Height system unification and estimation of the lithospheric structure beneath Vietnam through high-resolution gravity field and quasigeoid modeling

Dinh Toan Vu

Université Fédérale
Toulouse Midi-Pyrénées

THÈSE

En vue de l'obtention du
DOCTORAT DE L'UNIVERSITÉ DE TOULOUSE

Délivré par l'Université Toulouse 3 - Paul Sabatier

Présentée et soutenue par

Dinh Toan VU

Le 25 février 2021

Unification du système de hauteur et estimation de la structure lithosphérique sous le Vietnam utilisant la modélisation du champ de gravité et du quasigéoïde à haute résolution

Ecole doctorale : **SDU2E - Sciences de l'Univers, de l'Environnement et de l'Espace**

Spécialité : **Sciences de la Terre et des Planètes Solides**

Unité de recherche :
GET - Geosciences Environnement Toulouse

Thèse dirigée par
Sylvain BONVALOT et Sean BRUINSMA

Jury

M. Riccardo BARZAGHI, Rapporteur
M. George VERGOS, Examinateur
Mme Marie-Françoise LALANCETTE, Examinatrice
M. Pierre EXERTIER, Examinateur
Mme Lucia SEOANE, Examinatrice
M. Sylvain BONVALOT, Directeur de thèse
M. Sean BRUINSMA, Co-directeur de thèse
M. Michel DIAMENT, Président

Height system unification and estimation of the lithospheric structure beneath Vietnam through high-resolution gravity field and quasigeoid modeling

Thesis Dissertation

of

Dinh Toan VU

Toulouse, 2020

Acknowledgements

The present doctoral dissertation was done at the laboratory Géosciences Environnement Toulouse (GET, UMR 5563) during the academic years from 2016 to 2020 under the supervision of Dr. Sylvain Bonvalot and Dr. Sean Bruinsma. I sincerely thank my supervisors for their inspirational advice, attention, suggestions and encouragement throughout the work, without their supervision this work would not have been successful. This thesis was prepared for the Doctoral School (Ecole Doctorale-ED) of "Geosciences, Astrophysics, Space and Environmental Sciences" ("Sciences de l'Univers, de l' Environnement et de l' Espace"-SDU2E) at Paul Sabatier University-Toulouse III. I would also like to thank the management of the SDU2E doctoral school for their support.

I would like to thank the Vietnamese government for giving me a scholarship for four years. I also want to thank GET-UPS and BGI for providing me an additional scholarship. I would also like to thank Campus France for facilitating administrative procedures. I wish to thank the laboratory GET, allowing me to conduct my research in the best conditions. I am also very grateful for the support of the research team Géophysique et Géodésie Spatial (ER3-GGS) GET-OMP.

I am very grateful to the VIGAC, IGP-VAST and BGI that supplied gravity data for this work. I would like to thank the authors of GRAVSOFT (DTU) for providing their software.

To the members of the jury, Dr. Michel Diament, Pr. Riccardo Barzaghi, Pr. George Vergos, Dr. Marie-Françoise Lalancette, Dr. Lucia Seoane, Dr. Pierre Exertier and Dr. Georges Balmino, I would like to express my gratitude for their willingness to read and examine my work and for their objective judgement. Additionally, I show appreciation to the members of my thesis committee Pr. George Vergos (GravLab, AUTH), Dr. Lucia Seoane (GET-OMP) that followed my progress every year and gave me their helpful advice.

Last but not least, I would like to express my deepest gratitude to my family. My wife and my son, they were always giving me their faith, support and patience. I am indebted to my parents for encouraging me to do this PhD. I also thank my sisters and brothers for their encouragement. Finally, thanks to all my friends for their encouragement.

Thank you all!!!

Abstract

The goal of this work was twofold. The first part was devoted to the research of the size and physical shape of the Earth in Vietnam through the determination of a local gravimetric quasigeoid model. The second part was to better constrain the Earth's interior structure beneath Vietnam by determining the Moho and Lithosphere-Asthenosphere Boundary (LAB) depth models. For the first objective, a high-resolution gravimetric quasigeoid model for Vietnam and its surrounding areas was determined based on new land gravity data in combination with fill-in data where no gravity data existed. The resulting quasigeoid model was evaluated using 812 GNSS/levelling points in the study region. This comparison indicates that the quasigeoid model has a standard deviation of 9.7 cm and 50 cm in mean bias. This new local quasigeoid model for Vietnam represents a significant improvement over the global models EIGEN-6C4 and EGM2008, which have standard deviations of 19.2 and 29.1 cm, respectively, when compared to the GNSS/levelling data. An essential societal and engineering application of the gravimetric quasigeoid is in GNSS levelling, and a vertical offset model for Vietnam and its surrounding areas was determined based on the GNSS/levelling points and gravimetric-only quasigeoid model for this purpose. The offset model was evaluated using cross-validation technique by comparing with GNSS/levelling data. Results indicate that the offset model has a standard deviation of 5.9 cm in the absolute sense. Thanks to this offset model, GNSS levelling can be carried out over most of Vietnam's territory complying to third-order levelling requirements, while the accuracy requirements for fourth-order levelling networks is met for the entire country. To unify the height system towards the International Height Reference Frame (IHRF), the zero-height geopotential value for the Vietnam Local Vertical Datum W_0^{LVD} was determined based on two approaches: 1) Using high-quality GNSS/levelling data and the estimated gravimetric quasigeoid model, 2) Using the Geodetic Boundary Value Problem (GBVP) approach based on the GOCE global gravity field model enhanced with terrestrial gravity data. This geopotential value can be used to connect the height system of Vietnam with the neighboring countries. Moreover, the GBVP approach was also used for direct determination of the gravity potential on the surface at three GNSS Continuously Operating Reference Station (CORS) stations at epoch 2018.0 in Vietnam. Based on time series of the vertical component derived from these GNSS observations as well as InSAR data, temporal variations in the geopotential were also estimated on these permanent GNSS stations. This enables monitoring of the vertical datum and detect possible deformation. These stations may thus contribute to increase the density of reference points in the IHRF for this region.

For the second objective, the local quasigeoid model was first converted to the geoid. Then, high-resolution Moho and LAB depth models were determined beneath Vietnam based on the local isostatic hypothesis using the geoid height derived from the estimated

geoid, elevation data and thermal analysis. From new land gravity data, a complete grid and map of gravity anomalies i.e., Free-air, Bouguer and Isostatic was determined for the whole of Vietnam. The Moho depth was also computed based on the gravity inversion using the Bouguer gravity anomaly grid. All new models are computed at 1' resolution. The resulting Moho and LAB depth models were evaluated using available seismic data as well as global and local lithospheric models available in the study region. These comparisons indicate a consistency of the Moho depth estimations with the seismic data within 1.5 km in standard deviation for the whole of Vietnam. This new Moho depth model for Vietnam represents a significant improvement over the global models CRUST1.0 and GEMMA, which have standard deviations of 3.2 and 3.3 km, respectively, when compared to the seismic data. The high resolution of the new Moho and LAB depth models may contribute to a better understanding of the lithospheric structure as well as tectonic and geodynamic processes of this region. The differences in Moho depth visible in the northeast and southwest sides of Red River Fault Zone confirmed that the Red River Fault Zone may be considered to be the boundary between two continental blocks: the South China and Indochina blocks.

Keywords: Regional quasigeoid, GNSS/levelling, Gravity anomaly, Least-Squares Collocation, Stokes FFT, Local Vertical Datum, Height system unification, Gravity potential, GBVP approach, GNSS-CORS, Geoid height, Moho depth, LAB depth, Gravity inversion

Résumé

Le but de ce travail était double. La première partie a été consacrée à la recherche de la taille et de la forme de la Terre au Vietnam à travers la détermination d'un modèle quasigeoïde gravimétrique local. La deuxième partie consistait à étudier la structure intérieure de la Terre sous le Vietnam en déterminant la profondeur du Moho et de la limite entre Lithosphère-Asthénosphère. Pour le premier objectif, un modèle quasigeoïde gravimétrique à haute résolution pour le Vietnam et ses environs a été déterminé sur la base de nouvelles données issues de campagnes gravimétriques terrestres en combinaison avec des observations satellites dans les régions non couvertes par les observations au sol. Le modèle quasigeoïde a été évalué en utilisant 812 points GNSS/nivellement dans la région d'étude. Cette comparaison indique que le modèle quasigeoïde a un écart type de 9.7 cm et un biais moyen de 50 cm. Ce nouveau modèle quasigeoïde local pour le Vietnam représente une amélioration significative par rapport aux modèles globaux EIGEN-6C4 et EGM2008, qui ont des écarts-types de 19.2 et 29.1 cm, respectivement, par rapport aux données GNSS/nivellement. Une application sociétale et technique essentielle du quasigeoïde gravimétrique est le nivellement par GNSS, et un modèle de décalage vertical pour le Vietnam et ses environs a donc été déterminé sur la base des points GNSS/nivellement et du modèle quasigeoïde gravimétrique. Le modèle de décalage (ou modèle de correction) a été évalué en comparant avec des données GNSS/nivellement. Les résultats indiquent que le modèle obtenu a un écart type de 5.9 cm au sens absolu. Grâce à ce modèle de décalage, le nivellement par GNSS peut donc être effectué dans la plupart du territoire vietnamien conformément aux exigences de nivellement du troisième ordre, tandis que les exigences de précision pour les réseaux de nivellement du quatrième ordre sont satisfaites pour tout le pays. Pour tenter d'unifier le système de hauteur ainsi déterminé vers l'IHRF (International Height Reference System), la valeur géopotentielle à zéro-hauteur pour le système de référence vertical local du Vietnam W_0^{LVD} a été déterminée en fonction de deux approches: 1) Utilisation de données GNSS/nivellement de haute qualité et du modèle quasigeoïde gravimétrique. 2) Utilisation de l'approche du problème de la valeur aux limites géodésiques basée sur le modèle de champ de gravité global GOCE amélioré avec des données de gravité terrestres. Cette valeur géopotentielle est utilisée pour rattacher le système de hauteur du Vietnam avec les pays voisins. De plus, l'approche du problème de la valeur des limites géodésiques a également été utilisée pour la détermination du potentiel de gravité à la surface de trois stations GNSS-CORS à l'époque 2018.0 au Vietnam. Sur la base de séries chronologiques de composantes verticales dérivées des observations GNSS ainsi que des données InSAR, les variations temporelles du géopotentiel ont également été estimées sur ces stations GNSS permanentes. Cela permet de surveiller la référence verticale et de détecter d'éventuelles déformations. Ces stations peuvent ainsi contribuer à augmenter la densité

des points de référence dans l'IHRF pour cette région.

Pour le deuxième objectif, le modèle de quasigéoïde local a d'abord été converti en géoïde. Ensuite, des modèles de profondeur du Moho et de la limite entre Lithosphère-Asthénosphère à haute résolution ont été déterminés sous le Vietnam sur la base de l'hypothèse isostatique locale en utilisant la hauteur du géoïde dérivée du géoïde, des données de hauteur et d'analyse thermique. À partir de nouvelles données de gravité terrestre issues de campagnes récentes, des cartes d'anomalies gravimétriques d'Air-libre et de Bouguer et Isostatique corrigées de la topographie ont été déterminées pour l'ensemble du Vietnam. La profondeur de Moho a également été calculée sur la base de l'inversion gravimétrique en utilisant la grille d'anomalies gravimétriques de Bouguer. Tous les nouveaux modèles sont calculés à une résolution de 1'. Les modèles de profondeur du Moho et de la limite entre Lithosphère-Asthénosphère ont été discutés et évalués en utilisant des données sismiques disponibles ainsi que des modèles lithosphériques mondiaux et locaux disponibles dans la région d'étude. Ces comparaisons indiquent une cohérence des estimations de profondeur Moho avec les données sismiques à moins de 1.5 km d'écart type pour l'ensemble du Vietnam. Ce nouveau modèle de profondeur du Moho pour le Vietnam représente une amélioration significative par rapport aux modèles mondiaux CRUST1.0 et GEMMA, qui ont des écarts-types de 3.2 et 3.3 km, respectivement, par rapport aux données sismiques. La haute résolution des nouveaux modèles de profondeur du Moho et de la limite entre Lithosphère-Asthénosphère peut contribuer à une meilleure compréhension de la structure lithosphérique ainsi que des processus tectoniques et géodynamiques de cette région. Les différences de profondeur du Moho visibles entre les côtés nord-est et sud-ouest de la zone de faille de la Rivière Rouge confirment que cette zone de faille peut être considérée comme la frontière entre deux blocs continentaux: les blocs de Chine sud et d'Indochine.

Mots clés: Quasigeoïde régional, GNSS/nivellement, Anomalie de gravité, Collocation des moindres carrés, Stokes FFT, Référence verticale locale, Unification du système de hauteur, Potentiel de gravité, approche GBVP, GNSS-CORS, Hauteur du géoïde, Profondeur de Moho, Profondeur du LAB, Inversion de gravité

Acronyms

BGI	Bureau Gravimétrique International
CHAMP	Challenging Minisatellite Payload
CNES	Centre National d'Étude Spatiales
CORS	Continuously Operating Reference Station
CRF	Chay River Fault
d/o	degree/order
DBM	Digital Bathymetry Model
DBPF	Dien Bien Phu Fault
DORIS	Doppler Orbitography and Radio-positioning Integrated by Satellite
DRF	Da River Fault
DTM	Digital Terrain Model
FFT	Fast Fourier Transform
GAMIT/GLOBK	GNSS at MIT/Global Kalman Filter
GBVP	Geodetic Boundary Value Problem
GGM	Global Gravity field Models
GLONASS	Global'naya Navigatsionnaya Sputnikovaya Sistema
GMSL	Global Mean Sea Level
GMT	Generic Mapping Tools
GNSS	Global Navigation Satellite System
GOCE	Gravity field and steady-state Ocean Circulation Explorer
GPS	NAVSTAR Global Positioning System
GRACE	Gravity Recovery And Climate Experiment
HSU	Height System Unification
IAG	International Association of Geodesy
ICGEM	International Center for Global Earth Models
IGP	Institute of Geophysics
IHRF	International Height Reference Frame
IHRS	International Height Reference System
InSAR	Interferometric Synthetic Aperture Radar
ITRF	International Terrestrial Reference Frame
ITRS	International Terrestrial Reference System
LAB	Lithosphere-Asthenosphere Boundary
LAGEOS	LAser GEOdynamics Satellite
LLR	Lunar Laser Ranging
LRF	Lo River Fault
LSC	Least-Squares Collocation
LVD	Local Vertical Datums

MIIGAiK	Moscow State University of Geodesy and Cartography
MRF	Ma River Fault
MSL	Mean Sea Level
MT	Mean Tide
NGS	National Geodetic Survey
PPP	Precise Point Positioning
RCR	Remove–Compute–Restore
RET	Rock-Equivalent Topography
RINEX	Receiver Independent Exchange Format
RRF	Red River Fault
RRFS	Red River Fault System
RTM	Residual Terrain Model
SLF	Son La Fault
SLR	Sea Level Rise
SLR	Satellite Laser Ranging
SRTM	Shuttle Radar Topography Mission
STD	Standard deviation
TC	Terrain corrections
TF	Tide Free
VAST	Vietnam Academy of Science and Technology
VDSM	Vietnam Department of Surveying and Mapping
VIGAC	Vietnam Institute of Geodesy and Cartography
VLBI	Very Long Baseline Interferometry
VLVD	Vietnam Local Vertical Datum
WG	Wong-Gore
ZT	Zero Tide

Table of contents

Chapter 1: INTRODUCTION

1.1. General background

The mass distribution of the Earth is highly inhomogeneous. It comprises surface features such as mountains, plains, rivers, oceans, valleys, trenches as well as sub-surface or internal mass structures like core and mantle. This inhomogeneity of the Earth's structure is closely related to the variations in its gravity field, which is a useful tool especially for geodetic, geological or geophysical studies. Gravity data can be classified into surface data (from land, marine and airborne surveys) measured and collected by various governmental and private organizations, and satellite data acquired from space mission. Over the past 70 years, the global knowledge to the Earth's gravity has been continuously upgraded leading to Global Gravity field Models (GGMs) (Rapp, 1998) with increasing accuracies and resolutions (See the International Center for Global Earth Models (ICGEM) website (Ince et al., 2019)): from the early spherical harmonic models of degree 8 (Zhongolovich, 1952) to the present solution that extends to degree 2190 such as EGM2008 (Pavlis et al., 2012) or EIGEN-6C4 (Förste et al., 2014). GGM was significantly improved during the last 25 years with the space gravity data from dedicated missions: Challenging Minisatellite Payload (CHAMP; Reigber et al., 1996), Gravity Recovery And Climate Experiment (GRACE), and Gravity field and steady-state Ocean Circulation Explorer (GOCE; Drinkwater et al., 2003). Thanks to these satellite gravity missions, a new generation of GGM was developed providing accurate information of the Earth's gravity at long and medium wavelengths. A uniform coverage over open seas was also provided thanks to altimetric gravity observations. Over land, the high resolution of the Earth's gravity field remains provided by surface measurements such as those provided from the national services or private organizations or made available from international gravity organizations e.g., the Bureau Gravimétrique International (BGI) (See Geodesist's Handbook 2020 (Bonvalot, 2020)). Due to various reasons, the accuracy and spatial distribution of surface gravity data are often heterogeneous even at the national scale and their combination with satellite observations and GGMs is often required for characterizing the Earth's gravity variations on a given area. The combination of these heterogeneous data is often difficult and needs specific and rigorous approaches for obtaining the best determination of the expected products (geoid, gravity anomalies, Moho depths...).

From a geodetic point of view, one of the fundamental applications of the gravity data is to determine the size and physical shape of the Earth. The geoid as a fundamental surface of physical geodesy is currently most often defined as an equipotential surface which best fits the global Mean Sea Level (MSL), and therefore it is commonly known as the physical

figure of the Earth. Since the geoid is an equipotential surface, it is dependent on the mass distribution within the Earth and hence geoid determination is related directly to the Earth's gravity field. The geoid serves as a reference surface for the modern vertical system (Torge, 2001).

Until the 1990s, the most commonly used observing techniques for determining physical height were spirit levelling and gravimetry, which requires much time and consequently is expensive. Global Navigation Satellite System (GNSS) technology is used for positioning and navigation because of its speed, convenience and accuracy. The ellipsoidal height derived from GNSS technology can be achieved with an accuracy of a few millimeters (Alber et al., 1997). However, a drawback of GNSS is that the ellipsoidal height is not physically meaningful – it does not inform on in which direction water will flow. To convert an ellipsoidal height to a physical height, a high accuracy and resolution geoid model is needed. This approach is very convenient because of its simplicity. However, the accuracy of this relatively new technique is dependent on the accuracy of the geoid model. Geoid accuracy is still a complex issue to date, especially for many developing countries where the availability of gravity data might be limited. Therefore, from the 1990s, along with the strong development of satellite positioning technology, high accuracy geoid determination became a focus for geodetic researchers. Height systems can be divided into two main categories: orthometric and normal height. The orthometric height is the geometric distance between the geoid and the earth's surface that follows the curved plumb line. The normal height is the distance between a surface, identical to the geoid over the oceans and very close to it anywhere else, and the earth's surface. This surface is called the quasigeoid by Molodensky. Some countries use the orthometric height while the remaining countries use normal height. Therefore, instead of the geoid, countries using normal height determine the quasigeoid according to the theory of Molodensky to construct their national height system.

The geoid/quasigeoid is not a regular surface. This irregularity is highly correlated to the inhomogeneous mass distribution of the Earth. Therefore, different sources of information are required for the determination of a precise geoid/quasigeoid. First, a detailed Digital Terrain Model (DTM) is required in the computation procedure. The new DTMs (up to 3 arc second resolution), such as derived from the Shuttle Radar Topography Mission (SRTM), are now currently used for geoid/quasigeoid developments. Secondly, a GGM is required. A new generation of GGM based on GRACE and GOCE satellite data was developed. The high resolution GGMs are available for determining geoid or quasigeoid. Finally, precise gravity data are essential to determine the geoid/quasigeoid. However, establishing dense relative or absolute gravity networks remains challenging for most countries due to financial and practical difficulties. As stated earlier, the altimetric gravity field is of good quality over open sea, however, coastal zones remain problematic because

most altimeters cannot measure up to the coast on shallow waters areas. On the other hand, land gravity data is measured, collected and distributed by various governmental and private organizations since decades, and these data are often not equally accurate. Moreover, their spatial distribution is often limited due to various difficulties, but mainly due to challenging access (e.g., mountains, wetlands, rain forests) and remoteness. Therefore, in most areas, gravity measurements are limited to the more accessible low elevation regions. Airborne gravimetry (Forsberg & Olesen, 2010) is used preferentially to fill data gaps over mountainous regions as well as to close the gap between gravity data on land and over open sea. However, it has only been applied in a few countries so far. Another problem of enhancing the gravity data coverage is the cost and effort required to make such observations, which may not be affordable for many developing countries.

Current height systems are based on the MSL. It should also be noted that countries define regional MSL determined from tide gauge observations over a long period of time (at least the longest lunar tide, 18.6 years). Due to the oceanic variability and the effect of sea surface topography, MSLs as defined from tide gauge observations at various locations will not necessarily lie on a common equipotential surface. As a result, there are currently more than 100 Local Vertical Datums (LVD) in the world. Moreover, many vertical datums may even exist within a single country, especially for archipelagic countries such as the Philippines (Reyes et al., 2015), Indonesia (Kasenda & Kearsley, 2002), New Zealand (Amos & Featherstone, 2009), and Greece (Vergos et al., 2018), where the MSL may be subject to variations. The variability of the MSL is one of the reasons why the geoid/quasigeoid surface can be rigorously used to unify the different LVDs. The deviation of the MSL from the equipotential surface of the geoid/quasigeoid, known as the (stationary) mean dynamic topography, is quite significant and in some parts may reach the order of ±2m (Rapp & Balasubramania, 1992; Ihde et al., 2017). It will affect the definition and the unification of LVDs separated by oceans if the MSL is to be used as the height reference. Unification of the national vertical datums is required to implement engineering projects between countries and improve flooding observations and modeling at regional scales as well as monitor and manage rising of sea level at global scales (Ihde et al., 2017). The unification of height systems has been discussed by the geodetic scientific community for decades (Rummel & Teunissen, 1988; Rapp & Balasubramania, 1992; Ihde et al., 2000; Grigoriadis et al., 2014; Vergos et al., 2018). However, a reliable approach to a global height reference system is becoming possible only recently thanks to the availability of modern geodetic techniques, especially the precise determination of geometrical coordinates by GNSS positioning, and a high resolution and accuracy reference surface, the geoid/quasigeoid. Moreover, due to Sea Level Rise (SLR), recorded in some areas with tide-gauge and satellite altimetry observations, MSL actually varies over time. Despite this rate of sea level rise, levelling networks have most often not been

re-adjusted in order to accommodate this change. This is a disadvantage when using MSL as reference for the height system. In short, determination of an accurate geoid/quasigeoid is a necessary task today.

From a geophysical point of view, gravity inversion has long been known to be a helpful tool for detecting, understanding and interpreting several kinds of geophysical structures and geodynamical processes. The gravity field also gives information on the Earth's crustal evolution and isostatic compensation, as well as stress patterns in the lithosphere. The gravity method remains attractive as the gravity data is comparatively cheap and easy to collect in comparison with other geophysical methods. Moreover, large scale studies and applications also benefit from the availability of high-resolution GGMs. Geoid height, after removing long wavelength components, is also useful information for geophysical studies.

In 1909, Andrija Mohorovičič, who was seismologist, used seismic waves to discover the presence of the crust-mantle boundary (the Mohorovičič discontinuity, or Moho). The Moho is a physical/chemical boundary between the crust and mantle where both the crust and mantle are defined by material properties, which can cause large changes in geophysical properties, such as seismic wave velocity, density, pressure, temperature. Having information about this Moho surface is important for various purposes such as plate tectonics, better understanding of earthquake mechanisms, the heat flux and heat distribution inside the Earth, and thermal evolution of the Earth itself (Carbonell et al., 2013). Basically, seismic and isostatic-gravimetric methods are used to determine this Moho surface. Seismic methods usually provide a realistic way of imaging the Moho. However, seismic surveys are expensive and hence in many areas sufficient seismic information for depth estimation of the crust is sparse or lacking, inferring poor Moho depth models. Today, large scale gravity surveys by means of satellite gravity missions are much more cost-effective. The gravity data collected are global, but with lower spatial resolution. The Moho depth can be estimated by gravity inversion under the assumption of some kind of isostatic model (e.g., the models of Airy, Pratt and Vening Meinesz), where the gravity anomaly is mainly assumed to be the effect of variations in the Moho depth. The isostatic Moho models are complementary to seismic models, in particular in areas where seismic data is sparse. Hence, the problem of seismic data gaps can be solved by gravimetric-isostatic methods. After removing all terrain effects, non-geological components, the Bouguer gravity anomalies correlate mainly with lateral density variations within the crust and Moho topography. The Bouguer gravity anomalies are commonly used in the inversion method for determining the Moho depth. Deeper, the Lithosphere-Asthenosphere Boundary (LAB) is also fundamental in plate tectonics. The actual depth of this boundary remains a topic of debate and study (Rychert & Shearer, 2009). Several types of geophysical data have been used to determine the LAB, e.g.

seismic, thermal, electromagnetic, gravity and rheological. However, the resultant LAB depth models differ significantly (Artemieva, 2011). According to Fullea et al., (2006), the geoid heights in combination with elevation data are also used to determine the Moho and LAB depths based on the local isostatic hypothesis. This is an application of the geoid in the study of the Earth's interior structure.

In brief, gravity data is vital for geodetic, geophysical and geological studies. It can be used for defining the shape of the Earth to determining its internal structure, from a global scale down to a region or country. The following research topics, using gravity data in Vietnam, for which assimilation of surface gravity data in GGMs is very limited, are addressed: 1) Calculation of a complete map of gravity anomalies, 2) Computation of the gravimetric quasigeoid model towards resolving the issue of height system unification, 3) Application of the estimated gravimetric quasigeoid in the determination of the lithospheric structures and 4) Determination of the Moho depth surface from the gravity anomaly data employing an inversion method.

1.2. Scientific context and motivations for the thesis project

1. Geoid/quasigeoid and height system unification

In Vietnam, GGMs have been used in GNSS levelling applications since the late 1990s: EGM96 (Lemoine et al., 1998) at first and currently EGM2008 (Pavlis et al., 2012). However, EGM2008 is inadequate for GNSS levelling over Vietnam. A few studies attempted to match global models such as EGM2008 to GNSS/levelling data called VIGAC2014 and VIGAC2017 (Ha, 2017). However, according to Rummel et al., (2014), the expected mean accuracy after applying EGM2008 is about ±4 to ±6 cm in well-surveyed regions and about ±20 to ±40 cm with extreme cases of ±1 m in sparsely surveyed regions. Vietnam is representative of a sparsely surveyed region, where fill-in data had to be used in the EGM2008 model. As a result, its accuracy is insufficient to comply with fourth-order levelling specifications (a misclosure of $25\sqrt{k}$ mm over a distance of k km) in Vietnam. This will be clarified in chapter 4 of this study. A local gravimetric quasigeoid of Vietnam was so far never calculated. There is presently a strong need for a high-accuracy and high-resolution gravimetric quasigeoid model of Vietnam and its vicinity for the purpose of modernizing the height system using GNSS instead of spirit levelling, as well as for other applications such as geology, geophysics, and oceanography. It should be noted that normal height is currently used in the national height system of Vietnam; therefore, this study focuses on the determination of the quasigeoid. For applications in geology and geophysics, the geoid can be determined by applying a correction to the estimated quasigeoid.

As mentioned previously, the deviation of the MSL and the equipotential surface of the gravimetric geoid/quasigeoid can be quite significant. This leads to large mean biases

between existing height systems determined from levelling referring to the national MSL and the estimated geoid/quasigeoid referring to a global reference system, i.e., an international reference gravity potential W_0 = 62,636,853.4 m^2/s^2. With such a large mean bias, a gravimetric geoid/quasigeoid model does not allow accurate transformation of GNSS ellipsoidal heights to physical heights in the LVD. Most often, the gravimetric quasigeoid or geoid model is forced to fit onto the local vertical datum using GNSS/levelling data. Such a hybrid quasigeoid/geoid model is used to convert GNSS ellipsoidal heights to physical heights. Most countries make continuous efforts to determine and improve their geoid or quasigeoid model successfully based on gravity data collected from the national database as well as the GGMs. For comparison, Table 1.1 shows the accuracy of several local geoid or quasigeoid models, and notably of neighboring countries in Asia. The resulting standard deviations (STD) obtained for the most recent gravimetric models range from a few cm up to 30 cm, whereas for hybrid models from a few cm up to 10 cm, depending on the quality of the available gravity and GNSS/levelling data for the geoid/quasigeoid determination. A geoid/quasigeoid with an accuracy of a few centimeters is required for the GNSS levelling technique towards modernization of the national height systems nowadays.

Table 1.1. Statistics of selected local geoid or quasigeoid models

No	Country, region	Name	Year	STD (cm)	Geoid type	Reference
1	Australia	AUSGeoid98	1998	36.4	Gravimetric quasigeoid	Featherstone et al., 2001
		AUSGeoid09	2009	22.2	Gravimetric quasigeoid	Featherstone et al. 2011
		AUSGeoid2020	2018	2.7	Hybrid quasigeoid	Brown et al., 2018
2	Argentina	GAR	2007	29.0	Gravimetric geoid	Piñón et al. 2018
		GEOIDEAR	2017	27.0	Gravimetric geoid	Piñón et al. 2018
3	Japan	GSIGEO2000	2002	4.0	Hybrid geoid	Kuroishi et al. 2002
		GSIGEO2011	2014	1.8	Hybrid geoid	Miyahara et al. 2014
4	South Korea	KGEOID98	1998	42.2	Gravimetric geoid	Yun 2002
		KNGeoid13	2013	5.4	Hybrid geoid	Lee et al. 2017

		KNGeoid14	2014	5.2	Hybrid geoid	Lee et al. 2017
5	Thailand	THAI12G	2012	15.1	Gravimetric geoid	Dumrongchai et al. 2012
6	Philippines	PGM2014	2014	30.0	Gravimetric geoid	Forsberg et al., 2014
		PGM2016	2016	2.2	Hybrid geoid	Gatchalian et al. 2016
7	Peninsular (Malaysia)	VMGEOID04	2018	5.0	Hybrid geoid	Ismail et al. 2018
	Sabah and Sarawak (Malaysia)	EMGEOID05	2018	10.0	Hybrid geoid	Ismail et al. 2018
8	Hong Kong	HKGEOID-2000	2004	1.7	Hybrid geoid	Chen & Luo, 2004
9	Shenzhen	SZGEOID-2001	2004	1.4	Hybrid geoid	Chen & Luo, 2004

Presently, all conditions for accurate high-resolution quasigeoid determination using the Remove–Compute–Restore (RCR) technique (Sansò & Sideris, 2013; Barzaghi, 2016) of Vietnam are met thanks to:

- A new generation of GGMs based on GOCE data;
- High-resolution DTMs: SRTM3arc_v4.1 (Farr et al., 2007) on land and SRTM15arc_plus (Becker et al., 2009) over sea;
- New relative and absolute gravity measurements covering the entire country from the project "Measurement and Improvement of Vietnam National Gravity Data", carried out in collaboration between the Vietnam Institute of Geodesy and Cartography (VIGAC) with the Moscow Institute of Geodesy, Cartography and Aerial Images, Moscow State University of Geodesy and Cartography (MIIGAiK), Russia, from 2003-2011 (Final Report of VIGAC 2012) plus the gravity data collected from projects of geological survey, exploration geophysics, and mineral prospecting, as well as high-resolution altimeter-inferred gravity anomaly data over sea (Andersen & Knudsen, 2016). These gravity surveys were jointly carried out with GNSS and/or levelling measurements to determine the height of gravity stations.
- Well-distributed, high-quality GNSS/levelling network for validation, as well as to determine the offset model for GNSS levelling using the gravimetric quasigeoid.

Vietnam is located on the eastern margin of the Indochinese peninsula with a coastline of about 3,260 km and many islands. The country is divided into the highlands and the Hong River Delta in the north, the Annamite Range along with the coastal lowlands in the centre,

and the Mekong Delta in the south. The mountain plateaus in the northwest and centre are irregular in elevation and form. The country's highest peak, Fan Si Pan, rises to 3,142 meters in the extreme northwest. Limited gravity data is available in these mountainous regions of Vietnam and its neighboring countries. Secondly, the quality of gravity data from geological surveys, exploration geophysics, and mineral prospecting in the 1980s will make it challenging to achieve a high accuracy quasigeoid of Vietnam. Moreover, an airborne gravimetry project, the preferred method to close the gap between gravity data on land and marine altimetric gravity fields, has not been implemented yet in Vietnam. The accuracy of the quasigeoid in coastal zones is also a complex problem to research and improve.

The elongated roughly S shaped country has a north-to-south distance of about 2,000 km while the original point of the national height system is located in the north. Therefore, a north–south tilt would be present in the vertical network of Vietnam and thus influence the GNSS/levelling data. Vietnam is among the most affected countries by global climate change. A large number of studies show that Vietnam is experiencing climate change and will be severely negatively affected in coming decades. These negative effects include Sea Level Rise (SLR), salinity intrusion and other hydrological problems like flood as well as the increasing frequency of natural hazards such as storm surges. Some issues, such as land subsidence further worsen some effects that climate change (sea level rise) will bring especially in areas such as the Mekong Delta. The land subsidence might also affect the quality of GNSS/levelling in this delta. Taking into account these two effects on the GNSS/levelling data is a challenge in this study.

The height offsets between the 100 LVDs existing in the world today are often unknown to connect the height systems. The connection of height systems located on one continent can be done by geodetic sprit levelling in combination with gravity measurements, but height systems separated by sea cannot be unified in this manner. Even at the national scale, the Vietnam LVD is only valid for the continental territory but not for the islands and territorial waters of Vietnam. The determination of a high-resolution quasigeoid model together with GNSS will enable us to determine the height of all islands and unify the height references for Vietnam. Such a gravimetric quasigeoid model will be also used in combination with high-quality GNSS/levelling data (referred to the Vietnam LVD) to estimate the zero-height gravity potential value of the Vietnam LVD in order to connect the height system of Vietnam with that of the neighboring countries.

2. Gravity anomalies and lithosphere structures

Vietnam is situated immediately southeast of the eastern Himalayan syntaxis and hence remotely influenced by the collision between Indian and Eurasian plates. The study region is located in the active tectonic region with interactions of four tectonic plates: Indian, Eurasian, Philippine and Australian plates (Figure 1.1). This creates a complex

topographic and geological structure with a number of active faults especially the northern part of Vietnam. Earthquake intensity in this region is moderate but it remains active. The geophysical information beneath Vietnam is fundamental for understanding tectonic and geodynamic processes of the region.

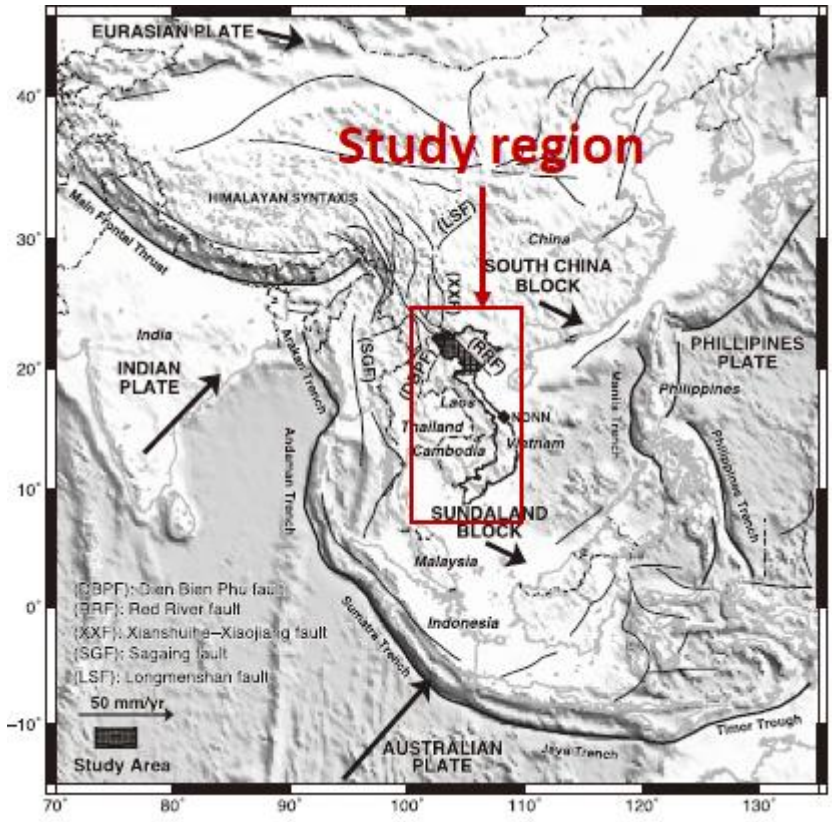

Figure 1.1. Regional tectonic map

In 2011, a map of Bouguer gravity anomalies has been released at 1:500,000 scale for mainland Vietnam using 12,579 gravity measurements by the Geophysical Division, General Department of Geology and Minerals of Vietnam (Lai et al., 2012). The density of these data is very limited. The new and very accurate gravity data from the VIGAC project, the new generation of GGM and altimetric gravity fields, and a high-resolution DTM were used here to improve the accuracy and resolution of the gravity anomaly maps of Vietnam. A unified gravity anomaly map (Free-air, Bouguer and Isostatic) for the whole of Vietnam (including the sea) has so far never been made, and the new maps will certainly help improve the accuracy of geophysical and geological applications in Vietnam. The gravity anomalies from WGM2012 (Bonvalot et al., 2012), grids and maps of the Earth's gravity anomalies computed at global scale and available at 2' resolution, will be used as reference.

One of the applications of gravity data in geophysics is to determine Moho depth surface based on the concept of isostasy. Even early studies of the Earth's interior structure started from this concept i.e., the different hypothesizes proposed by Pratt and Airy from the middle of the nineteenth century, long before seismic investigations started (Kaban et

al., 2004). Global Moho depth models were developed using different data sources, for example: CRUST5.0 (Mooney et al., 1998), CRUST2.0 (Laske et al., 2000) and the most recent CRUST1.0 (Laske et al., 2013) at $5x5^0$, $2x2^0$ and $1x1^0$ resolution, respectively, using seismic data, and GEMMA (Reguzzoni & Sampietro, 2014) has been computed by inverting the global grid of second radial derivatives of the gravitational potential observed by the ESA mission GOCE and considering the density of the crust as defined in the CRUST2.0 model. The GEMMA model is available with resolution $0.5x0.5^0$. The Moho depths based on seismic data have good quality where denser seismic data is available, such as over North America and Europe. According to Mooney et al., (1998) and Sjöberg & Bagherbandi (2017) the seismic data is sparse in large portions of Africa, South America, Asia and Greenland and also open ocean areas, hence the CRUST model is much worse, in terms of accuracy as well as resolution, in these regions. The local or regional Moho depth surfaces based on the gravity inversion are preferentially used to complement a seismic model. These global models can be used as the reference model in computation and validation of the local models.

Several isostatic-gravimetric Moho depth surfaces were developed for the northern part and sea of Vietnam (Bui, 1983; Dang, 2003; Braitenberg et al., 2006; Dinh, 2010; Nguyen & Nguyen, 2013; Nguyen et al., 2018) using gravity data derived from geological surveys, exploration geophysics and mineral prospecting as well as marine gravity fields derived from global altimetric gravity models. However, the results derived from these studies differ considerably (Nguyen et al., 2013) due to several reasons such as the precision and resolution of gravity data used, approach used in computation, and lack of independent constrained conditions (i.e., seismic data). The Moho depth in the study region has also been investigated using seismic data (Lebedev & Nolet, 2003; Wu et al., 2004; Dinh, 2010; Li & Hilst, 2010; Bai et al., 2010; Huang et al., 2009; Nguyen et al., 2013; Yu et al., 2017; Su et al., 2018). However, the resolutions of these studies are relatively low because of the sparse distribution of seismic stations or the limited number of profiles covering the study area. Most of the stations are located in the northern part of Vietnam, and there are no measurements over sea. Consequently, the knowledge of the Moho structure beneath Vietnam is still poor. From the high accuracy and high resolution gravimetric quasigeoid in combination with elevation data derived from DTM, a new Moho depth model is determined here for the whole of Vietnam based on the local isostatic assumption. For comparison, the Moho depth model is also estimated for this region from the Bouguer gravity anomaly grid calculated using the new gravity data. The objective of this study is to test the accuracy of these two approaches in the computation of the Moho depth. The LAB depth, including the crust and the uppermost mantle, is also determined based on the approach using the geoid height and elevation data. These high-resolution new Moho and LAB depth models are expected to better contribute to the understanding of the

lithospheric structure as well as the tectonic and geodynamic processes of this region.

1.3. Objectives of the study

The objectives of this thesis are:

- To determine maps and grids of gravity anomalies for Vietnam and its surrounding areas.
- To determine a high-accuracy and high-resolution gravimetric quasigeoid for Vietnam.
- To determine a vertical offset model based on the differences between gravimetric quasigeoid and GNSS/levelling data. This offset model is used for GNSS levelling technique in Vietnam.
- To determine the zero-height geopotential (W_0^{LVD}) as well as offset height value of Vietnam LVD with respect to the global equipotential surface realized by a conventional value towards unification of height system. Two method are used for computing the local geopotential value: 1) using the local gravimetric quasigeoid and GNSS/levelling data and 2) using the Geodetic Boundary Value Problem (GBVP) approach based on the gravity data. Moreover, determination of the geopotential value on the permanent GNSS stations will be also performed based on the GBVP approach towards realization of International Height Reference System (IHRF) in the study region.
- To determine a high-accuracy and high-resolution Moho and LAB depth based on the estimated gravimetric geoid and elevation data.
- To determine a high-accuracy and high-resolution Moho depth map based on new gravity anomaly grid for Vietnam and its surrounding areas.

1.4. Structure of the thesis

This study focuses on two principal topics: 1) determination of gravimetric geoid and its application in GNSS levelling technique and in unification of height system and 2) creation of gravity anomaly grids to determine lithospheric structures beneath Vietnam. These contents consist of seven chapters. This work has been also the subject of 4 articles published which make part of this manuscript. Below is a short preview on the contents of these chapters.

Chapter 1 is the introduction of the research. It provides the motivation and the main objectives of this thesis.

Chapter 2 gives the necessary information on the determination of gravimetric geoid/quasigeoid. The gravimetric quasigeoid determination techniques, such as the Stokes integral using the Fast Fourier Transform (FFT) approach and deterministic kernel modification proposed by Wong–Gore, as well as by means of Least-Squares Collocation

(LSC), are discussed in detail. Gravity reductions, Free-air, Bouguer and Isostatic, are described. The information regarding the height data types employed in this study i.e., ellipsoidal and physical height, is also explained.

Chapter 3: the data used in the research as well as their pre-processing procedures are given. The gravity data is reduced and the maps of gravity anomalies are determined. The validation of these gravity anomaly maps is presented.

Chapter 4: the results of the gravimetric quasigeoid computations using Stokes-FFT method as well as LSC will be presented and discussed in detail. Then, the validation of these gravimetric quasigeoid models with GNSS/levelling data is presented. The results from this chapter have been published in Vu et al., (2019).

Chapter 5 provides analysis of the quality of the GNSS/levelling data in Vietnam. The GNSS/levelling data will be corrected using land subsidence results in the Mekong Delta. A vertical offset model is determined for GNSS levelling application using GNSS/levelling-corrected land subsidence and estimated gravimetric quasigeoid. Finally, the gravity potential as well as datum offset value of Vietnam vertical datum are determined based on two approaches: 1) using gravimetric quasigeoid and GNSS/levelling data and 2) using the gravity data based on the GBVP approach. The results from this chapter have been published in Vu et al., (2020) and Vu et al., (2021).

Chapter 6 gives and compares two methods to determine the lithospheric structures under Vietnam: 1) using the geoid height derived from the local gravimetric geoid and elevation data and 2) using the Bouguer gravity anomaly and the gravity inversion method. The results from this chapter have been published in Vu et al., (2021).

Chapter 7 summarizes the outcomes of this study. The main conclusions of this research are drawn and recommendations for future work will be presented.

1.5. Introduction en français

Les données gravimétriques sont un outil utile pour les études géodésiques, géologiques ou géophysiques. D'un point de vue géodésique, l'une des applications fondamentales des données gravimétriques est de déterminer la taille et la forme physique de la Terre à l'aide d'un modèle géoïde/quasigéoïde gravimétrique. Dans la réalisation du système vertical moderne, le géoïde/quasigéoïde sert de surface de référence. À partir des années 1990, parallèlement au fort développement de la technologie de positionnement par satellite GNSS, la détermination du géoïde à haute précision est devenue une priorité des géodésiens pour l'application du nivellement par GNSS au lieu du nivellement, ce qui nécessite beaucoup de temps et par conséquent coûte cher. Actuellement, pour l'application locale ou régionale du nivellement par GNSS, un géoïde/quasigéoïde d'une précision de quelques centimètres est nécessaire. D'un point de vue géophysique, l'inversion gravimétrique est aussi connue depuis longtemps pour être un outil majeur pour la détermination de la profondeur du Moho et de la limite entre Lithosphère-Asthénosphère. La méthode gravimétrique reste intéressante car les données gravimétriques sont comparativement à d'autres méthodes d'investigation géophysiques bon marché et faciles à collecter. Pour les études et applications à de vastes régions, cette méthode est d'autant plus facilitée de nos jours grâce à des modèles de champ de gravité globaux de mieux en mieux résolus et de plus en plus précis.

Au Vietnam, les modèles de champ de gravité globaux sont utilisés dans les applications de nivellement par GNSS depuis la fin des années 1990: EGM96 (Lemoine et al., 1998) dans un premier temps et actuellement EGM2008 (Pavlis et al., 2012). Cependant, le modèle EGM2008 (5' de résolution) reste insuffisant pour le nivellement par GNSS au Vietnam. Quelques études ont essayé d'ajuster des modèles mondiaux tels que EGM2008 aux données GNSS/nivellement appelées VIGAC2014 et VIGAC2017 (Ha, 2017). Cependant, selon Rummel et al., (2014), la précision moyenne attendue après application d'EGM2008 est d'environ ±4 à ±6 cm dans les régions bien mesurées et d'environ ±20 à ±40 cm avec des cas extrêmes de ±1 m dans les régions peu mesurées. Le Vietnam est représentatif d'une région très peu mesurée, où des données de remplissage ont dues être utilisées lors de la réalisation du modèle EGM2008. En conséquence, sa précision est insuffisante pour se conformer aux spécifications de nivellement du quatrième ordre (une erreur de fermeture de $25\sqrt{k}$ mm sur une distance de k km) au Vietnam. Cela sera clarifié au Chapitre 4 de cette étude. Un quasigeoïde gravimétrique local du Vietnam n'a jusqu'à présent jamais été calculé. Il existe donc actuellement un fort besoin d'un modèle quasigeoïde gravimétrique à haute précision et haute résolution du Vietnam et de ses environs dans le but de moderniser le système de hauteur en utilisant GNSS au lieu du nivellement, ainsi que pour d'autres applications telles que la géologie, la géophysique, et l'océanographie. Il convient de noter que la hauteur normale est actuellement utilisée

dans le système national de hauteur du Vietnam; par conséquent, cette étude se concentre sur la détermination du quasigéoïde. Pour les applications en géologie et géophysique, le géoïde peut être déterminé en appliquant une correction au quasigéoïde.

L'écart du niveau moyen de la mer et de la surface équipotentielle du géoïde/quasigéoïde gravimétrique est assez grande. Cela conduit à des larges biais entre les systèmes de hauteur existants déterminés à partir du nivellement se référant au niveau moyen de la mer à l'échelle nationale et le géoïde/quasigeoïde estimé se référant à un système de référence global, c'est-à-dire un potentiel de gravité de référence international W_0 = 62,636,853.4 m^2/s^2. Avec un large biais, un modèle géoïde/quasigéoïde gravimétrique ne permet pas une transformation précise des hauteurs ellipsoïdales GNSS en hauteurs physiques dans le système de référence vertical local. Le plus souvent, le modèle quasigeoïde ou géoïde gravimétrique est ajusté au référentiel vertical local à l'aide de données GNSS/nivellement. Un tel modèle quasigeoïde/géoïde hybride est utilisé pour convertir les hauteurs ellipsoïdales GNSS en hauteurs physiques. Le problème avec cette méthode est que le modèle quasigeoïde/géoïde hybride n'est plus une surface équipotentielle, donc sa signification physique et ses applications dans le reste des géosciences sont limitées. Une méthode alternative pour la définition d'une référence verticale par nivellement par GNSS est d'utiliser le modèle quasigeoïde gravimétrique local pour déterminer un modèle de décalage vertical (distance entre le quasigéoïde gravimétrique et le système de référence vertical local). Cette procédure est plus réaliste parce qu'elle ne contraint pas le quasigeoïde gravimétrique local à coïncider avec le système de référence vertical local.

Actuellement, toutes les conditions pour la détermination un quasigeoïde à haute résolution à l'aide de la technique Retrait – Calcul – Restauration (Sansò & Sideris, 2013; Barzaghi, 2016) du Vietnam sont réunies grâce à:

- une nouvelle génération de modèles globaux de champ de gravité basés sur les données GOCE;
- des modèles numériques de terrain à haute résolution: SRTM3arc_v4.1 (Farr et al., 2007) sur terre et SRTM15arc_plus (Becker et al., 2009) sur mer;
- de nouvelles mesures relatives et absolues de gravité couvrant tout le pays grâce au projet «Mesure et amélioration des données de gravité nationales du Vietnam», réalisé en collaboration entre l'Institut vietnamien de géodésie et de cartographie et l'Institut de géodésie, de cartographie et d'images aériennes de Moscou, Moscou Université d'État de géodésie et de cartographie, Russie, de 2003 à 2011 (rapport final du VIGAC, 2012) complétées par des données gravimétriques issues de levés géologiques, d'exploration géophysique et de prospection minière, ainsi que par des données d'altimétrie à haute résolution permettant de déterminer les anomalies gravimétriques en mer (Andersen &

Knudsen, 2016).

- des données bien distribuées et de haute qualité issues du réseau national de stations de nivellement/GNSS exploitable pour valider le calcul de géoide, ainsi que pour déterminer le modèle de décalage pour le nivellement par GNSS à l'aide du quasigeoïde gravimétrique.

Cependant, malgré ces observations nouvelles, plusieurs limites subsistent. Des données gravimétriques sont en effet indisponibles dans les régions montagneuses du Vietnam et dans ses pays voisins. La qualité des données gravimétriques issus de levés plus anciens réalisés dans les années 1980 (levés géologiques ou géophysique de reconnaissance ou de prospection minière) rend aussi difficile la réalisation d'un quasigéoïde à haute précision sur l'ensemble du Vietnam. De plus, un projet de gravimétrie aéroportée, la méthode préférée pour combler l'écart entre les données gravimétriques sur la terre et les champs gravimétriques altimétriques marins, n'a pas encore pu être mis en œuvre au Vietnam. La précision du quasigéoïde dans les zones côtières est enfin un problème complexe à aborder et à améliorer.

Les décalages de hauteur entre les cents systèmes de référence verticale existant dans le monde aujourd'hui sont souvent inconnus pour connecter les systèmes de hauteur. La connexion des systèmes de hauteur situés sur un continent peut être effectuée par nivellement en combinaison avec des mesures de gravité, mais les systèmes de hauteur séparés par la mer ne peuvent pas être unifiés de cette manière. Même à l'échelle nationale, le système de référence vertical local du Vietnam n'est valable que pour le territoire continental mais pas pour les îles et les eaux territoriales du Vietnam. Grâce au modèle quasigéoïde à haute résolution associé au GNSS, il est possible de déterminer la hauteur de toutes les îles et d'unifier les références de hauteur pour le Vietnam. Le modèle quasigeoïde gravimétrique pourra également être utilisé en combinaison avec des données GNSS/nivellement de haute qualité (référencées au système de référence vertical local du Vietnam) pour estimer la valeur potentielle de gravité à zéro-hauteur du système de référence vertical local du Vietnam afin de connecter le système de hauteur du Vietnam à celui des pays voisins.

Concernant l'imagerie gravimétrique du Vietnam, une carte des anomalies gravimétriques de Bouguer sur le Vietnam continental a été publiée en 2011 à l'échelle 1:500,000 pour en utilisant 12,579 mesures gravimétriques par la Division Géophysique, Département Général de Géologie et Minéraux du Vietnam (Lai et al., 2012). La densité de ces données est toutefois relativement limitée. Les nouvelles données de gravité très précises issues des campagnes récentes, la nouvelle génération des modèles globaux de champ issus de la gravimétrie ou de l'altimétrie satellitaires et les modèles numériques de terrain à haute résolution ont été utilisés dans cette étude pour améliorer la précision et la résolution des cartes des anomalies de gravité du Vietnam. Une première cartographie complète des

anomalies gravimétriques (Free-air, Bouguer et Isostatique) pour l'ensemble du Vietnam (y compris la mer) a ainsi été réalisée, et les nouvelles cartes aideront certainement à améliorer la précision des applications géophysiques et géologiques au Vietnam.

L'une des applications des données gravimétriques en géophysique est de déterminer localement la profondeur du Moho sur la base du concept d'isostasie. Les premières études de la structure intérieure de la Terre partaient de ce concept, c'est-à-dire des différentes hypothèses proposées par Pratt et Airy à partir du milieu du XIXe siècle, bien avant le début des études sismiques (Kaban et al., 2004). Les modèles globaux de profondeur du Moho ont été développés à l'aide de différentes sources de données, par exemple: CRUST5.0 (Mooney et al., 1998), CRUST2.0 (Laske et al., 2000) et le plus récent CRUST1.0 (Laske et al., 2013) à une résolution de $5x5^0$, $2x2^0$ et $1x1^0$, respectivement, en utilisant principalement des données sismiques; le modèle GEMMA (Reguzzoni & Sampietro, 2014) a été calculé en inversant la grille globale des dérivées secondes radiales du potentiel gravitationnel observé par la mission ESA GOCE et en considérant la densité de la croûte telle que définie dans le modèle CRUST2.0. Le modèle GEMMA est disponible avec une résolution de $0.5x0.5^0$. Les profondeurs de Moho basées sur des données sismiques sont supposées fiables là où des données sismiques plus denses sont disponibles, comme sur l'Amérique du Nord et l'Europe. Selon Mooney et al., (1998) et Sjöberg & Bagherbandi (2017), les données sismiques sont rares dans de grandes parties de l'Afrique, de l'Amérique du Sud, de l'Asie et du Groenland ainsi que dans les zones océaniques ouvertes, où le modèle CRUST est bien moins fiable en termes de précision ainsi que de résolution, dans ces régions. Les profondeurs de Moho locales ou régionales basées sur l'inversion gravimétrique sont préférentiellement utilisées pour compléter un modèle sismique. Ces modèles globaux peuvent être utilisés comme modèle de référence dans le calcul et la validation des modèles locaux.

Des modèles de Moho isostatiques-gravimétriques ont été précédemment développées pour la partie nord et la mer du Vietnam (Bui, 1983; Dang, 2003; Braitenberg et al., 2006; Dinh, 2010; Nguyen et Nguyen, 2013; Nguyen et al., 2018) à partir de données gravimétriques issus de levés d'exploration et/ou de modèles de champs globaux. Cependant, les résultats dérivés de ces études diffèrent considérablement (Nguyen et al., 2013) à cause de plusieurs raisons telles que la précision et la résolution des données gravimétriques utilisées, l'approche utilisée dans le calcul et le manque de conditions contraintes indépendantes (données sismiques). La profondeur de Moho dans la région d'étude a également été étudiée à partir de données sismiques (Lebedev & Nolet, 2003; Wu et al., 2004; Dinh, 2010; Li & Hilst, 2010; Bai et al., 2010; Huang et al., 2009; Nguyen et al., 2013; Yu et al., 2017; Su et al., 2018). Cependant, les résolutions de ces études sont relativement faibles en raison de la faible répartition des stations sismiques ou du nombre limité de profils couvrant la région d'étude. La plupart des stations sont situées dans la

partie nord du Vietnam et il n'y a pas de mesures sur la mer. La connaissance de la structure Moho sous le Vietnam est donc encore faible. À partir du quasigeoïde gravimétrique à haute précision et haute résolution en combinaison avec les données de hauteurs dérivées du modèle numérique de terrain, une nouvelle carte de profondeur de Moho est déterminée pour l'ensemble du Vietnam sur la base de l'hypothèse isostatique locale. Une même détermination est également faite à par inversion de l'anomalie de Bouguer calculée à partir des nouvelles données gravimétriques compilées sur l'ensemble du Vietnam et des régions voisines. L'objectif de cette étude est de tester la précision de ces deux approches dans le calcul de la profondeur de Moho. La profondeur de la limite entre Lithosphère-Asthénosphère, y compris la croûte et le manteau supérieur, est également déterminée en fonction de l'approche utilisant des hauteurs du géoïde et des données de hauteur. Ces nouvelles cartes de profondeur du Moho et de la limite entre Lithosphère-Asthénosphère devraient contribuer à mieux comprendre la structure lithosphérique ainsi que les processus tectoniques et géodynamiques de cette région.

Chapter 2: THEORETICAL BASIS

Two approaches to solve the third GBVP for determination geoid/quasigeoid: Stokes' approach, classic theory, and Molodensky' approach, modern theory, are clarified. This will be the main content of this chapter. The theoretical basis and methodology required for geoid/quasigeoid determination will be presented. First, the gravitational, centrifugal, gravity, anomaly and normal potentials will be described as well as gravities and free-air gravity anomalies. The gravity reduction, Bouguer and Isostatic reduction, will be also described. Then, the fundamental equation of physical geodesy, the third GBVP, which leads to the conventional Stokes' integral formulation for determining geoid/quasigeoid is discussed. The RCR technique is a well-known method used for determining geoid/quasigeoid models as well as the methods for modifying Stokes' kernel function to solve the truncation error in calculation geoid using Stokes' formula are introduced. Moreover, the LSC method for determination of the gravimetric geoid/quasigeoid is also presented. Finally, various height systems, geometric and physical height, will be also discussed in this chapter. The procedures for height determination related and not-related to the Earth's gravity field and their physical meaning will be described.

2.1. Gravity field of the Earth

2.1.1. Gravity potential

According to Newton's law of gravitation, the Earth's gravity potential W at a point on or outside Earth's surface is the sum of the attraction potential V and the centrifugal potential Φ:

$$W = V + \Phi = G \iiint_v \frac{\rho dv}{r} + \frac{(l\omega)^2}{2} \tag{2.1}$$

where G – the Newtonian gravitational constant,

dv – an element of unit volume inside the Earth of total volume ν,

r – the distance from the mass element to a specified point,

ω – the angular velocity of the Earth,

ρ – the density of the Earth's mass,

and l – the perpendicular distance from the axis of rotation.

It can be shown that the attraction potential V satisfies Poisson's equation:

$$\nabla^2 V = -4\pi G\rho \tag{2.2}$$

where ∇^2 is called the Laplace operator. Outside the masses the density ρ is zero and V satisfies Laplace's equation

$$\nabla^2 V = 0 \tag{2.3}$$

thus, V is a harmonic function in empty space

The surfaces of W = constant are called equipotential surfaces of Earth's gravity. A specific equipotential surface very close to the MSL of the oceans is defined as the geoid. A sphere is the first-order approximation and an ellipsoid of rotation is the second-order approximation of the geoid. This ellipsoid is called the Earth' mathematical reference and its parameters define geodetic reference system.

The shape of the Earth can be approximated to an ellipsoid of revolution. The gravity potential associated with the reference ellipsoid is called the normal potential. The difference between the normal gravity field and the actual gravity field is small enough to disregard second and higher order terms. Thus it is considered linear, called disturbing potential (Heiskanen & Moritz, 1967). Hence, defining normal gravity potential makes it easy to handle the gravity potential mathematically. The Earth's gravity field is split into a normal and disturbing field as follows:

$$W = U + T \tag{2.4}$$

The disturbing potential outside of the earth satisfies Laplace's equation, which means the Laplace operator applied to T is zero, because the centrifugal potentials are cancelled and it is assumed to be a mass-free area.

The normal potential can be determined based on the reference ellipsoid whereas the disturbing potential can be estimated using gravity data for determining geopotential in height system unification. A geopotential number (C_P) is the difference between the geopotential surface of the Earth (W_0) and a geopotential surface of interest (W_P), and it can be expressed by

$$C_P = W_0 - W_P \tag{2.5}$$

In unification of height system, the determination of geopotential and/or geopotential number plays an important role. It is considered a physical component in realization of IHRF. The determination of T, U and W will be described in chapter 5.

2.1.2. Gravity

After having presented the gravity potential a new concept called gravity can be introduced. The gravity is the total force acting on a body at rest on the Earth's surface (Heiskanen & Moritz, 1967) derived from the gravitational, associated with the gravitational potential, and centrifugal, associated with centrifugal potential, forces. Moreover, the gravity vector g can be also defined as the total force that acts on a unit mass, and it can be expressed as the gradient of the gravity potential (W):

$$\bar{g} = grad\ W \tag{2.6}$$

The direction of g is the vertical known as the plumb line.

Similarly, corresponding to the normal potential is normal gravity. The normal gravity vector is perpendicular to the level ellipsoid and is denoted by γ. In analogy of equation (2.6), it is possible to establish that

$$\bar{\gamma} = grad\ U \tag{2.7}$$

According to (Moritz, 1980), γ can be expressed by the rigorous close formula of Somigliana (1929)

$$\gamma = \frac{a\,\gamma_e\,cos^2\varphi + b\,\gamma_p\,sin^2\varphi}{\sqrt{a^2cos^2\varphi + b^2sin^2\varphi}} \tag{2.8}$$

where γ_e and γ_p are the normal gravity values at the equator and poles respectively, a and

b are the semi-major and semi-minor axes of the ellipsoid respectively, and φ is the latitude of the calculating point.

From this formula, a linear formula can be derived, called approximation of Chebychev, which doesn't require a square root extraction:

$$\gamma = \gamma_e (1 + f_2 sin^2\varphi + f_4 sin^4\varphi + \cdots) \tag{2.9}$$

with $f_2 = -f + \frac{5}{2} m + \frac{1}{2} f^2 - \frac{26}{7} f m + \frac{15}{4} m^2$

$f_4 = -\frac{1}{2} f^2 + \frac{5}{2} f m$

$m = a \frac{\omega^2}{\gamma_e}$

f is ellipsoidal flattening

ω angular velocity

This linear formula is more accurate than the conventional formula below:

$$\gamma = \gamma_e (1 + f^* sin^2\varphi - \frac{1}{4} f_4 sin^2 2\varphi) \tag{2.10}$$

where $f^* = \frac{\gamma_p - \gamma_e}{\gamma_e} = f_2 + f_4$ is gravity flattening

The normal gravity above the level ellipsoid is also obtained by considering the normal gravity gradient as proposed by Bruns (Heiskanen & Moritz, 1967). Considering the ellipsoidal height h in m, in a rigorous form, the normal gravity above the level ellipsoid (γ_h) is given by:

$$\gamma_h = \gamma - \frac{2\gamma_e}{a}(1 + f + m - 2f sin^2\varphi)h + \frac{3\gamma_e}{a^2} h^2 \tag{2.11}$$

and considering a simplification given by the mean value for the normal gravity gradient, the normal gravity above the level ellipsoid is given in mGal by:

$$\gamma_h = \gamma - 0.3086h \tag{2.12}$$

where -0.3086 is the derivative of the normal gravity γ with height.

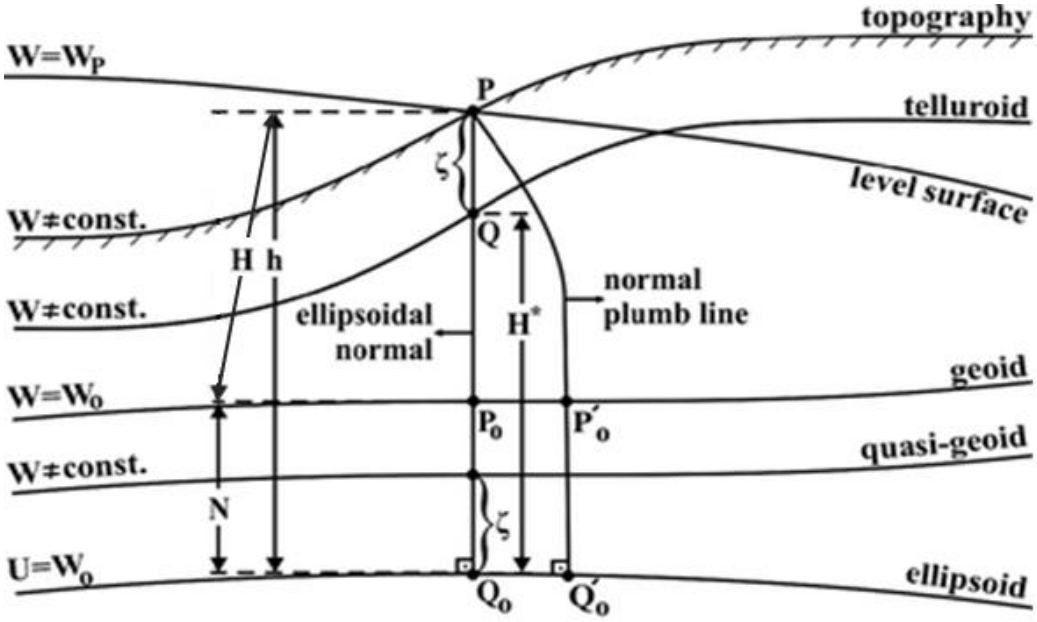

Figure 2.1. Reference surfaces for heights in the geopotential space

Free-Air anomaly (Δg_{FA}) is defined as the difference between observed gravity on the physical surface (P) and normal gravity on the telluroid ($\bar{Q}$) (Heiskanen & Moritz, 1967). The telluroid is defined as that surface where the potential of normal gravity is equal to the actual potential on the physical surface (Figure 2.1). Considering Eq. (2.12), the formula for calculating the Free-air gravity anomaly is as follows:

$$\Delta g_{FA} = g_P - \gamma_{\bar{Q}} = g_P - \gamma - 0.3086 H_P^* \tag{2.13}$$

where H_P^* is the normal height of point P on the physical surface to quasigeoid, it is also the elevation from the ellipsoid to telluroid. This will be presented at the end of this chapter.

It should also be noted that, according to classical theory of Stokes, the gravity anomaly is the difference in magnitude between the gravity at P_0 on geoid and the normal gravity at Q_0 on ellipsoid. This means that the terrestrial gravity measured on the physical surface must be up/downward continued to geoid considering the gravity effects of topographic masses. To do that, the vertical gradient (along the plumb line) of the Earth's gravity field ($\delta g/\delta H$) interior and sometimes exterior (e.g. for airborne data) to the Earth's gravitating masses is required. In practice, however, this vertical gravity gradient along the plumb line is difficult to estimate accurately, especially inside the topography. Instead, the vertical gradient of normal gravity ($\delta\gamma/\delta h$), which is used to compute the Free-air gravity anomaly (Hackney & Featherstone, 2003). In order to avoid the removal of the topographic masses, Molodensky (Molodensky et al., 1962) selected the Earth's surface, instead of the geoid. Therefore, there is no need to reduce the gravity observations from the Earth's surface down to the geoid. On the other hand, because the vertical gradient of

the Earth's gravity field is extremely difficult to determine, in geophysics, large-scale gravity effects are removed by subtracting a theoretical value of gravity from the measured value of gravity. This theoretical value is determined by correcting the value of normal gravity on the ellipsoid to the measurement level. This only requires knowledge of the mathematically defined vertical gradient of the normal gravity field ($\delta\gamma/\delta h$). The same quantity with geodetic perspective i.e., downward-continue observed gravity to the geoid is used to correct normal gravity to the level of the measurement.

2.2. Gravity reduction

The Free-air anomalies depend on the topography, because gravity itself contains the attractive effect of topographic masses. A map of Free-air anomalies shows the same small details as seen in the topographic map i.e., high degree of correlation between the Free-air gravity anomaly and elevation. By removing the effect of the topography, a so-called Bouguer gravity anomaly is obtained. The purpose of the Bouguer reduction of gravity is to completely remove of the topographical contribution outside the geoid, i.e. non-geological components, in order to represent mainly the effects of lateral density variations within the crust and Moho topography. However, the Bouguer anomalies in mountainous areas are strongly negative. This means that there is some kind of mas deficiency under the mountains (Heiskanen & Moritz, 1967). In order to compensate for this discrepancy, gravity anomalies can be balanced based on isostasy. By subtracting the effect of the isostatically compensated crust/lithosphere from free-air gravity anomaly, Isostatic anomaly is determined. The isostatic reduction is an important reduction applied for various geological and geophysical study.

2.2.1. Bouguer reduction

The Free-air anomaly grid was used to derive the complete Bouguer gravity anomaly grid by subtracting the Bouguer reduction. There are two approaches for the computation of the Bouguer reduction: the planar and spherical approach. In the planar approach, the complete Bouguer reduction can be divided into two parts: the Bouguer plate reduction and the terrain correction. In the spherical approach, presented by Bullard (1936), the gravitational attraction of the topography is divided into three parts: Bullard A (as the infinite Bouguer plate), Bullard B (the correction caused by the curvature of the Earth) and Bullard C (as the terrain correction). Bullard B reduces the infinite Bouguer plate to a spherical cap of the same thickness and a surface radius of 166.7 km (see LaFehr, (1991)). For geophysical application, the planar approximation has often been used to determine the Bouguer gravity anomalies (Kuhn et al., 2009). In this study, the planar approach is used to compute topographic reductions.

The computation of the complete Bouguer anomalies was carried out using the following formula:

$$\Delta g_B = \Delta g_{FA} - A_B + TC \tag{2.14}$$

where Δg_{FA} are the free-air anomalies, A_B is the effect of the Bouguer plate, and TC is the terrain correction. The effect of the Bouguer plate was computed for values over land using:

$$A_B = 2\pi G \rho_c H \tag{2.15}$$

Over sea, the corresponding effect was computed by:

$$A_B = 2\pi G(\rho_w - \rho_c)(-H) \tag{2.16}$$

Here, $\rho_c = 2670\ kg/m^3$ and $\rho_w = 1030\ kg/cm^3$ are the density of the crust and water, respectively, and H is the elevation of the calculation point.

Terrain corrections (TC) can be computed using the rectangular prism method. The terrain effect at P (considered the origin point) due to a rectangular prism bounded by (x_1, y_1, z_1) and (x_2, y_2, z_2) in Cartesian coordinates is given as follows (Forsberg, 1984):

$$TC = G\rho\left(x\ ln(y+r)\ + y\ ln(x+r)\ -\ z\ arctan\ \left(\frac{xy}{zr}\right)\right)|_{x_1}^{x_2}|_{y_1}^{y_2}|_{z_1}^{z_2} \tag{2.17}$$

where $r = \sqrt{x^2 + y^2 + z^2}$; x, y, z are the coordinate components (z is also elevation component) of the integration point.

ρ is the density, whose value depends on the sign of elevation (i.e. onshore/offshore grid point): $\rho = \rho_c$ if elevation>0; $\rho = \rho_c - \rho_w$ if elevation<0.

Terrain corrections can also be computed using the FFT method (Forsberg, 1984) and Gaussian quadrature (Hwang et al., 2003).

The Free-air reduction neglects the attraction of the topography between the Earth's surface and vertical datum surface. In geodesy, the Free-air reduction is effectively a condensation reduction, where all topographic masses are condensed on to the geoid. Then, the terrain correction is used as part of a condensation reduction. This condensation reduction is required to make the gravity anomaly field a harmonic function, thus permitting the solution of the GBVP by Stokes' method. Essentially, the terrain correction is applied to the Free-air gravity anomaly to yield the Faye gravity anomaly. The terrain correction is also used during the gridding and prediction of gravity data to reduce aliasing prior to computation of the geoid. In geophysics, the complete Bouguer correction comprises the Bouguer plate and the terrain correction. This correction is applied to the Free-air gravity anomaly to yield the complete Bouguer gravity anomaly. The terrain correction is used to model and remove the gravitational effects of the topography

residual to the Bouguer plate. Formula (2.14) is rewritten as follows:

$$\Delta g_B = \Delta g_{FA} - \Delta g_{Topo} \tag{2.18}$$

where $\Delta g_{Topo} = A_B - TC$ are the Bouguer reductions or the topographic reductions which include the effect of the Bouguer plate and the terrain corrections.

More recently, Balmino et al., (2012) and Hirt & Kuhn, (2012) used spherical harmonic series expansions for conversion of spherical harmonic topography models to the implied gravitational potential in spherical approach. This new approach is suitable for calculations on a global scale.

2.2.2. Isostatic reduction

There are two classical isostatic theories for such a compensation. Both were developed at almost the same by:

1) J.H. Pratt and J. F. Hayford in 1854 developed the mathematical tools for the so-called the Pratt-Hayford model. According to their hypothesis, the density of the "root" under a mountain varies with the height of the mountain, so that under the highest mountains would be the lightest material. The boundary between this light root material and the denser material of the Earth's crust is at a fixed depth.

2) G.B. Airy in 1855, and V.A. Heiskanen used it extensively and developed the mathematical form of the so-called Airy–Heiskanen model. According to Airy-Heiskanen the mass density of the "root" is constant, and the isostatic compensation is realized by varying the depth to which the root extends down into the Earth's crust. Nowadays, the results derived from seismic data indicate that the Airy-Heiskanen model corresponds better to what is really happening inside the Earth (Vermeer, 2020). Both models assume the compensation to be strictly local and that it takes place along vertical columns. This presupposes free mobility of the masses to a degree that is obviously unrealistic in this strict form. For this reason, Vening Meinesz modified the Airy floating theory in 1931 by introducing regional instead of local compensation (Heiskanen & Moritz, 1967). In this study, the Airy-Heiskanen model is used to compute the Isostatic gravity anomalies.

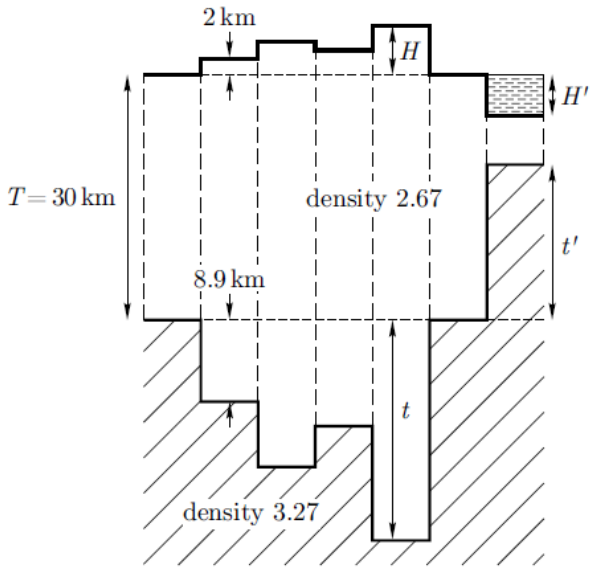

Figure 2.2. Airy-Heiskanen isostasy model (Heiskanen & Moritz, 1967)

According to the Airy-Heiskanen model the relation between the height of the topography (H) and the corresponding root (t) using the condition of floating equilibrium is as follows:

$$t\Delta\rho = H\rho_c \tag{2.19}$$

where $\Delta\rho$ is the difference between the density of crust (ρ_c) and mantle (ρ_m):

$$\Delta\rho = \rho_m - \rho_c \tag{2.20}$$

So, the thickness of root can be determined:

$$t = \frac{\rho_c}{\Delta\rho} H \tag{2.21}$$

For the oceans, the corresponding condition is:

$$t'\Delta\rho = H'(\rho_c - \rho_w) \tag{2.22}$$

where ρ_w is the density of sea water and t' is the thickness of the antiroot, so the thickness of root can be determined:

$$t' = \frac{\rho_c - \rho_w}{\Delta\rho} H' \tag{2.23}$$

From the thickness of root and antiroot, the rectangular prism method can be also used (Eq (2.17)) to compute isostatic reductions (A_C). Isostatic gravity anomalies are then determined as follows:

$$\Delta g_T = \Delta g_{FA} - A_C \tag{2.24}$$

More recently, the modern approaches are developed without using an isostasy assumption to derive the isostatic response function, i.e., local as well as regional, such as experimental isostasy (Dorman & Lewis, 1970) and mechanical behavior of the lithosphere (Poudjom Djomani et al., 1992). The experimental isostasy method directly computed the isostatic response function from gravity data while the mechanical behavior of the lithosphere was based on the coherence function between the gravity and the topography.

2.3. Geodetic Boundary Value Problem condition

The GBVP refers to the problem of determining the earth's physical surface and exterior gravity field from geodetic measurements such as gravity and potential difference (Moritz, 1980; Torge, 2001). There are three GBVPs in physical geodesy. The first of all is called Dirichlet's problem, or the first boundary-value problem: "given an arbitrary function on a surface S, to determine a function V which is harmonic either inside or outside S and which assumes on S values of the prescribed function" (Heiskanen & Moritz, 1967). The second GBVP is called Neumann's problem, or the second boundary-value problem, in which "the normal derivative $\partial V/\partial n$ is given on the surface S, instead of the function V itself" (Heiskanen & Moritz, 1967). The last GBVP is called the third boundary-value problem, in which "a linear combination of V and its normal derivative is given on S" (Heiskanen & Moritz, 1967). The third GBVP for the potential T will be solved below.

The Bruns' formula expresses the relationship between the geoid undulation (N) or height anomaly (ζ) with the disturbing potential (T) and the normal gravity (γ) (Heiskanen & Moritz, 1967):

$$N = \frac{T(P_0)}{\gamma} \tag{2.25}$$

$$\zeta = \frac{T(P)}{\gamma} \tag{2.26}$$

The relationship between gravity anomaly, disturbing potential and its first derivative is as follows:

$$\Delta g = -\frac{\partial T}{\partial n} + \frac{1}{\gamma}\frac{\partial \gamma}{\partial n}T \tag{2.27}$$

This expression is called "the fundamental equation of physical geodesy", because it relates the measured gravity anomaly Δg to the unknown anomalous potential and it can be used as a boundary condition. The solution of Eq. (2.27) gives T and then the geoid height can be obtained via Bruns formula Eq. (2.25) as well as height anomaly from Eq. (2.26). Due to the assumption that Δg is known at every point of the geoid, a linear

combination of T and $\partial T/\partial n$ is given on the geoid. Therefore, the determination of the geoid from gravity measurements can be considered as the third GBVP.

The spherical approximation of equation (2.27) is given by

$$\Delta g = -\frac{\partial T}{\partial r} - \frac{2T}{R} \tag{2.28}$$

where R is the mean radius of the Earth and r represents the radius vector of the calculating point.

2.4. Stokes' formula and Molodensky's approach

Considering the boundary condition (2.28), Stokes' formula is as follows:

$$T = \frac{R}{4\pi}\iint_{\sigma} \Delta g S(\psi) d\sigma \tag{2.29}$$

By Bruns' theorem, N = T/γ, Stokes' formula for computation geoid height is as follows:

$$N = \frac{R}{4\pi\gamma}\iint_{\sigma} \Delta g S(\psi) d\sigma \tag{2.30}$$

This formula was published by G.G. Stokes in 1949, therefore it is called Stokes' integral. It is by far the most important formula of physical geodesy because it performs to determine the geoid from gravity data. S(ψ) is known as Stokes' function.

$$S(\psi) = \frac{1}{\sin(\frac{\psi}{2})} - 6\sin\frac{\psi}{2} + 1 - 5cos\psi \ln(sin\frac{\psi}{2} + sin^2\frac{\psi}{2}) \tag{2.31}$$

Heiskanen & Moritz, (1967) provides the Stokes' function in terms of Legendre polynomials to use for zonal harmonics

$$S(\psi) = \sum_{n=2}^{\infty} \frac{2n+1}{n-1} P_n(cos\psi) \tag{2.32}$$

The Stokes' function in terms of Legendre polynomials (Eq. (2.32)) does not contain zero- and first-degree terms. Therefore, any gravimetric geoid determination computed using this Stokes' function deficient with zero- and first-degree effects. Zero-degree term represents the mass difference between the actual Earth and the reference ellipsoidal Earth. The first-degree term will only be zero if the reference ellipsoid is geocentric, the center of the ellipsoid coincides with the center of the Earth. The generalization of Stokes'

formula accounts for the effect of zero-degree term. The zero-degree term of the anomalous potential (T) at the surface of the earth is given by:

$$T_0 = \frac{G\delta M}{R} \tag{2.33}$$

where δM = M – M' is the difference between the mass M of the earth and the mass M' of the ellipsoid. The first-degree can be always assumed to be zero but the exact mass of the earth is unknown to make M' equal to M to be able to remove T_0. Thus, Eq. (2.29) is rewritten:

$$T = \frac{G\delta M}{R} + \frac{R}{4\pi}\iint_{\sigma} \Delta g S(\psi) d\sigma \tag{2.34}$$

This Stokes' formula holds for an arbitrary reference ellipsoid whose center coincides with the center of the earth.

Stokes' formula represents a global integration i.e., gravity anomalies are needed over the whole geoid. This is virtually impossible. Moreover, due to the fact that evaluating Stokes' integral world-wide is time consuming. In practice, a spherical cap with a limited radius ψ around the point of calculation is usually applied in the integration (Sansò & Sideris, 2013) and a global model is used for outer zones. However, a truncation error is introduced when the gravity data are limited within the spherical cap. Many approaches have been introduced in the last decades to solve the truncation error by modifying Stokes' kernel function such as (Molodensky et al., 1962; Witte, 1967; Wong & Gore, 1969; Meissl, 1971; Heck, 1987; Vaníček & Sjöberg, 1991 and Featherstone et al., 1998). In this research, the Wong & Gore, (1969) modification for Stokes' kernel function was used. In this modification, the removing of the low-degree Legendre polynomials is performed since they make distortions the long-wavelength signal of the geoid when integrating over a spherical cap of radius ψ_0. The modification equation as follows:

$$S_{mod}(\psi) = S(\psi) - \sum_{n=2}^{N_2} \alpha(n) \frac{2n+1}{n-1} P_n(cos\psi) \tag{2.35}$$

$$\alpha(n) = \begin{cases} 1 & for\ 2 \le n \le N_1 \\ \dfrac{N_2 - n}{N_2 - N_1} & for\ N_1 \le n \le N_2, n = 2, \dots, N \\ 0 & for\ N \ge n \ge N_2 \end{cases}$$

where $S(\psi)$ comes from equation (2.31), N_2 is the maximum degree of the Legendre polynomial or truncation degree and $\alpha(n)$ is the linear tapering coefficient. The original Stokes' kernel function is modified by setting the low harmonics (up to N_1) to zero, thus

the influence of the local data at long wavelengths is eliminated, and then linearly tapered to N_2. N_1 and N_2 are selected according to data and the GGM used in the removing step, but they should be less than or equal to degree n_{max} of the GGM. This selection will be clarified in chapter 4.

In Stokes' approach of geoid determination, gravity data must be available on the geoid surface. This involves the reduction of gravity measurements from the Earth's surface to geoid which requires the knowledge of density distribution of the topographical masses above the geoid. But usually, this information is not available and an assumption of constant density (e.g., ρ=2670 kg/m^3) is used. Therefore, this leads to some errors in the final geoid heights. Molodensky et al., (1962) has proposed solve this problem without this hypothesis. In Molodensky's approach, GBVP deals with the gravity measurements just on the Earth's surface instead of gravity measurements refer to the geoid in the Stokes' approach. Molodensky applied Stokes' boundary value problem to the Earth surface. It may be expected that height anomaly (ζ) is connected with the ground-level anomalies (Δg) by an expression analogous to Stokes' formula for the geoid height (N). This is indeed true. However, the telluroid, reference surface of the physical height where normal geopotential is equal to the actual potential on the physical surface, is not a level surface, and every point P on the Earth's surface corresponds in general a different geopotential surface $W = W_P$. Therefore, the relation between Δg and ζ in the new theory is considerably more complicated than for the geoid. The height anomalies are plotted above the ellipsoid to get a surface that is identical with the geoid over the oceans and is very close to the geoid anywhere else. This surface has been called the quasigeoid by Molodensky, however, the quasigeoid is not an equipotential surface and has no physical meaning whatever. Therefore, the normal height of a point is its elevation above the quasigeoid, as the orthometric height is its elevation above the geoid.

According to Heiskanen & Moritz, (1967) the boundary conditions for the Molodensky problem on the earth's surface is the same form as in the classic case of geoid:

$$\Delta g = g_P - \gamma_Q = -\frac{\partial T}{\partial h} + \frac{1}{\gamma}\frac{\partial \gamma}{\partial h}T \tag{2.36}$$

and the Stokes' formula can be used for Molodensky problem adding correction to ground-level free-air anomalies (Δg), the height anomaly is determined as follows:

$$\zeta = \frac{R}{4\pi\gamma}\iint_{\sigma}(\Delta g + g_1)S(\psi)d\sigma \tag{2.37}$$

where g_1 is the first term in the Molodensky expansion represents the effect of topography.

The geoidal undulation (N) can be also obtained from height anomaly calculated using Stokes' formula:

$$N = \zeta + \frac{\bar{g} - \bar{\gamma}}{\bar{\gamma}} H = \frac{R}{4\pi\gamma} \iint_{\sigma} (\Delta g + g_1) S(\psi) d\sigma + \frac{\bar{g} - \bar{\gamma}}{\bar{\gamma}} H \tag{2.38}$$

where $\bar{g}$ is the mean gravity along the plumb line between geoid and ground and $\bar{\gamma}$ is the mean normal gravity along the normal plumb line between ellipsoid and telluroid.

$\bar{g} - \bar{\gamma}$ represents the distance between the geoid and the quasigeoid. According to Heiskanen & Moritz, (1967), $\bar{g} - \bar{\gamma} \approx \Delta g_B$ is the Bouguer gravity anomaly. Hence, the geoid can be determined from modern theory of Molodensky using Stokes' formula. The advantage of this method for the determination of the geoid is that the density of the masses above sea level enters only indirectly as an effect on the orthometric height (H) through the mean gravity. Hence, the geoid height as obtained by this method is as accurate as the orthometric height.

If the RCR technique is used in the determination of the quasigeoid, this is described in the following section, with terrain effects applying in the remove procedure, the Molodensky correction g_1 term will generally be insignificant in computation the residual height anomalies (ζ_{res}) (Forsberg & Sideris, 1989; Schwarz et al., 1990).

2.5. Remove-Compute-Restore technique

The RCR technique is a well-known method for determining geoid/quasigeoid models. In practical gravimetric geoid/quasigeoid, Stokes' integral is evaluated over a spherical cap of limited radius around the computation point and a global spherical harmonic gravity model is used for outer zones. Therefore, the long-wavelength parts of the Earth's gravity field are removed from the observed gravity anomalies using a GGM before Stokes' integral is calculated. Also, terrain effects are reduced in order to obtain the smoothed gravity anomalies. The residual gravity anomalies, obtained by removing the long-wavelength components derived from GGM and the short-wavelength components calculated from DTM, are used to compute the residual height anomalies. The final height anomalies are obtained by restoring the long- and short-wavelengths components in the height anomaly sense. Hence, the RCR technique implies a spectral decomposition of the Earth's gravity field into three parts: the long-wavelength contributions from the GGM, the medium-wavelength signals from regional gravity observations and the short-wavelength parts of the gravity spectrum from the topography (Sideris & Forsberg, 1991; Sjöberg, 2005). As a result, the height anomaly can be expressed by:

$$\zeta = \zeta_{GGM} + \zeta_{RTM} + \zeta_{res} \tag{2.39}$$

where ζ_{GGM} is the long-wavelength components of height anomaly derived from GGM, ζ_{RTM} is the terrain effect computed from DTM and ζ_{res} is the residual height anomaly computed from the residual gravity anomaly using Stokes' integral or LSC method.

The height anomaly derived from GGM are given by:

$$\zeta_{GGM} = \frac{GM}{r\gamma} \sum_{n=2}^{n_{max}} \left(\frac{a}{r}\right)^n (\bar{C}_{nm} cosm\lambda + \bar{S}_{nm} sinm\lambda)\, \bar{P}_{nm}(cos\varphi) \tag{2.40}$$

with φ, λ are the spherical coordinates of the computation point.

GM and a are the geopotential constant and the semi-major axis of the reference ellipsoid.

$\bar{P}_{nm}$ is the fully normalized associated Legendre function.

$\bar{C}_{nm}$ and $\bar{S}_{nm}$ are the fully-normalized spherical harmonic coefficients

γ is the normal gravity on reference ellipsoid.

The Residual Terrain Model (RTM) technique (Forsberg, 1984) is usually used to compute the terrain effect in RCR method to avoid the short-wavelength topographic gravity field noise. Gravity anomalies reduced with the RTM are generally smoother than those resulting from other terrain reduction methods (Sansò & Sideris, 2013). The RTM reduction uses a smooth mean elevation surface to remove topographic masses above the reference surface and fill the deficits below the smooth surface (Figure 2.3). The smooth surface can be constructed by low-pass filtering of the detailed DTM to transform it into a coarse and smooth topography grid. The spatial resolution of the smoothed reference surface must be equivalent to that of the GGM used to represent the low frequencies of the gravity field. According to (Torge & Müller, 2012), the spatial resolution of the GGMs is related to their maximum degree expansion, and can be calculated according to the expression:

$$resolution_{GGM} = \frac{180^0}{n_{max}}\,(degree)\ or\ resolution_{GGM} = \frac{20.000\ km}{n_{max}}\,(km) \tag{2.41}$$

The corresponding RTM residual gravity anomaly is given by:

$$\Delta g_{RTM} = 2\pi G\rho\left(H - H_{ref}\right) - TC \tag{2.42}$$

where H_{ref} and H are the heights of the reference grid and the detailed grid, respectively

TC is the classical terrain correction

G is the universal gravitational constant

ρ is the density of the crust

The advantage of RTM method is that it only accounts for the topographic effect that has not been included in the spherical harmonic model of the gravity field of the Earth thanks to using the smoothed reference surface equivalent to that of the GGM used.

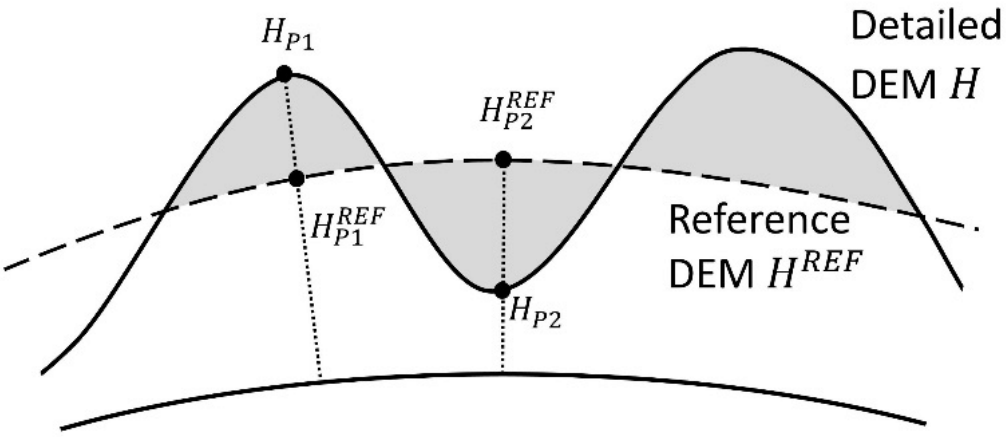

Figure 2.3. The geometry of the RTM reduction

The residual height anomalies are computed from the residual height anomalies using Stokes' formula according to Molodensky approach. The residual gravity anomalies used to determine ζ_{res} are computed in the remove procedure as follows:

$$\Delta g_{res} = \Delta g_{FA} - \Delta g_{GGM} - \Delta g_{RTM} \tag{2.43}$$

where Δg_{FA} is the Free-air gravity anomaly, Δg_{GGM} is the gravity anomaly computed with a GGM, and Δg_{RTM} is the RTM effect on the gravity anomaly.

2.6. Stokes-1D FFT method

According to Schwarz et al., (1990), the FFT technique can be used to efficiently solve the Stokes' integral given in the RCR technique. However, residual gravity anomalies must be expressed in a regular grid (Sansò & Sideris, 2013).

There are two approximations used to solve the Stokes' integral (Sansò & Sideris, 2013): the planar approximation, which is given by

$$\zeta_{res}(x_P, y_P) = \frac{1}{2\pi\gamma} \iint_E \frac{\Delta g_{res}(x, y)}{\sqrt{(x_P - x)^2 + (y_P - y)^2}} dx\, dy \tag{2.44}$$

and the spherical approximation, expressed by

$$\zeta_{res}(\varphi_P, \lambda_P) = \frac{R}{4\pi\gamma} \iint_E \Delta g_{res}(\varphi, \lambda)\, S(\varphi_P, \lambda_P, \varphi, \lambda)\, cos\varphi\, d\varphi\, d\lambda \tag{2.45}$$

The both approximations can be obtained using the FFT technique in a two-Dimensional (2D) discrete convolution integral (Schwarz et al., 1990; van Hees, 1991). Haagmans et al., (1993) proposed a new spherical approach to obtain the Stokes' integral using the FFT technique in a one-dimensional (1D) convolution integral. It does not need the simplification of Stokes' kernel and so is a much faster algorithm than the other approaches (Featherstone & Sideris, 1998). According to Haagmans et al., (1993), residual height anomaly can be expressed as:

$$\zeta_{res}(\varphi_l, \lambda_k) = \frac{R\Delta\varphi\Delta\lambda}{4\pi\gamma} F_1^{-1}\left\{\sum_{j=0}^{N-1} F_1\{\Delta g(\varphi_j, \lambda_k) cos\varphi_j\} F_1\{S(\varphi_l, \varphi_j, \lambda_k)\}\right\} \quad (2.46)$$

where F_1 and F_1^{-1} represent 1D Fourier transform operators and its inverse, respectively. In this study, the 1D-FFT technique of Haagmans et al., (1993) is used to calculate the Stokes' integral.

2.7. Least Squares Collocation (LSC) method

The determination of anomalous potential (T) is normally made from a set of linear functionals of observations e.g., Free-air gravity anomalies or height anomalies. A generalization of this linear model may be expressed as (Moritz, 1980)

$$y_i = A_i^T X + L_i(T) + e_i \quad (2.47)$$

where y_i is the i-th observation of the available dataset, L_i is any linear functional of the anomalous potential associated with y_i, e_i is the error of observations, A_i is a vector of partial derivatives and X is the vector of parameters. By using the RCR technique, the linear model of Eq. (2.47) changes to

$$y_{i,res} = A_i^T X + L_i(T_{res}) + e_i \quad (2.48)$$

where $y_{i,res}$ is the residual observation. Eq. (2.48) is the basic observation equation for LSC (Tscherning, 2015). In matrix form, it becomes

$$Y_{res} = AX + L(T_{res}) + E \quad (2.49)$$

where Y_{res} is the vector of the residual observations, L is a vector of linear functionals, and E is the vector of the observation errors.

A crucial part of the LSC procedure is the covariance modeling, in which the available observations are used to model the local or regional characteristics of the gravity field in the study area. The covariance between two observable quantities is defined as

$$cov(L_i, L_j) = C_{ij} \tag{2.50}$$

In case one of the two functionals is the evaluation of T in a point P, the covariance is indicated as

$$cov(T_P, L_i) = C_{Pi} \tag{2.51}$$

while the base covariance of T on two points P and Q is

$$cov(T_P, T_Q) = C_{PQ} \tag{2.52}$$

In this study, the Tscherning-Rapp function (Tscherning and Rapp, 1974) is used to define Eq. (2.52), and consequently Eqs. (2.51) and (2.50), written by:

$$\begin{aligned} cov(T_P, T_Q) = \alpha \sum_{n=2}^{N} \left(\frac{R_E^2}{r_P r_Q}\right)^{n+1} \sigma_n^2 P_n(cos\psi) \\ + \sum_{n=N+1}^{\infty} \left(\frac{R_B^2}{r_P r_Q}\right)^{n+1} \frac{a}{(n-1)(n-2)(n+4)} P_n(cos\psi) \end{aligned} \tag{2.53}$$

where r_P and r_Q are the radii of the Earth in points P and Q, R_E is the mean radius of the Earth, N is the maximum degree of the GGM, P_n is the Legendre polynomial of degree n, y is a spherical distance between two points P and Q, and σ_n^2 is the error degree variance of the used GGM. In this equation, the unknown variables of the covariance function are the two scale factors a and a (the former related to the GGM error, the latter to the residual signal at higher degrees), and the Bjerhammer radius R_B. These unknowns are determined by fitting this analytic covariance function with the values of an empirical covariance. The empirical covariances are determined using the following formula:

$$cov_{\Delta g_{res}}(\psi_i) = \frac{1}{N_i} \sum_{n=1}^{N_i} \Delta g_{res} \Delta g'_{res} \tag{2.54}$$

where ψ_i is the spherical distance and the products are calculated for all pairs of points (N_i), where the distance is in the interval:

$$\psi_i - \frac{\Delta\psi}{2} \leq \psi \leq \psi_i + \frac{\Delta\psi}{2} \tag{2.55}$$

where $\Delta\psi$ is the sampling interval length selected depending on the density of the gravity data.

Denoting the variance-covariance between noises e_i and e_j by s_{ij} and defining the n ³ n

covariance matrix as $C = \{\text{cov}(L_i, L_j) + s_{ij}\}$, where n is the number of observations, the least-squares estimate of X results in

$$X = (A^T C^{-1} A)^{-1} (A^T C^{-1} Y_{res}) \tag{2.56}$$

Based on the LSC procedure, T_{res} is then obtained as (Sadiq et al., 2009)

$$T_{res} = C_P^T C^{-1} (Y_{res} - A^T X) \tag{2.57}$$

where C_P is the vector of components C_{Pi}. Based on the Bruns formula, the residual height anomalies can be estimated from residual anomaly potentials. Finally, the accuracy can be assessed using the following formula (Sansò & Sideris, 2013):

$$\delta^2_{T,res} = C_{PQ} - C_P^T C^{-1} C_P \tag{2.58}$$

2.8. Height system

A height system is a "one-dimensional coordinate system used to define the metric distance of some points from a reference surface along a well-defined path" (Featherstone & Kuhn, 2006). The height systems can be classified into two principal groups: geometric height systems and physical height systems. The formers are not linked to the Earth's gravity field, but the latter are associated with this field. Fluids are attracted by the gravity force of the Earth rather than height differences. Thus, the physical height system is used for describing the flow direction of fluids. There are many forms of physical height systems, depending on the treatment of gravity and the reference surface (Featherstone & Kuhn, 2006).

2.8.1. Geometric height

The GNSS is a satellite-based navigation system included the USA's NAVSTAR Global Positioning System (GPS), Europe's GALILEO, Russia's Global'naya Navigatsionnaya Sputnikovaya Sistema (GLONASS) and China's BeiDou Navigation Satellite System. It was designed to provide positioning and timing information everywhere on the Earth. The GNSS has been used to provide high precise Cartesian coordinates with respect to a terrestrial reference frame (Torge, 2001), i.e. WGS-84. A Cartesian coordinate system (X, Y, Z) can be transformed to a geodetic coordinate system (geodetic latitude φ, geodetic longitude λ and ellipsoidal height h) by applying closed-form formulas, provided the Cartesian coordinate system origin coincides exactly with the geometric center of the ellipsoid used (W. E. Featherstone & Claessens, 2008). In the case that coincidence between the coordinate system origin and the center of the ellipsoid is not possible, other transformations methods can be applied to obtain ellipsoidal height. Ellipsoidal height differences can be achieved with cm-accuracy over distances up to some 100 km or more

applying differential methods and long observation times (e.g., 24 hours). For short distances, even sub-cm accuracy can be obtained (Torge, 2001). This accuracy of ellipsoidal height appeals to researchers with the goal of using GNSS levelling technique to substitute time-consuming geometric levelling. However, an ellipsoidal height is measured positively from the surface of the reference ellipsoid to the point of interest on the Earth' surface along the (straight) ellipsoidal normal. Thus, ellipsoidal heights are defined separately from the Earth's gravity field, hence they have no physical meaning (Featherstone et al., 1998) and that the reduction of ellipsoidal heights to normal or orthometric heights, the height systems contain physical meaning, is necessaire. The geoid/quasigeoid is often used for this procedure.

The solution of the inverse problem was given to transform from high precise Cartesian coordinate system (X, Y, Z) to geodetic coordinate system (φ, λ, h) as follows

$$h = \frac{\sqrt{X^2 + Y^2}}{cos\varphi} - N \tag{2.59}$$

$$\varphi = arctan\frac{Z}{\sqrt{X^2 + Y^2}}\left(1 - e^2\frac{N}{N + h}\right)^{-1} \tag{2.60}$$

$$\lambda = arctan\frac{Y}{X} \tag{2.61}$$

where N is radius of curvature in the prime vertical:

$$N = \frac{a}{\sqrt{1 - e^2 sin^2\varphi}} \tag{2.62}$$

φ and h are also present on the right-hand of Eqs. (2.59) and (2.60) so the equation can only be solved by iteration.

2.8.2. Physical height

Due to the non-parallelism of the level or geopotential surfaces, the sum of all the consecutive height differences in a closed loop of levelling measurements is not equal to zero even if levelling has been measured with perfect precision. Since the optical level and the rods are always aligned with the direction of the local gravity, consecutive height differences observed in different places may use slightly different vertical alignments. These variations of vertical alignments will accumulate, resulting in the misclosure of the levelling loop. Hence, the unique height cannot be provided by raw spirit levelling results. Gravity reductions have to be applied to these levelling results to provide a unique height defined in the gravity field. A simple geometrical relationship of levelling difference can be obtained, between the point of interest on the Earth (P) and its reference point on geoid

(P_0), and gravity potential difference can be given if the gravity is measured along the plumb line:

$$\int_0^H g dh = W_0 - W_P = C_P \tag{2.63}$$

where dh is the height difference at each levelling station. C_P is the geopotential number of P as Eq (2.5).

1. Orthometric height

Orthometric height is the height from the geoid to the point of interest on the Earth surface measured along the plumb line at the point. From Eqs. (2.5) and (2.63), the formula for determining the orthometric height is as follows:

$$H = \frac{C}{\bar{g}} \tag{2.64}$$

where $\bar{g}$ is the mean value of the gravity along the plumb line between the geoid (P_0) and the surface point (P). The computation of the exact value of $\bar{g}$ requires the complete knowledge of mass density of the crust. However, physically it is not possible to compute gravity along the plumb line. Therefore, a simple approximation is given to compute this value using the gravity observed at each levelling station. According to Heiskanen & Moritz, (1967) $\bar{g}$ is computed using the following formula:

$$\bar{g} = g - \left(\frac{1}{2}\frac{\partial \gamma}{\partial h} + 2\pi G\rho\right) H \tag{2.65}$$

where g is the observed gravity at each levelling station. Hence, in order to determine the orthometric height, gravity measurement needs be performed on each levelling station.

2. Normal height

In order to avoid using the approximation formula in calculation of the mean value of the gravity along the plumb line ($\bar{g}$), it is replaced by the normal gravity. It gives the normal height (H^*):

$$H^* = \frac{C}{\bar{\gamma}} \tag{2.66}$$

where $\bar{\gamma}$ is the mean normal gravity along the plump line. It is computed as follows:

$$\bar{\gamma} = \gamma\left[1 - (1 + f + m - 2f\sin^2\varphi)\frac{H^{*2}}{a} + \frac{H^{*2}}{a}\right] \tag{2.67}$$

The mean theoretical gravity itself depends on the normal height but not strongly, so that an iterative solution is very simple. The key difference between orthometric and normal height is that the latter refers to a different reference surface termed as telluroid. This difference is also the difference between height geoid and height anomaly given by Eq. (2.38). If geoid and/or quasigeoid are determined, the orthometric and normal height can be computed, the orthometric height is given as follows:

$$H = h + N \tag{2.68}$$

and the normal height is expressed by the following formula:

$$H^* = h + \zeta \tag{2.69}$$

These are the basic formulas of GNSS levelling. Normal height is currently used in the national height system of Vietnam so this study focuses on this height system as well as quasigeoid.

Chapter 3: DATA AND MAP OF GRAVITY ANOMALIES

In this chapter, all data used for the thesis project i.e., terrestrial gravity data, GGMs, DTMs, altimetry satellites model and GNSS/levelling data, will be described. The gravity anomaly derived from GGMs and DTMs is used to fill-in data where the terrestrial gravity is not available. Moreover, they are also used in the RCR technique to compute the gravimetric quasigeoid. For the best result, one must determine and use the optimal GGM and DTM.

The terrestrial gravity data are presented in detail. A preprocessing procedure must first be applied to clean up the gross errors in the gravity data. Using these cleaned gravity data, a complex procedure follows, which combines the heterogeneous gravity data i.e., the terrestrial gravity and fill-in data, and a map of Free-air gravity anomalies is then determined for the study region. The Bouguer and Isostatic reductions are computed and applied to Free-air gravity anomalies to obtain the Bouguer and Isostatic gravity anomalies maps. These are the first complete (Free-air, Bouguer and Isostatic) grids and maps of gravity anomalies for Vietnam. Finally, the validation is done by comparing with a global map e.g., WGM2012. The discussions on applicability of these gravity anomalies grids and maps will be also detailed.

The GNSS/levelling data are needed to validate the estimated gravimetric quasigeoid and to determine the vertical offset model for GNSS levelling technique using gravimetric quasigeoid. The GNSS/levelling data are also presented in this chapter.

3.1. Data and pre-processing

3.1.1. Global Gravity field Model

To calculate the gravimetric quasigeoid, gravity anomaly data are reduced for the long and medium wavelengths, using GGMs, and the terrain effect, using DTMs, in order for the residual gravity anomalies to be smooth before gridding or prediction. The GGM has to best represent the gravity anomalies and height anomalies in the selected area. GGMs, enhanced with RTM effects, are also used to generate fill-in data where gravity measurements are not available. The GGMs are available on the ICGEM website (see http://icgem.gfz-potsdam.de/home).

The high resolution EGM2008 model, developed up to degree/order (d/o) 2190, has well-known errors due to datum inconsistencies and variability of the measurement density and accuracy (Gilardoni and al. 2013), in the low-medium frequency band, and because it is a pre-GOCE model. In Gilardoni et al. (2013), the geoid model accuracy was improved by combining spherical harmonic coefficients of the EGM2008 model with a GOCE gravity model. Following previous studies that successfully used mixed GOCE and EGM2008 models for the removal of the long and medium wavelengths to compute geoids/quasigeoids of Malaysia (Jamil et al., 2017), Nepal (Forsberg, Olesen, Einarsson, et al., 2014) and the Philippines (Forsberg, Olesen, Gatchalian, et al., 2014), a combined model is constructed to remove the long to medium wavelength components of the gravity field up to d/o 719. The fifth release of GOCE the global potential model obtained from the direct approach, named GOCE DIR-R5 (Bruinsma et al., 2014), is used for this combination, called the mixed DIR/EGM model. The blending was done in the following way:

- Degrees 2-260: GOCE DIR-R5
- Degrees 270-2190: EGM2008
- Degrees 260-270 are computed by weighted mean of the two models with the weights determined as the inverse of degree variances as follows (Gilardoni & al, 2013):

$$T_{mn} = \left[\frac{T_{mn}^{E}}{\left(\sigma_{T_{mn}}^{2}\right)^{E}} + \frac{T_{mn}^{D}}{\left(\sigma_{T_{mn}}^{2}\right)^{D}} \right] \left[\frac{1}{\left(\sigma_{T_{mn}}^{2}\right)^{E}} + \frac{1}{\left(\sigma_{T_{mn}}^{2}\right)^{D}} \right]^{-1} \tag{3.1}$$

where T_{mn}^{E} and $\left(\sigma_{T_{mn}}^{2}\right)^{E}$ are the coefficients and degree variances, respectively, derived from EGM2008. T_{mn}^{D} and $\left(\sigma_{T_{mn}}^{2}\right)^{D}$ are the coefficients and degree variances, respectively, derived from GOCE DIR-R5.

All recent GGMs, such as GOCO05s (Mayer-Guerr, 2015), GOCE TIM-R5 (Brockmann et al., 2014) and GOCE SPW-R5 (Gatti et al., 2016), were tested in this study, in steps of 10 degrees, to determine the best GGM and its optimum maximum degree in combination

with EGM2008. Figure 3.1 indicates the STD of the differences between the GOCE GGMs in combination with EGM2008 (up to d/o 2190) and the GNSS/levelling data, described in Section 3.1.4. It can be seen that thanks to the GOCE, STD of GGMs significantly improves (from 0.29 m down to 0.16 m). The GOCE DIR-R5 at d/o 260 plus EGM2008 is the best model with the smallest STD of 0.16 m. The results of the differences between the GGMs and the GNSS/levelling data are shown in appendix 1. Moreover, the EIGEN-6C4 model (Förste et al. 2014), computed from the combination of LAGEOS (LAser GEOdynamics Satellite), GRACE, GOCE and a reconstruction of EGM2008 beyond d/o 235, was also tested. The combination model described above best reproduces the gravity data. In particular, the Experimental Gravity Field Model XGM2016 (Pail et al., 2018), computed with improved terrestrial data especially over continental areas such as South America, Africa, parts of Asia, and Antarctica, up to the same d/o 719, was also used to compute quasigeoid for this region but the result was slightly worse than when using the mixed DIR/EGM model.

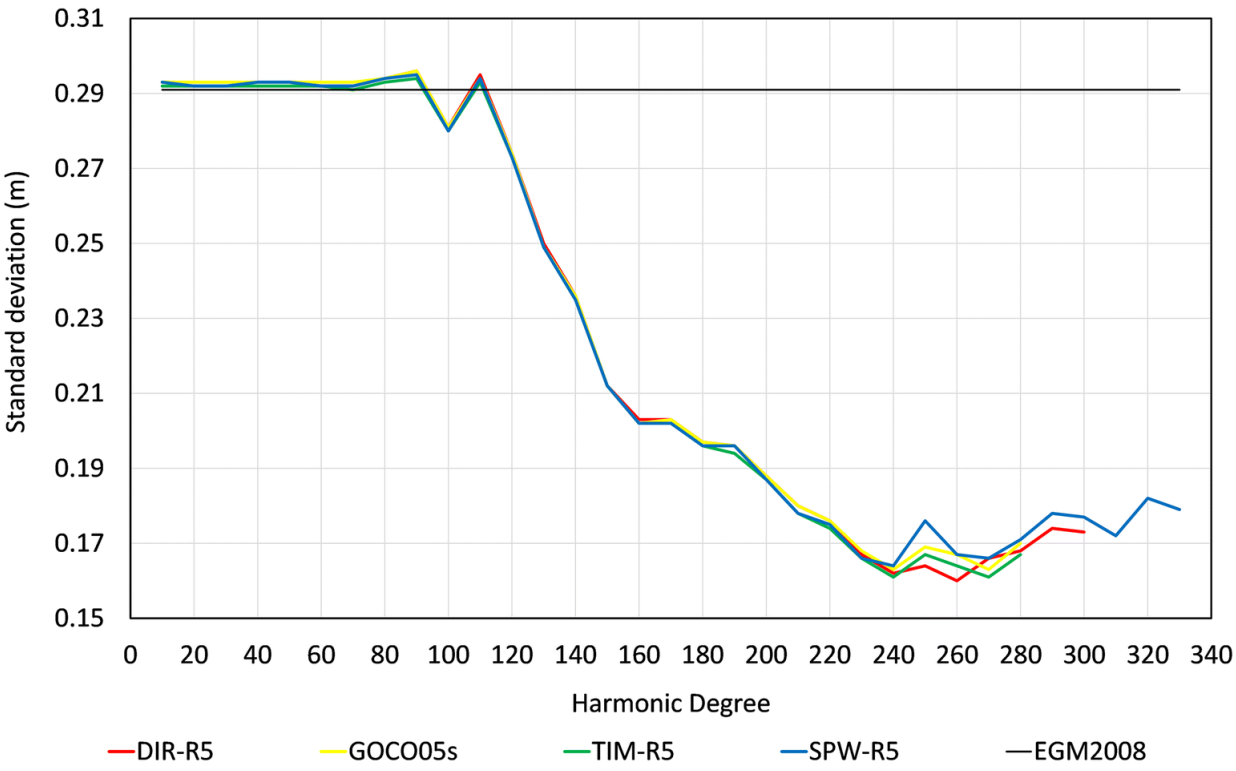

Figure 3.1. Standard deviation of the differences between the GOCE GGMs in combination with EGM2008 and the GNSS/levelling data

3.1.2. Digital Terrain Model

The DTM provides information on the short wavelengths of the gravity field. RTM was selected to calculate the terrain effects, and the smoothing effect on gravity data can reach 50% if elevations are accurate (Forsberg, 1984). The RTM effect is also used to enhance fill-in data on land through addition to the gravity field derived from GGMs. Finally,

elevation data from the DTM in combination with the geoid heights are also used to determine the lithospheric structure. The detailed DTM in this study over land areas is the 90-m resolution SRTM3arc_v4.1 (Farr et al., 2007). The 15" resolution Digital Bathymetry Model (DBM) SRTM15arc_plus (Becker et al., 2009) was used over sea, and after re-gridding to 3'' it was merged with SRTM3arc_v4.1 using the full-resolution coastline in Generic Mapping Tools (GMT) (Wessel & Smith, 1998); the result is called the mixed SRTM model. Several DTMs, such as Earth2012 (Hirt, 2013), DTM2006 (Pavlis et al., 2012) and ETOPO1 (Amante & Eakins, 2009), were also evaluated on land, but the best model is SRTM3arc_v4.1 (the STD of residual gravity anomalies using this model is the smallest, as will be shown in the next section). To avoid the need to distinguish between different density values (mass density of water (ρ_w) and mass density of rock (ρ_r)), the Rock-Equivalent Topography (RET) approach (Balmino et al. 1973; Balmino et al. 2012) is used.

3.1.3. Gravity measurements and fill-in data

For the purpose of determining the quasigeoid and the lithospheric structure beneath Vietnam, a compilation of all gravity data available from the Institute of Geophysics (IGP), Vietnam Academy of Science and Technology (VAST), the VIGAC, and the BGI has been performed. The total number of gravity points is 31,102. Distribution of land gravity data is shown in Figure 3.2. IGP conducted surveys between 1961 and 1984 for the purpose of geological survey, exploration geophysics and mineral prospecting when positioning was of poor quality, especially for heights, which were determined using barometers (19,267 green points in Figure 3.2). As errors in the elevation will propagate into the computed gravity anomaly, gross-error detection methods were first applied to clean up the IGP data (see below). Fortunately, most of the country has been re-surveyed from 2003 to 2011, through the project ±Measurement and Improvement of Vietnam National Gravity Data±, carried out in collaboration with the Moscow Institute of Geodesy, Cartography and Aerial Images, MIIGAiK, Russia. This new dataset comprises 10,940 points, including an absolute gravity network of 11 base reference stations with an accuracy of better than ° 5 mGal and their tie points, 29 1st order gravity stations with an accuracy of better than ° 15 mGal and their tie points and 92 3rd order gravity points and more than 10,000 detailed points measured from 2005 to 2009 (red points in Figure 3.2). The base reference stations and 1st order gravity network were determined from absolute measurements using GBL instrument (Final Report of VIGAC 2012). For the VIGAC gravity surveys, GNSS has been used to determine coordinates and heights, so this is less prone to positioning errors. The IGP data is less accurate than the VIGAC data. However, the combination of the IGP and VIGAC data enhances the coverage considerably, especially in the South of Vietnam. Finally, the land gravity data set was also complemented by a set of gravity data provided by BGI for Vietnam and surrounding areas (895 points in Vietnam, 229 points in Cambodia and 351 points in Thailand).

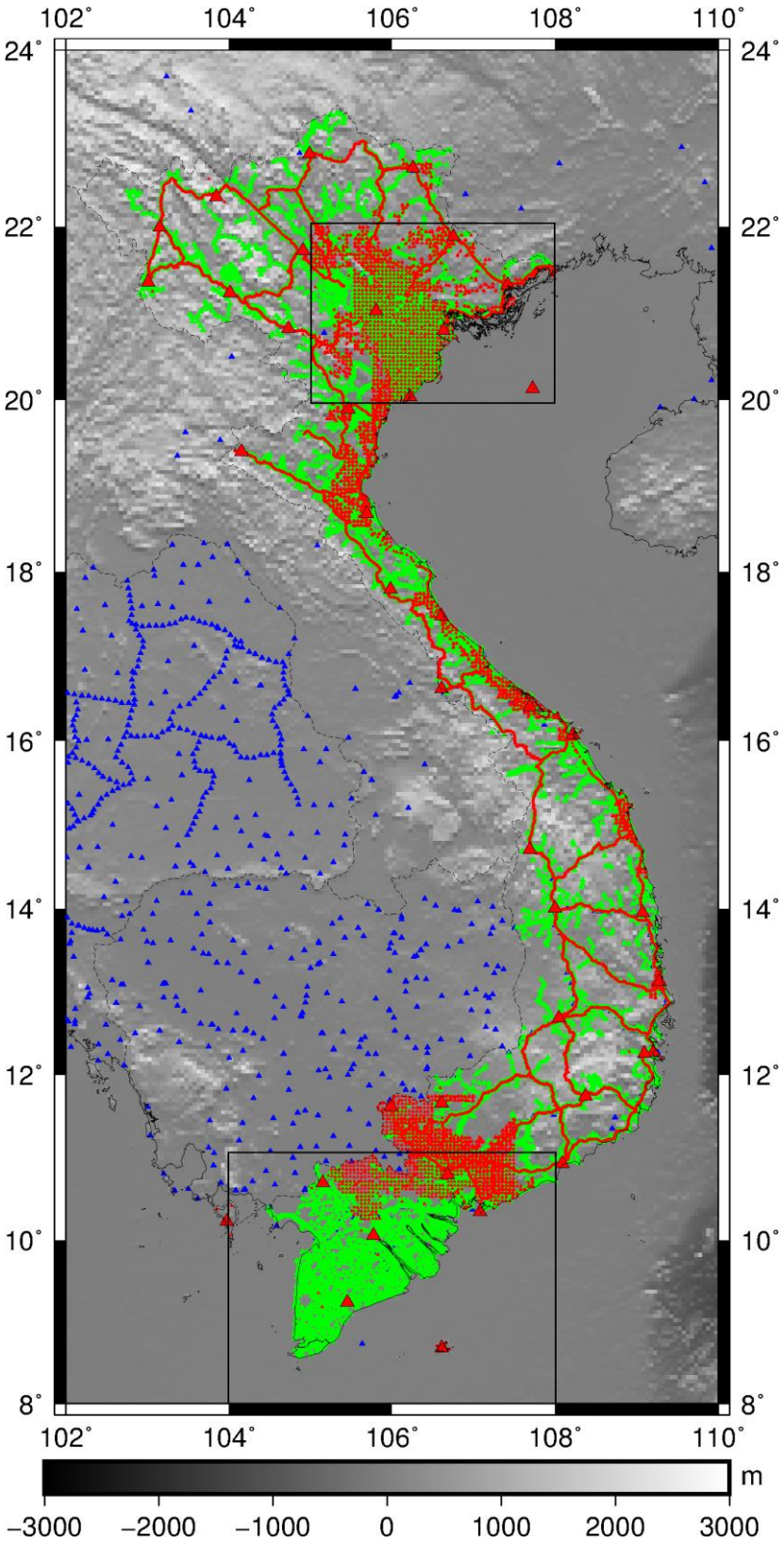

Figure 3.2. Distribution of land gravity data used in this study: red dots are the VIGAC relative measurements, green dots are the IGP relative measurements and blue dots are obtained from the BGI database. The VIGAC absolute gravity measurements are indicated by red triangles

Two procedures were used to detect localized gross errors in the gravity data. The first uses SRTM3arc data to verify the gravity observation elevations in the IGP data. The results are listed in Table 3.1. For the purpose of evaluating the accuracy of the DTM, the good quality of heights at GNSS/levelling points are used to compare with these derived from SRTM3arc. The differences at GNSS/levelling points show a STD of 6.86 m and an average bias of -3.13 m, which are in line with results of Denker (2005) for Germany. The VIGAC data show a STD of 23.46 m and average bias of -4.23 m, while SRTM3arc has a reported vertical accuracy of better than 16 m (Farr et al., 2007). This proves that SRTM provides very good height information. The differences of the gravity observation elevations in the IGP data with SRTM3arc are 73.50 m in STD and -14.95 m in mean bias. This indicates that the elevations in the IGP data, which were determined from barometric levelling, have gross errors. A horizontal error in gravity data will also result in a discrepancy between the gravity observation elevations in the IGP data and those derived from DTM, especially in areas of steep elevation changes; consequently, a different procedure is needed to better detect gross errors in the IGP data.

Table 3.1. Statistics of the differences between the observation elevations and the SRTM3arc model [Unit: (m)]

Data	Mean	STD	Min	Max
GNSS/levelling (812 points)	-3.13	6.86	-50.13	32.94
VIGAC data (10,940 points)	-4.23	23.46	-403.20	434.95
IGP data (all: 19,267 points)	-14.95	73.50	-789.00	715.46
Rejected points of IGP data (1,960 points)	-57.97	171.68	-782.32	715.46
Accepted points of IGP data (17,307 points)	-10.08	49.42	-789.00	491.80

The second procedure involves comparisons with the GOCE DIR-R5 model. To reduce the effect of the omission error in the GGM, GOCE DIR-R5 augmented with high-resolution RTM effects beyond its selected resolution (degree 260) has been used. The RTM effects were computed using the GRAVSOFT TC program (Forsberg & Tscherning, 2008) with a radius of 20 km for the detailed DTM, and 200 km for the coarse grid. Thus, three models are needed to calculate the RTM effects with the TC program: the detailed (the mixed SRTM model), coarse, and reference DTMs in which the reference height grid was estimated by low pass filtering the detailed DTM in order to represent the topographic signal above the maximum degree of the GGM used (Forsberg, 1984) i.e., degree 260 in this case. The coarse and reference DTM models were created as follows:

- The coarse grid is computed by simple averaging (e.g., 3'×3' grid) of the detailed DTM model using the GRAVSOFT SELECT program.

- The coarse grid (3'×3') is then filtered with a moving average operator to the required resolution using the GRAVSOFT TCGRID program; in this case, the required resolution is

d/o 261.

The 3" resolution DTM is equivalent to a spherical harmonic expansion to d/o 216000. Therefore, the reduction of gravity data has been evaluated in the following way:

$$\Delta g_{res} = \Delta g_{FA} - \Delta g_{DIR5}|_{2}^{260} - \Delta g_{RTM}|_{261}^{216000} \quad (3.2)$$

The results are given in Table 3.2. The differences of VIGAC data show a STD of 9.1 mGal and average bias of -0.6 mGal, whereas IGP data show a STD of 19.1 mGal and average bias of 4.5 mGal. This again indicates that the IGP gravity dataset contains gross errors. Aiming for IGP data with the same precision as the VIGAC gravity data (i.e., 9.1 mGal in STD), and assuming a normal distribution, IGP data for which differences are greater than three STD of the VIGAC data (i.e., 27.3 mGal) were eliminated. There are 1,960 points greater than this threshold, which were rejected. Table 3.1 indicates that the differences in elevation of these points (compared to SRTM) have a STD of 171.68 m and average bias of -57.97 m, while the 17,307 accepted points have a STD of 49.42 m. There is still a big difference in the IGP cleaned data due to horizontal errors as indicated above.

To confirm that these gross errors in IGP gravity anomaly are due to elevation errors, the tests were done using different subsets of the gravity points according to an elevation threshold (100 m). The results of these tests are also given in Table 3.2. The higher elevation points in the IGP data increase by 12 mGal the average bias and by 9 mGal the STD, while VIGAC results change by less than 2 mGal. For the lower altitude points, the accuracy of VIGAC and IGP data is 8.4 and 9.5 mGal, respectively. This proves that there is a small effect of elevation in VIGAC data, whereas it is large in IGP data. After editing the IGP dataset, they are at the same level as the VIGAC data (about 9 mGal in STD when comparing with GOCE DIR-R5 together with RTM effect).

Table 3.2. Statistics of the differences between the observed gravity anomalies and the GGM GOCE DIR-R5 [Unit: (mGal)]

Data	Mean	STD	Max	Min
VIGAC-(GOCE DIR-R5+RTM) (10,940 points)	-0.7	9.1	158.4	-62.7
IGP-(GOCE DIR-R5+RTM) (19,267 points)	4.5	19.1	153.4	-54.8
VIGAC-(GOCE DIR-R5+RTM) (H<100m) (6,980 points)	-0.1	8.4	158.4	-35.6
IGP-(GOCE DIR-R5+RTM) (H<100m) (13,497 points)	-0.6	9.5	121.8	-54.8
VIGAC-(GOCE DIR-R5+RTM) (H>100m) (3,960 points)	-1.6	10.1	105.6	-62.7
IGP-(GOCE DIR-R5+RTM) (H>100m) (5,770 points)	16.4	28.4	153.4	-39.0
IGP cleaned - (GOCE DIR-R5+RTM) (17,307 points)	0	8.9	27.3	-27.1
All data (VIGAC cleaned, IGP cleaned, BGI) – GOCE DIR-R5 (29,121 points)	-12.0	21.7	125.6	-154.5
All data (VIGAC cleaned, IGP cleaned, BGI) – (GOCE DIR-R5+RTM) (29,121 points)	-0.3	9.0	158.4	-62.7

As with the IGP data, 21 gravity points of VIGAC data were detected with large differences and were excluded from the computation. Thus, a total of 1981 points was eliminated. After cleaning, the difference between the observed gravity anomalies with GOCE DIR-R5 (d/o = 260) together with RTM effects is -0.3 mGal on average and 9.0 mGal STD, whereas with only GOCE DIR-R5 (d/o=260) it is -12.0 mGal and 21.7 mGal, respectively. This result clearly shows that the terrain effect is the most important parameter to consider in order to enhance the consistency of available terrestrial gravimetric data and GGMs and to produce a unified database. The RTM data succeed largely in filling the spectral gap between land gravity measurements and GGMs. Figure 3.3a also indicates the presence of a height-correlated bias in the data, but this bias in residual anomaly is significantly reduced by taking RTM effects into account (Figure 3.3b).

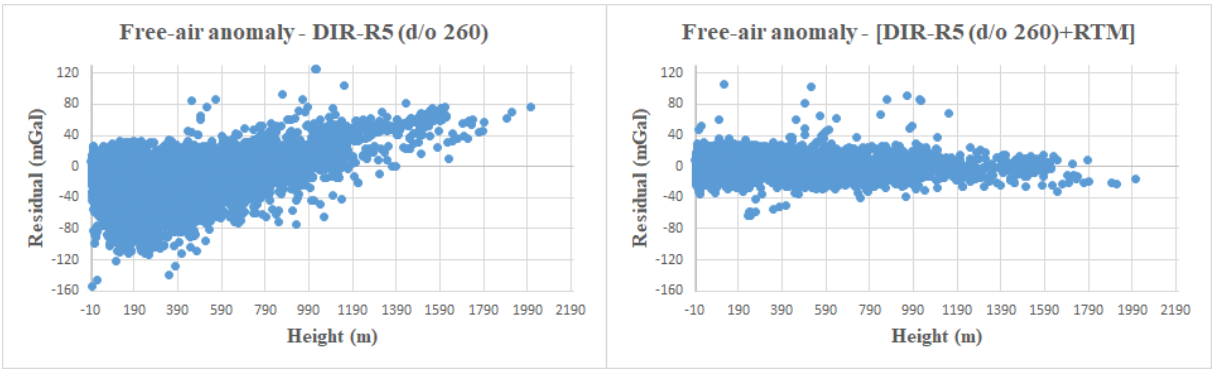

(a) (b)

Figure 3.3. Differences between measurements with a) GOCE DIR-R5 and b) GOCE DIR-R5+RTM

The mixed DIR/EGM model up to d/o 2159 together with topographic effects was used to fill-in data on land. The fill-in data have been evaluated following a spectral enhancement approach as:

$$\Delta g^{\text{fill-in}} = \Delta g_{\text{DIR/EGM}}|_{2}^{2159} + \Delta g_{\text{RTM}}|_{2160}^{216000} \tag{3.3}$$

The use of the mixed DIR/EGM model instead of GOCE DIR-R5 only in combination with RTM effect is because of EGM2008, which performs better than RTM effect within the spectral window 260-2159 in Vietnam. This issue will be further clarified in the next section.

The DTU15 gravity field model (Andersen & Knudsen, 2016) was used for marine areas. Altimetric gravity is of good quality over the open seas. However, coastal zones remain problematic because most altimeters cannot measure up to the coast (Hirt, 2013). Airborne (Forsberg & Olesen, 2010) or shipborne (Featherstone, 2010) gravimetry is used preferentially to close the gap between gravity data on land and marine altimetric gravity fields if it is available. These observations are not available for Vietnam's coastal

zones, so the accuracy of the quasigeoid there is a difficult problem. DTM and DBM provide information on the short wavelengths of the gravity field in coastal zones and can be used to augment and improve global gravity fields (Hirt, 2013). In this study, the RTM effects together with GGM are used in coastal zones instead of using the altimetric gravity field. This significantly improves the accuracy of the quasigeoid.

3.1.4. GNSS/Levelling data

In the past, the Vietnam height system was divided into two different parts and the 17th parallel was the provisional demarcation line; North Vietnam used the MSL at Hon Dau tide gauge station and in South Vietnam the Ha Tien tide gauge was used (Pham, 2009). After the war, the height system was calculated uniformly for the entire country. From 2001-2003, the Vietnam national levelling network has been re-measured, and then it was readjusted in 2007 using the MSL over 1950 - 2005 at the Hon Dau tide gauge station (Pham, 2009). From 2009 – 2010, the Vietnam Department of Surveying and Mapping (VDSM) carried out GNSS observations on the levelling points. The GNSS baselines were observed using dual-frequency instruments in static mode with a minimum measurement time of 6 hours per session. The GNSS data were processed with the Bernese software to obtain ellipsoidal heights referred to the WGS84 ellipsoid. A total number of 812 GNSS/levelling observations was used in this study (see station location on Figure 3.4). The GNSS/levelling points are relatively well distributed over the entire country. GNSS/Levelling data include horizontal coordinates (latitude, longitude) and the computed height anomalies.

Of the 812 GNSS/levelling points, 428 points are 1st and 2nd order (yellow triangles) and 384 points are 3rd order (purple circles) of the national levelling networks. 1st, 2nd and 3rd order levelling in Vietnam allows misclosure of $5\sqrt{k}$, $12\sqrt{k}$ and $25\sqrt{k}$ mm over a distance of k km, respectively. Normal height is currently used in the national height system of Vietnam. Figure 3.4 shows that gravity measurements of VIGAC (black dots) have been made alongside the 1st and 2nd order levelling.

The GNSS/levelling geometric height anomalies were compared with those derived from the GOCE DIR-R5 or the mixed DIR/EGM model together with RTM effects. The RTM effect is used as augmentation of GGMs beyond their selected resolution as:

$$\Delta\zeta = \zeta^{\text{GNSS/levelling}} - \zeta_{\text{DIR5}}\big|_{2}^{260} - \zeta_{\text{RTM}}\big|_{261}^{216000} \tag{3.4}$$

$$\Delta\zeta = \zeta^{\text{GNSS/levelling}} - \zeta_{\text{DIR/EGM}}\big|_{2}^{2159} - \zeta_{\text{RTM}}\big|_{2160}^{216000} \tag{3.5}$$

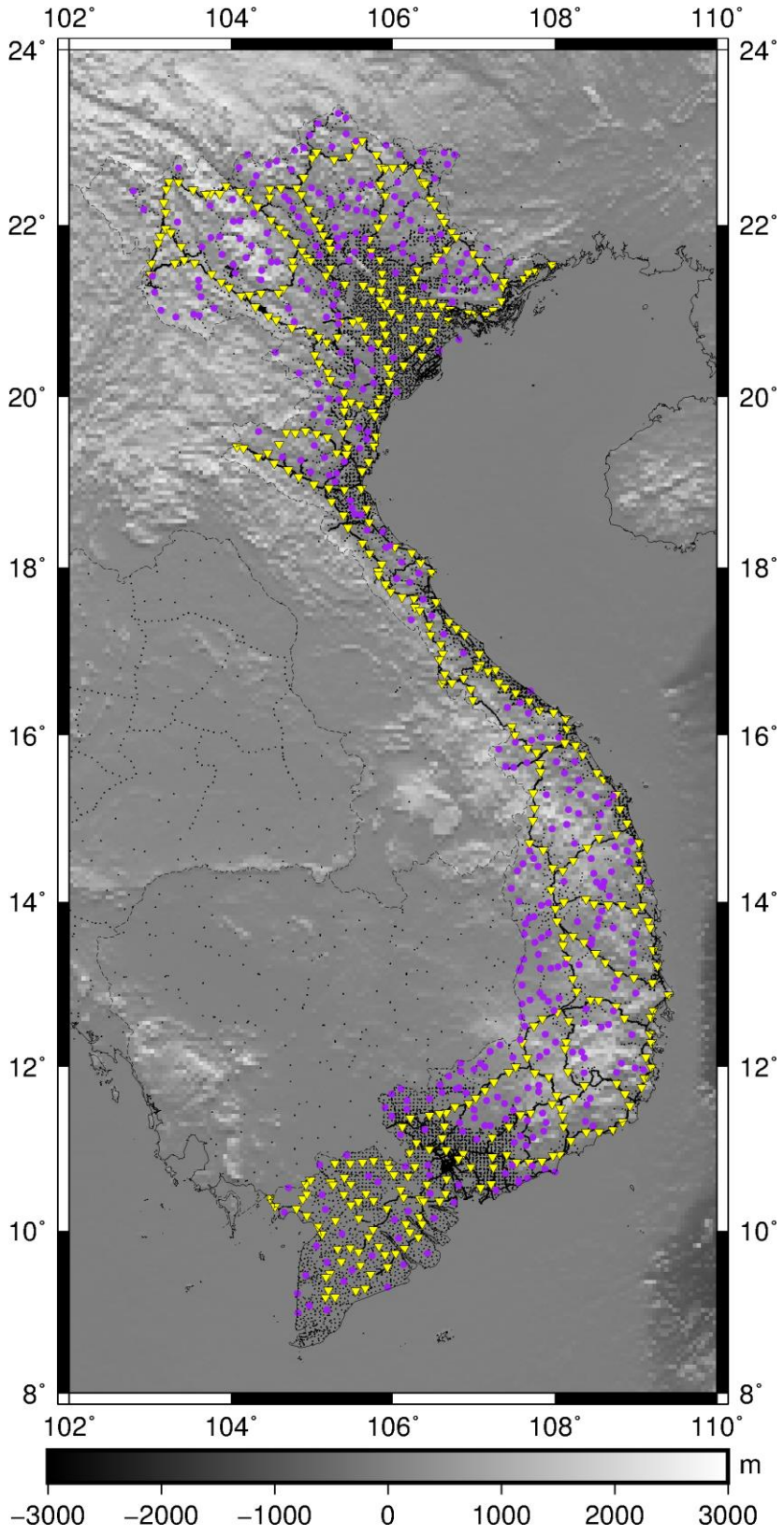

Figure 3.4. GNSS/levelling data: yellow dots are 1st and 2nd order of the national levelling networks, whereas purple dots are 3rd order

The results are listed in Table 3.3. These results clearly show significant improvement (2.7 cm in STD) when using the mixed DIR/EGM instead of using GOCE DIR-R5 only in

combination with RTM effects. This demonstrates that EGM2008 performs better than RTM effects computed with TC program within the spectral window d/o 260-2159 in Vietnam, even if fill-in data were used. It should be noted that the zero-degree term is not included in this evaluation.

Table 3.3. Statistics of the differences between the GNSS/levelling points and the GGM [Unit: (m)]

GGMs	d/o of GGM	Mean	STD	Max	Min
DIR-R5	260	0.455	0.235	1.281	-0.305
DIR-R5+RTM	260	0.543	0.184	1.138	-0.155
DIR/EGM+RTM	2159	0.515	0.157	1.018	-0.103

3.2. Map of gravity anomalies

3.2.1. Map of Free-air gravity anomalies

The cleaned terrestrial gravity data together with the fill-in data (the mixed DIR/EGM model up to d/o 2159 plus RTM effect over land and the DTU15 gravity field model over open sea) are used to determine the Free-air gravity anomalies. The resolution of the terrestrial gravity data plus the fill-in data over land is equivalent to d/o 216000 (3" resolution DTM), and the gravity anomaly field deduced from the DTU15 altimetry satellites model is at 1' resolution in the marine domain. A 1×1' map of gravity anomalies is determined for the study region. The heterogeneous gravity data, i.e., measured gravity data and fill-in data, are merged in a complex procedure described below:

- A 1x1' grid is interpolated with the GRAVSOFT GEOGRID program using the LSC method on the gravity anomaly measurements. Then, only grid nodes lying within 5' radius circles centered on each of the terrestrial gravity points were kept;
- The grid nodes lying 50 km and more beyond the 5' radius circles were filled in with the mixed DIR/EGM model together with RTM effect over land (green points in Figure 3.5) and with DTU15 over sea (blue points in Figure 3.5). The full-resolution GMT coastline was used to determine marine and land regions.
- The transition areas between observations and fill-in models (land transitions starting at the 5' radius circles to 50 km beyond, coastal transitions starting at the coastline to 50 km on sea) were filled using a combination of data and models.

  From measurement points, the differences between observations and fill-in data were calculated in the following way:

$$\Delta g_{dif} = \Delta g_{FA} - \Delta g_{DIR/EGM}|_{2}^{2159} - \Delta g_{RTM}|_{2160}^{216000} \quad (3.6)$$

  The differences in the fill-in grids (beyond 50 km from the 5' radius circles) were set to zero. The LSC method in GEOGRID program was then used to interpolate

these differences to the transition points (Δg_{dif}^{grid}). Gravity anomalies of transition points were then constructed by adding Δg_{dif}^{grid} to the fill-in data of transition points as follows:

$$\Delta g_{trans}^{grid} = \Delta \mathrm{g}_{\mathrm{DIR/EGM}}|_{2}^{2159} + \Delta \mathrm{g}_{\mathrm{RTM}}|_{2160}^{216000} + \Delta g_{dif}^{grid} \tag{3.7}$$

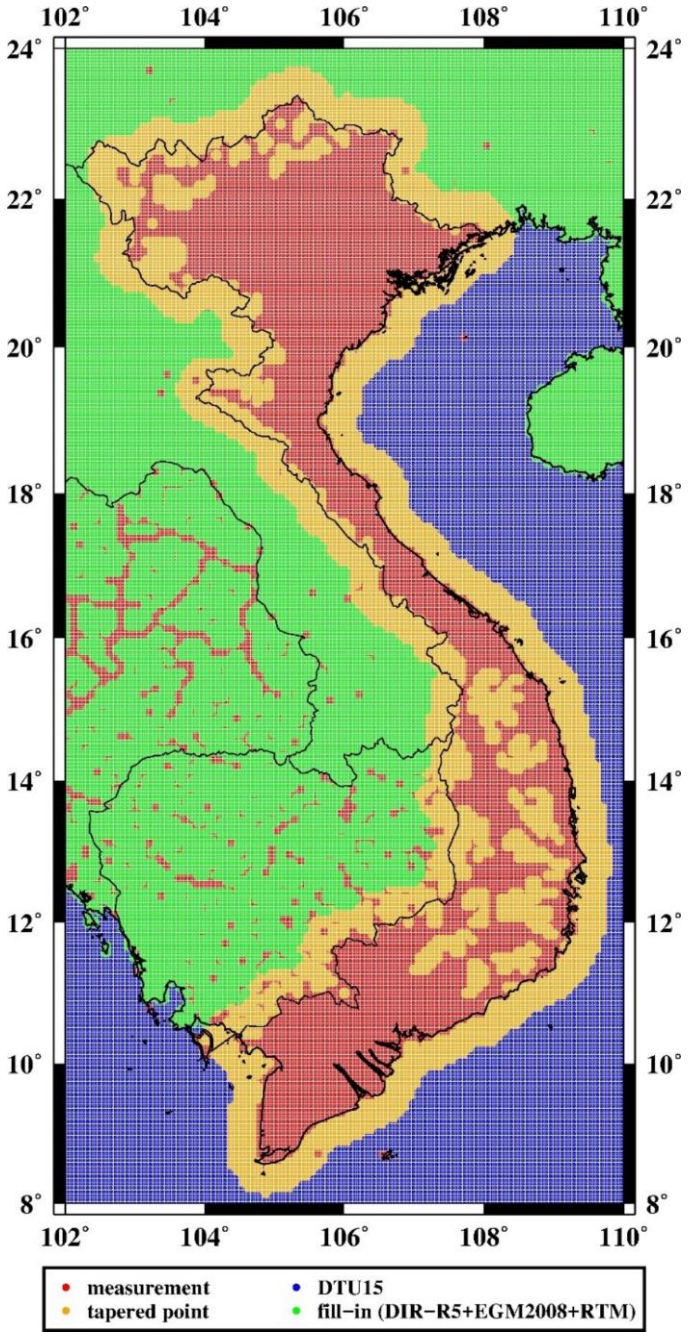

Figure 3.5. Geographical display of the combination of the gravity data: red dots are from land gravity points, orange dots are tapered transition points from fill-in data on land or on the sea to land gravity data, green dots are fill-in points on land and blue dots are DTU15 marine gravity points

The grid of Free-air gravity anomalies is shown in Figure 3.6a. They vary from -213.0 to

175.8 mGal with mean and STD of -12.8 and 26.9 mGal, respectively. Large negative values, -150 to -200 mGal, are seen in the northwestern region. The short wavelengths of the Free-air gravity anomalies correlate strongly with topography. This map of Free-air anomalies shows the same small details as seen in the topographic map (Figure 3.4). In order to see the contribution of terrestrial gravity data in the new grid, the Free-air gravity anomalies derived from the WGM2012 (Bonvalot et al., 2012) and EIGEN-6C4 global models are also shown in Figures 3.6b and 3.6c. Statistics of this grid in the study region are listed in Table 3.4.

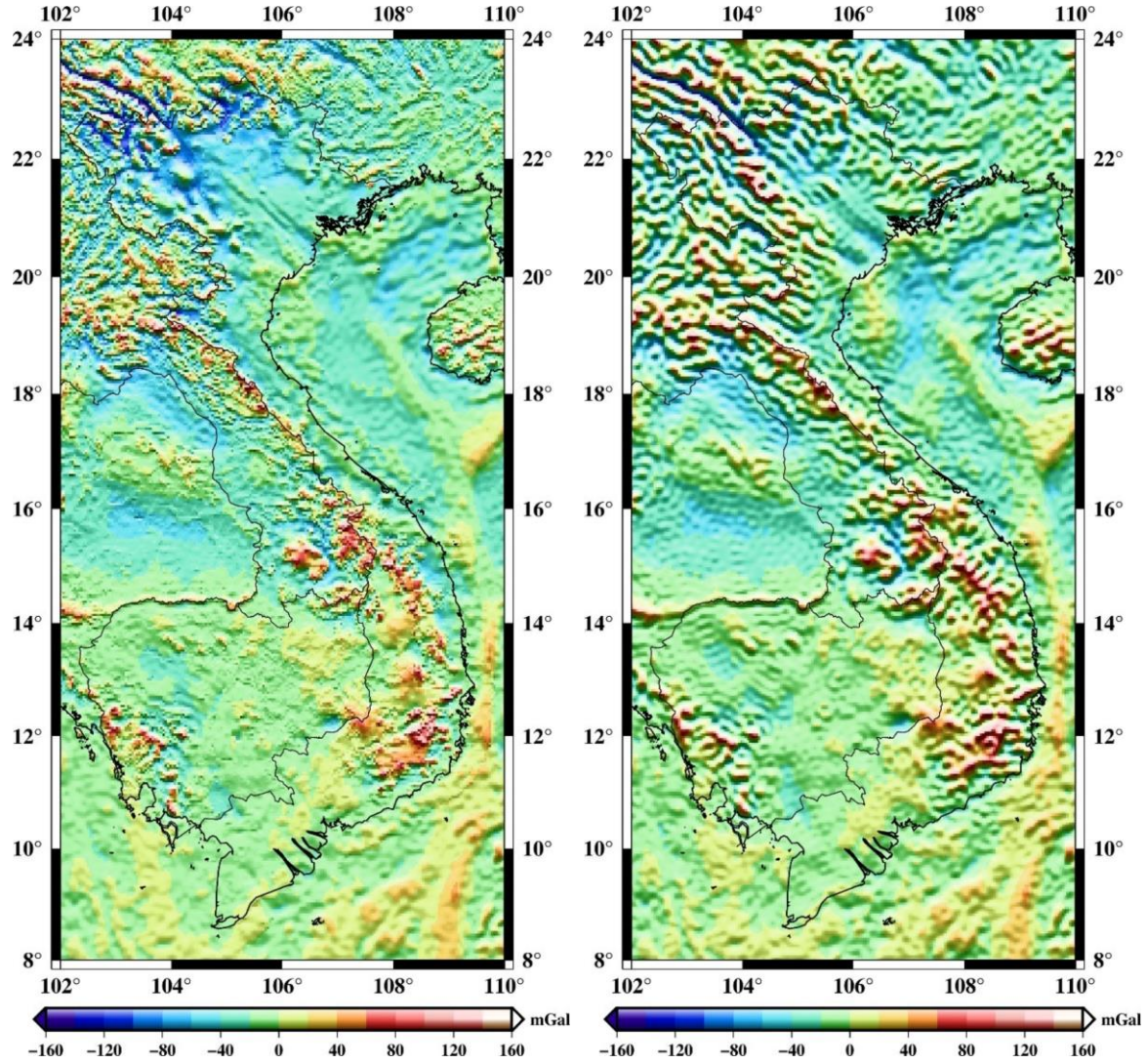

(a) (b)

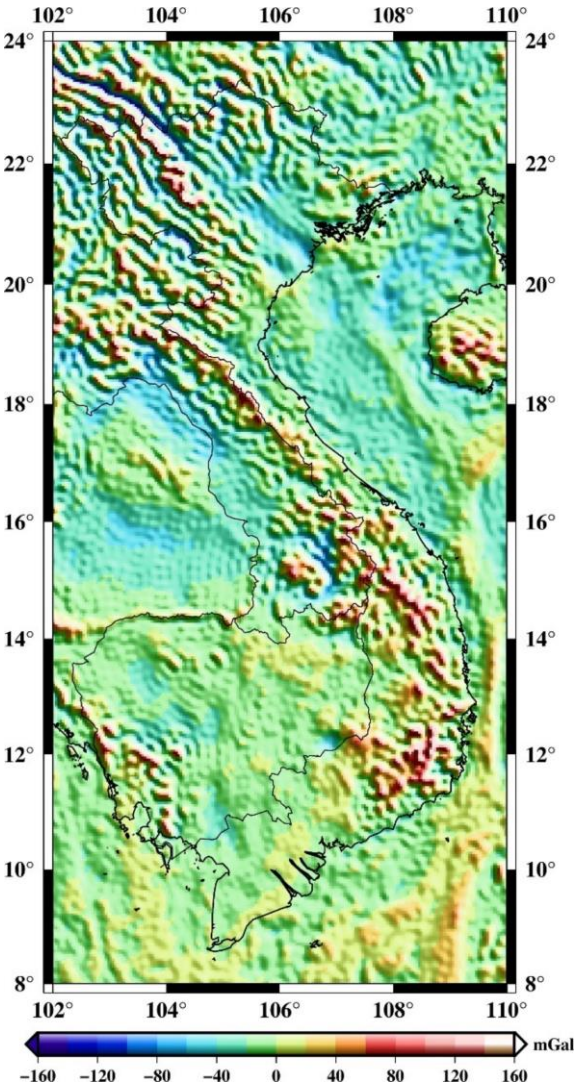

(c)

Figure 3.6. Map of Free-air gravity anomalies from: a) new grid, b) EIGEN-6C4 global model and c) WGM2012 global model

Table 3.4. Statistics of the gravity anomalies and their reductions

	Min	**Max**	**Mean**	**STD**
Δg_{FA} (Free-air anomaly)	-213.0	175.8	-12.8	26.9
A_B (effect of the Bouguer plate)	-161.6	328.1	27.0	49.9
TC (terrain correction)	0	48.4	1.8	3.0
Δg_B (complete Bouguer anomaly)	-377.6	166.7	-38.0	49.5
A_C (Isostatic reduction)	-129.0	188.2	3.1	21.8
Δg_I (Isostatic anomaly)	-274.7	99.0	-15.9	21.2
Differences Δg_{FA} and EGM2008	-247.5	81.4	-4.0	16.6
Differences Δg_{FA} and EIGEN-6C4	-243.1	81.4	-4.0	15.8

The Free-air gravity anomalies derived from high resolution global models e.g., EGM2008 and EIGEN-6C4 are used to compare with the new gravity anomalies. Statistics of the

comparisons are listed in Table 3.4. The differences between the new Free-air anomalies with EGM2008 are 16.6 and -4.0 mGal in STD and mean bias, respectively, while with EIGEN-6C4 are 15.8 and -4.0 mGal. The EIGEN-6C4 is a little more accurate than EGM2008 thanks to the assimilated GOCE data.

3.2.2. Bouguer reduction and map of Bouguer gravity anomalies

The mixed SRTM model was used to compute topographic reductions (TC and A_B). Terrain corrections were calculated within a radius of 20 km for inner zone using the detailed DTM grid at 3" and 200 km for outer zone using the coarse DTM grid at 3'. Constant values for crustal density (ρ_c) of 2670 kg/m^3 and for sea water (ρ_w) of 1030 kg/m^3 were used. The estimated terrain corrections vary from 0 to 48.6 mGal. Large terrain corrections, at the 20–30 mGal level, are in the northwest region. The Bouguer plate corrections were also computed using the elevation derived from the mixed SRTM model. The estimated Bouguer plate corrections vary from -161.6 to 328.1 mGal. Large Bouguer plate corrections, at the 200–300 mGal level, are also in the northwest region. Finally, the Bouguer gravity anomalies are obtained by subtracting the Bouguer plate and adding the terrain corrections to the Free-air anomalies. The Bouguer plate corrections, the terrain effects and the Bouguer gravity anomalies are shown in Figures 3.7a, 3.7b and 3.7c, respectively, and their statistics are given in Table 3.4. The Bouguer gravity anomalies vary from -377.6 to 166.7 mGal with mean and STD of -38.0 and 49.5 mGal, respectively. A southeast-northwest trend is visible in Figure 3.7c with large negative anomalies up to 150-200 mGal in the northwest.

The Free-air anomalies depend on the topography, because gravity itself contains the attractive effect of topographic masses. A map of Free-air anomalies shows the same small details as seen in the topographic map. By removing the effect of the topography, a so-called Bouguer gravity anomaly is obtained. The purpose of the Bouguer reduction of gravity is to completely remove of the topographical contribution outside the geoid, i.e. non-geological components, in order to represent mainly the effects of lateral density variations within the crust and Moho topography. However, the Bouguer anomalies in mountainous areas are strongly negative. This means that there is some kind of mas deficiency under the mountains (Heiskanen & Moritz, 1967). In order to compensate for this discrepancy, gravity anomalies can be balanced based on isostasy. By subtracting the effect of the isostatically compensated crust/lithosphere from free-air gravity anomaly, Isostatic anomaly is determined. The isostatic reduction is an important reduction applied for various geological and geophysical study.

Figure 3.7c shows that, even if the standard deviation of the Free-air anomalies is smaller, the Bouguer gravity anomalies are smoother. For this reason, the Bouguer anomalies are suited especially for the interpolation and prediction of gravity anomalies (Featherstone

& Kirby, 2000). However, the Free-air anomalies vary randomly closer to zero than Bouguer anomalies (mean value of Free-air anomalies is -12.8 mGal whereas this of Bouguer anomalies is -38.0 mGal). As mentioned in Section 2.2, this is due to the Bouguer anomalies are strongly negative, especially in the mountains. The lowest values of complete Bouguer gravity anomalies occur in the mountainous region of northwest and central Vietnam. The isostatic concept will be used to get more balanced gravity anomalies. This is presented in the following section.

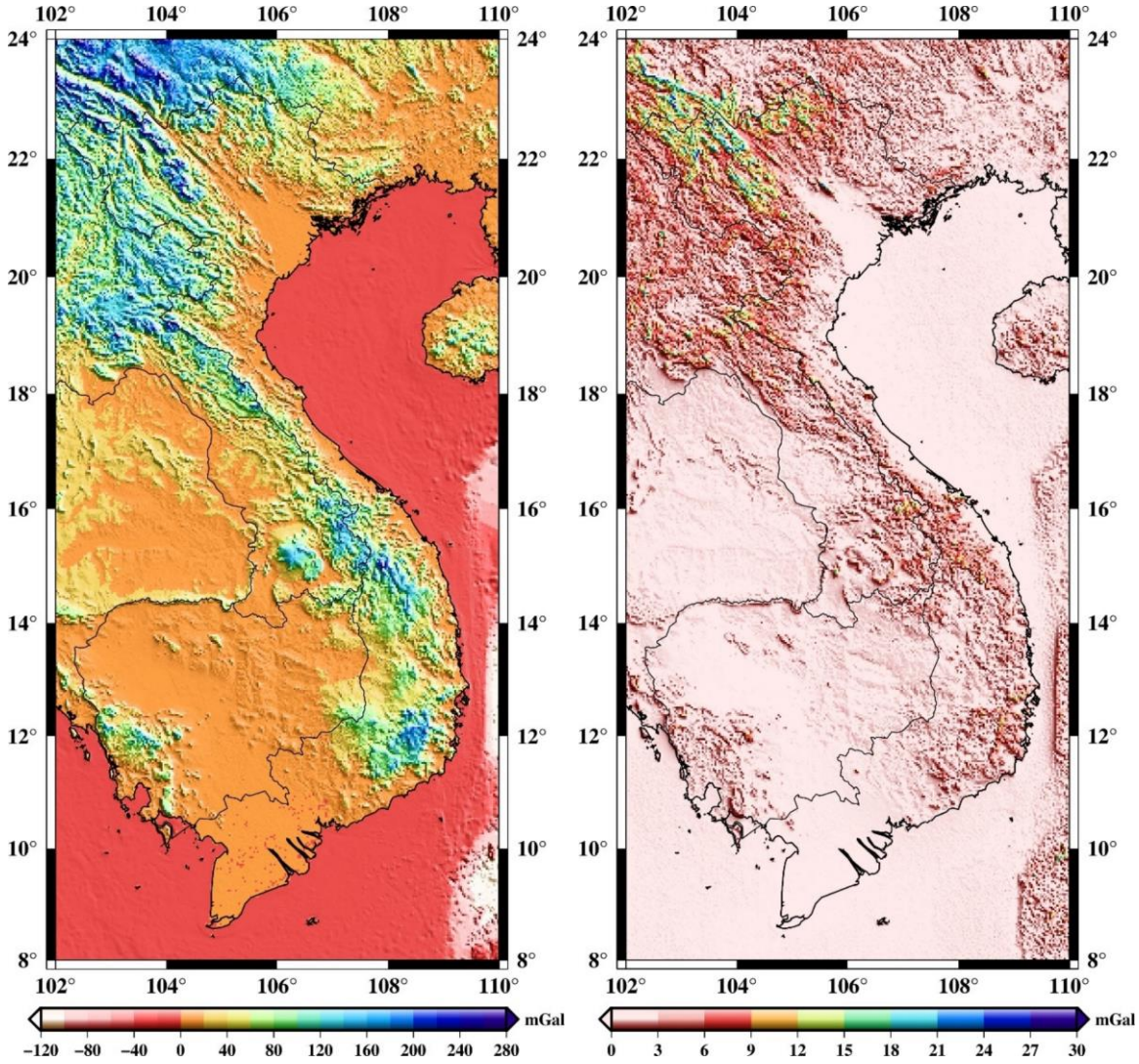

(a) (b)

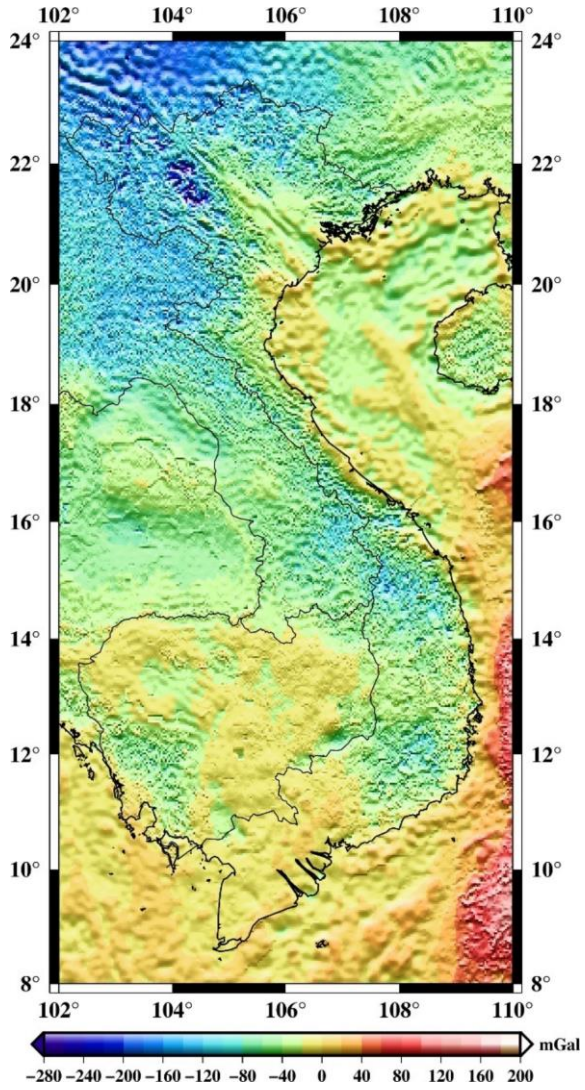

(c)

Figure 3.7. a) Bouguer plate, b) Terrain corrections and c) Complete Bouguer gravity anomalies

3.2.3. Isostatic reduction and map of Isostatic gravity anomalies

Isostatic reductions (A_C) were computed using Airy-Heiskanen model to derive the Isostatic gravity anomalies. A constant density contrast of 507 kg/m^3 and average Moho depth of 28.5 km (these selections will be explained in the determination of Moho depth in Chapter 6) were used in the estimation of A_C. The Isostatic reductions vary from -129.0 to 188.2 mGal with mean bias and STD of 3.1 and 21.8 mGal, respectively. The largest values of Isostatic reductions occur in the mountainous region of northwest and central Vietnam. The Isostatic gravity anomalies are then determined by subtracting Isostatic reductions from the Free-air gravity anomalies. The Isostatic reductions and Isostatic Airy-Heiskanen gravity anomalies are shown in Figures 3.8a and 3.8b, respectively. Statistics of these results were listed in Table 3.4.

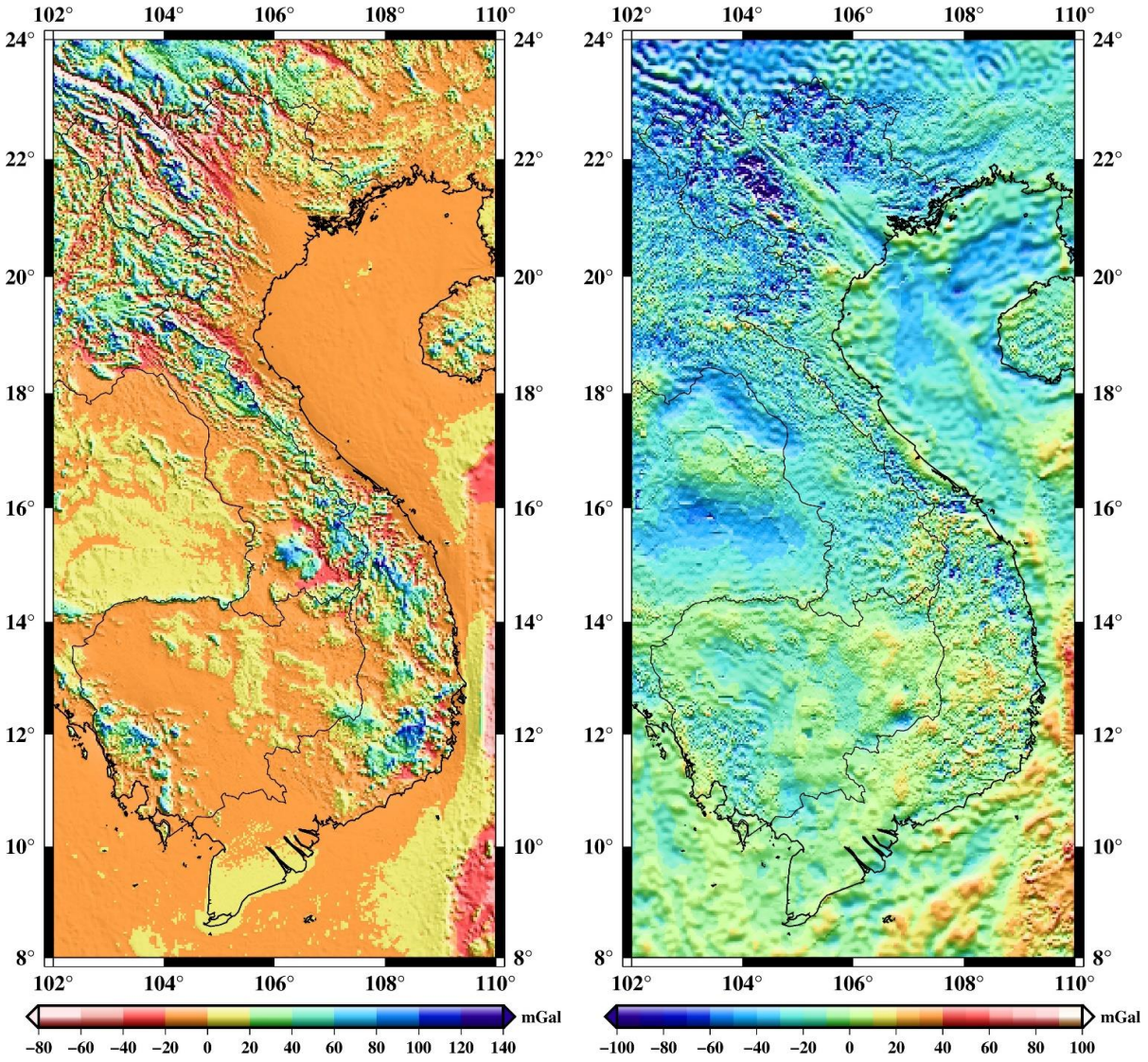

(a) (b)

Figure 3.8. a) Isostatic Airy-Heiskanen reductions and b) Isostatic Airy-Heiskanen gravity anomalies

The Isostatic Airy-Heiskanen gravity anomalies vary from -274.0 to 99.0 mGal with mean bias and STD of -15.9 and 21.2 mGal, respectively. Large negative of the Isostatic anomalies can be seen in the northwest but only about 100 mGal in magnitude while with Bouguer anomalies, it is about 200 mGal. By removing as many as possible "superficial" effects from the gravity field i.e., removing both the topography and its isostatic compensation, the gravity field is only affected by the Earth's remaining deep layers. This is a useful tool for geophysical studies. After applying topographic-isostatic reduction to Free-air anomalies, the Isostatic anomalies obtained are very smooth. Moreover, the magnitude of Isostatic anomalies is smaller and smoother than Bouguer and Free-air gravity anomalies (STD of Isostatic anomalies is 21.2 mGal whereas of Bouguer and Free-air anomalies are 49.5 and 26.9 mGal, respectively), and unlike the Bouguer gravity anomalies, the Isostatic gravity anomalies are closer to zero (mean bias of Isostatic

anomalies is -15.9 mGal with Bouguer anomalies it is -38.0 mGal). However, as the topographic masses are always closer to the point of observation than the compensating roots, their combined effect on observed gravity anomalies is non-zero (in this case, mean bias is -15.9 mGal), even in the case of a complete isostatic balance (Kaban et al., 2004). Moreover, the Isostatic anomalies are also affected by all heterogeneities within the Earth which are not accounted for in the Airy-Heiskanen as well as Pratt-Hayford isostatic model, for example the isostatic anomalies might contain an effect of sedimentary layers. This is an issue that needs to be investigated to improve the homogeneity of Isostatic anomalies in this region. However, the isostatic reductions applied largely compensate for the mass deficiency under mountains and the Isostatic anomaly field is much more homogeneous than the Bouguer anomaly. This is the advantage of the Isostatic gravity anomaly. This anomaly plays an important in geological and geophysical applications.

3.3. Validation of the gravity anomaly map

These are the first complete grids and maps, i.e., Free-air, Bouguer and Isostatic gravity anomaly at 1' resolution, for the whole of Vietnam and its surrounding region including the sea of Vietnam. The gravity anomalies from global WGM2012 map at 2' resolution (Bonvalot et al., 2012) were used to validate these new gravity anomaly grids. The new grids were re-gridded to 2' to compared with those derived from the WGM2012. The differences are listed in Table 3.5 and shown in Figure 3.9.

Table 3.5. Statistics of the differences between the new grids and the WGM2012 model [unit: mGal]

	Min	**Max**	**Mean**	**STD**
Differences Δg_{FA} and WGM2012	-246.4	81.3	-3.9	16.6
Differences Δg_{FA} and WGM2012+RTM	-318.3	139.3	-2.5	15.6
Differences Δg_{B} and WGM2012	-353.3	-11.5	-127.3	16.1
Differences Δg_{I} and WGM2012	-225.7	84.6	-4.3	18.0

Figure 3.9a shows the differences between the Free-air anomalies derived from the new grid and those derived from the WGM2012. The results of comparison in the Free-air gravity anomalies show that the EGM2008 and WGM2012 are identical, 16.6 and -3.9 mGal in STD and mean bias, respectively. This is expected because the grid of Free-air gravity anomalies of WGM2012 was calculated using EGM2008. The differences vary from -246.4 to 81.3 mGal. Large differences at 70-100 mGal level in magnitude occur in the northwest and central mountainous region. This is considered since the fill-in data used in the EGM2008 while the terrestrial gravity data significantly improved the new grid. The mean bias of -3.9 mGal between the new Free-air anomaly grid and WGM2012 is due to the omission error in WGM2012, because EGM2008 was only developed up to d/o 2190. To make this point clear, the resolution of WGM2012 was increased by adding RTM effects

(beyond d/o 2190 up to 216000, equivalent of 3” resolution DTM); the average value of the differences decreased to 2.5 mGal and the STD decreased to 15.6 mGal. The mean value of the differences between the new grids and the WGM2012 gravity anomalies is -127.3 and -4.3 mGal for Bouguer and Isostatic anomalies, respectively. It appears that the Bouguer anomalies are largely shifted, which is considered to come from terrain reductions. The differences between the new grid and the WGM2012 gravity anomalies after removing the large shift in Bouguer anomalies are shown in Figure 3.9b. There is a slight difference of STD and mean bias in the results of the comparison in Free-air and Isostatic anomaly. It should be noted that the Isostatic reduction is computed with a constant density contrast of 507 kg/m^3 and average Moho depth of 28.5 km in this study while in the WGM2012 used a constant density contrast of 600 kg/m^3 and average Moho depth of 30 km. This explained for the differences in the STD and mean terms of Isostatic and Free-air anomaly, with Isostatic anomaly are 18.0 and -4.3 mGal, respectively, while with Free-air are slight lower 16.6 and -3.9 mGal, respectively.

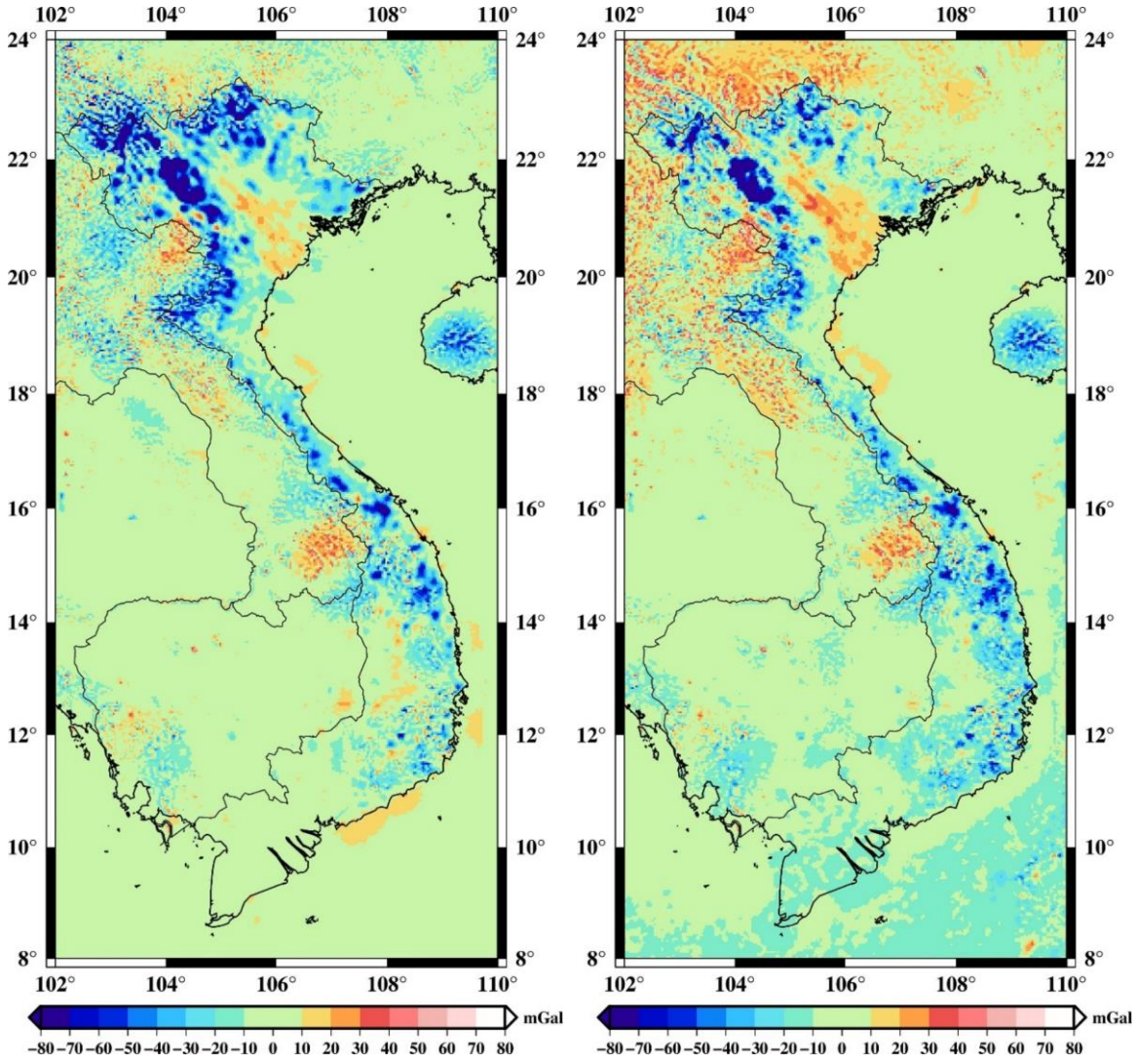

(a) (b)

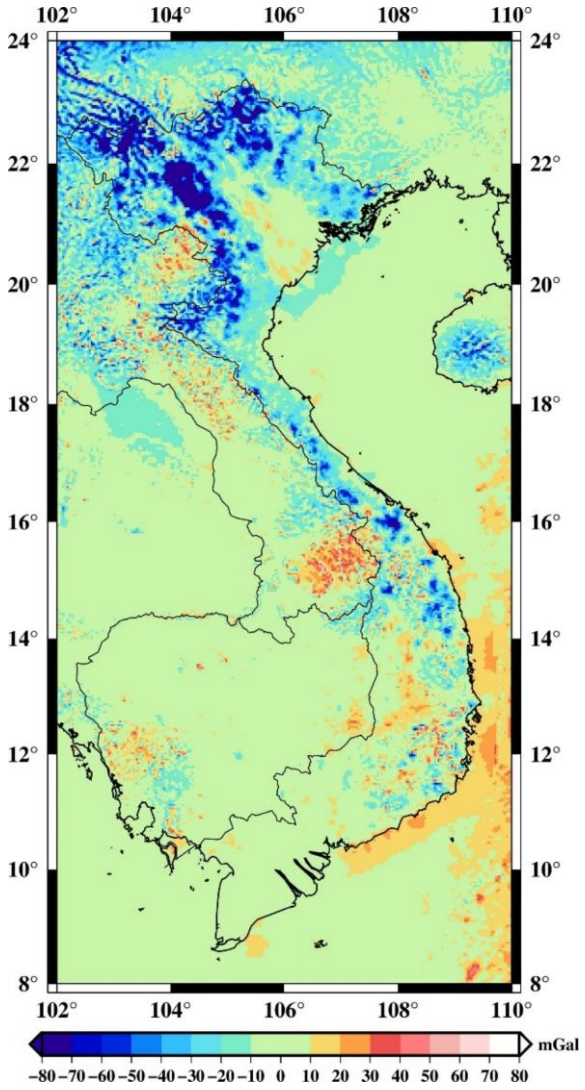

(c)

Figure 3.9. Differences between new gravity anomaly maps with WGM2012: a) Free-air, b) complete Bouguer after subtraction of 123.4 mGal and c) Isostatic Airy-Heiskanen gravity anomalies

Figure 3.9c shows the differences between the new grid and the WGM2012 in the Isostatic gravity anomalies. Figures 3.9a, 3.9b and 3.9c indicate significant improvement in the Bouguer and Isostatic anomalies of the new grids in the area where the topographic relief is very rugged e.g., the mountainous regions in the northwest and the sea ridges in the southeast. This is thanks to using the DTM up to 3" resolution to compute the topographic reduction. This issue will be clarified next.

WGM2012 used the 1×1' resolution ETOPO1 (Amante & Eakins, 2009) for computation of terrain effects, whereas the mixed SRTM model at 3" resolution was used in this study. Again, while the classical integration of prism contribution is used to evaluate Newton's integral on a local or regional scale, called the planar approximation or spatial domain, terrain reductions in the WGM2012 was calculated on a global scale with Newton's

integral was evaluated in the spherical approximation or spectral domain. Moreover, WGM2012 used spherical harmonic series expansions for conversion of spherical harmonic topography models to the implied gravitational potential. Some studies have indicated significant differences of these two technique domains in evaluation of Newton's integral of topographic gravity in the mountainous region. Kuhn et al., (2009) indicated an almost constant bias of about −18.7 mGal within a variation interval of 2.5 mGal over 92% of differences in Australia. However, over the mountainous areas magnitudes larger than 10 mGal were seen when using two approaches for computing the topographic reduction for Australia. Wang et al. (2010) encountered notable discrepancies at the 10–30 mGal level over steep mountain slopes of Earth's major mountain ranges, with a maximum disagreement at the 60 mGal level over the Himalayas. Balmino et al. (2012) compared topographic gravity from the spatial and spectral method to ultrahigh degree of 10,800 (equivalent to 1 km resolution), yielding maximum differences of about 40 mGal and a RMS of about 2.3 mGal over parts of Northern Africa. However, this difference increases over the Atlas mountain range to the about 10 mGal level. Thus, the differences in the used DTMs and/or terrain reduction techniques could be considered as the reason for large shift in Bouguer gravity anomalies between the new grid with WGM2012. To clarify this issue, the ETOPO1 at 1' resolution, which was used in the WGM2012, was compared with the mixed SRTM model in Vietnam after re-gridding to 1'. The differences are -0.9 and 44.3 m in mean and STD, respectively. This proves that no bias comes from two DTMs used. Therefore, the differences in topographic reductions approach are the possible reason for this large shift.

Topographic reductions calculated with different approaches i.e., planar and spherical, and with different DTMs i.e., the mixed SRTM model and ETOPO1, are listed in Table 3.6. The differences are also given in this table and displayed in Figure 3.10. A difference of about 124 mGal between the two approaches of terrain reduction using in the new grid and WGM2012 is revealed over Vietnam. This value explained for the large shift in the Bouguer anomalies derived from the new grid and WGM2012. Figure 3.10b shows the differences after removing the mean bias value between two approaches, planar and spherical, using the same DTM, ETOPO1. After removing this mean value, discrepancies at the 20–30 mGal level over steep mountain slopes in northwestern regions can be seen. The discrepancy is consistent with the results of recent research mentioned above. The differences are significant in the mountains of the study area. The northwest–southeast trend visible in Figures 3.10a and 3.10b is the result of the relative location of the computation points with respect to the global topographic masses. For example, the differences are more negative in the northwest due to the closer proximity to the Hoang Lien Son Mountain Range, with its Fansipan peak at the height of about 3,140 m above the sea level, which causes the spherical topographic reductions to be more positive, whereas

the southeast is sea ridges with the depth up to 2,500 m below the sea level and so the spherical topographic reductions to be more negative. Finally, a comparison of the planar approach using the different DTMs, the mixed SRTM and ETOPO1 model, is shown in Figure 3.10c and listed in Table 3.6. The results show that there is not a bias in both DTMs (only -0.7 mGal in mean bias and 4.8 mGal in STD). Differences are mainly in the areas where the topographic relief is very rugged since the mixed SRTM model up to 3" resolution (15" on the sea) represents the real topographic relief very well, whereas ETOPO1 does not. Elevation data of ETOPO1 cannot provide information at wavelengths shorter than the grid spacing (1') so the elevation derived from the mixed SRTM and ETOPO1 are significantly different where the topographic relief is very rugged. It is clear that the mixed SRTM model is undoubtedly suitable for these rugged areas thanks to its high resolution. Fullea et al., (2008) indicated that the accuracy of the terrain correction is strongly dependent on the resolution of the DEM used by comparing terrain correction computed from the ETOPO2 at 2' resolution (Smith & Sandwell, 1994; Hastings et al., 2000) and the SRTM at 3" resolution. Therefore, the large shift in differences between the new Bouguer anomalies grid and WGM2012 is mainly from the approach used in the calculation of the topographic reductions. It corresponds to the far-zone effect of the topographic reduction in the spherical approximation. This represents the gravitational effect of the whole global topographic masses while excluding masses in the localized area of several hundred kilometers around the calculation point that have been considered in the planar terrain correction. More specific, the oceans occupy about 71% of the globe and land the remaining 29%, and differences between ocean and land are the reason for the differences between planar and spherical approaches. A simple example by Vermeer (2020) indicated a bias of about 155 mGal between planar and spherical Bouguer reductions by assuming the mean height of the land topography and density for crustal rock are 800m and 2,670 kg/m^3, respectively, and mean ocean depth and density for sea water are 3,700m and 1,030 kg/m^3, respectively.

Table 3.6. Statistics of differences in topographic reductions [unit: mGal]

	Min	**Max**	**Mean**	**STD**
Planar (SRTM)	-162.2	295.9	25.2	48.6
Planar (ETOPO1)	-157.3	301.3	25.9	49.3
Spherical (ETOPO1) (derived from WGM2012)	-287.0	219.0	-98.2	54.2
Planar (SRTM)-spherical (ETOPO1)	23.5	185.9	123.4	10.6
Planar (ETOPO1)-spherical (ETOPO1)	39.6	160.3	124.1	8.3
Planar (SRTM)-planar (ETOPO1)	-61.8	47.9	-0.7	4.8

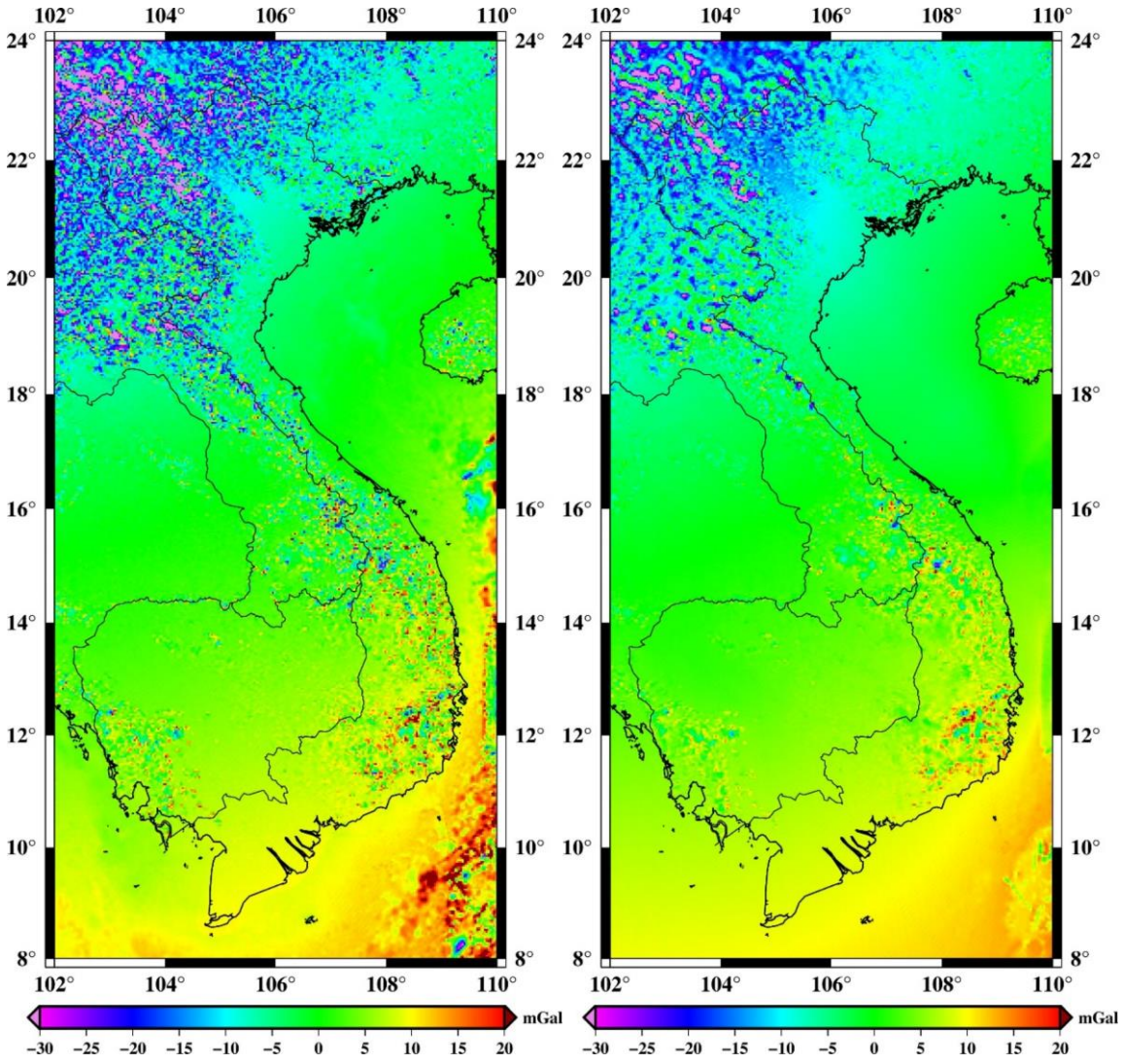
102°
104°
106°
108°
110°
24°
22°
20°
18°
16°
14°
12°
10°
8°
mGal
−30
−25
−20
−15
−10
−5
0
5
10
15
20

(a) (b)

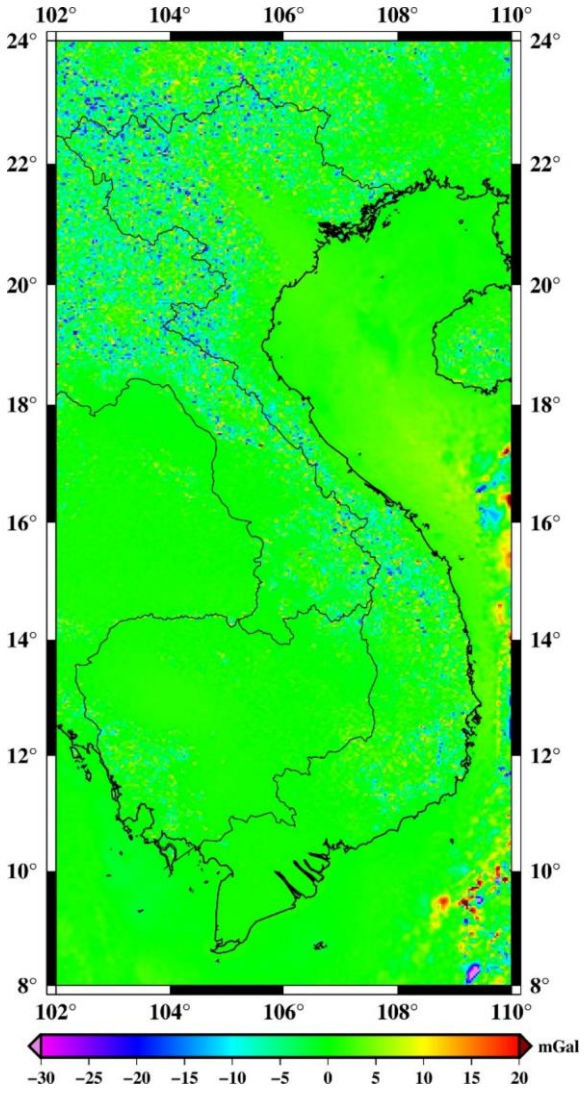

(c)

Figure 3.10. Differences in topographic reductions (after removing the mean bias) between: a) planar approach using the mixed SRTM3arc and spherical approach using ETOPO1, b) planar and spherical approach using ETOPO1 and c) planar approach using the mixed SRTM3arc and ETOPO1

In this chapter, all data used for the thesis project was described. A pre-processing procedure on these data has been carried out, especially the terrestrial gravity data. A set of complete gravity anomaly maps was determined. These maps were validated by comparing with those derived from the WGM2012 map. The results indicated that the new maps significantly improved the accuracy and resolution in the study region thanks to using the new gravity data and the fill-in data derived from the RTM effects (using SRTM at 3" resolution) plus the GOCE gravity. This set of maps is the basic data for the study area. In the following chapters, these data will be used for geodetic, geophysical and geological applications e.g., determination of the quasigeoid model as well as the Moho and LAB depth.

Chapter 4: THE GRAVIMETRIC QUASIGEOID SOLUTION

In this chapter, a high resolution gravimetric quasigeoid model for Vietnam and its surrounding areas is determined based on the new gravity data. Like the Free-air gravity anomaly map, here GGM plus RTM effects and gravity field derived from altimetry satellites are used to provide the fill-in information over land and marine areas. First, the cleaned land gravity measurements as well as the fill-in data are removed the long wavelengths using GGM and the short wavelengths using RTM effects. The mixed DIR/EGM model up to d/o 719 and the RTM effect calculated from the mixed SRTM model are used for the remove-restore procedure. The residual gravity anomalies are then interpolated to regular grid using LSC method in the GRAVSOFT GEOGRID program. The residual height anomalies are determined employing the Stokes integral using the FFT approach and deterministic kernel modification proposed by WG in the GRAVSOFT SPFOUR program, as well as by means of LSC in GRAVSOFT GEOCOL17 program. Finally, the gravimetric quasigeoid is determined by restoring the long wavelengths using GGM and the short wavelengths using RTM effects. The accuracy of the estimated quasigeoid models is evaluated by comparing with geometric height anomalies derived from the GNSS/levelling points. The global models EIGEN-6C4 and EGM2008 are also used for this validation.

This study has been subject to the following paper:

Vu, D. T., Bruinsma, S., & Bonvalot, S. (2019). A high-resolution gravimetric quasigeoid model for Vietnam. *Earth, Planets and Space*, *71*(1), 65. https://doi.org/10.1186/s40623-019-1045-3

4.1. Chart of steps for determination of quasigeoid

All computations have been performed by GRAVSOFT program (Forsberg & Tscherning, 2008). The quasigeoid model was developed according to the diagram shown in Figure 4.1, which presents the different steps, inputs and modules for RCR operations.

All computations have been performed with the reference ellipsoid WGS84, of which the constants are: a=6378137.00 m, f=1/298.257223563, GM_0=3.986004418 x 10^{14} m^3/s^2, and in the Tide Free (TF) system. When a GGM is referred to the Zero Tide (ZT) system or the Mean Tide (MT) system, the $C_{2,0}$ coefficient is converted to the TF system using the formula reported in (Rapp, 1989). In Vietnam, where the height system refers to the MT system, the conversion from MT system to the TF system is done according to (Ekman, 1989).

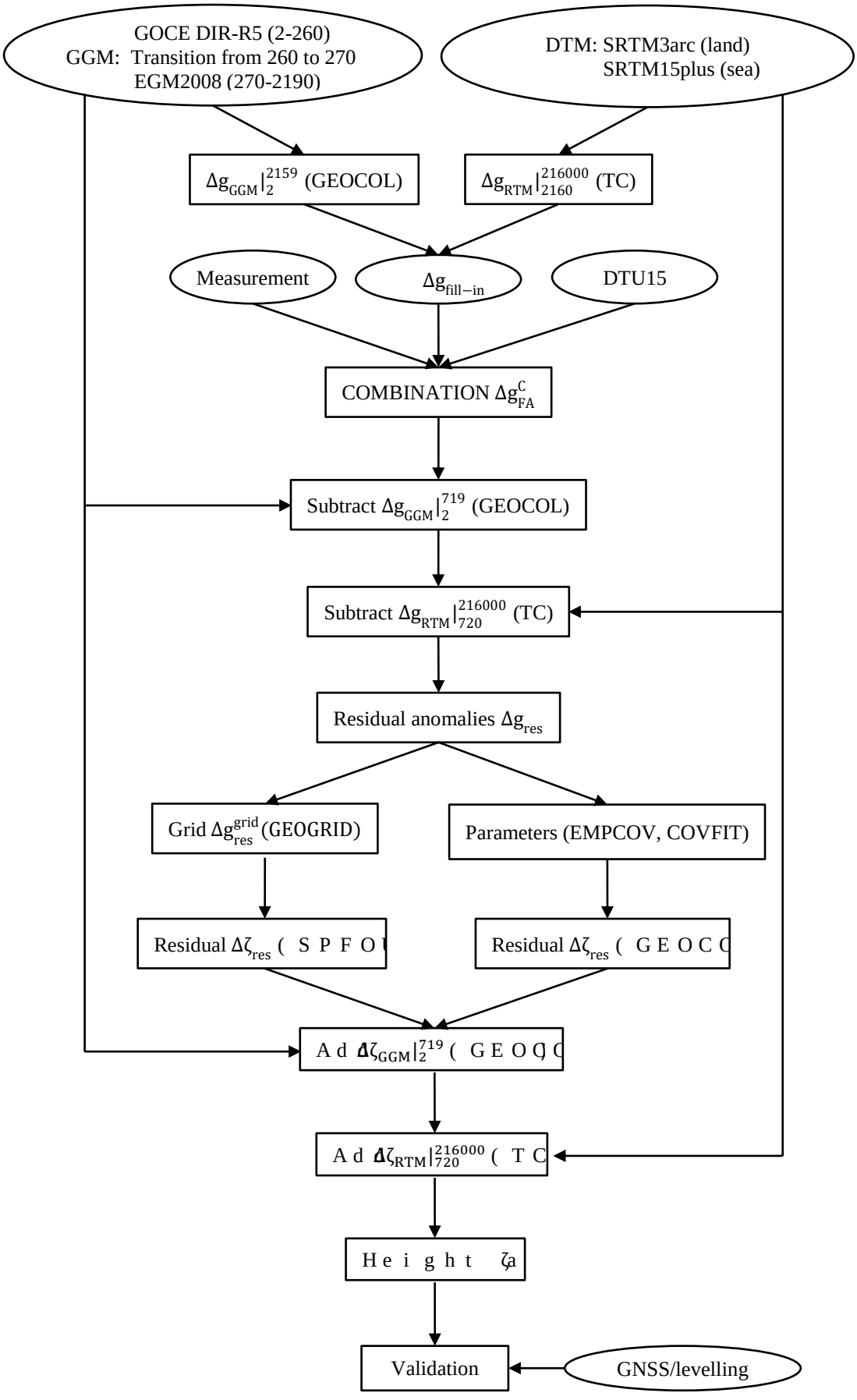

Figure 4.1. Diagram of sequential steps (top to bottom) in the calculation of the quasigeoid

4.2. Gravimetric quasigeoid

After removing long and short wavelength components from GGM and RTM effect, respectively, the residual gravity anomalies are much smoother than the Free-air gravity anomalies. Hence, using these residual gravity anomalies for interpolating to regular grid is better than the Free-air gravity anomalies. Consequently, the grid of residual gravity anomalies was determined as follows: First, the removal procedure is applied for the cleaned terrestrial gravity data as well as the fill-in data to obtain the residual gravity anomalies. The mixed DIR/EGM model up to d/o 719 plus RTM effect derived from the mixed SRTM model is used in this procedure. Then, a 5x5' regular grid of residual gravity anomalies is created with the complex procedures for merging the heterogeneous residual data are performed as presented in Section 3.2 for creating the grid of Free-air gravity anomalies. A grid at higher resolution, e.g., 2.5', was also tested to estimate the gravimetric quasigeoid but the result was slightly worse than when the 5' grid was used. The 5x5' regular grid is used to calculate quasigeoid according to the Stokes' integral in the 1D-FFT approach. For LSC method, the actual measurements were used; however, the same fill-in and transition grid data were used.

Statistics of the merged grid of residual gravity anomalies are given in Table 4.1 and shown in Figure 4.2. These residual gravity anomalies are generally small (<30mGal in magnitude). Large residual gravity anomalies occur in mountainous regions (e.g., the northwest and central parts of the study area) where the altitude is greater than 1000 m. The reason for the large residuals is that errors of the DTM and terrestrial gravity in mountainous regions are larger than in flat regions. The topography is relatively complicated with the active faults system, which will be discussed in chapter 6. However, with STD and mean bias of residual anomalies grid are only 7.8 and -0.8 mGal, respectively, much lower than these of Free-air anomalies grid (26.9 and -12.8 mGal, respectively), a much smoother grid was obtained for computing gravimetric quasigeoid.

Table 4.1. Statistics of the residual gravity anomalies [Unit: (mGal)]

	Mean	**STD**	**Max**	**Min**
Residual	-0.9	10.2	117.2	-127.2
Grid of residual	-0.8	7.8	-59.2	49.1

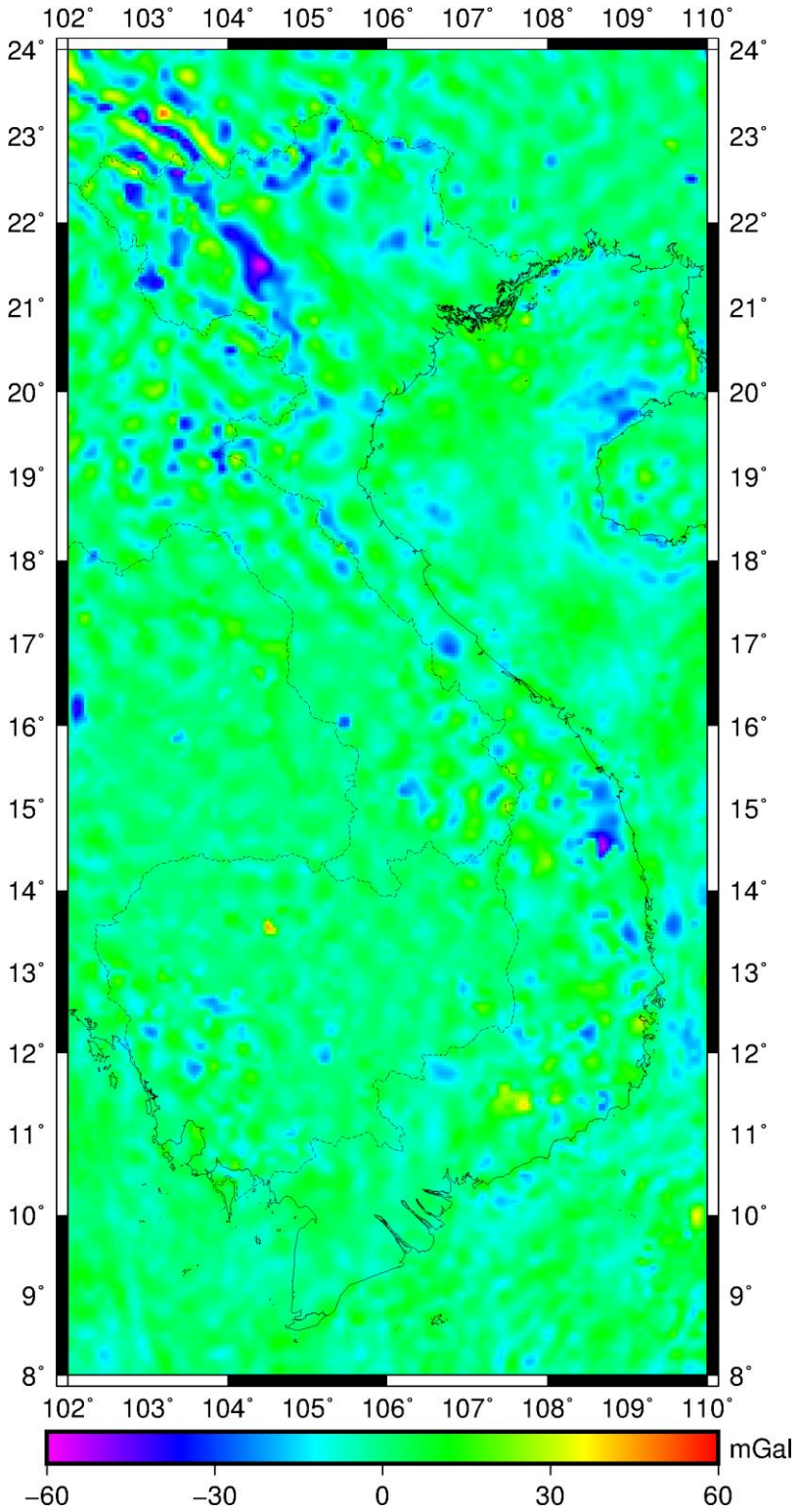

Figure 4.2. Grid of residual gravity anomalies

The residual height anomalies have been determined using the regular grid of residual gravity anomalies employing the Stokes' integral in the 1D-FFT approach implemented in the GRAVSOFT SPFOUR program with the WG modification of the Stokes' kernel function. WG removes low harmonics up to degree N_1, so the influence of the local data at long wavelengths is eliminated, and then linearly tapered to N_2 (Rene Forsberg & Tscherning,

2008). N_1 and N_2 are selected according to data and the GGM used in the remove step, but they should be less than or equal to degree n_{max} of the GGM in the remove step. To find out the optimum N_1 and N_2 degrees the quasigeoid was computed by the Stokes-FFT using WG with N_1 and N_2 were tested from 100 to 260 (maximum degree of the GOCE DIR-R5 model used in combination with EGM2008) in steps of 10 degrees. The computed quasigeoid models were then compared to GNSS/levelling data. Finally, the best quasigeoid model was obtained when the low harmonics were completely removed from Stokes' function up to degree $N_1 = 220$ and then linearly tapered to $N_2 = 230$. The results of this test are shown in appendix 2.

Residual height anomalies were also calculated with the LSC method, using the GRAVSOFT GEOCOL program. Computation of the empirical and fitted covariance functions of the gravity anomalies is required in LSC to estimate the residual height anomalies. The error degree-variances of the mixed DIR/EGM model up to 719 and the fourth model of Tscherning and Rapp for the degree-variances of degree greater than 719 (Tscherning & Rapp, 1974) were used. Degree 719 agrees best with the empirical data for fitting the model covariance function. The empirical covariance function of the data has been computed using the GRAVSOFT EMPCOV program, and was fitted to the Tscherning and Rapp model using the GRAVSOFT COVFIT program. The output result of the GRAVSOFT COVFIT program is shown in appendix 3. The optimum parameters: the depth to the Bjerhammar sphere $R\text{-}R_B = -0.028$ km and the variance of the gravity anomalies at zero height VARG = 131.06 $mGal^2$ have been determined for inputs of GRAVSOFT GEOCOL program. Figure 4.3 shows the plot of the empirical covariance (blue line) and fitted covariance functions for the residual gravity anomalies Δg_{res} (red line).

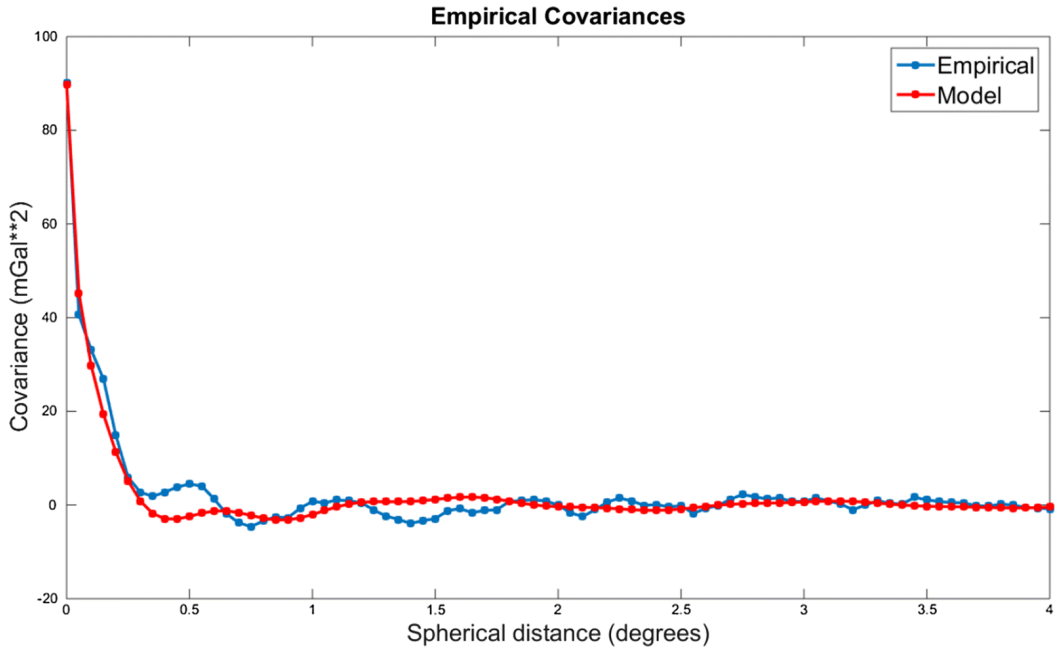

Figure 4.3. Empirical and fitted covariance functions for residual gravity anomalies Δg_{res}

The residual height anomalies ($\Delta\zeta_{res}^{FFT}$) computed with the SPFOUR program vary from -0.701 to 0.402 m. The height anomalies (ζ_{FFT}), obtained by restoration of ζ_{GGM} and ζ_{RTM}, vary from -35.097 to 16.684 m (GEOID_FFT solution). The residual height anomalies were also computed with the GEOCOL program: $\Delta\zeta_{res}^{LSC}$ varies from -0.779 to 0.432 m and ζ_{LSC} from -34.969 to 16.688 m (GEOID_LSC solution).

Figures 4.4a and 4.4b show the residual height anomalies ($\Delta\zeta_{res}^{FFT}$) and GEOID_FFT, and the differences between GEOID_FFT with GEOID_LSC are shown in Figure 4.4c. The differences range from -0.232 to 0.244 m. The large differences between GEOID_FFT and GEOID_LSC occur in the regions where the residual gravity anomalies are large (>30 mGal in Figure 4.2). This issue will be discussed in the following section.

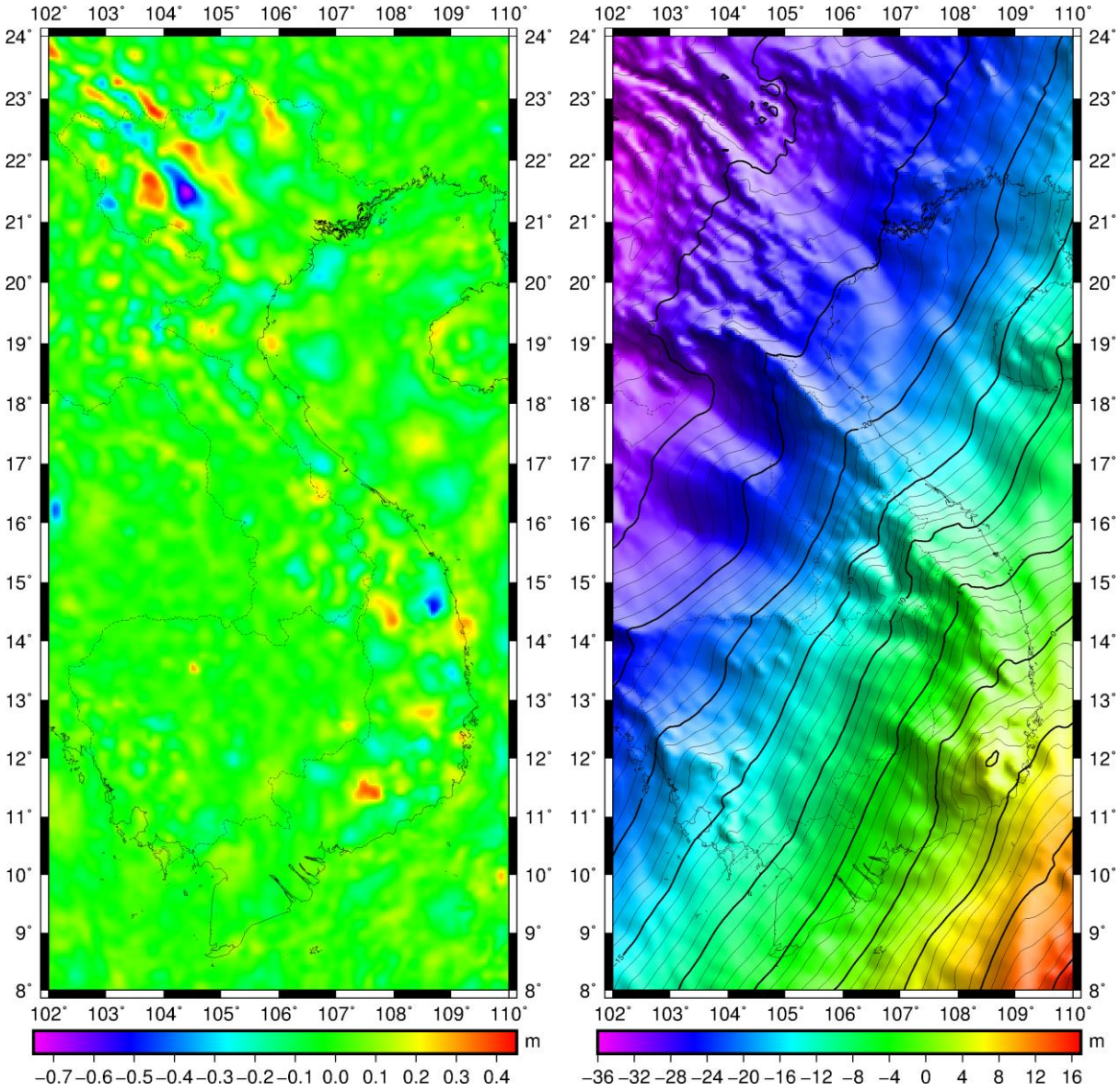

(a) (b)

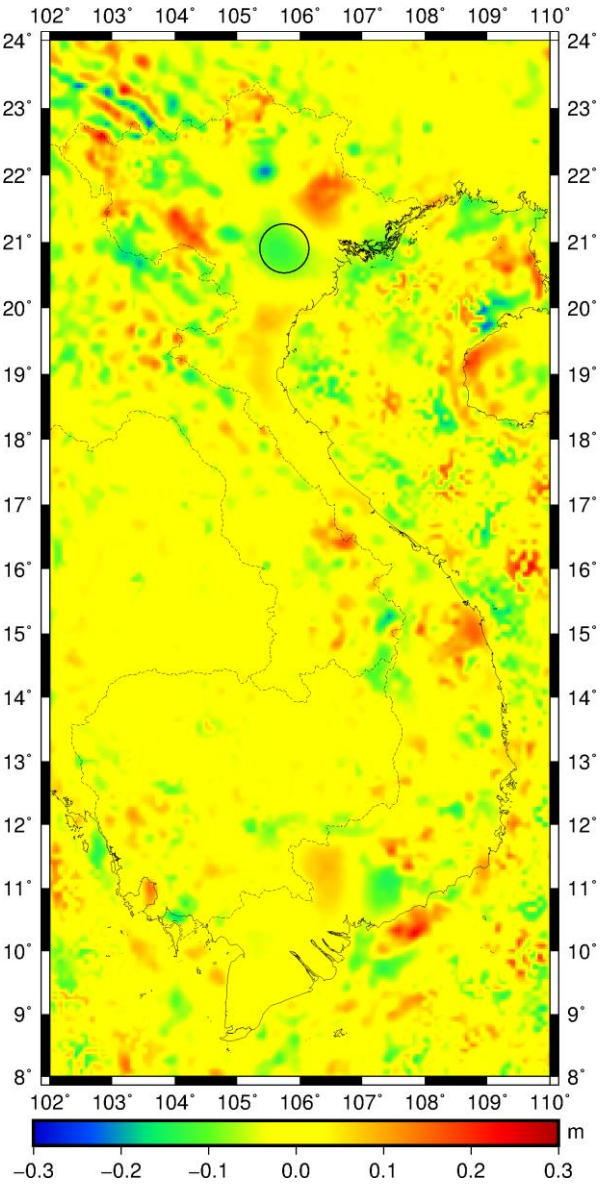

(c)

Figure 4.4. a) Residual height anomalies ($\Delta\zeta_{res}^{FFT}$), b) GEOID_FFT and c) Differences between GEOID_FFT with GEOID_LSC

4.3. Validation of the gravimetric quasigeoid

For validation, the height anomalies were compared with those inferred from 812 GNSS/levelling reference points ($\zeta^{\text{GNSS/levelling}}$). In order to clearly see the improvements of two new gravimetric quasigeoid models, the height anomalies derived from EGM2008 and EIGEN-6C4 were compared with these GNSS/levelling points. Figures 4.5a, 4.5b and 4.5c show the plots of the differences of ζ^{FFT}, ζ^{LSC} and ζ^{EGM2008} with $\zeta^{\text{GNSS/levelling}}$ and the statistics are listed in Table 4.2. The differences for GEOID_FFT range from 0.136 to 0.816 m with a STD of 0.097 m and average bias of 0.506 m; for GEOID_LSC, from 0.138 to 0.815 m with a STD of 0.097 m and average bias of 0.508 m. The results show that both methods reach the same precision, with a STD at the 9.7 cm level. The reason for the large average bias is

datum inconsistencies. These quasigeoids refer to a global reference system while heights have been determined from levelling refer to national MSL. This issue will be solved in the next chapter. It should also be noted that here the zero-degree term is not included in this average bias. The results of the comparison indicated significant improvement of the local quasigeoids over EGM2008 and EIGEN-6C4 in Vietnam, which have STD of 29.1 and 19.2 cm, respectively. Figure 4.5 shows this improvement over EGM2008, especially in the north and the mountainous regions.

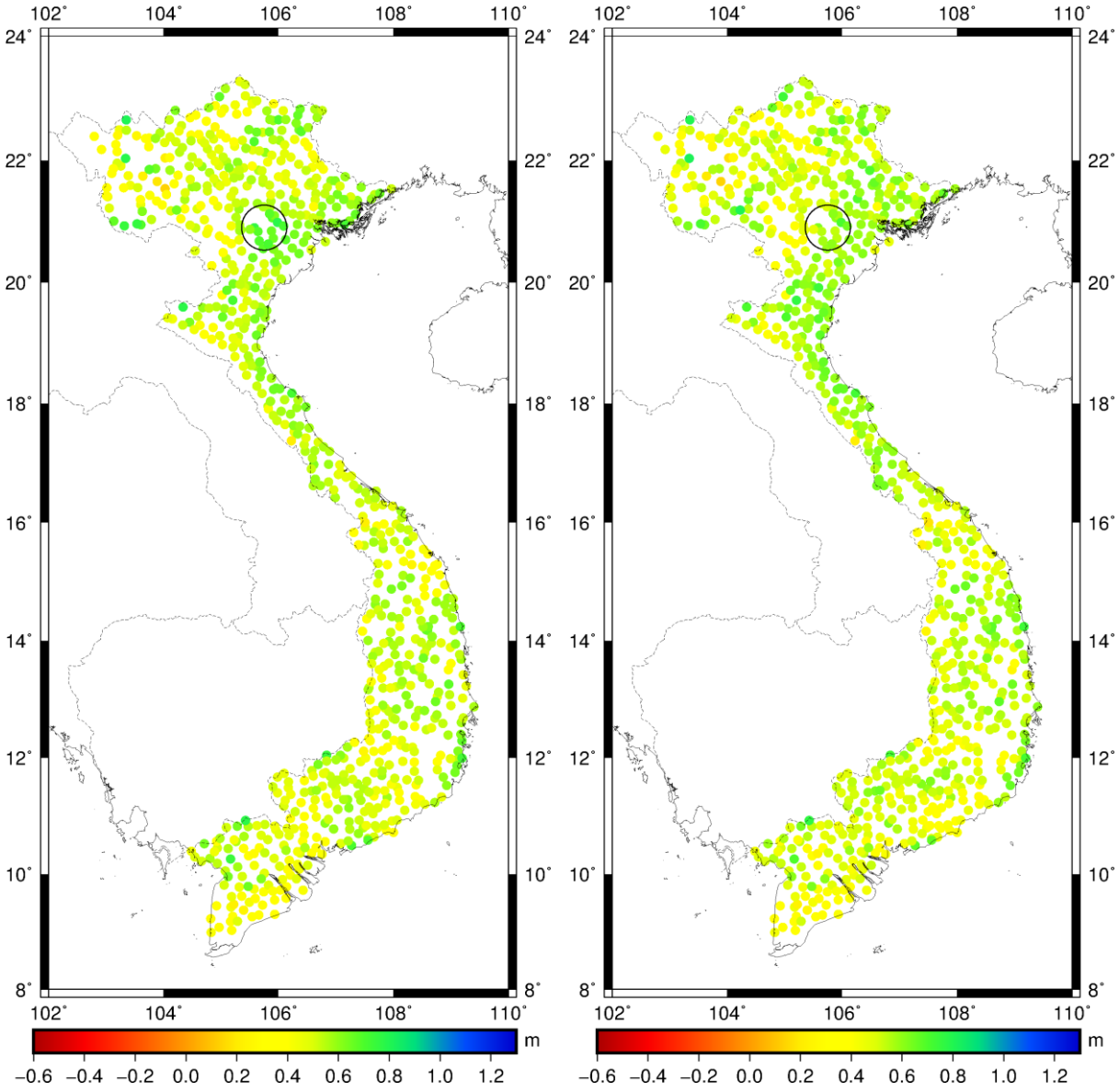

(a) (b)

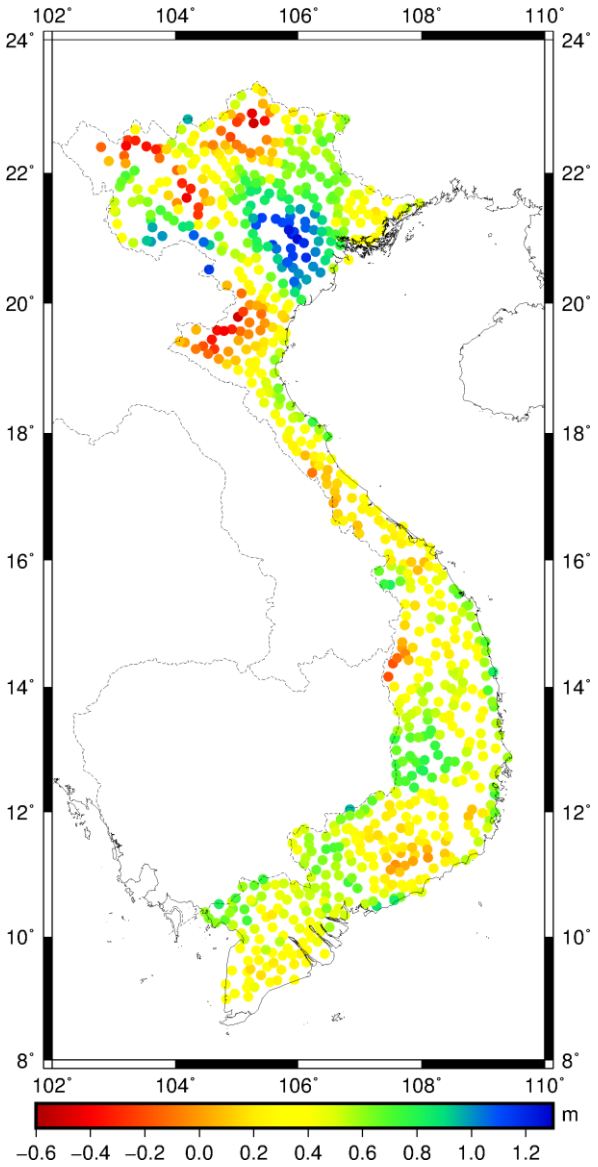

(c)

Figure 4.5. Differences between the developed quasigeoid and GNSS/levelling: a) GEOID_FFT, b) GEOID_LSC and c) EGM2008

Table 4.2. Statistics of the quasigeoid and their validation with GNSS/levelling data [Unit: m]

	Mean	**STD**	**Max**	**Min**
$\Delta\zeta_{res}^{FFT}$	-0.005	0.084	0.402	-0.701
ζ^{FFT}	-16.169	11.781	16.684	-35.097
$\Delta\zeta_{res}^{LSC}$	0	0.080	0.432	-0.779
ζ^{LSC}	-16.164	11.778	16.688	-34.969
$\zeta^{GNSS/levelling} - \zeta^{FFT}$	0.506	0.097	0.816	0.136
$\zeta^{GNSS/levelling} - \zeta^{LSC}$	0.508	0.097	0.815	0.138
$\zeta^{GNSS/levelling} - \zeta^{EIGEN-6C4}$	0.514	0.192	1.057	-0.348
$\zeta^{GNSS/levelling} - \zeta^{EGM2008}$	0.428	0.291	1.272	-0.516

The height anomalies from these quasigeoids were also compared with GNSS/levelling points split according to order: 428 points of 1st and 2nd order levelling, and 384 points of 3rd order levelling. The results of GEOID_LSC show a STD of 8.7 cm for the 1st and 2nd order points (where gravity was measured) and 10.8 cm for the 3rd order points (where gravity was not measured), while GEOID_FFT has a STD of 9.1 cm for the 1st and 2nd order points and 10.4 cm for the 3rd order points (Table 4.3). These results show that the LSC method is a little more precise than the Stokes_1D FFT where gravity data is available. To further clarify this issue, the quasigeoid was evaluated in two areas (two rectangles in Figure 3.2) where there is sufficient terrestrial gravity as well as GNSS/levelling data (136 GNSS/levelling points in a northern area defined by $20^0 \le \varphi \le 22^0$ in latitude and $105^0 \le \lambda \le 108^0$ in longitude, 120 GNSS/levelling points in a southern area defined by $8^0 \le \varphi \le 11^0$ in latitude and $104^0 \le \lambda \le 108^0$ in longitude). For the northern area, the STD of the LSC and Stokes_1D FFT methods is 7.4 cm and 8.2 cm, respectively; for the southern area, the STDs are 9.2 cm and 10.0 cm, respectively. The results of the comparison indicated that the LSC method is more precise than the Stokes_1D FFT method, improved 0.8 cm of STD for each area. However, quality of the available gravity data in Vietnam is not homogeneous (bias, precision between IGP, VIGAC and fill-in data) and these data have not enough information on the accuracy, which is challenging with the LSC method while with the Stokes-FFT method a good data density is required. It is the reason why these two methods have the same accuracy for the whole study area. The circles on Figures 4.4c, 4.5a and 4.5b show the area where the difference between the two quasigeoid solutions is significant (and where terrestrial gravity data is available). The higher accuracy of LSC, which uses all observations, may be due to the higher density of measurements in these areas than for other areas; a denser residual gravity grid could have been computed for the Stokes-FFT method. This hypothesis was confirmed by computing and using denser grids (2.5'×2.5') for the two test areas with the Stokes-FFT method. The results are shown in the last 2 rows of Table 4.3 and they indicate that the Stokes-FFT method has the same accuracy as the LSC method over these two areas when GEOID_FFT is computed with the denser grids.

Table 4.3. Differences between the quasigeoid and GNSS/levelling data according to the order of levelling network [Unit: m]

	Number of points	**Mean**	**STD**	**Min**	**Max**
$\zeta^{GNSS/levelling} - \zeta^{FFT}$ (1st and 2nd order)	428	0.508	0.091	0.217	0.781
$\zeta^{GNSS/levelling} - \zeta^{LSC}$ (1st and 2nd order)	428	0.515	0.087	0.182	0.807
$\zeta^{GNSS/levelling} - \zeta^{FFT}$ (3rd order)	384	0.503	0.104	0.136	0.816
$\zeta^{GNSS/levelling} - \zeta^{LSC}$ (3rd order)	384	0.500	0.108	0.116	0.815
$\zeta^{GNSS/levelling} - \zeta^{EIGEN-6C4}$ (3rd order)	384	0.488	0.186	-0.348	0.990

$\zeta^{GNSS/levelling} - \zeta^{EGM2008}$ (3rd order)	384	0.402	0.274	-0.512	1.143
$\zeta^{GNSS/levelling} - \zeta^{FFT}$ (northern area)	136	0.551	0.082	0.290	0.781
$\zeta^{GNSS/levelling} - \zeta^{LSC}$ (northern area)	136	0.540	0.074	0.287	0.707
$\zeta^{GNSS/levelling} - \zeta^{FFT}$ (southern area)	120	0.465	0.100	0.224	0.776
$\zeta^{GNSS/levelling} - \zeta^{LSC}$ (southern area)	120	0.462	0.092	0.230	0.765
$\zeta^{GNSS/levelling\_coast} - \zeta^{FFT}$	69	0.532	0.090	0.333	0.719
$\zeta^{GNSS/levelling\_coast} - \zeta^{FFT-DTU}$	69	0.524	0.098	0.322	0.746
Quasigeoid computed with Stokes-FFT with grid 2.5' × 2.5					
$\zeta^{GNSS/levelling} - \zeta^{FFT}$ (northern area)	136	0.575	0.073	0.319	0.762
$\zeta^{GNSS/levelling} - \zeta^{FFT}$ (southern area)	120	0.446	0.096	0.234	0.829

The STD of the differences between EGM2008 and EIGEN-6C4 with 384 GNSS/levelling points of the 3rd order levelling is 27.4 cm and 18.6 cm (Table 4.3), respectively, whereas the STD of GEOID_FFT and GEOID_LSC is 10.8 and 10.4 cm, respectively, slightly reduced accuracy when compared to the 1st and 2nd order. These numerical findings signify that the addition of the RTM effects to DIR/EGM has significantly improved the accuracy of the height anomalies in the area where no data existed.

Moreover, a quasigeoid was computed using DTU15 data ($\zeta^{FFT-DTU}$) instead of using the mixed DIR/EGM model together with RTM effect within 50 km from the coastline. The height anomalies derived from these quasigeoids were compared with those derived from 69 GNSS/levelling points near the coast ($\zeta^{GNSS/levelling\_coast}$ in Table 4.3). An improvement can be seen when using RTM effects together with the mixed DIR/EGM model instead of using DTU15 gravity within 50 km from the coastline. This suggests that RTM effects together with the DIR/EGM model can be used to fill the gap between gravity data on land and marine altimetric gravity if airborne or shipborne gravity is not available in coastal zones.

A large bias was found between gravimetric quasigeoid and GNSS/levelling data (50 cm) in which the zero-degree term also needs to be taken into account to determine the true vertical datum offsets for Vietnam with respect to a global equipotential surface. Such offsets value must be removed for before using a quasigeoid in GNSS levelling. These issues will be solved in Chapter 5. It is important that there are two high resolution gravimetric quasigeoid models having the same precision of 0.97 m in STD for the study region. In the next chapters, the applications of the gravimetric quasigeoid model in geodesy as well as in geophysics and geology will be presented.

Chapter 5: QUASIGEOID APPLICATION FOR GNSS LEVELLING AND HEIGHT SYSTEM UNIFICATION

This study has been subject to the following papers:

Vu, D. T., Bruinsma, S., Bonvalot, S., Remy, D., & Vergos, G. S. (2020). A Quasigeoid-Derived Transformation Model Accounting for Land Subsidence in the Mekong Delta towards Height System Unification in Vietnam. *Remote Sensing*, *12*(5), 817. https://doi.org/10.3390/rs12050817

Vu, D. T., Bruinsma, S., Bonvalot, S., Bui, K. L., & Balmino, G. (2021). Determination of the geopotential value on the permanent GNSS stations in Vietnam based on the Geodetic Boundary Value Problem approach. *Geophysical Journal International*, *226*(2), 1206–1219. https://doi.org/10.1093/gji/ggab166

5.1. Background for using quasigeoid in GNSS levelling

A drawback of GNSS is that it provides to the user a high precision ellipsoidal height, which is not physically meaningful. To convert an ellipsoidal height (h) to a physical height, i.e., orthometric (H) and/or normal height (H*), one has to subtract the height anomaly (ζ), being the vertical distance between the quasigeoid and the reference ellipsoid, as follows:

$$H^* = h - \zeta \tag{5.1}$$

This is the basic formula in GNSS levelling. For local or regional applications, a geoid/quasigeoid with an accuracy of few cm is required to determine the height anomalies. However, a large mean bias was indicated in the gravimetric-only quasigeoid when compared with GNSS/levelling data in Vietnam. The principal reason for the large mean bias is that there is an inconsistency in the reference systems in these vertical datum realizations. The quasigeoid refers to a global reference system i.e. an international reference gravity potential W_0=62,636,853.4 m^2/s^2 whereas the height anomalies determined from the GNSS/levelling data refer to the national MSL, called the Vietnam Local Vertical Datum (VLVD). The MSL over 1950 - 2005 for a single tide gauge in the north of Vietnam, called Hon Dau (20°40', 106°49'), was assigned to zero height on the VLVD. With its large mean bias, the gravimetric quasigeoid model does not allow the accurate transformation of GNSS ellipsoidal heights to physical heights in the VLVD. Most often, the gravimetric quasigeoid or geoid model is forced to fit onto the local vertical

datum. Such a hybrid quasigeoid/geoid model is used to convert GNSS ellipsoidal heights to physical heights.

It is well known that the LVD determination by levelling contains the distortions caused by vertical crustal movement and systematic cumulative errors associated with levelling surveys over long distances (Entin, 1959; Vanicek et al., 1980). So, the problem with this fitting method is that the surface realized after the transformation, despite providing more or less rigorous results for the application of levelling with GNSS, is not an equipotential surface anymore, hence its physical meaning and applications in the rest of the geosciences are limited. This hybrid geoid/quasigeoid model aims only at providing a model of the separation between the reference ellipsoid and the LVD rather than determining the classical geoid/quasigeoid as an equipotential surface of the Earth's gravity field. An alternative method for the definition of a vertical datum by GNSS levelling is to use the local gravimetric-only quasigeoid model for determining a vertical offset model (distance between the gravimetric-only quasigeoid and a LVD). This procedure is more realistic because it does not constrain the local gravimetric quasigeoid to be coincident to the LVD. This vertical offset model can be used to convert ellipsoidal heights into the local physical heights where the current LVD needs to be maintained. On the contrary, this offset model can also be used to redefine and recalculate a modern LVD by adding it to the available levelling data. Such an offset model has been successfully applied in modernizing the height reference system for instance in New Zealand (Amos, 2010) and Canada (https://www.nrcan.gc.ca/earth-sciences/geomatics/geodetic-reference-systems/9054). The GEOID_LSC model is used to estimate the vertical offset model.

Significant trends in national levelling networks have been documented in several countries as in Thailand (a significant tilt of -0.126 mm/km in north-south direction and 0.008mm/km in east-west direction (Dumrongchai et al., 2012)), in Canada (a tilt of -0.26 cm/degree in the north-south direction and 0.52 cm/degree in the west-east direction (Hayden et al., 2013)) as well as in the USA (a large northwest-southeast tilt in NAVD88 data with respect to the GOCE geoid (Amjadiparvar et al., 2013) or Western Australia (a tilt of 0.27 mm/km in the north-south direction and 0.07 mm/km in the east-west direction (Featherstone & Filmer, 2008). Therefore, it is likely that The tilts would be also present in the vertical network of Vietnam, thus inherited in the levelling data that will be analyzed in this study. Moreover, thanks to recent studies, the Mekong Delta is known to be affected by significant land subsidence (Erban et al., 2014; Minderhoud et al., 2017). With an average subsidence rate of 1.6 cm/year and extreme locals up to over 2.5 cm/year (Erban et al., 2014; Minderhoud et al., 2017), the influence of land subsidence is significant on the quality and maintenance of levelling data in the Mekong Delta when compared to the rest of Vietnam. As such, distortions might be expected in the GNSS/levelling data in Vietnam and because the computation of an offset model using LSC assumes stochastic

observations, any deterministic biases and trends must be removed.

The objective is to determine an offset model for converting ellipsoidal heights into the local normal heights in Vietnam. This offset model is applied to the local gravimetric-only quasigeoid model for GNSS levelling technology giving an accuracy that complies with 3rd order levelling specifications. The accuracy of the offset model depends on the quality of the height anomalies derived from the GNSS/levelling data used in the calculation. Therefore, analyzing and improving the accuracy of the GNSS/levelling data will also be performed. The effects of local subsidence in South Vietnam is also discussed from the analysis of ground deformation measurements derived from permanent GNSS stations and InSAR (Interferometric Synthetic Aperture Radar) time series. Based on the results of land subsidence derived from InSAR, the corrections were applied on the GNSS/levelling data in the Mekong Delta. Finally, high quality GNSS/levelling data was used to assess the accuracy of the developed offset models based on the cross-validation technique (Fotopoulos, 2003).

5.2. Estimation of GNSS/levelling data

To estimate the GNSS/levelling data, the so-called geometric height anomalies, i.e. derived through Eq (5.1), of the 812 GNSS/levelling points ($\zeta^{\text{GNSS/levelling}}$) were compared with those derived from the GEOID_LSC (ζ) in the absolute sense as follows:

$$\varepsilon = \zeta^{GNSS/levelling} - \zeta - \zeta_0 \tag{5.2}$$

where is called the offset of the existing VLVD with respect to the local gravimetric-only quasigeoid.

ζ_0 represents the contribution of the zero-degree harmonic term to the GGM with respect to a specific reference ellipsoid (Hofmann-Wellenhof & Moritz, 2006).

$$\zeta_0 = \frac{GM - GM_0}{R\gamma} - \frac{W_0 - U_0}{\gamma} \tag{5.3}$$

The parameters GM_0 and U_0 are the geocentric gravitational constant of the reference ellipsoid and the normal gravity potential, respectively. The WGS-84 ellipsoid is used as the reference ellipsoid for computation GEOID_LSC, GM_0=398,600.4418×10^9 m^3/s^2 and U_0 = 62,636,851.7146 m^2/s^2 (report of NIMA 2000 (NIMA, 2000)) while the Earth's geocentric gravitational constant GM and the gravity potential Wo are set to GM=398,600.4418109×10^9 m^3/s^2 and W_0=62,636,853.4 m^2/s^2. The mean Earth radius R is taken equal to 6371 km and the normal gravity γ at the surface of the ellipsoid is computed by using Eq. (4-60) of Hofmann-Wellenhof and Moritz (2006).

The results of this comparison are listed in Table 5.1 and shown in Figure 5.1a. Outliers were determined assuming a normal distribution of the residuals, and the three sigma (3σ) rejection led to elimination of 9 points. Linear regressions on the differences of

GNSS/levelling data and GEOID_LSC in northern (> 21° in latitude) and near coast (calculation for GNSS/levelling points within 50 km from the coastline defined by GMT (Wessel & Smith, 1998) are shown in Figure 5.1b, there are tilts in the east-west direction in the north of Vietnam and in the north-south direction. The tilt in the north is 0.30 mm/km whereas the tilt in the north-south direction is 0.11 mm/km. These tilts are significant over long distances and may be due to two reasons: first, trends in the local gravimetric quasigeoid model caused by long and medium wavelength errors, steep gravity gradient and/or terrestrial gravity errors, and second, trends of levelling data caused by vertical crustal movements and/or systematic cumulative errors associated with levelling surveys over long distances. This will be investigated and clarified later in this section.

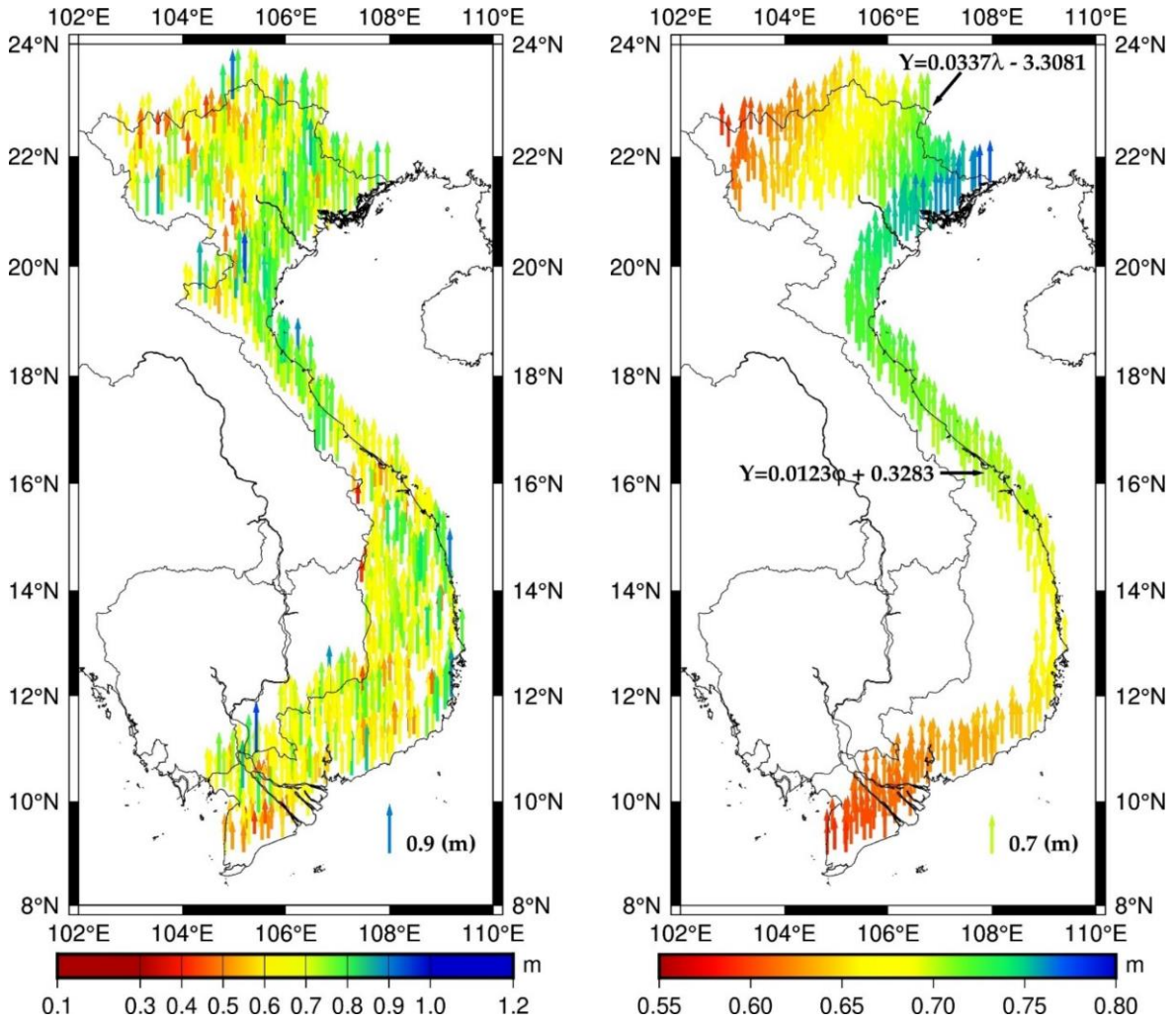

(a) (b)

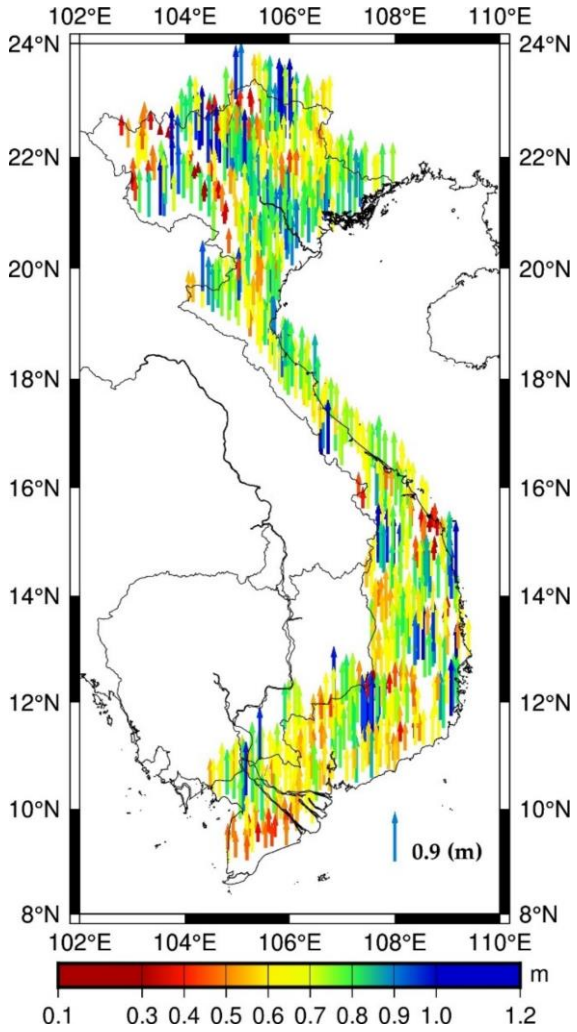

(c)

Figure 5.1. a) Differences between GNSS/levelling data and GEOID_LSC; b) Linear regression on the differences of GNSS/levelling data and GEOID_LSC in northern (> 21° in latitude) and near coast (points within 50 km from the coastline) and c) Differences between GNSS/levelling data and DIR/EGM (d/o 719) plus RTM effects

Table 5.1. Descriptive statistics of the absolute (residuals) and relative differences between the 812 GNSS/levelling stations and GEOID_LSC. [Unit: (m)]

Absolute differences					
	Mean	**STD**	**Max**	**Min**	**Outlier points**
$\zeta^{GNSS/levelling} - \zeta^{LSC}$ (812 points)	0.680	0.097	0.987	0.310	9
$\zeta^{GNSS/levelling} - \zeta^{LSC}$ (excluding outliers) (803 points)	0.682	0.092	0.937	0.396	0
$\zeta^{GNSS/levelling} - \zeta^{DIR/EGM+RTM}$ (803 points)	0.682	0.168	1.138	0.119	
$\zeta^{GNSS/levelling} - \zeta^{LSC}$ (North-east part) (190 points)	0.705	0.077	0.879	0.459	

$\zeta^{GNSS/levelling} - \zeta^{LSC}$ (Southern, <11°) (120 points)	0.634	0.092	0.937		0.402	
Relative differences						
	Mean	**STD**	**Max**	**Min**	**Outlier 3rd order**	**Outlier 4th order**
$\Delta\zeta^{GNSS/levelling} - \Delta\zeta^{LSC}$ (803 points) (21,423 baselines)	0.087	0.071	0.518	0	8153 (38.06%)	2052 (9.58%)

Thanks to GOCE, global geoids with an accuracy of 1-2 cm and gravity field models with an accuracy of 1 mGal at a spatial resolution of approximately 100 km are available. The GEOID_LSC model is expected to be less prone to long and medium wavelength errors thanks to using a mixed DIR/EGM model, and its enhanced resolution allows better detection of distortions in the terrestrial gravity and levelling data. To further clarify the issue of possible trends in local gravimetric quasigeoid models caused by errors in the terrestrial gravity data, the GNSS/levelling geometric height anomalies were compared with those derived from the DIR/EGM model up to d/o 719, (this d/o gave the best result in the removal of the long and medium wavelengths and the calculation of the quasigeoid restore effects in computation GEOID_LSC), plus RTM effects up from d/o 720 to 216000. The results are listed in Table 5.1 and shown Figure 5.1c. The average bias is similar (0.682 m) with GEOID_LSC, whereas the standard deviation is 0.168 m due to the omission error in the mixed DIR/EGM model. It is significantly improved when terrestrial gravity data are used to determine the GEOID_LSC model (the STD of GEOID_LSC is only 0.092 m). This proves that trends in the local gravimetric quasigeoid model caused by bias in the terrestrial gravity data are insignificant in GEOID_LSC model on the scale of the country. Therefore, the tilts are due to steep gravity gradient and trends in levelling data.

The comparison in a relative sense was carried out with 803 GNSS/levelling points over 21,423 baselines. The results are shown in Figure 5.2 and listed in Table 5.1. The magnitude of relative differences of the height anomalies of GNSS/levelling points and the GEOID_LSC increases with the baseline length can be seen in Figure 5.3. To clarify this, the height anomalies of 803 GNSS/levelling points were compared with those derived from the GEOID_LSC in the relative sense per baseline length (10 km). The results are listed in Table 5.2. These results indicate that the mean bias and STD increase linearly with baseline length. This is due to error in the spirit levelling depending on the baseline length. Relative accuracy of spirit levelling decreases 2.9 cm in STD and 3.8 cm in mean when baseline length increases from 10 km to 100 km. This is significant over long distance. This is due to systematic cumulative errors in levelling. It causes the tilts in the levelling data as discussed above. The comparison in relative sense in the northern part (>21° in latitude) and the points near the coast (within 50 km from the coastline) were also carried out. The results are listed in Table 5.2. In the northern part, the mean bias ranges between

4.4 cm and 9.3 cm, while the STD from 3.0 cm and 7.2 cm when the baseline length varies from 10 km to 100 km, respectively. In the region near the coast, mean bias is 4.2 cm and 7.5 cm, STD is 3.7 cm and 6.9 cm when baseline length is 10 km and 100 km, respectively. The relative accuracy of spirit levelling in the northern part decreases faster than in the region near the coast. The tilt in the region near the coast is only 0.11 mm/km whereas in the northern part it is 0.30 mm/km. This means that besides the errors in levelling there is also a contribution of the quasigeoid to the error in the northern part. This tilt of the quasigeoid in the northern part can be attributed to the steep gravity gradient over the northern mountainous regions (the altitude is greater than 1000 m in the northwest).

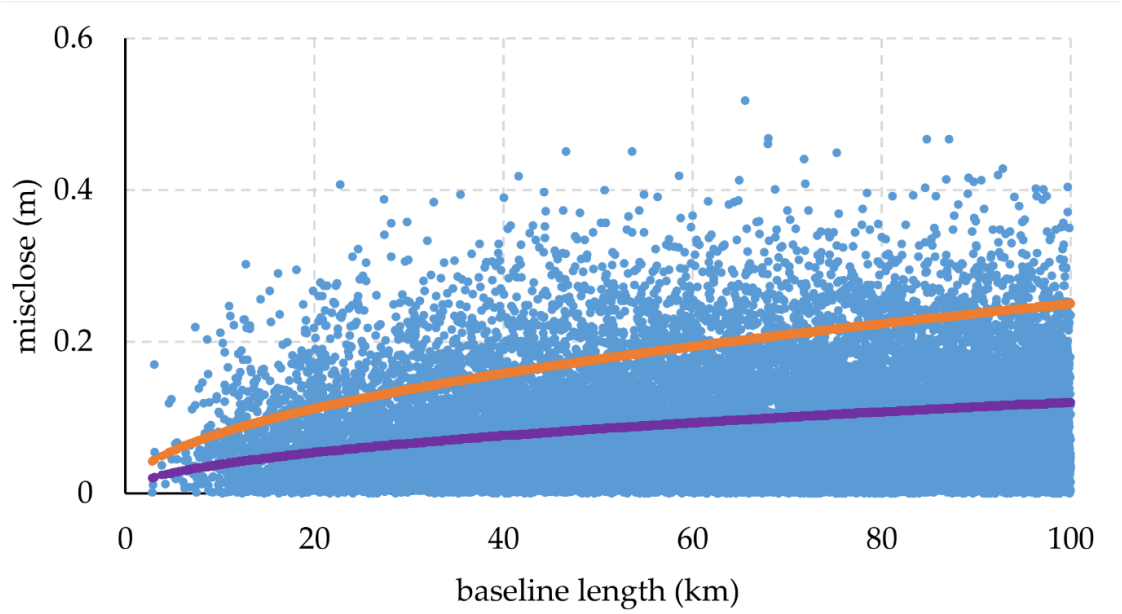

Figure 5.2. Magnitude of relative differences between GEOID_LSC with 803 GNSS/levelling points over 21,423 baselines (blue), 4th order tolerance (orange) and 3rd order tolerance (purple)

Table 5.2. Relative differences between 803 GNSS/levelling points and GEOID_LSC, per baseline length (every 10 km) (NoB: Number of Baselines). [Unit: (m)]

	10km	**20km**	**30km**	**40km**	**50km**	**60km**	**70km**	**80km**	**90km**	**100km**	**All**
NoB	96	760	1356	1776	2215	2505	2845	3068	3334	3468	21423
mean	0.055	0.065	0.077	0.082	0.084	0.089	0.089	0.091	0.090	0.093	0.087
STD	0.045	0.055	0.063	0.066	0.070	0.072	0.073	0.072	0.073	0.074	0.071
Max	0.219	0.302	0.407	0.394	0.451	0.451	0.518	0.449	0.467	0.428	0.518
min	0.001	0	0	0	0	0	0	0	0	0	0
Northern part											
NoB	34	231	376	530	647	751	854	868	1004	998	6294
mean	0.044	0.075	0.080	0.084	0.083	0.089	0.092	0.094	0.093	0.093	0.089
STD	0.030	0.061	0.066	0.066	0.069	0.071	0.071	0.069	0.072	0.072	0.070
Max	0.120	0.295	0.322	0.316	0.390	0.400	0.468	0.396	0.392	0.404	0.468
min	0.001	0	0	0	0	0	0	0	0	0	0
Points near the coast (within 50 km from the coastline)											
NoB	18	202	312	357	380	369	347	361	336	321	3003

mean	0.042	0.055	0.067	0.073	0.072	0.079	0.078	0.074	0.074	0.75	0.073
STD	0.037	0.049	0.055	0.066	0.067	0.067	0.065	0.060	0.069	0.069	0.064
Max	0.138	0.290	0.388	0.333	0.418	0.363	0.384	0.408	0.467	0.352	0.467
min	0.007	0	0	0	0	0.001	0	0	0	0	0

Figure 5.1a indicates that there are two distinct biases, one in the north-east part of the northern region (>105° in longitude and >20° in latitude) and another for the southern region (<11° in latitude). Hence, the GNSS/levelling geometric height anomalies were compared with those derived from the GEOID_LSC for these two regions. The results are listed in Table 5.1. The difference in average bias between these two regions is 7.1 cm (average bias of 0.705 m in the north-east part and 0.634 m in the southern region). These differences, provided by GNSS and levelling which were not measured at the same time (GNSS measurements were taken about 7 years after levelling), may be due to the effect of land subsidence, which has been documented for the southern region of Vietnam (Mekong Delta). Most of the Mekong Delta lies within 2 m of current sea level and is well-known as a region strongly affected by climate change phenomena such as land subsidence and SLR. In a recent study, Featherstone et al., (2019) assessed that the land subsidence effect on the accuracy of height anomalies derived from the GNSS/levelling data, which were not measured at the same time, is an important candidate (together with the poor quality of the altimeter data and steep gravity gradients) to explain for 1mm/km tilt in the quasigeoid in Perth, Australia whereas the land subsidence effect on the computed quasigeoid is very small. As the differences in the GNSS/levelling could be due to ongoing displacements affecting the Mekong Delta, detection such possible displacements through inspection of GNSS and InSAR data is performed. This hypothesis is discussed in the next section.

5.3. Land subsidence in the Vietnam

To assess the impact of land subsidence processes in the estimation of GNSS/levelling discrepancies, the complementary information provided by the permanent GNSS stations in Vietnam and by InSAR data is used to estimate the vertical land motion currently observed in the northern and southern parts of the country.

5.3.1. GNSS and InSAR data

The Continuously Operating Reference Station (CORS) network is under construction in Vietnam. Therefore, quite few GNSS stations measured continuously over long periods of time. Nevertheless, data from 11 GNSS stations (with continuous observation time of about 10 years) were used in this study (Figure 5.3). For 8 of them (named MTEV, MLAY, DBIV, SMAV, PHUT, VINH, HUES and BACL), a time series of heights processed with GNSS at MIT/Global Kalman Filter (GAMIT/GLOBK) software (King & Bock, 2009) were provided by the IGP–VAST. In addition, Receiver Independent Exchange Format (RINEX) data from 3 stations (named DSRS, QNRS and VTRS) provided by the Vietnam Department

of Surveying and Mapping (VDSM) and processed with GINS (Marty, 2009), the in-house software package developed by CNES (Centre National d'Étude Spatiales), using the Precise Point Positioning (PPP) methodology have been included to obtain time series of heights. The calculation results of all the stations are given in the reference frame ITRF2014.

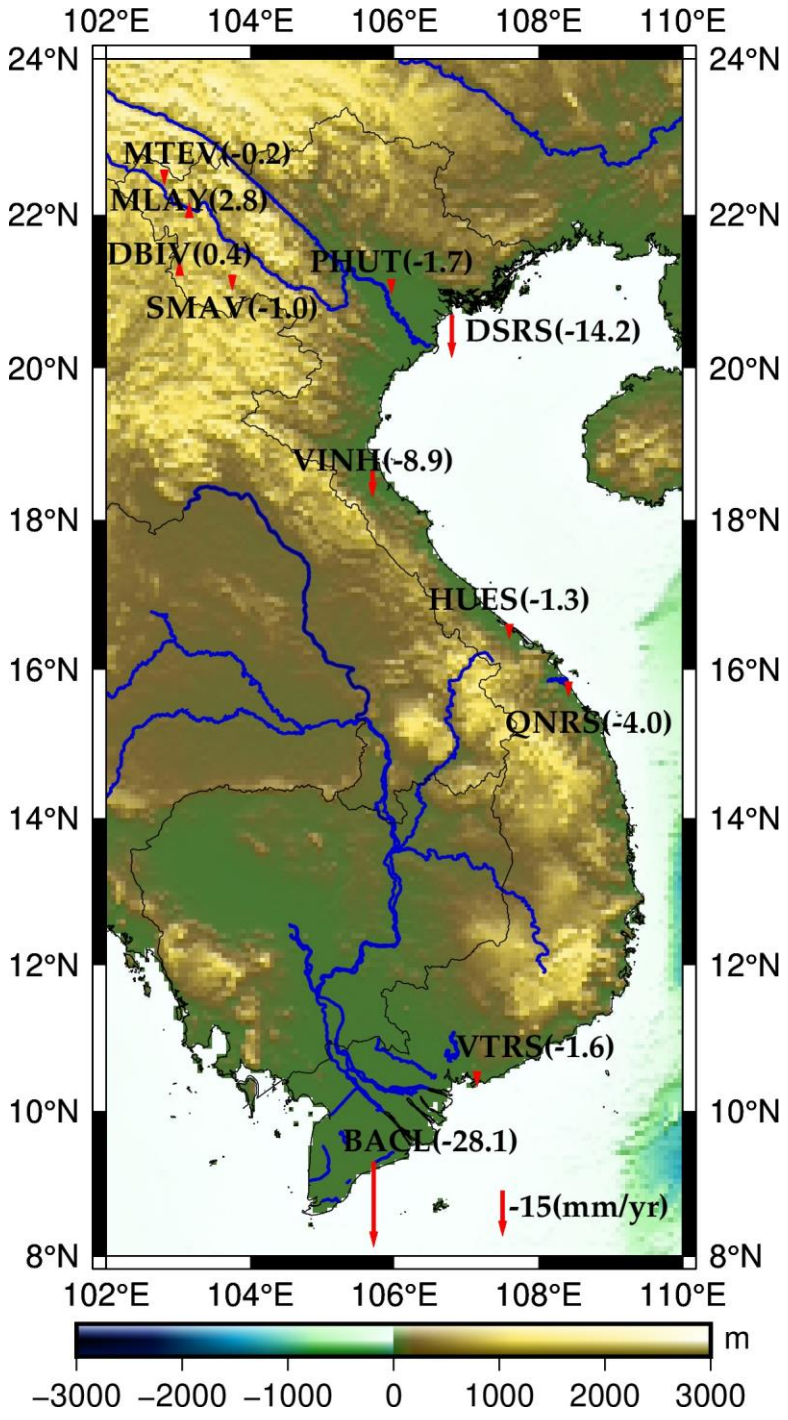

Figure 5.3. Vertical land motion rates from permanent GNSS stations

The annual average subsidence rates over the 2006-2010 period derived from a total of 121 ALOS-1 PALSAR images covering most of the Mekong Delta provided by Dr Laura E Erban (Erban et al., 2014) were used. These estimations are in good agreement with

ground-based measurements of land subsidence at hydraulic wells. The Sentinel-1 imagery time series over the 2015-2018 period for three areas Ca Mau (CM), Long Xuyen (LX) and Rach Gia (RG) situated in the Mekong delta were also used. These are available in the frame of the project "*EMSN057: Ground subsidence in Mekong Delta, Vietnam"* (Report of COPERNICUS, 2019). Average motion was estimated for every year from 2015 to 2018. From this, the annual subsidence for the period 2015-2018 is determined by simply averaging. The full description of the SAR processing for ALOS and Sentinel-1 data can be found in Erban et al. (2014) and project EMSN057 (Report of COPERNICUS, 2019), respectively.

5.3.2. Land subsidence and correcting GNSS/levelling data

The vertical land motion rates derived from permanent GNSS stations are shown in Figure 5.3, and the results of time series of heights are shown in appendix 4. The observation time is not continuous for two stations, DSRS and VINH, for which there are 2 or 3 long data interruptions (see appendix 4). Consequently, the results are not reliable for these two stations. A notable subsidence rate of -28.1 mm/year is observed for the BACL station, located in the Mekong Delta, whereas that of the remaining stations is only at the few mm/year level. As Mekong delta has been known to be deforming for decades, such a value is not surprising. Nevertheless, the length of the observation time span is too short (about 4 years from 2015 to 2019), and one should not disregard that the observed subsidence of the BACL station could be a local effect due to anthropogenic activity. It was then decided to carry out a careful analysis of ground displacement fields imaged by InSAR in the Mekong Delta.

The differences of GNSS/levelling and GEOID_LSC over the southern region are shown in Figure 5.4a. The linear regression on the differences is shown in Figure 5.4b. Ground displacement fields from InSAR confirms without ambiguity that subsidence affects the whole part of the Mekong Delta. The map of the annual average subsidence rates over the 2006-2010 period derived from ALOS-1 PALSAR provide useful indication about the structure and the magnitude of the subsidence affecting the Mekong Delta (Figure 5.4c). It shows that average subsidence rate of 1.6 cm/year for this delta with local extremes in the southeastern part over 2.5 cm/year. This result is in good agreement with land subsidence rate derived from BACL station (-28.1 mm/year). A southeast-northwest trend is evident in Figures 5.4b and 5.4c in the Mekong Delta with larger-rate subsidence in the southeast of this delta. In particular, Ho Chi Minh City (HCMC, blue ellipse in Figure 5.4a) where the highest rates (about 4 cm/year) were observed. However, a detailed analysis of HCMC by Minh et al. 2015 using ALOS-1 for the 2006-2010 period shows that average subsidence rate of HCMC is only 0.8 cm/year with larger-rate subsidence in the southwest of the city. This subsidence rate is in good agreement with the differences between the GNSS/levelling and the quasigeoid over HCMC. A slightly larger-rate of

subsidence can be seen in Figure 5.4a for HCMC than the surrounding areas. In addition, Sentinel-1 imagery time series confirms these estimations in some areas (Figure 5.4d).

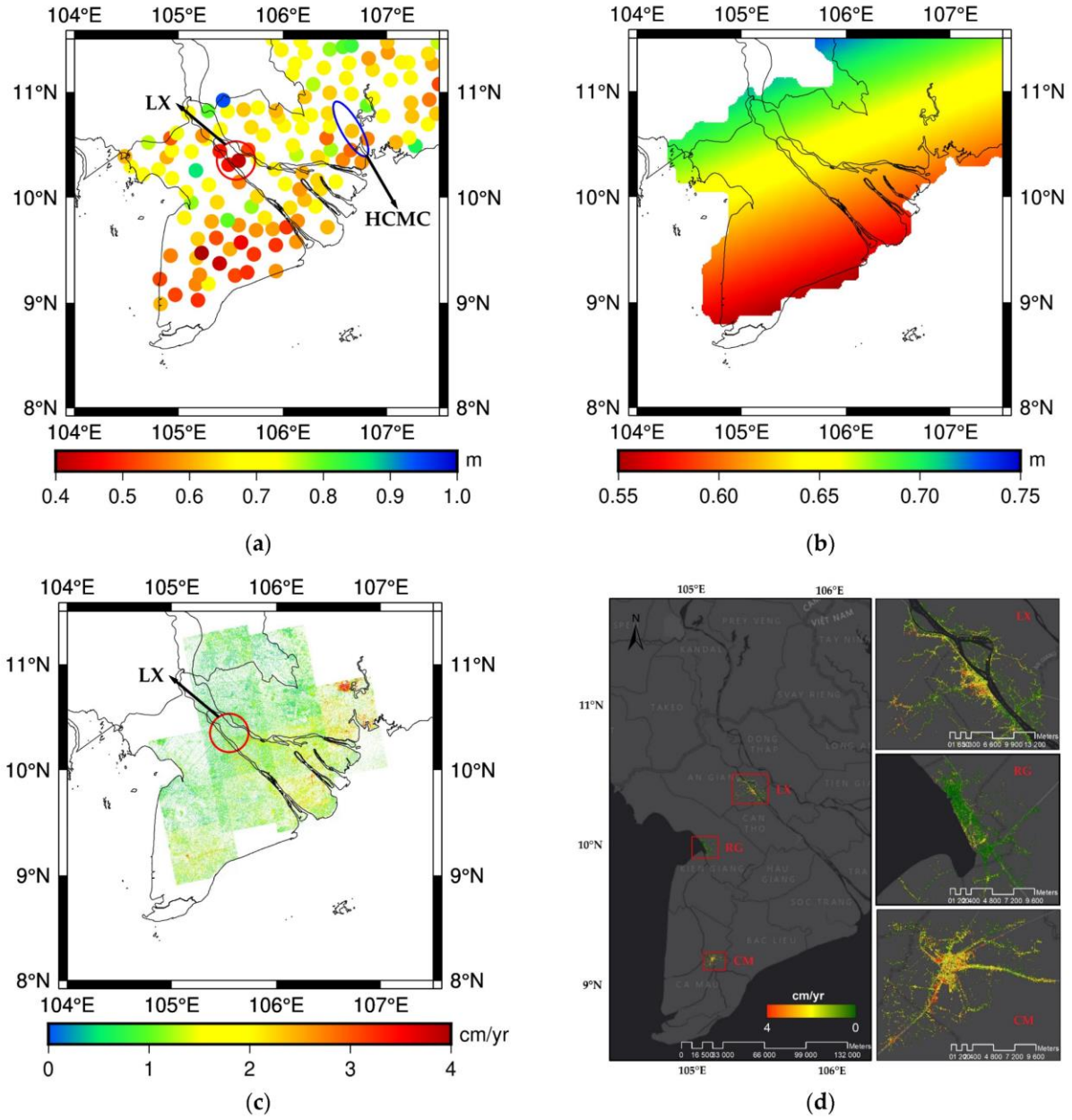

Figure 5.4. a) Differences of GNSS/levelling data and GEOID_LSC in the southern region; b) Linear regression on the differences of GEOID_LSC and GNSS/levelling data in the southern region; c) InSAR results derived for the period 2006-2010 from ALOS-1 (Erban et al., 2014) and d) InSAR results derived for the period 2015-2018 from Sentinel-1 (Report of COPERNICUS, 2019)

Good agreement between the results derived from ALOS-1, Sentinel-1 and quasigeoid in the areas CM and RG is shown in Figure 5.4. However, there is a slight inconsistency between the results derived from ALOS-1 and Sentinel-1 along the Mekong River, especially in the area LX (red circle in Figures 5.4a and 5.4c). The origin of this discrepancy is not known and could be due to a change in displacement rates between the 2006-2010

and the 2015-2018 periods, but there is better consistency between the result derived from Sentinel-1 and the quasigeoid over this area while GNSS and levelling were measured at the time closer to ALOS-1 than Sentinel-1. However, the salient fact is that the InSAR-based subsidence pattern appears to largely coincide with the trend pattern observed in the differences between the GNSS/levelling and the quasigeoid. All these observations strongly suggest that distortion in GNSS/levelling data of the southern region is mainly due to land subsidence, especially in the Mekong Delta. Obviously, the subsidence significantly affects the GNSS/levelling data as well as the offset model if it is determined without first correcting the GNSS/levelling points. To address this problem, the following approach and methodology are carried out.

The 683 GNSS/levelling points with latitudes greater than 11° are considered to be unaffected by subsidence. The height anomalies of these GNSS/levelling points were compared with those derived from the GEOID_LSC in the absolute sense. The results are listed in Table 5.3. Aiming for GNSS/levelling data of the same precision in the southern part (<11° in latitude), the GNSS/levelling height anomalies are corrected using the annual subsidence rate grid calculated with ALOS-1. To avoid affecting the edge, the remaining grid nodes (not calculated by ALOS-1) were set to zero. Height anomalies of 47 points were corrected considering a 7-year lag between levelling and GNSS measurement periods. On the height anomalies of GNSS/levelling points ($\zeta^{\mathrm{GNSS/levelling}}$), the correction was performed according to the following formula:

$$\zeta^{\mathrm{GNSS/levelling\_cor}} = \zeta^{\mathrm{GNSS/levelling}} + \mathrm{t.V} \qquad (5.4)$$

where V is the annual average subsidence rate of the GNSS/levelling point interpolated from the rate grid calculated from ALOS-1 SAR data, t is 7-year lag between levelling and GNSS measurement periods.

Table 5.3. Descriptive statistics of the differences between the GNSS/levelling data corrected in Mekong Delta and GEOID_LSC. [Unit: (m)]

	Mean	**STD**	**Max**	**Min**	**Outlier points**
$\zeta^{\mathrm{GNSS/levelling}} - \zeta^{\mathrm{LSC}}$ (Southern, <11°) (120 points)	0.634	0.092	0.937	0.402	
$\zeta^{\mathrm{GNSS/levelling}} - \zeta^{\mathrm{LSC}}$ (>11°) (683 points)	0.690	0.089	0.933	0.396	
$\zeta^{\mathrm{GNSS/levelling\_\mathbf{cor}}} - \zeta^{\mathrm{LSC}}$ (Southern, <11°) (120 points)	0.664	0.085	0.937	0.459	
$\zeta^{\mathrm{GNSS/levelling\_\mathbf{cor}}} - \zeta^{\mathrm{LSC}}$ (803 points)	0.686	0.089	0.937	0.396	1
$\zeta^{\mathrm{GNSS/levelling\_\mathbf{cor}}} - \zeta^{\mathrm{LSC}}$ (excluding outliers) (802 points)	0.687	0.088	0.937	0.423	

The corrected result is listed in Table 5.3. After the correction, the mean bias of the difference between GNSS/levelling data and GEOID_LSC in the southern part increases by 3 cm (mean bias before and after correcting are 0.634 m and 0.664 m, respectively). This mean is much closer to that in the remaining part of the country (0.690 m in 683 points with latitudes greater than 11°). The STD also decreases by 0.7 cm (STD before and after correcting are 0.092 m and 0.085 m, respectively). Thus, thanks to this rather approximate correction the accuracy of GNSS/levelling data in the southern part is more similar to data for the rest of the country. On all 803 points, the STD is slightly improved 0.3 cm (STD before and after correcting are 0.092 m and 0.089 m, respectively). Under the assumption of a normal distribution, 1 point is rejected. A total of 802 points with mean and STD of 0.687 m and 0.088 m, respectively, are retained for computation of the offset model.

5.4. Offset model determination methodology

The offsets ( ) can be decomposed into two components, the distortion and the residual. The former may contain long and/or medium wavelength errors of local gravimetric geoid model, and/or some bias and trends of GNSS/levelling height anomalies due to vertical crustal movements and systematic cumulative errors associated with levelling surveys over long distances. A schematic flow of the strategy is shown in Figure 5.5.

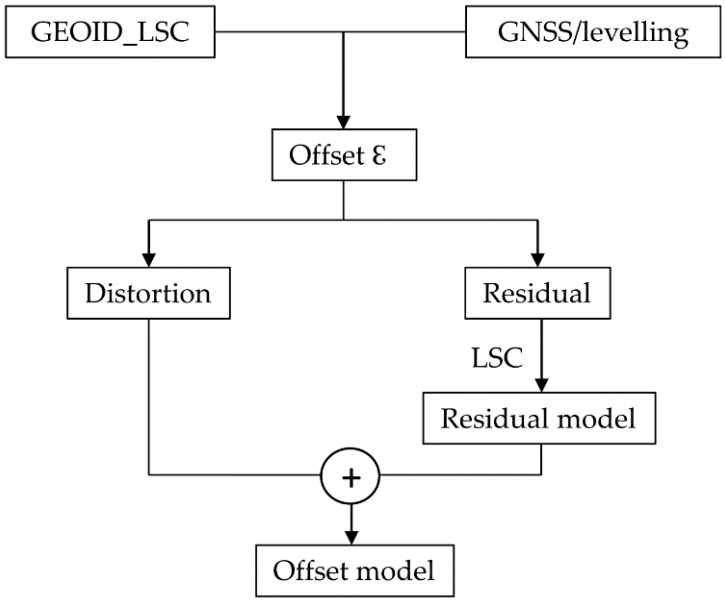

Figure 5.5. Schematic flow of offset model determination

In order to remove distortions in these offsets, a four parameter Helmert-type similarity transformation model is often employed for fitting gravimetric quasigeoid model to GNSS/levelling data (Iliffe et al., 2003; Forsberg & Tscherning, 2008). However, in the GNSS/levelling data of Vietnam inherent tilts may exist, so some models with parameters representing for spatial tilts, such as linear in φ and λ, 2^{nd} order polynomial, 3_{rd} order

polynomial, will also be tested:

¶ Linear in φ and λ model:

$$\varepsilon' = a_0 + a_1\varphi + a_2\lambda + \varepsilon \tag{5.5}$$

¶ 2nd order polynomial model:

$$\varepsilon' = a_0 + a_1\varphi + a_2\lambda + a_3\varphi^2 + a_4\varphi\lambda + a_5\lambda^2 + \varepsilon \tag{5.6}$$

¶ 3rd order polynomial model:

$$\varepsilon' = a_0 + a_1\varphi + a_2\lambda + a_3\varphi^2 + a_4\varphi\lambda + a_5\lambda^2 + a_6\varphi^3 + a_7\varphi^2\lambda + a_8\varphi\lambda^2 + a_9\lambda^3 + \varepsilon \tag{5.7}$$

¶ four parameter Helmert model:

$$\varepsilon' = a_1 cos\varphi\, cos\lambda + a_2 cos\varphi\, sin\lambda + a_3 sin\varphi + a_4 + \varepsilon \tag{5.8}$$

After removing distortions from the offsets of GNSS/levelling points residual offsets (Δ = - ') will be obtained, these residuals will be then interpolated to a 5' grid with LSC using the GRAVSOFT GEOGRID program. The covariance function was evaluated using a second-order Gauss Markov model as:

$$K_N(\rho) = K_o(1 + A\rho)e^{-A\rho} \tag{5.9}$$

where, K_o is the variance of the observations Δ ; A is a parameter related to the correlation length; ρ is the distance measured in km. An offset model is created by adding the residual offset to the distortion component. Thus, a gravimetric quasigeoid model and an offset model on 5' grids can be determined. The normal height at a point is then obtained as:

$$\mathrm{H}^* = \mathrm{h} - \zeta - \varepsilon \tag{5.10}$$

where, the gravimetric quasigeoid height anomaly (ζ) and offset ( ) are interpolated from the grids.

Most often, the same GNSS/levelling data are used both to create and test the hybrid model. This strategy is flawed because it is insensitive to errors in the GNSS/levelling data. Specifically, any error in the GNSS/levelling data will cause the same error in the combined model. However, this error will not be apparent when compared to the same GNSS/levelling data (the error of the hybrid quasigeoid in this case is only a few centimeters, this will be clarified in the following section). Therefore, a cross-validation technique is used in this study, in which one GNSS/levelling point at a time is omitted from each offset model prediction, and that point is then used to assess the hybrid model. This is repeated for all points in the dataset. Importantly, this gives a more objective

assessment of the gravimetric quasigeoid and vertical offset model.

5.5. Vertical offset model estimation

Thanks to the offset modelling into two components (distortion and residual), the distortions for different regions instead of calculation the homogeneous distortion parameter for the entire country can be calculated. As a result, the residuals will be smaller. Figure 5.1a indicates that there are two distinct distortions between the two parts, one in the northern part (>17° in latitude) and another for the southern one. In the following section, distortion and residual will be calculated to determine two offset models as follows:

- using all 802 GNSS/levelling points and calculation the homogeneous distortion parameter (case 1);
- using all 802 GNSS/levelling points and calculation two distortion parameters for two regions: southern (<17° in latitude) and northern part (>17° in latitude) (case 2).

On the other hand, to select the best model for removing distortions in the differences between GNSS/levelling data and the GEOID_LSC model, all 802 GNSS/levelling points (case 1) are used to calculate the distortion employing the four models which were shown in Section 5.4. The results of residuals are listed in Table 5.4. The third-order polynomial model had the highest precision with an STD of 0.082 m. The fourth- and fifth-order polynomial models were also used to remove the distortions, but the STD was not significantly improved, i.e., 8.1 cm for these two models. Moreover, a height-dependent parameter (Kotsakis et al., 2012) was also added into the third-order model to remove the distortions, but STD had no improvement, i.e., 8.2 cm with the third-order model added height-dependent parameter, because Kotsakis et al., (2012) and Hayden et al., (2013) warned that using this parameter will only be successful in the region that has a significant height variability. The third-order model will be used to calculate the distortions for case 2, i.e., two distortion parameters for two different regions. The STDs of case 1 with one distortion parameter for the entire country and case 2 calculating two different distortion parameters for two regions were 8.2 and 7.8 cm, respectively. Thanks to calculating the distortions for different regions, more accurate results are obtained (0.4 cm). Six GNSS/levelling points were detected with large residuals. These points were rejected from the computation according to the assumption of a normal distribution. Therefore, 796 points with STD of 7.5 cm will be used to calculate the offset model. The distortions and residuals in this case are shown in Figures 5.6a and 5.6b.

Table 5.4. Residual of the differences between GNSS/levelling data and GEOID_LSC model. Unit: (m)

	Mean	STD	Max	Min	Outlier Points
Linear (802 points)	0	0.087	0.285	−0.296	
Second-order (802 points)	0	0.085	0.265	−0.326	
Third-order (802 points)	0	0.082	0.262	−0296	
Helmert model (802 points)	0	0.086	0.285	−0.316	
case 2 (Third-order) (802 points)	0	0.078	0.252	−0.288	6
case 2 (Third-order) outlier (796 points)	0	0.075	0.225	−0.223	

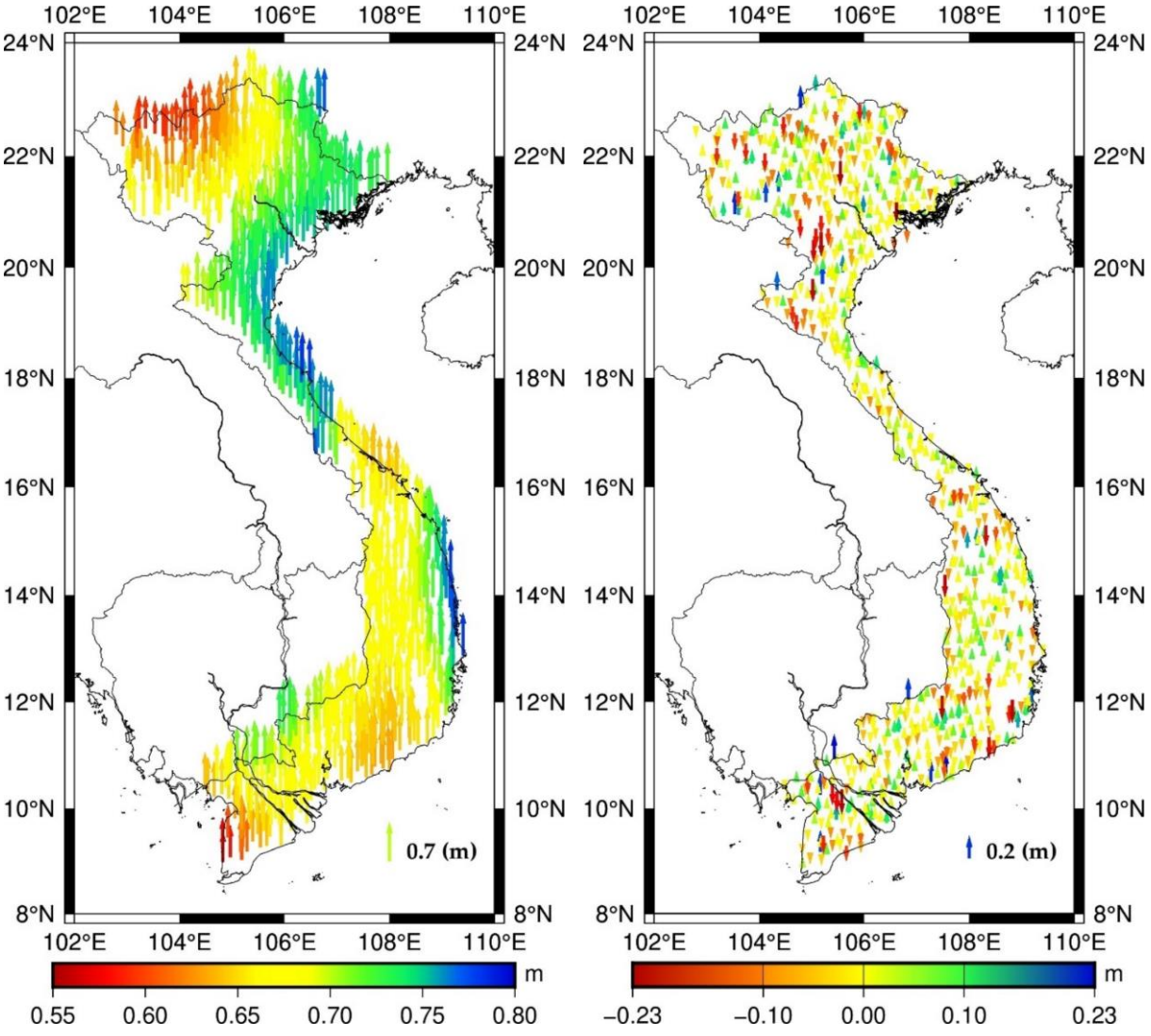

(a) (b)

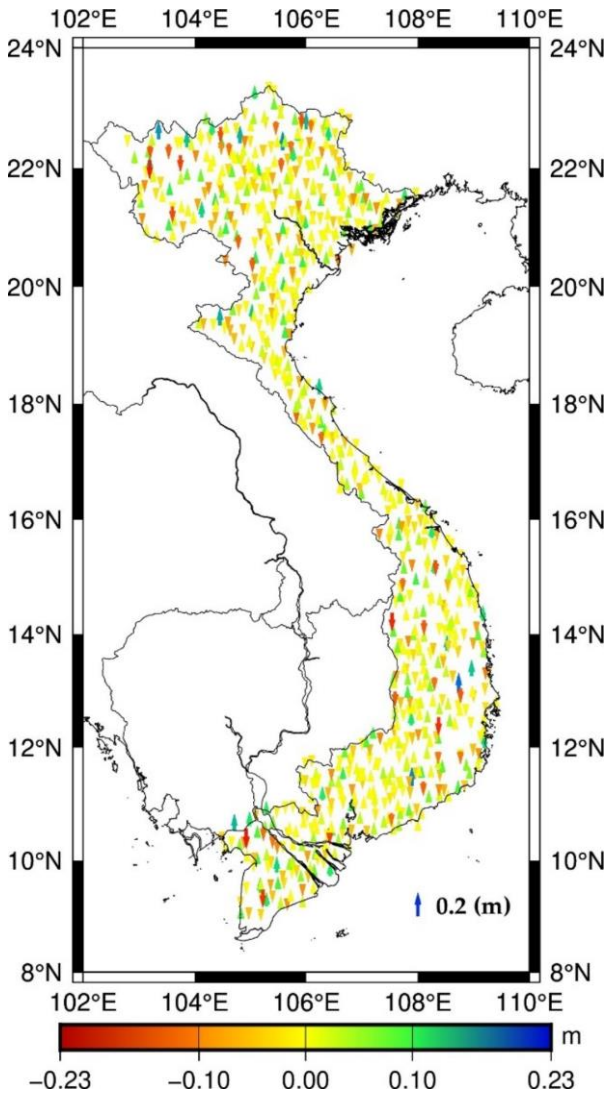

(c)

Figure 5.1. a) Distortions, b) residuals and c) differences between the 779 GNSS/levelling points and gravimetric quasigeoid model adding offset model

From the residuals calculated above, the LSC method in GRAVSOFT GEOGRID program was used to interpolate to a 5' grid. Computation of the empirical and fitted covariance functions of the residual height anomalies is required in LSC. The empirical covariance of the data has been computed and then fitted to the second-order Gauss Markov model (Eq. (5.9)). A correlation length of 16 km was found. The GRAVSOFT GEOGRID program was used to simulate employing 796 residual height anomalies with the correlation lengths of 10, 16, 30 and 40 km. The best result was obtained when the correlation length was 30 km. Therefore, a correlation length of 30 km was used to calculate a 5' grid of the residual height anomalies. An offset model was then created by adding residual offset to the distortion component. The cross-validation technique was used to assess the gravimetric quasigeoid and offset model employing GNSS/levelling points with 796 LSC runs in this case.

Table 5.5 shows the absolute differences between the 796 GNSS/levelling points and gravimetric quasigeoid model adding offset model. The descriptive statistics for the cross-validation technique are presented (first row), with the STD being 0.065 m. The outliers were determined according to the assumption of a normal distribution. There were 17 points that were rejected. So, a total of 779 points was used to calculate and validate the models. The case when all the GNSS/levelling data (779 points) were used to create and test the offset model was also presented (third row). Using all the GNSS/levelling data to create and test the offset model had an STD of 0.034 m, whereas using the cross-validation technique had an STD of 0.059 m. This demonstrates the importance of applying a cross-validation technique, which gives a more realistic error estimate than the pure fit statistics. The results are shown in Figure 5.6c.

Table 5.5. Descriptive statistics of the differences between the GNSS/levelling data and gravimetric quasigeoid adding offset model with baseline length < 100 km. Unit: (m)

Absolute Differences					
	Mean	**STD**	**Max**	**Min**	**Outlier Points**
$\zeta^{GNSS/levelling} - \zeta^{LSC}$ (796 points) (cross-validation)	0	0.065	0.250	−0.291	17
$\zeta^{GNSS/levelling} - \zeta^{LSC}$ (779 points) (excluding outliers) (cross-validation)	0	0.059	0.170	−0.170	
$\zeta^{GNSS/levelling} - \zeta^{LSC}$ (779 points)	0	0.034	0.099	−0.109	
$\zeta^{GNSS/levelling} - \zeta^{LSC}$ (Hanoi) (32 points)	−0.004	0.047	0.109	−0.092	
$\zeta^{GNSS/levelling} - \zeta^{LSC}$ (HCMC) (29 points)	−0.001	0.055	0.104	−0.139	

Relative Differences						
	Mean	**STD**	**Max**	**Min**	**Outlier 3rd Order**	**Outlier 4th Order**
$\Delta\zeta^{GNSS/levelling} - \Delta\zeta^{LSC}$-Δ (779 points) (20,243 baselines)	0.026	0.020	0.109	0	377 (1.86%)	14 (0.07%)
$\Delta\zeta^{GNSS/levelling} - \Delta\zeta^{LSC}$-Δ (Hanoi) (469 baselines)	0.024	0.018	0.074	0.003	8	0
$\Delta\zeta^{GNSS/levelling} - \Delta\zeta^{LSC}$-Δ (HCMC) (384 baselines)	0.025	0.019	0.085	0.085	13	0

Table 5.5 also shows the descriptive statistics for the relative case, using 779 GNSS/levelling points. The results indicated that the gravimetric quasigeoid model plus the offset model can be used to convert ellipsoidal heights to local normal heights with an accuracy that complies with fourth-order levelling specifications for the whole of Vietnam (99.93%), while 98.14% of the baselines complied with third-order levelling specifications. This suggests that these models allow GNSS levelling to comply with third-order levelling specifications over most of Vietnam, except for some mountainous areas where quality and distribution of gravity data were not good. Especially over the areas of

the two major cities of Vietnam, Hanoi (20.5° to 21.5° in latitude, 105° to 106° in longitude) and HCMC (10° to 11° in latitude, 106° to 107° in longitude), the third-order levelling network specifications were met with only 8/468 and 13/384 baselines, respectively, out of specifications.

5.6. Background for the unification of height systems

An LVD is considered as an equipotential surface defined by a geopotential value (W_0^{LVD}); hence, in the traditional sense of height systems, W_0^{LVD} is the potential of the MSL. As mentioned, more than 100 LVDs exist in the world today, so unification of these vertical datums is required to implement engineering projects between countries and improve flooding observations and modeling at regional scales. Even at the national scale, the Vietnam LVD is only valid for the continental territory but not for the islands and territorial waters of Vietnam. Thanks to the high-resolution GEOID_LSC model, the height can be determined for the whole islands towards unifying the height references for Vietnam. Moreover, this model is also used in combination with high-quality GNSS/levelling data (referring to the VLVD) for estimating the gravity potential value of the VLVD to connect the height system of Vietnam with that of the neighboring countries. According to the International Association of Geodesy (IAG) resolution No.1, 2015 (Drewes et al., 2016), the international conventional reference gravity potential, denoted by W_0, is considered equal to 62,636,853.4 m^2s^{-2} (Sánchez et al., 2016). From this value, Height System Unification (HSU) can be realized to connect height systems together by determining potential differences or gravity potentials referring to this conventional value (Rapp & Balasubramania, 1992; Ihde et al., 2000; Grigoriadis et al., 2014; Vergos et al., 2018). Knowing the gravity potential of LVD, the gravity potential difference of every LVD and the LVD offset values between all the LVDs can be determined. Therefore, determining the gravity potential value of LVD plays an important role in the HSU. Thanks to the availability of the GNSS/levelling data and the GEOID_LSC model, the geopotential value can be determined for the VLDV using the differences in height anomalies derived from them. Moreover, the gravity potential value can be directly determined based on the GBVP approach using the available gravity data. Besides estimation of the geopotential, its variation in time ($\dot{W}$) should also be determined from this approach. This is an advantage of the GBVP approach in building a modern height system. In this thesis, two approaches will be used to determine the geopotential value for Vietnam.

5.7. Estimation of the geopotential value using gravimetric quasigeoid and GNSS/levelling data

The geopotential number (C) is the potential difference between an equipotential surface (W_i) and a reference equipotential surface. National vertical datum from traditional levelling realizes by selecting as their zero-point O a coastal tide gauge and setting it a

geopotential value W_0^{LVD}, while a geoid/quasigeoid model realizes the origin of a global vertical datum (W_0). The geopotential number for point *i* can be written as (Tocho & Vergos, 2016; Vergos et al., 2018):

$$C_i = W_0 - W_i \tag{5.11}$$

$$C_i^{LVD} = W_{0,\mathrm{i}}^{LVD} - W_i \tag{5.12}$$

where C_i^{LVD} is referring to a LVD reference surface (W_0^{LVD}) while C_i is referring to global vertical datum (W_0). Their difference (δW^{LVD}) at given i points can be given from Equations (5.11) and (5.12):

$$= C_i - C_i^{LVD} = W_0 - W_{0,\mathrm{i}}^{LVD} \tag{5.13}$$

Therefore, the zero-height geopotential for the LVD can be determined from Eq (5.13) if the geopotential number difference δW^{LVD} is known. Over the GNSS/levelling points these difference values can be calculated based on the differences between height anomalies from GNSS/levelling measurements and those derived from GEOID_LSC i.e., the offset value in Eq (5.2), and the mean normal gravity value ($\bar{\gamma}$) is computed by Equation (4-60) in Hofmann-Wellenhof and Moritz (2006):

$$\delta W_i^{LVD} = \varepsilon_i \bar{\gamma}_i \tag{5.14}$$

Consequently, the mean zero-height geopotential value for the LVD can be determined by simply averaging of $W_{0,\mathrm{i}}^{LVD}$:

$$W_0^{LVD} = \frac{\sum_{i=1}^{m} W_{0,\mathrm{i}}^{LVD}}{m} = W_0 - \frac{\sum_{i=1}^{m} \delta W_i^{LVD}}{m} = W_0 - \delta W^{LVD} \tag{5.14}$$

where m is the number of the GNSS/levelling points.

It should be noted that the indirect bias term, due to the unknown offset value of LVD, is affecting the GEOID_LSC model and hence, it also affects the potential difference as well as geopotential value estimated using this quasigeoid model. This problem will be calculated and clarified for this region in the next section.

Given the preceding analysis, distortions i.e., tilts and biases, existed in the GNSS/levelling data; hence, they should be removed from the observations in the computation of . However, only tilts were removed here because the datum offset between LVD and reference equipotential surface should be retained in this case. Equation (5.2) is rewritten as follows:

$$\bar{\varepsilon} + a_i^T \mathrm{x} + v_i = \zeta_i^{GNSS/levelling} - \zeta_i - \zeta_0 \quad (5.16)$$

where $\bar{\varepsilon}$ is mean of the differences between height anomalies from GNSS/levelling measurements and those derived from GEOID_LSC (ε_i). It is a tilted offset of VLVD (this offset value that differs from the true LVD offset value) because the tilts exist in the levelling data. The term a_i^Tx absorbs the tilts, and v_i represents the random error of the height anomalies.

Therefore, the third-order polynomial model was also used for removing tilt effects. However, it should be noted that this model should not contain any constant components to retain the datum offset, which in turn implies that the constant term a_0 must be omitted in this computation. The height anomalies from good 779 GNSS/levelling points after correcting the subsidence for the Mekong Delta was used for estimating W_0^{LVD}. Calculation of two tilt parameters for two regions, southern (<17° in latitude) and northern part (>17° in latitude), was also used in this case. The results are shown in Table 5.6 where the improvement in the STD between the null and third-order model with two parameters was significant. Therefore, the results calculated from the third-order model with two parameters were used to estimate W_0^{LVD} employing Equation (5.14). A gravity potential W_0^{LVD} = 62,636,846.81 ± 0.70 m^2/s^2 for the LVD of Vietnam has been determined as an offset to the equipotential surface realized by the conventional value W_0 = 62,636,853.4 m^2/s^2.

Table 5.6. Descriptive statistics of the differences between the GNSS/levelling data removed tilt effects and GEOID_LSC. Reference geopotential values W_0^{LVD} for the VLVD with the global reference level realized by the conventional value W_0 = 62,636,853.4 m^2/s^2. Unit: (m)

	Mean	**STD**	**Max**	**Min**
Null model	0.688	0.083	0.912	0.435
Third-order	0.693	0.075	0.897	0.458
Third-order (two parameters)	0.689	0.071	0.902	0.478
δW^{LVD}(m^2/s^2)	6.60 ± 0.70	W_0^{LVD}	62,636,846.81 ± 0.70	

5.8. Estimation of the geopotential value using the Geodetic Boundary Value Problem (GBVP) approach

Until relatively recently, reference datums in the world were invariable in time, and "control points" in such reference datums were generally considered stable and reliable over decades. With the advent of space geodesy, observations can be performed to understand the physical changes occurring on the Earth and to realize a dynamic reference datum. A dynamic International Terrestrial Reference System (ITRS) and its

realization, the International Terrestrial Reference Frame (ITRF), based on a global network of Satellite Laser Ranging (SLR), Lunar Laser Ranging (LLR), Very Long Baseline Interferometry (VLBI), and Doppler Orbitography and Radio-positioning Integrated by Satellite (DORIS) stations co-located with Global Navigation Satellite System (GNSS) (Altamimi et al., 2002; Altamimi & Collilieux, 2009), indicated change in such control points at the level of centimeters per year. At the request of the International Association of Geodesy (IAG) resolutions (Drewes et al., 2016), the IHRF, a realization of the International Height Reference System (IHRS) is also defined and realized following the same structure as that of the ITRF (Ihde et al., 2017). The IHRS/IHRF includes a geometric component given by a coordinate vector (X) in ITRS/ITRF and a physical component given by the determination of the potential value (W) or potential difference (C) with respect to the conventional value (W_0) at (X). According to Resolution No. 1 of the IAG (Drewes et al., 2016), the international conventional reference gravity potential is equal to 62,636.853.4 m^2/s^2 (Sánchez et al., 2016) for the purpose of implementing the IHRS. Moreover, besides estimation of the physical component, its variation in time ($\dot{W}$) should also be determined like the variation in the geometric component ($\dot{X}$) in the ITRF, to continuously monitor deformation as well as regularly update the height reference frame. Temporal geometric height changes can be accurately determined from observations on permanent GNSS stations whilst deformation of the topography around these GNSS stations can be estimated by InSAR. Thus, the variation of the geopotential value in time can be determined (even if imperfectly because of mass change in the crust, e.g. aquifer depletion) on these GNSS CORS. Therefore, this realization should be conducted on the GNSS-CORS stations as reference points, i.e., estimation of geopotentials and their variations at these stations on the Earth's surface but not on the geoid or quasigeoid. In 2017, the first proposal for the IHRF reference network included 163 stations co-located with GNSS worldwide, but with poor coverage in particular over Africa and Asia (Sánchez, 2017 and Sánchez, 2019). Presently, the IHRF is still the issue of discussion and studied for implementation (Ihde et al., 2017 and Sánchez, 2019). At the national or regional scale, despite vertical movement of the Earth, most countries do not model the vertical datum change. The US National Geodetic Survey (NGS), a pioneer in the matter, is in the process of building a dynamic vertical datum for North America by providing a dynamic component of the geoid through the Geoid Monitoring Service. The project is expected to be published in 2022 (report of NGS, 2019). Together with the realization of the IHRS on a global scale, the implementation of the IHRS on the GNSS-CORS stations on a national or regional scale is an important task in which the determination of potential plays a key role. It may contribute to increase the density of reference points in the IHRF, especially over poorly covered areas.

There are two categories that should be considered in potential changes with time: 1)

changes in potential related to MSL rise and 2) changes in mass redistribution leading to potential variations. The geoid is the equipotential surface which best fits to Global Mean Sea Level (GMSL) (Gauss, 1828; Listing, 1873). However, presently GMSL is rising at a rate of approximately 3.2 millimeters per year (IPCC, 2014), so the value of the gravity potential (W_0) should also change to maintain the best fit to GMSL. The variation of gravity potential caused by sea level rise was studied by Burša et al., (1997), Ardalan et al., (2002), Burša et al., (2007) and Dayoub et al., (2012). Sánchez et al., (2016) recommended using a potential value obtained for a certain epoch as the reference value W_0 and monitoring the changes of the MSL i.e., changes in potential value at the sea surface W_S. When large differences appear between W_0 and W_S (e.g., > 2 m^2/s^2), the adopted W_0 should be updated. At national or regional level, LVD refers to local MSL. Analogously, the geopotential of a LVD (W_0^{LVD}) should also change in order to accommodate the change in local MSL. The second category is the focus of this study. Change in elevation, e.g., due to land subsidence, will lead to changing redistribution of masses within the Earth, and its gravity field will change as well. One has to re-measure gravity to determine these changes, but like levelling this is a costly and time consuming effort. Therefore, an alternative method is applied in this study, which is based on forward modelling residual terrain effects to determine temporal gravity variations as well as disturbing potential variations due to observed changes in topography.

The geopotential value for the LVD of Vietnam was estimated using local gravimetric-only quasigeoid and GNSS/levelling data in Section 5.7. However, tilts, caused by accumulated systematic levelling errors and land subsidence, existed in the GNSS/levelling data. The latter effects have been partly corrected through modelling based on the land subsidence derived from InSAR, but residual effects, due to the inconsistency between levelling and GNSS measurements (e.g., differences in accuracy level and tide systems (Sánchez, 2012)), remain in the GNSS/levelling data. Based on the GBVP approach (Hofmann-Wellenhof & Moritz, 2006), the geopotential value on the surface can be directly determined using the gravity data without height anomalies derived from GNSS/levelling data. As a result, the inconsistency that existed between the levelling and GNSS measurements is completely removed.

In this thesis, the zero-height geopotential value of the LVD is firstly determined on the GNSS/levelling points using the GBVP approach to validate the proposed method as well as to show its advantages by comparing with the results derived from the GNSS/levelling data and gravimetric-only quasigeoid in Section 5.7. Then the GBVP approach will be used for determination of geopotential values including variations in time on GNSS-CORS stations. This work aims to prepare the integration of the existing national height system of Vietnam into the IHRS. It also contributes to enhancing the density and distribution of IHRF stations in this part of the world, where the IHRF has few reference stations.

In the GBVP approach, the geopotential value is directly determined based on the normal potential (U_P) and the disturbing potential (T_P) as follows:

$$W_P = U_P + T_P \tag{5.17}$$

The normal potential is computed with the reference level ellipsoid (Hofmann-Wellenhof & Moritz, 2006), and the disturbing potential is determined based on the GBVP approach using the gravity data. In this approach, the core is to determine the disturbing potential value by the GBVP approach applying the RCR technique (Sansò & Sideris, 2013; Barzaghi, 2016) will be described in Section 5.8.1. Thanks to the GOCE (Drinkwater et al., 2003b), GGMs with an accuracy of 1–2 cm and gravity field models with an accuracy of 1 mGal at a spatial resolution of approximately 100 km are available to compute potential values. In this thesis, terrestrial gravity data is used to reduce the omission error of the GOCE model by increasing its resolution. Using the modern theory of Molodensky (Molodensky, 1962) in the GBVP approach, the determination of W_P is straightforward on the Earth's surface, and is unaffected by levelling errors or inconsistency between levelling and GNSS measurements. Additionally, from the potential values (W_P) on the reference points, the zero-height geopotential value of LVD (W_0^{LVD}) can be determined based on the physical height of these reference points.

From the geopotential values on the surface (W_i) of each point i, the zero-height geopotential value for the LVD (W_i^{LVD}) on this point can be determined based on physical height (H^*) as follows:

$$W_i^{LVD} = W_i + H_i^* \bar{\gamma}_i \tag{5.18}$$

where $\bar{\gamma}$ is the mean normal gravity value along the plumb line from the reference ellipsoid to the telluroid (Hofmann-Wellenhof and Moritz, 2006) [Eq. 4-60]. For each GNSS/levelling point, a geopotential value can be calculated, and the zero-height geopotential value for the LVD is obtained by averaging:

$$W_0^{LVD} = \frac{\sum_{i=1}^{m} W_i + H_i^* \bar{\gamma}_i}{m} \tag{5.19}$$

The zero-height gravity potential value is calculated from physical heights, but not height anomalies. This is advantageous since only the normal heights (H^*) are taken into account, thereby avoiding any errors due to inconsistency in the difference between GNSS ellipsoidal height (h), physical height derived from levelling and quasigeoid height (ζ). Moreover, this approach is impervious to the effects of land subsidence which occurred during the temporal separation between GNSS and levelling measurement.

5.8.1. Determination of the disturbing potential based on the GBVP approach

As mentioned, in the GBVP approach, the disturbing potential needs to be estimated. Stokes' formula Eq. (2.34) derived from the boundary condition Eq. (2.28) is used to

determine the disturbing potential from gravity data. The Free-air terrestrial gravity anomalies are derived from measured gravity (g) and normal gravity (γ). The Free-air reduction is calculated from the normal height (for the purpose of gravity reduction from the surface to the quasigeoid) according to Hofmann-Wellenhof and Moritz (2006) is:

$$\Delta g = g - \frac{\partial \gamma}{\partial H^*} H^* - \gamma = g + \frac{2\bar{\gamma}}{r}\frac{C}{\bar{\gamma}} - \gamma = g + \frac{2C}{r} - \gamma \qquad (5.20)$$

The normal height (H*) is biased due to datum offset (δH^*) between LVD and the global equipotential surface, so the gravity anomalies will also be biased by:

$$\Delta g^b = \frac{\partial \gamma}{\partial H^*}\delta H^* = -\frac{2\bar{\gamma}}{r}\frac{\delta W^{LVD}}{\bar{\gamma}} = -\frac{2\delta W^{LVD}}{r} = 0.3086\ \delta H^* \qquad (5.21)$$

So, it should also be pointed out that

$$\Delta g^{ub} = \Delta g - \Delta g^b = \Delta g + \frac{2\delta W^{LVD}}{r} = \Delta g - 0.3086\ \delta H^* \qquad (5.22)$$

is the unbiased (ub) gravity anomaly after correction for the datum offset.

Insertion of (5.22) into (2.34) gives:

$$T = \frac{G\delta M}{R} + \frac{R}{4\pi}\iint_\sigma (\Delta g - 0.3086\delta H^*)\, S(\psi) d\sigma \qquad (5.23)$$

Setting $T_0 = \frac{G\delta M}{R}$ is called zero-degree term of the disturbing potential (Hofmann-Wellenhof and Moritz, 2006), $T^{Stokes} = \frac{R}{4\pi}\iint_\sigma \Delta g\, S(\psi) d\sigma$, and $T^{ind} = \frac{R}{4\pi}\iint_\sigma \frac{2\delta W^{LVD}}{R} S(\psi) d\sigma$ is called the indirect bias term, which is affected by the offset from local (W_0^{LVD}) to global datum (W_0). Eq. (5.23) can now be expressed as follows:

$$T = T_0 + T^{Stokes} + T^{ind} \qquad (5.24)$$

The datum offset δH^* is unknown prior to height unification and only the biased anomalies Δg can be used to determine disturbing potential from terrestrial gravity data. So T^{ind} cannot be calculated. Amos & Featherstone, (2009) have solved this issue by determining and correcting datum offsets for different local datums in New Zealand in an iterative manner. In this study, the effect of the indirect bias term will be assessed for Vietnam and its surrounding areas through simulation, presented in Section 5.8.2.

The RCR technique is used to calculate T^{Stokes}. It is realized by summation of three terms:

$$T^{Stokes} = T_{GGM} + T_{RTM} + T_{res} \qquad (5.25)$$

where T_{GGM} is computed using a GGM, T_{RTM} expresses the RTM effect (Forsberg, 1984), and T_{res} is computed from residual gravity anomalies employing the Stokes' integral Eq. (2.34). The residual gravity anomalies for determining T_{res} are computed using Eq. (2.43). Like the residual height anomaly, the residual disturbing potential obtained from Stokes' integral with Stokes kernel should be modified to reduce truncation errors (Molodensky

et al., 1962; Witte, 1967; Wong & Gore, 1969; Meissl, 1971; Heck, 1987; Vaníček & Sjöberg, 1991 and Featherstone et al., 1998). The WG modification (Eq (2.35)) is commonly used. A program was developed for computation of the disturbing potential by means of Stokes' integration employing the WG modification of the Stokes' kernel function using Free-air gravity anomaly data on the surface according to Molodensky's theory.

5.8.2. Effect of omission error and indirect bias effect

Several recent studies have been done on the effects of indirect bias on the HSU for different regions in the world e.g., in Europe (Gerlach & Rummel, 2013) and North America (Amjadiparvar et al., 2016). Its effect on the estimated disturbing potential for this study region is also determined. The datum offset value (δH^*) was estimated in the previous section at 69 cm with the global equipotential surface realized by the conventional value W_0 = 62,636853.4 m^2/s^2. This offset value was used for simulation data, in which terrestrial gravity anomalies are biased according to: $\Delta g^b = 0.3086\ \delta H^* \approx$ 0.2 (mgal). The simulation data are made as follows: the grid points derived from the land gravity points (red dots on Figure 3.5) are set to 0.2 (mGal), while the remaining grid points (fill-in and tapered grids) are set to 0 (mGal). Here, the fill-in grid points derived from a global model are assumed to do not have a datum offset. It should be noted that the red dots lying on the surrounding areas i.e., Thailand, China, Laos and Cambodia (Figure 3.5) are also set to 0. Firstly, the indirect bias term is computed using the Stokes integral (Eq (2.34)) with the original Stokes kernel. The results are shown in Figure 5.7a and listed in Table 5.7. The effect computed using the original Stokes kernel is significant and ranges from 0 to 0.386 m^2/s^2. Secondly, the indirect bias term is computed with different modified-degree kernels. The results are listed in Table 5.7 and shown for two cases in Figures 5.7b and 5.7c. The effect decreases for higher degrees of truncation. The indirect bias term is less than 0.1 m^2/s^2 (equivalent to 1 cm) for all truncation degrees higher than 60. Therefore, with the aim of determining the height reference system with cm level accuracy, the indirect bias term value can be safely neglected if the GGM is used in the computation of the disturbing potential to degree higher than 60. According to the study done by Gerlach & Rummel, (2013) for Europe, this value is smaller than 1 cm when a GGM is used in the RCR technique and the residual geoid undulation is computed using a modified Stokes kernel with degree of GGM n > 200. Similarly for North America, Amjadiparvar et al., (2016) recommended using n > 180 for omitting this indirect effect. The degree of truncation in this study is smaller because the offset value of this study region is smaller e.g., for Alaska it is 148 cm, for Belgium 232 cm while for Vietnam it is 69 cm, furthermore, here the smoother WG modification was used for the Stokes' kernel (Amjadiparvar et al., 2016).

Table 5.7. Indirect bias effect term on disturbing potential (unit: m^2/s^2)

Truncation degree	Min	Max	Mean	STD
N_1=0; N_2=0	0	0.386	0.089	0.097
N_1=50; N_2=60	-0.020	0.110	0.015	0.033
N_1=60; N_2=70	-0.031	0.088	0.007	0.027
N_1=100; N_2=110	-0.055	0.041	-0.007	0.015
N_1=150; N_2=160	-0.030	0.030	-0.002	0.009
N_1=220; N_2=230	-0.026	0.026	0.002	0.006

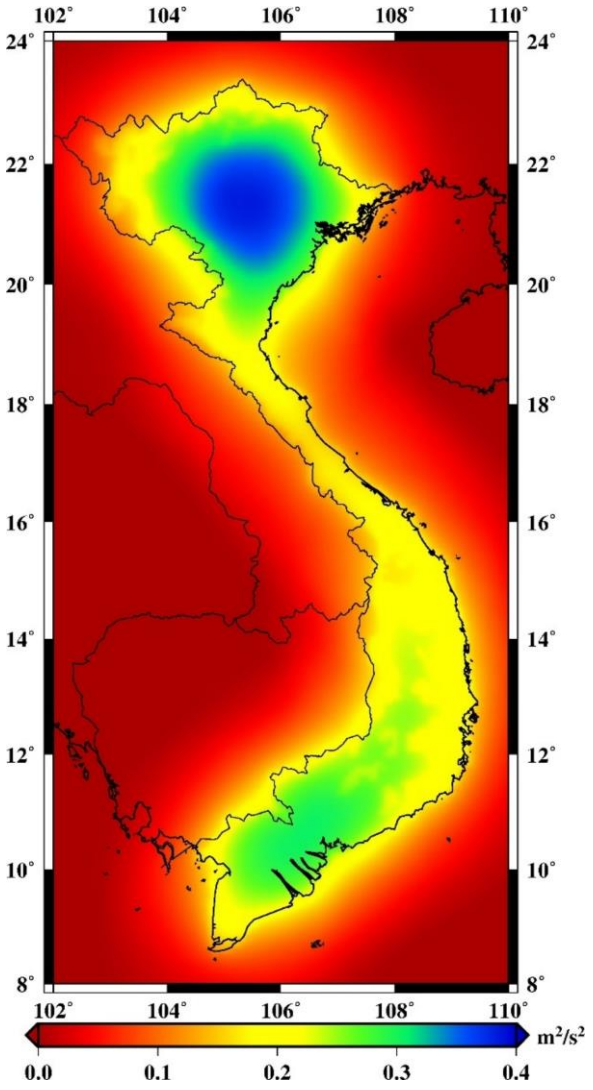

(a)

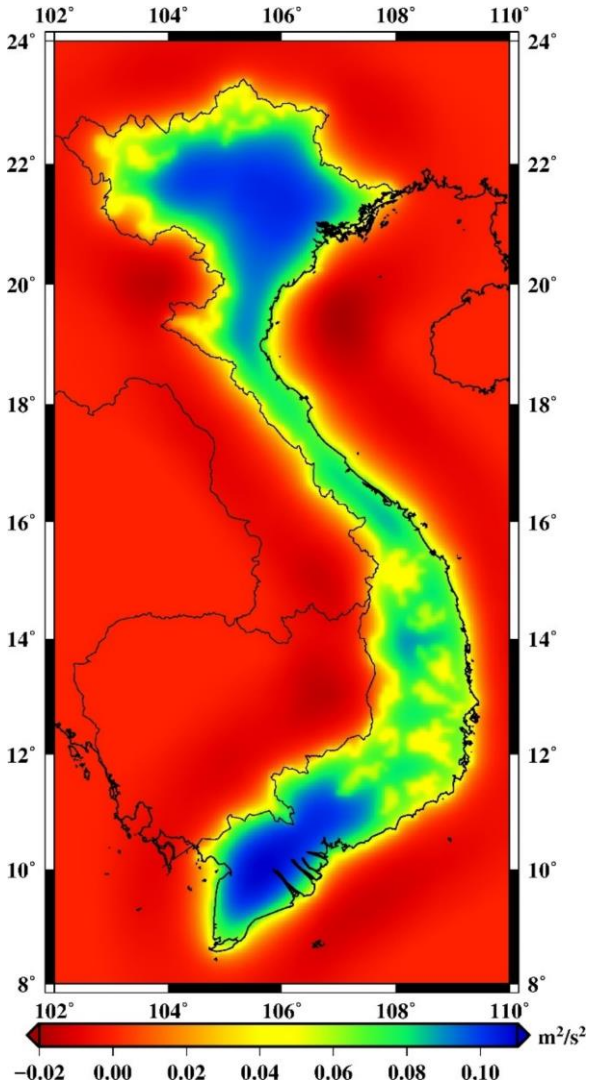

(b)

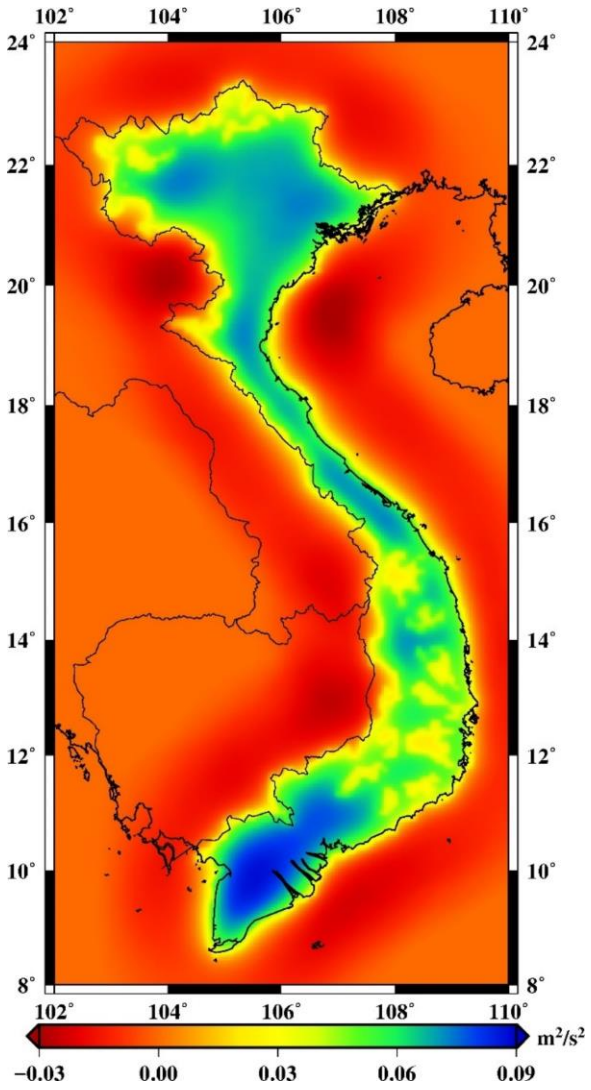

(c)

Figure 5.2. Indirect bias effect term on disturbing potential: a) N_1=0; N_2=0, b) N_1=50; N_2=60 and c) N_1=60; N_2=70

A GOCE GGM is used for the computation of the geopotential values, and its omission error is estimated here. D/o 260 of GOCE DIR-R5 (Bruinsma et al., 2014) was found to be optimum for this study region, so the omission error of this model is estimated for that d/o. It is evaluated on 779 GNSS/levelling points, for GOCE DIR-R5 at d/o 260, and after extending with EGM2008 from d/o 261-2190, as well as for the gravimetric-only quasigeoid GEOID_LSC. Table 5.8 shows the gravity potential offset value for the LVD with respect to W_0 = 62,636,853.4 m^2/s^2 calculated on 779 GNSS/levelling points. It is evident that the GOCE DIR-R5 model up to d/o 260 has quite significant omission error. The potential offset value computed with mixed DIR/EGM up to its full resolution is 6.64 m^2/s^2 and that computed with GEOID_LSC is 6.68 m^2/s^2 while the GOCE DIR-R5 only and mixed DIR/EGM up to d/o 719 yield 6.12 and 6.45 m^2/s^2, respectively. Thus, the effect of the GOCE GGM omission error on the offset value is estimated at 0.5 m^2/s^2 (equivalent to 5

cm) and that of the mixed DIR/EGM to d/o 719 to about 0.2 m^2/s^2 (equivalent to 2 cm). These results indicate that the contributions of the smaller scales of the gravity field are very important when evaluating the potential as well as the datum offset. The offset values computed with DIR/EGM at full resolution and the GEOID_LSC model are very close. This does not necessarily mean that omission errors of both models are equal over the entire country. It may be due to the locations of the GNSS/levelling points, most of which are in lowland areas where the effect of omission error is smaller when compared to mountainous areas (Hirt et al., 2010). To clarify this issue for the study region, the tests were done using different subsets of the GNSS/levelling points according to an elevation threshold (1000 m). With 755 points having elevation <1000 m, the potential offset value is very similar (6.69 and 6.65 m^2/s^2 for GEOID_LSC and DIR/EGM at full resolution, respectively). This value is 6.52 and 6.14 m^2/s^2 for GEOID_LSC and DIR/EGM, respectively, on 24 points having elevation >1000 m. This means that the effect of the mixed DIR/EGM omission error at full resolution is 0.4 m^2/s^2 when the comparison is done in the mountainous areas. The higher frequency information from the terrestrial gravity data in the GEOID_LSC also significantly reduces the STD of the estimated potential offset value (0.86 and 1.53 m^2/s^2 for GEOID_LSC and DIR/EGM at full resolution, respectively). It is also clear that DIR/EGM at d/o 719 significantly reduces the STD of the estimated potential offset value when compared to the only GOCE DIR-R5 model at d/o 260 (1.69 and 2.29 m^2/s^2 for DIR/EGM and GOCE DIR-R5, respectively). Similar to the case of quasigeoid determination, the mixed DIR/EGM model at d/o 719 is used for the RCR procedure.

Table 5.8. Gravity potential offset for LVD with respect to W_0 = 62,636,853.4 m^2/s^2 on 779 GNSS/levelling points (unit: m^2/s^2)

Model	δW^{LVD}	STD
GOCE DIR-R5 (d/o 260)	6.12	2.29
DIR/EGM (d/o 719)	6.45	1.69
DIR/EGM (d/o 2190)	6.64	1.53
GEOID_LSC	6.68	0.86
DIR/EGM (d/o 2190) (<1000 m, 755 points)	6.65	1.50
GEOID_LSC (<1000 m, 755 points)	6.69	0.82
DIR/EGM (d/o 2190) (>1000 m, 24 points)	6.14	2.26
GEOID_LSC (>1000 m, 24 points)	6.52	1.08

5.8.3. Zero-height geopotential for LVD on the GNSS/levelling points using the GBVP approach

The regular grid of residual gravity anomalies for computation gravimetric quasigeoid is also used to calculate the residual disturbing potentials (T_{res}) on 779 GNSS/levelling

points. The GBVP approach based on Molodensky's theory using the Stokes' integral with the WG modification of the kernel function, called Stokes_WG_GBVP, at degrees N_1=220 and N_2=230 is used to compute residual disturbing potentials. These optimum degrees for the study region were determined in computation of quasigeoid, and as a result the effect of indirect bias terms can be omitted in the estimation disturbing potential. The residual disturbing potentials vary from -7.15 to 3.81 m^2/s^2. The disturbing potentials ($T^{Stokes\_WG\_GBVP}$) are obtained by restoration of T_{GGM} (using the mixed DIR/EGM model up to d/o 719) and T_{RTM} (using the mixed SRTM from degree 720-216000). The results are listed in Table 5.9. Figure 5.8 shows the estimated disturbing potentials, which vary from -329.21 to 48.79 m^2/s^2.

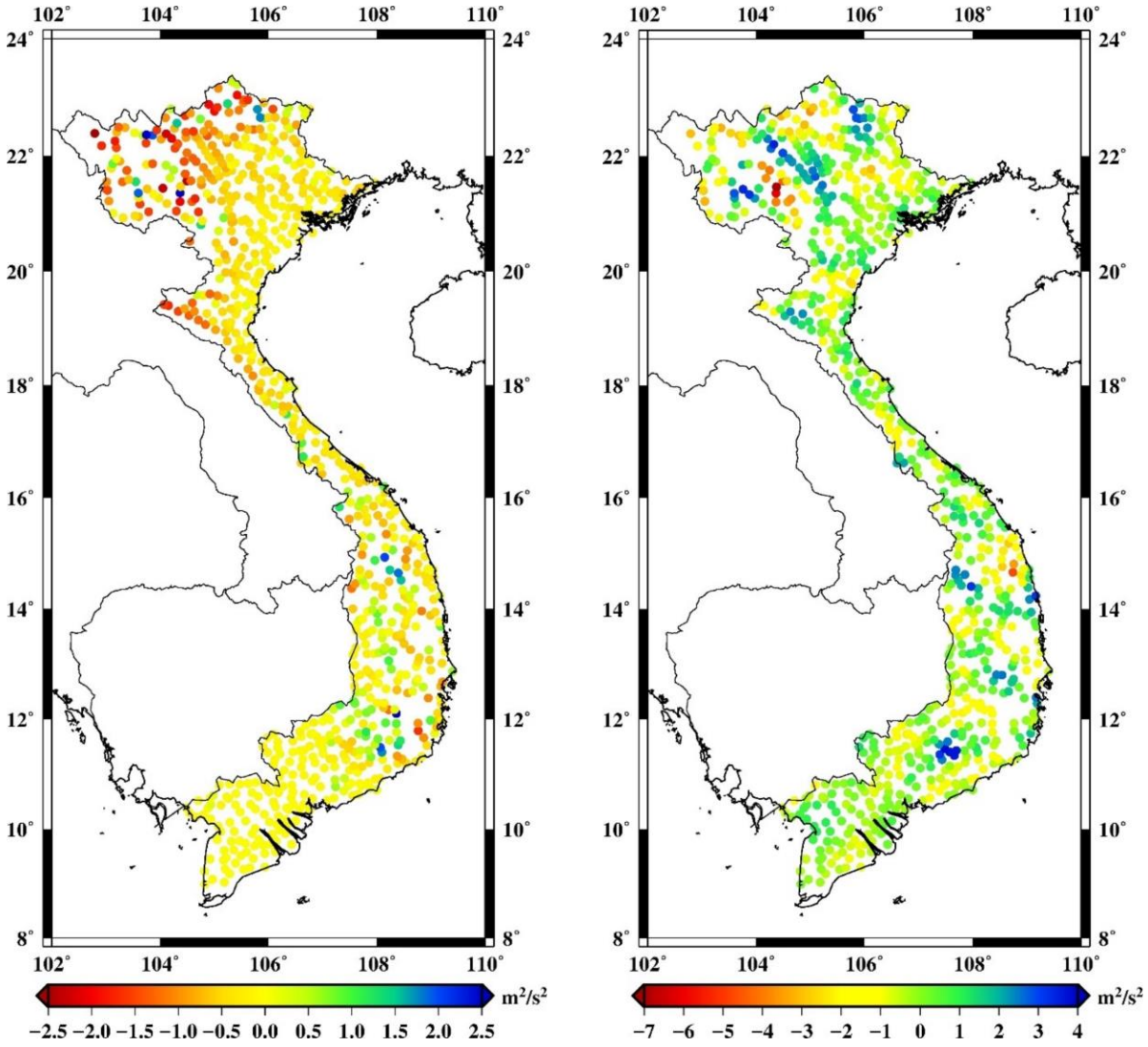

(a) (b)

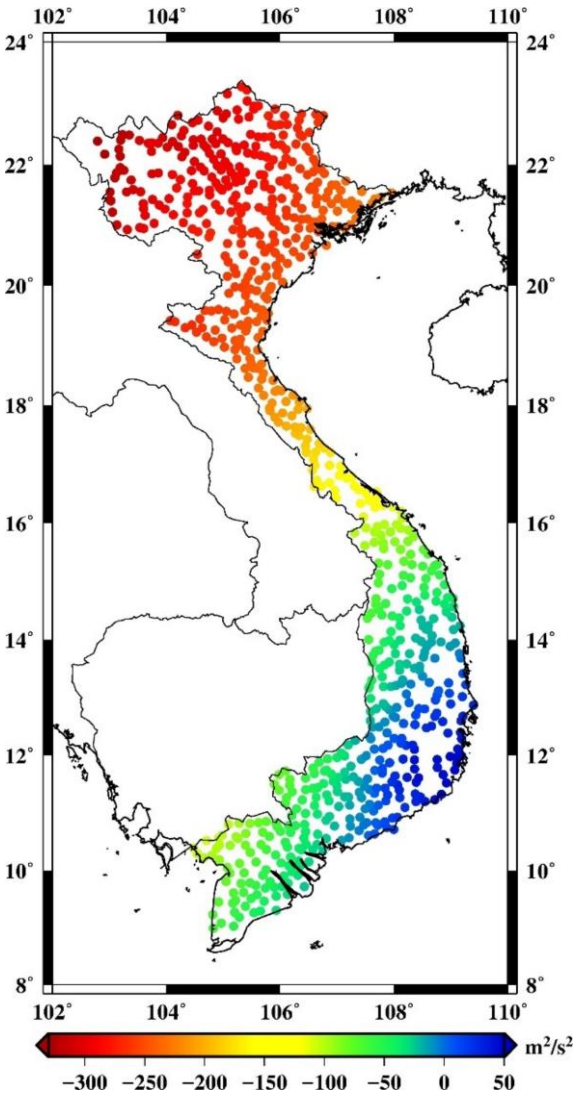

(c)

Figure 5.3. Estimated disturbing potential: a) T_{RTM}, b) T_{res} (N_1=220; N_2=230) and c) $T^{Stokes\_WG\_GBVP} = T_{GGM} + T_{RTM} + T_{res}$

Table 5.9. Statistics of the disturbing potential (unit: m^2/s^2)

	Min	**Max**	**Mean**	**STD**
$T_{DIR/EGM}$ (d/o 719)	-323.70	47.90	-147.28	120.11
T_{RTM}	-2.50	2.84	-0.24	0.63
T_{res}	-7.15	3.81	-0.13	1.34
$T^{Stokes\_WG\_GBVP}$	-329.21	48.79	-147.65	120.40
W_i	62,620,927.52	62,636,844.69	62,634,717.26	2,931.87

From the disturbing potential on 779 GNSS/levelling points ($T^{Stokes\_WG\_GBVP}$), the geopotential values on the surface (W_i) can be determined by adding the normal potential U_i on the reference ellipsoid (WGS-84 in this case) and then the zero-height geopotential level (W_i^{LVD}) can be obtained based on the normal height (H^*) of the GNSS/levelling points

using Eq (5.18). By simply averaging of W_i^{LVD} according to Eq (5.19), the mean zero-height gravity potential (W_0^{LVD}) for the LVD can be obtained. The results are listed in Table 5.10 and shown in Figure 5.9. The zero-height geopotential value varies from 62,636,843.89 to 62,636,849.28 m^2/s^2. The mean zero-height gravity potential of the VLVD was estimated equal to W_0^{LVD} = 62,636,846.69 m^2/s^2 with STD of 0.82 m^2/s^2. There is slight improvement in the STD when compared to W_0^{LVD} estimated from GNSS/levelling data and the GEOID_LSC model (0.86 m^2/s^2 in Table 5.8, correction is not applied to GNSS/levelling data in this case) thanks to using GBVP approach in computation. This will be clarified next.

Table 5.10. Zero-height gravity potential (W_i^{LVD}) on the GNSS/levelling points based on Stokes_WG_GBVP (unit: m^2/s^2)

	Min	**Max**	**Mean (W_0^{LVD})**	**STD**
Before de-trending	62,636,843.89	62,636,849.28	62,636,846.69	0.82
After de-trending	62,636,844.25	62,636,848.74	62,636,846.69	0.70

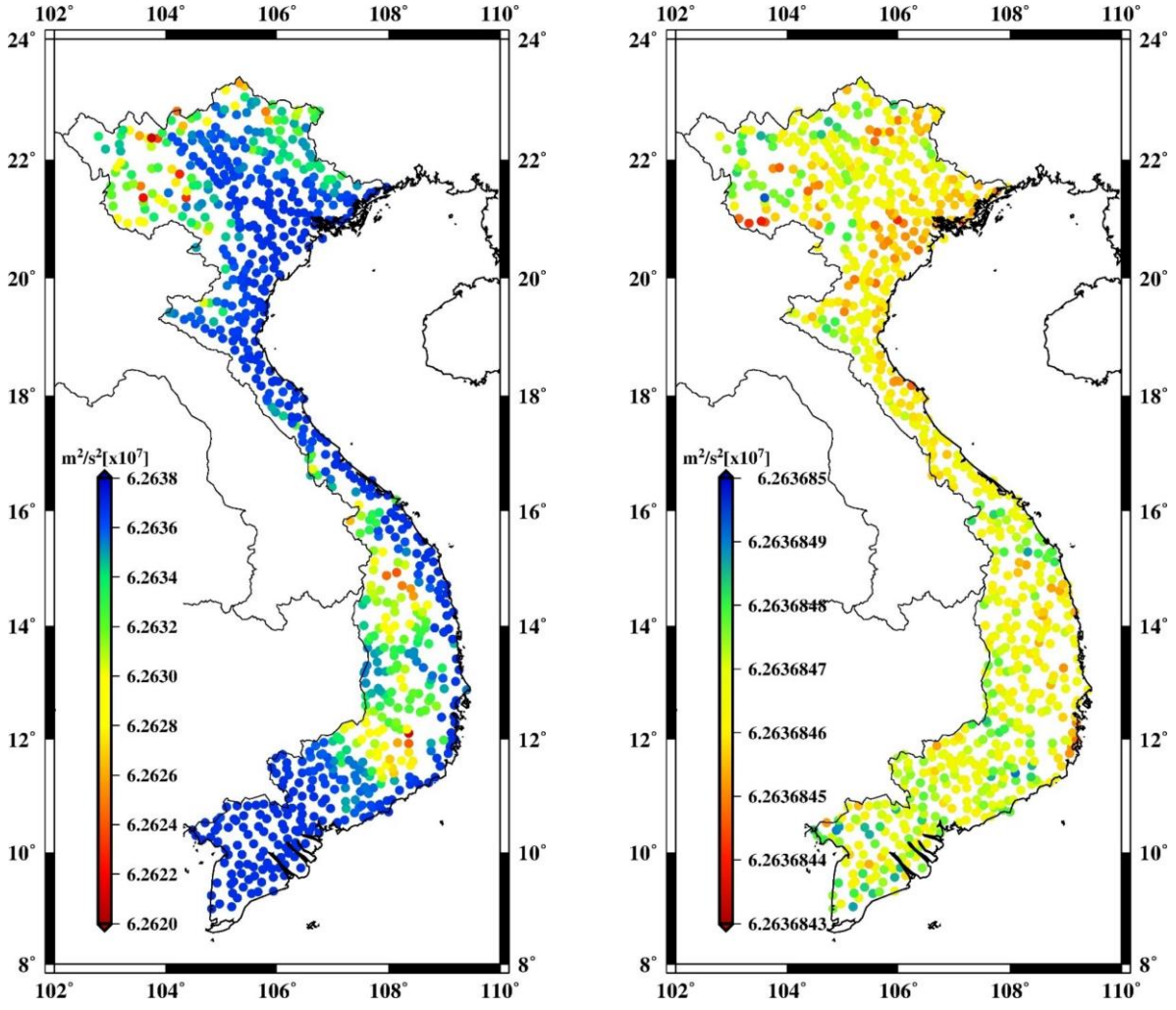

(a) (b)

Figure 5.4. Gravity potential on the GNSS/levelling points: a) $W_i=U_i+T_i$ and b) W_i^{LVD}

W_i^{LVD} is calculated from geopotential on the surface based on the normal heights, so without errors due to inconsistency between GNSS, levelling and gravimetric geoid/quasigeoid model for deriving height anomalies. Such errors are always present in the approach using GNSS/levelling and a gravimetric quasigeoid model for the determination of the potential value, e.g. effect of land subsidence on geometric height anomalies derived from GNSS and levelling data referring to different epoch times. GNSS/levelling is affected by land subsidence in the Mekong Delta, but this is not visible in Figure 5.9b. As a result, the STD of the geopotential calculated with the GBVP approach is slightly smaller. However, the systematic error in levelling data always affects W_i^{LVD}, which were converted from the geopotential on the surface using physical height derived from levelling. This systematic error was analyzed in Section 5.3 based on the differences between geometric height anomalies derived from GNSS/levelling data and those derived from the gravimetric-only quasigeoid model. However, when using GNSS and levelling data to derive the geometric anomalies, besides systematic errors in levelling data, errors in the GNSS measurements, as well as inconsistencies between GNSS and levelling measurements, are always present. This is the motivation to re-analyze the effect of systematic errors in the levelling data based on the estimated gravity potential where only levelling data is used for estimation. This effect can be seen in Figure 5.10 which shows the height residuals (e_i). The height residuals are computed as follows (Grigoriadis et al., 2014):

$$e_i = H_i^* - \frac{W_0^{LVD} - W_i}{\bar{\gamma}_i} \tag{5.26}$$

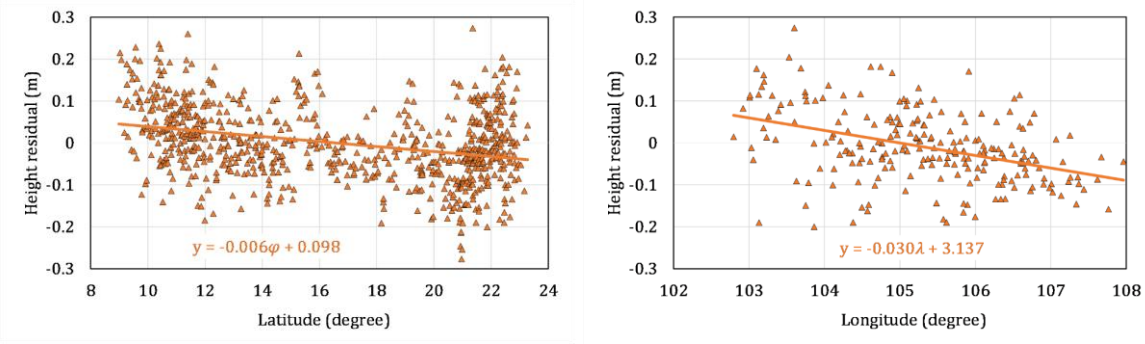

(a) (b)

Figure 5.5. Height residuals: a) The north-south direction of linear regression of all points and b) The east-west direction of linear regression of all points north of 21° latitude

A trend of 0.006 m/degree in the north-south direction may cause an error of about 8 cm over a distance of 15° (GNSS/levelling data located from 9°-23° in latitude). The tilt is 0.030 m/degree in the east-west direction in the north of Vietnam. These tilts are slightly smaller than those derived from GNSS/levelling and quasigeoid, but still significant over

long distances. The trends in W_i^{LVD} due to the systematic errors in the levelling data are shown in Figure 5.11. The orange triangles indicate potential residuals that were calculated corresponding to the height residuals.

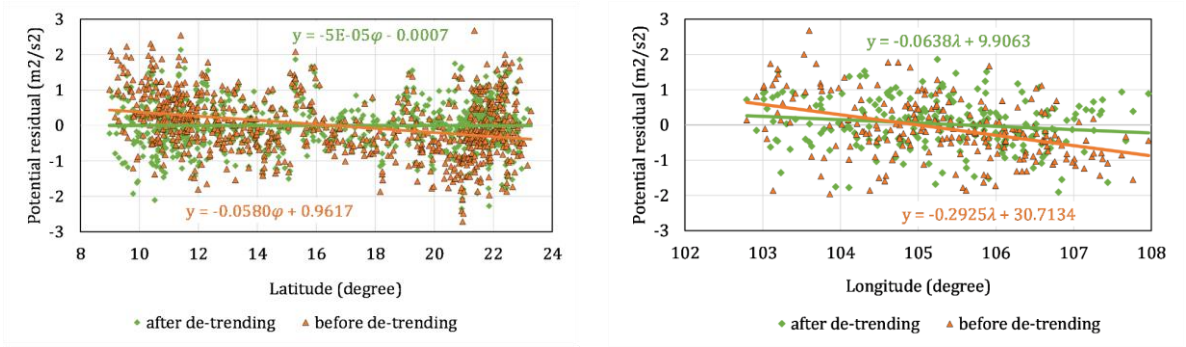

(a) (b)

Figure 5.6. Potential residuals, before and after de-trending, corresponding to height residuals in Figure 5.10: a) In north-south direction and linear regression of all points and b) In east-west direction and linear regression of all points in the north (>21° in latitude)

The trends in height residuals are modeled and removed using the third-order polynomial model with two distinct distortion parameters for the two parts, one for the northern part (>17° in latitude) and another for the southern. However, here the height residuals were modeled instead of vertical datum offset. In the model used for vertical datum offset, it cannot separate between the datum offset and tilt components within the levelling data i.e., only tilt needs to be removed and the mean bias in differences between GNSS/levelling data and quasigeoid (datum offset) was retained. This leads any constant components should not be contained in the estimated model (Kotsakis et al., 2012). In this case, the estimated model contains a constant component:

$$e_i = H_i^* - \frac{W_0^{LVD} - W_i^{LVD}}{\bar{\gamma}_i} - (a_0 + a_1\varphi + a_2\lambda + a_3\varphi^2 + a_4\varphi\lambda + a_5\lambda^2 + a_6\varphi^3 + a_7\varphi^2\lambda + a_8\varphi\lambda^2 + a_9\lambda^3) \quad (5.27)$$

On each GNSS/levelling point there is an equation like Eq. (5.27), and Least Square (LS) adjustment has been performed with equal weights. After de-trending, the corrected normal heights are used for computation of the gravity potentials and the results are listed in Table 5.10. The mean zero-height gravity potential value does not change (W_0^{LVD} = 62,636,846.69 m2/s2), but STD improves significantly (0.70 m^2/s^2 after de-trending, decreasing by 0.12 m^2/s^2). Figure 5.11 shows the improvements of the potential residuals after de-trending was applied for the levelling data (green dots). In the previous section, the gravity potential of the VLVD was estimated at W_0^{LVD} = 62,636,846.81 ± 0.70 m^2/s^2 after applying corrections for GNSS/levelling data due to effect of land subsidence in the

Mekong Delta, which improved the consistency between GNSS and levelling data significantly. Now there are two estimates for the gravity potential values for VLVD with a small difference of 0.12 m^2/s^2 (equivalent to 1 cm), which is insignificant. This proves that the applied method is reliable for directly calculating the gravity potential value on the Earth's surface. In Section 5.8.4, the gravity potential value and its variations will be determined based on this approach using GNSS-CORS stations as realization of the IHRS, to monitor deformation of the height reference system for Vietnam.

5.8.4. Geopotential and its variations on the GNSS-CORS stations

To avoid site motion, geodetic control points, horizontal as well as vertical, were usually set into structures with deep foundations. Such control points were considered as "fixed" in time. However, even when deeply embedded into the bedrock, these points are susceptible to vertical motion. Thanks to space geodetic techniques, the displacement phenomena can be measured in time. The coordinates of control points can be given at the reference epoch together with their variations in time, allowing continuous monitoring of the deformation of the reference datum. When differences exceed a given threshold, the reference coordinates should be updated. For this purpose, a vertical reference datum, at global as well as national or regional scale, should be realized based on the GNSS-CORS stations. In Section 5.4, continuous time series of heights from 11 permanent GNSS stations over long periods of time were used to determine the vertical land motion in Vietnam. From these 11 stations, three stations about equally spaced from north to south (named PHUT, QNRS and BACL) were selected to calculate the gravity potential used as the reference points for the vertical datum. The locations of these 3 stations are shown in Figure 5.4. Variations in geometric height derived from these GNSS stations can be used to infer change in the normal geopotential. Vertical land motion rates from InSAR reflect topography changes around the GNSS station and can be used to calculate time variations of the disturbing potential. From time variations in normal and disturbing potential, the gravity potential change on the GNSS stations is obtained as follows:

$$\dot{W}_P = \dot{U}_P + \dot{T}_P \tag{5.28}$$

For topography change, the annual average land subsidence rates over 2015–2018 derived from Sentinel-1 imagery time series covering most of the south of Vietnam were used, which are available in the frame of the project "EMSN062: Assessing changes in ground subsidence rates, Mekong Delta, Vietnam" (Report of COPERNICUS, 2019).

For the purpose of identifying the permanent GNSS stations as the reference points for the modern height system in Vietnam, the gravity potential values on the surface of these points are firstly determined based on the GBVP approach and then their variations are calculated.

The Stokes_WG_GBVP approach is used for computation of the residual disturbing potential in $4x4^0$ blocks surrounding each GNSS-CORS station. The disturbing potentials are obtained by restoring T_{GGM} and T_{RTM}. The geopotential value on the surface is determined by adding the normal potential on the reference ellipsoid. The computation procedure was performed in the same way as for the GNSS/levelling points. The results, listed in Table 5.11, were calculated using the ellipsoidal height at epoch 2018.0.

Table 5.11. Estimated potential on the GNSS stations at epoch 2018.0 (unit: m^2/s^2)

Name	T_{res}	$T^{Stokes\_WG\_GBVP}$	U_i	W_i
PHUT	-0.20	-264.84	62,636,982.30	62,636,717.46
QNRS	0.44	-89.37	62,636,797.04	62,636,758.62
BACL	-0.87	-38.43	62,636,734.76	62,636,645.40

The ellipsoidal heights time series derived from continuous measurements on the GNSS-CORS stations are shown in Figure 5.12.

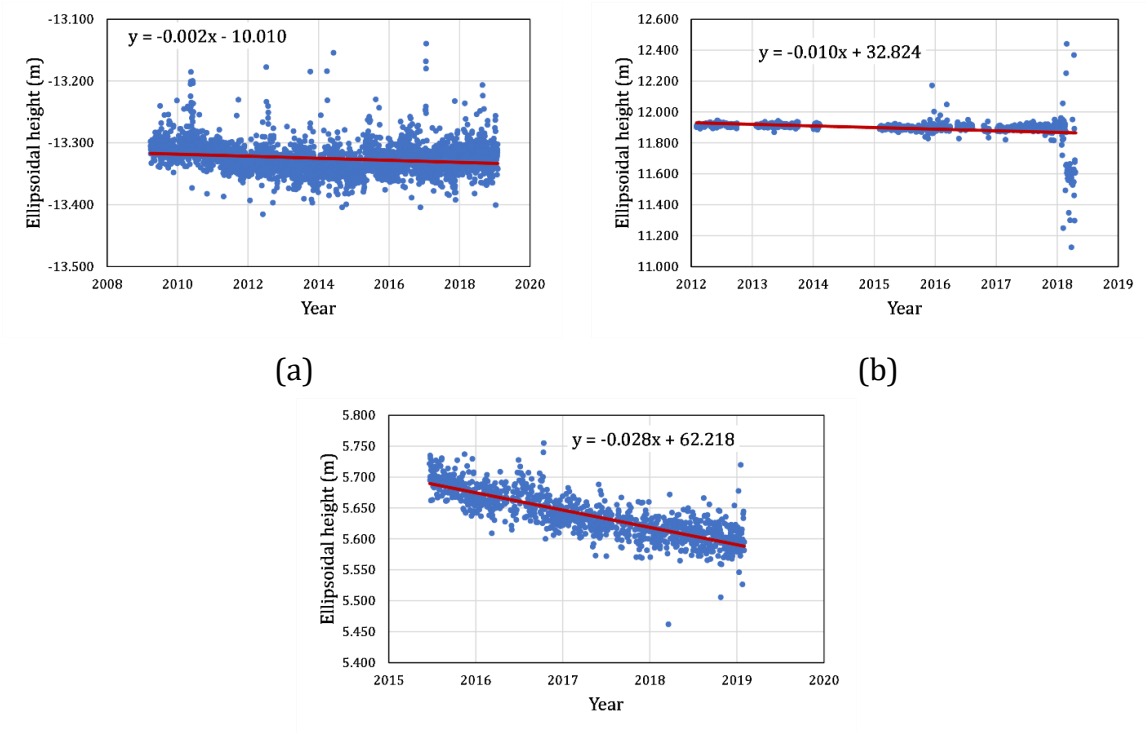

Figure 5.7. Ellipsoidal heights time series on the GNSS-CORS stations: a) PHUT station, b) QNRS station and c) BACL station

These time series of GNSS heights reveal signals induced by vertical deformation, but also outliers, especially for the QNRS station. The outliers were determined assuming a normal distribution of the residuals, and three sigma (3σ) rejection led to elimination of 90, 89 and 19 epoch times for the PHUT, QNRS and BACL stations, respectively. The height residuals are computed using the linear model as follows:

$$e^t = h^t - (a_0 + a_1 t) \quad (5.29)$$

where h^t is the ellipsoidal height at epoch time t; a_0 and a_1 are coefficients which are determined using LS adjustment.

The filtered ellipsoidal heights time series are used to calculate the normal potential time series, assuming that it does not change on the reference ellipsoid (U_0). From time series of the normal potential, the linear vertical movement rates can be determined. The results are shown in Figure 5.13. Rates in normal potential of 0.02 ± 0.00(12), 0.04 ± 0.00(15) and 0.28 ± 0.00(52) m^2s^{-2}/year were observed for the PHUT, QNRS and BACL stations, respectively. There clearly is a large change in the normal potential in the BACL station, located in the Mekong Delta, while it is insignificant for the other two. As the Mekong Delta is known to be deforming for decades, this result is not surprising.

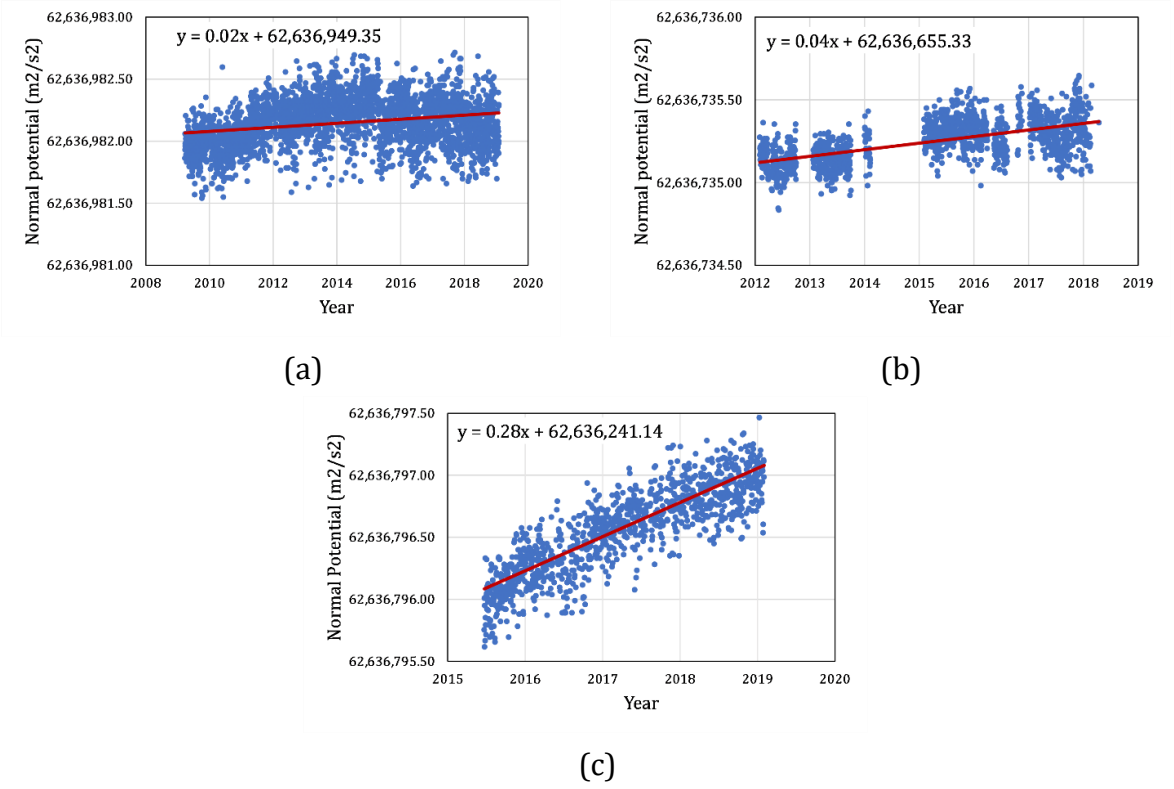

Figure 5.8. Normal potential time series on the GNSS-CORS stations: a) PHUT station, b) QNRS station and c) BACL station

To determine the time variations in the disturbing potential for the BACL station, the gravity change is firstly determined using the changed topography derived from Sentinel-1 InSAR data (Figure 5.14a) via forward modelling of residual terrain effects with constant density. Then the Stokes' integral is applied to this gravity change grid to determine the change in disturbing potential. This approach was used for the determination of the change in height anomalies caused by the 2016 Kaikoura earthquake (McCubbine et al., 2020). The gravity anomaly changes are computed as follows:

$$\Delta g^{change} = \Delta H \frac{\partial \gamma}{\partial h} - 2\pi G\rho\Delta H + TC(\Delta H) \quad (5.30)$$

where ΔH is the change in elevation given as the annual average land subsidence derived from Sentinel-1, $\frac{\partial \gamma}{\partial h}$ is the linear Free-air gravity gradient, ρ is density of crust, G is the universal gravitational constant and $TC(\Delta H)$ is terrain correction due to the change in topography. The latter two terms on the right-hand side in Eq. (5.30) are the RTM effects due to the change in topography determined by the InSAR data. Eq. (5.30) can be rewritten as follows:

$$\Delta g^{change} = \Delta H \frac{\partial \gamma}{\partial h} + \Delta g_{RTM}(\Delta H) \quad (5.31)$$

$\Delta g_{RTM}(\Delta H)$ has been computed with the same mixed SRTM model that was used as the detailed DTM. The reference DTM is created by adding the annual average land subsidence rates over 2015–2018 derived from Sentinel-1 (Report of COPERNICUS, 2019) into the mixed SRTM model. The grids of subsidence rates are not specified over sea (set to 0). Figure 5.14a shows the annual average land subsidence rates derived from Sentinel-1. Average subsidence rates range from 1-4 cm/year in built up areas whereas over agricultural areas it is less than 1 cm/year. Figure 5.14b indicates the forward modelled gravity anomaly changes using Eq. (5.31). The gravity anomaly changes vary from -0.07 to 0.20 (mGal).

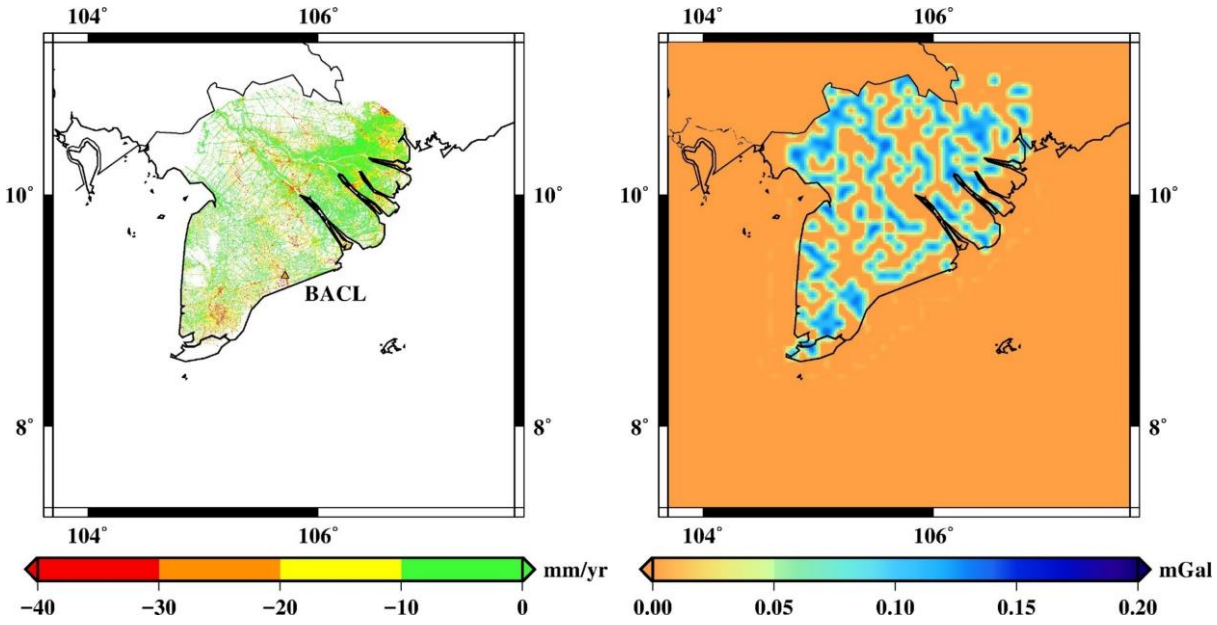

Figure 5.9. a) Annual average vertical deformation over the 2015-2018 period in the Mekong Delta determined from Sentinel-1 InSAR, project EMSN062 (Report of COPERNICUS, 2019), orange triangle is the BACL station and b) Gravity anomaly changes computed from the annual average vertical deformation [min: -0.07 (mGal), max: 0.20 (mGal)]

From the grid of gravity anomaly changes, the Stokes' integral is used for determining the change in disturbing potential at the BACL station. The change due to significant subsidence in the Mekong Delta is only 0.004 m^2s^{-2}/year, and is very small when compared to the change in normal potential. Hence, the time variations in geopotential are considered equal to the change in normal potential i.e., time variations in the disturbing potential can be omitted in the estimation of geopotential change. According to the recommendation in Sánchez et al., (2016), an update of W_0 is required if the cumulative change reaches 2 m^2/s^2. This value will be reached within 8 years at the BACL station at the current rate. This is why the geopotential value needs to be monitored and determined with the time-dependent component on the permanent GNSS stations.

In this chapter, the applications of gravimetric quasigeoid in geodesy i.e., using quasigeoid in GNSS levelling technique as well as determination of the zero-height gravity potential of VLVD, were presented. First, the gravimetric quasigeoid was used in combination with GNSS/levelling data to determine a vertical offset model. This offset model can be used for combination with a gravimetric quasigeoid model in GNSS levelling. The offset model was evaluated using cross-validation technique by comparing with GNSS/levelling data. Results indicate that the offset model has a standard deviation of 5.9 cm in the absolute sense. Based on this offset model, GNSS levelling can be carried out in most of Vietnam's territory complying third-order levelling requirements, while the accuracy requirements for fourth-order levelling networks is met for the entire country. This model in combination with the developed gravimetric quasigeoid model should also contribute to the modernization of Vietnam's height system. The high-quality GNSS/levelling data and the estimated quasigeoid model were also used to determine the zero-height geopotential value W_0 for the VLVD. The gravity potential of the VLVD is estimated equal to W_0^{LVD} = 62,636,846.81 ± 0.70 m^2/s^2 with the global equipotential surface realized by the conventional value W_0 = 62,636,853.4 m^2s^{-2}. The GBVP approach was also used to directly determine this W_0^{LVD}value. A similar result of W_0^{LVD}= 62,636,846.69 was also determined and the difference of 0.12 m^2/s^2 (equivalent to 1 cm) is within the limits of the study objective. This proves that the applied method is reliable for directly calculating the gravity potential value on the Earth's surface. Hence, the GBVP approach was used for determination of the gravity potential on the surface of three GNSS CORS stations at epoch 2018.0 in Vietnam. Based on time series of vertical component derived from the GNSS observations as well as InSAR data, time variations of geopotential were also estimated on these permanent GNSS stations. The purpose is to monitor deformation of the vertical datum. These are the reference stations of VLVD. The results indicated that the geopotential values need to be monitored and determined with the time-dependent component on the permanent GNSS stations in order to plan updates. These stations may contribute to increase the density of reference points in the IHRF for this region.

Chapter 6: QUASIGEOID APPLICATION FOR DETERMINATION OF THE LITHOSPHERIC STRUCTURE

This study has been subject to the following paper:

Vu, D. T., Bonvalot, S., Bruinsma, S., Bui, K. L., (2021). A local lithospheric structure model for Vietnam derived from a high-resolution gravimetric geoid. *Earth Planets Space* 73, 92 (2021). https://doi.org/10.1186/s40623-021-01415-2

The Earth is comprised three main internal structures: crust, mantle and core (Figure 6.1). These structures have different densities in different depths. The Moho discontinuity is 5 to 10 km below the ocean floor with an average depth of about 8 km and 20 to 90 km beneath continental crusts with an average of 32 km. In Vietnam, several isostatic-gravimetric Moho depth surfaces were developed for the northern part and the sea of Vietnam. However, the results of these studies differ considerably due to lack of independent constraint conditions (Nguyen et al., 2013). Therefore, these results are largely outdated now due to the initial gravity model was based on relatively sparse and irregular ground measurements. Recently, some studies were carried out using seismic data for determining the Moho depth. However, they are not sufficient to draw a detailed Moho depth model in this region. The isostatic-gravimetric method is needed to solve this problem.

Lithosphere of the Earth is composed of the crust and the portion of the upper mantle (Figure 6.1). The LAB beneath the continents is the most important surface in understanding the geochemical and geodynamic evolution of the planet (O'Reilly & Griffin, 2010) . Similar to the Moho depth, the choice of data and approach used has a strong influence on the final lithospheric model. Several geophysical data sets have been used to determine the LAB e.g., seismic, thermal, electromagnetic, gravity and rheological. However, the existing lithospheric thickness models differ significantly (Artemieva, 2011). The individual geophysical methods are contentious and sometimes poorly understood (Eaton et al., 2009; Artemieva, 2011). The structure of the lithosphere beneath Vietnam and its surrounding areas is even less well understood than the Moho topography.

Recently, through the local isostatic assumption, Fullea et al. (2006) developed a new method to model lithospheric structure using geoid heights derived from a GGM, in combination with elevation data from a DTM. A refinement of this approach was presented in Fullea et al. (2007) by considering the lithospheric mantle density variation with temperature instead of using a constant one. This method was successfully used in

the determination of the lithospheric structure of the Arabia–Eurasia collision (Iran) (Jiménez-Munt et al., 2012), Central Asia (Robert et al., 2012), southern India (Kumar et al., 2014), the Iberian Peninsula (Torne et al., 2015), Africa (Globig et al., 2016) and Central Eurasia (Robert et al., 2017). All of these studies used the geoid height and elevation data derived from the GGMs EGM96 at 30' resolution (Lemoine et al., 1998) or EGM2008 (Pavlis et al., 2012) at 5' resolution and the DTMs ETOPO2 at 2' resolution (Smith & Sandwell, 1997) or ETOPO1 (Amante & Eakins, 2009) at 1' resolution, respectively. The high-accuracy and high-resolution gravimetric quasigeoid model was determined for Vietnam and its surrounding areas based on new gravity data. This quasigeoid model is used in combination with the elevation data derived from the mixed SRTM model to compute the Moho and LAB depths in Vietnam. Moreover, the new Bouguer gravity anomaly map is also used based on the gravity inversion method to compute the precise Moho depth for the whole of Vietnam. The aim of the study is to constrain the different models proposed to explain the crustal and lithospheric structure of the study area. The Moho and LAB depths models will be discussed in relation with geological, topographic and gravity anomalies map. The recent local and global scale models of Moho and LAB depths are used to validate the resulting depth models. The results are also validated using the Moho depth derived from seismic data collected in the study region.

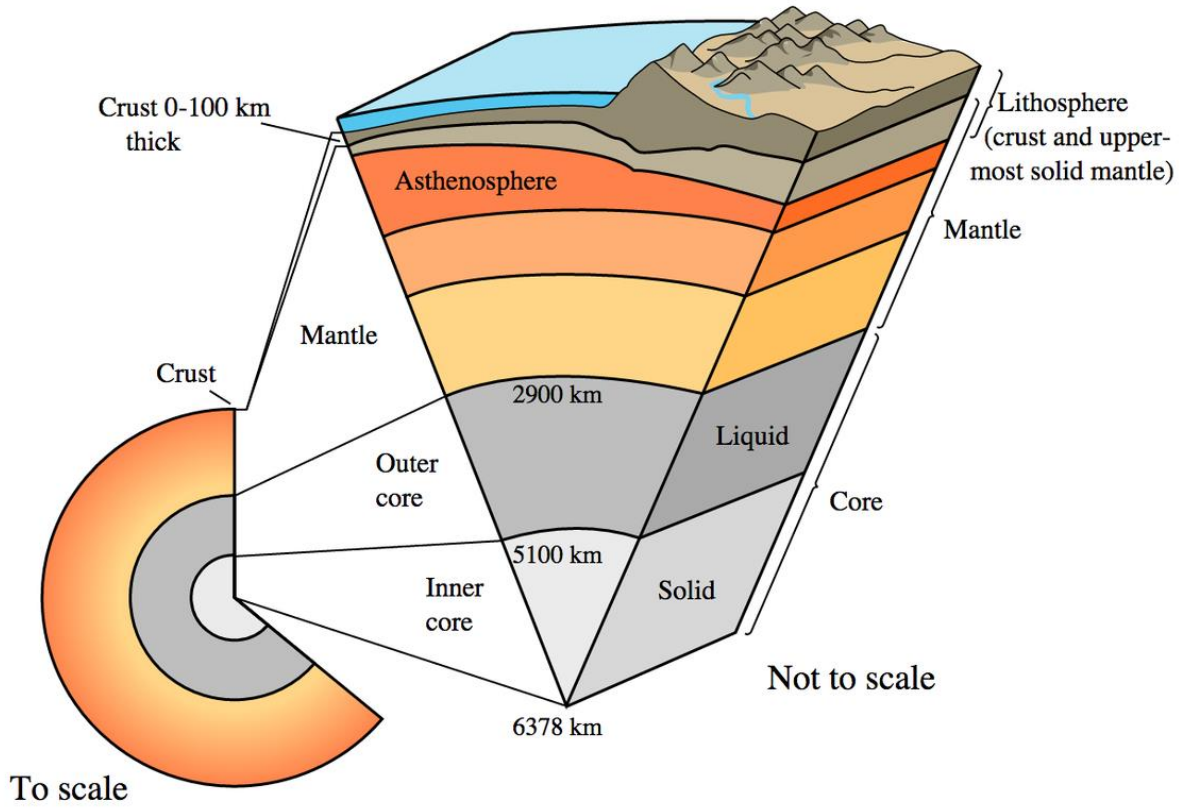

Figure 6.1. Earth's layered structure (source: https://www.usgs.gov/)

6.1. Moho and LAB depth determination methodology

6.1.2. Method using geoid height and elevation data

The Moho and LAB depths are calculated by combining elevation above mean sea level and geoid data together with thermal analysis in a 1D approach proposed by Fullea et al., (2007). In which elevation and geoid data provide different kinds of information concerning the density distribution in the lithosphere: topography reflects the average density, whereas geoid heights are produced by variations in the dipole moment of the density. This method assumes local isostasy with a compensation depth below the LAB, and a four-layer model: water, crust, lithospheric mantle and asthenosphere. The concept of local isostasy assumes that a series of rigid columns (the lithosphere) floats freely on an inviscid liquid (the asthenosphere) and below a certain level (the compensation level, z_{max}), the pressure does not vary laterally. This means that the elevation is a measure of the buoyancy of the lithospheric columns. Hence, the relation between the Moho and LAB depths with elevation data is as follows (Fullea et al., 2006):

$$z_c = \frac{\rho_a L_0 + E(\rho_c - \rho_w) + z_L(\rho_m - \rho_a)}{\rho_m - \rho_c} \tag{6.1}$$

where z_c is the depth of the Moho

z_L is the depth of the LAB

ρ_c is the mean density of the crust

ρ_m is the mean density of the lithospheric mantle

ρ_w is the density of the sea water

ρ_a is the density of the asthenosphere

L_0 is the depth of the free asthenospheric level

E is the elevation

The geoid height (N) can be determined using the following relation:

$$N = -\frac{\pi G}{g}[\rho_w E^2 + (z_c^2 - E^2)\rho_c + (z_L^2 - z_c^2)\rho_m + (z_{max}^2 - z_L^2)\rho_a] - N_0 \tag{6.2}$$

where z_{max} is the depth of the compensation level

G is the universal gravitational constant

g is the Earth's surface gravitational acceleration

As absolute densities are used in this approach, an integration constant N_0 is needed in order to adjust the zero level of the geoid heights (Fullea et al. 2006). N_0 is determined by

applying Eq. (6.2) to a selected lithospheric reference column (z_{cREF}, z_{LREF}) that eliminates geoid height.

The expressions (6.1) and (6.2) form a system of equations for the depths of the Moho (z_c) and LAB (z_L) and for the densities of the crust (ρ_c) and lithospheric mantle (ρ_m). Thus, there are four variables and only two constraints. If densities in the crust and lithospheric mantle are known for the whole model then variable depths for the crust/mantle and LAB can be retrieved from (6.1) and (6.2).

Fullea et al., (2007) proposed a refinement of this approach by considering a lithospheric mantle density variation with temperature and a linear density gradient from upper and lower crustal densities for the crustal layer instead of using a constant one. According to Parsons & Sclater, (1977), the lithospheric mantle density depends on the temperature as follows:

$$\rho_m(z) = \rho_a(1 + \alpha[T_a - T_m(z)]) \tag{6.3}$$

where α is the linear coefficient of thermal expansion (K^{-1}), T_a is the temperature at the LAB and $T_m(z)$ is the temperature at depth z in the lithosphere. This equation is solved with boundary conditions considering fixed temperature at the surface (T_s) as well as at the LAB. The temperature at the crust-mantle boundary (T_{mh}) is calculated using:

$$T_{mh} = \frac{(z_L - z_c)\theta + \delta}{z_c\Delta k + z_L k_{c+} E k_m} \tag{6.4}$$

where $\theta = k_c T_s + f$

$\delta = k_m T_a(z_c + E)$

$\Delta k = k_m - k_c$

f is heat production calculated according to crustal surface one (H_s)

k_c is the thermal conductivity of the crust

k_m is the thermal conductivity of the lithospheric mantle

The vertically average value of the lithospheric mantle density can be determined by integrating Eq. (6.3) between z_c and z_L:

$$\bar{\rho}_m = \rho_a\left(1 + \frac{\alpha}{2}[T_a - T_{mh}]\right) \tag{6.5}$$

The geoid height from Eq (6.2) with the density of the crust varying linearly with depth and the density of the lithospheric mantle depending on lithospheric temperature is rewritten as follows:

$$N = -\frac{\pi G}{g}\left[\rho_w E^2 + \frac{2\beta}{3}(z_c^3 - |E^3|) + (\beta E + \rho_c^T)(z_c^2 - E^2) + (z_{max}^2 - z_L^2)\rho_a + \rho_a \alpha \frac{T_a - T_{mh}}{3}[(z_L - z_c)(z_L + 2z_c)]\right] - N_0 \quad (6.6)$$

where $\beta = \frac{\rho_c^B - \rho_c^T}{z_c + E}$

ρ_c^T and ρ_c^B are the densities of the upper and the lower of the crustal layer.

In order to calculate $\bar{\rho}_m$, the depths of the Moho and LAB in Eq (6.4) should be known. Hence, an iterative manner is carried out to solve this problem. The initial values of z_c and z_L were estimated by assuming a constant density for the crust and lithospheric mantle. The iterative steps will stop when the difference between the geoid height calculated from Eq (6.6) and observed one becomes smaller than a desired value (see Fullea et al., (2007) for details). The geoid and DTM model, which are used for deriving geoid height and elevation data, respectively, contain signals representing all masses within the Earth. Therefore, to study lithospheric structure only, a filtering procedure must be applied to the data. A Matlab program was developed to filter geoid height and elevation data, and subsequently compute the Moho and LAB depth.

6.1.2. Gravity inversion method

The Parker´Oldenburg gravity inversion algorithms is also used to model the Moho depth in this study. It was proposed by Parker (1973) to apply FFT in the calculation, and then Oldenburg (1974) rearranged Parker's forward algorithm to determine the density interface from the observed gravity anomaly. The original form of Parker´Oldenburg's algorithms is two-dimensional (2D), its three-dimensional (3D) application with large data sets in the geophysical field can be frequently found now in Gómez-Ortiz & Agarwal, (2005); Shin et al., (2006), Shin et al., (2007) and Block et al., (2009). This method is briefly described below.

According to Parker (1973) the relation between the vertical gravity effect, Δg, and its causative mass topography, $h(\vec{r})$, with two-dimensional form in wavenumber domain is as follows:

$$F(\Delta g) = -2\pi G \rho e^{(-|k|z_0)} \sum_{n=1}^{\infty} \frac{|k|^{n-1}}{n!} F[h^n(\vec{r})] \quad (6.7)$$

where F(Δg) is the Fourier transform of the gravity anomaly

G is the universal gravitational constant

ρ is the density contrast across the interface

k is the wave number of the transformed function

$h(\vec{r})$ is the depth to the interface

z_0 is the mean depth of the horizontal interface

$\vec{r}$ denotes the projection of the position r = (x, y, z) onto x, y plane.

Oldenburg's rearrangement for Parker's scheme for the 3D case can be written as follows:

$$F[h(\vec{r})] = -\frac{F[\Delta g(\vec{r})]e^{(|k|z_0)}}{2\pi G\rho} - \sum_{n=2}^{\infty} \frac{|k|^{n-1}}{n!} F[h^n(\vec{r})] \tag{6.8}$$

The above equation may be solved by an iterative procedure where the mean depth z_0 and the density contrast ρ are predefined constant parameters, while the depth $h(\vec{r})$ at the right-hand side of the equation may be set for the first iteration, for example $h(\vec{r}) = 0$. The iteration stops when the difference in depths between two successive iterations is smaller than a predefined value. The final Moho surface depends on the pre-set parameters, the mean Moho depth z_0 and the density contrast of the interface ρ. Because of the term $e^{(|k|z_0)}$ in Eq (6.8), it highly affects short wavelengths. Therefore, the short wavelength features, usually coming from intra-crustal density inhomogeneity or noise, should be removed before the inversion process. A low-pass filter is used in this case. The low-pass filter is defined by the following equations:

$$LPF(k) = \begin{cases} \frac{1}{2}\left[1 + cos\left(\frac{k - 2\pi K_L}{2(K_H - K_L)}\right)\right] & for\ K_L < k < K_H \\ 0 & for\ k > K_H \\ 1 & for\ k < K_L \end{cases} \tag{6.9}$$

where k is the wavenumber which may be replaced with $1/\lambda$ where λ is the wavelength expressed in km.

K_H and K_L are the high and low cut-off wavenumbers.

In order to decide on the appropriate wavelength range of the features corresponding to Moho deflection the selection of K_H and K_L is complex. This is even more difficult if both continental and marine regions are in the study area since the target depth of marine regions is significantly lower than that of the continental areas. The choice of a filter and its parameters is based on the accuracy and resolution of the available gravity data, the topography of the study area, and the existing geological formations. Different researchers have selected various types of filters and parameters for different test areas. For computation, a Matlab code, 3DINVER.M, provided by Gómez-Ortiz & Agarwal, (2005) was used in this study.

6.2. Geological setting

The Vietnam region, lying on the south-east part of the Eurasian tectonic plate, has a complex tectonic history inherited from the tectonic evolution of South-East Asia. Molnar & Tapponnier, (1975) and Jolivet et al., (1990) have proposed that the tectonics of southeast Asia can be entirely related to the India-Eurasia collision initiated 80 My ago, which has influenced the structure of the Earth far beyond the Himalaya-Tibet orogeny. The study region is considered to be mainly on two tectonic blocks (Figures 6.2a and 6.2b): the Indochina (or Sundaland) terrane and the South China terrane. The Indochina terrane includes east Thailand, southwest part of Vietnam, Cambodia, a large portion of Laos, and small parts of Malaysia and Indonesia. These tectonic features have played an important role on the geological evolution of Vietnam and on the formation of economic resources of the country. The boundary between South China and Indochina blocks is located along the Ma River Fault Zone (MRFZ) (Helmcke, 1985; Hutchison, 1989; Findlay, 1997; Findlay & Trinh, 1997; Lepvrier et al., 1997; Lepvrier et al., 2011; Faure et al., 2014; Metcalfe, 2013). However, some authors suggested that the Red River Fault Zone (RRFZ) is the major geological discontinuity, which separates South China from Indochina block (Leloup et al., 1995; Leloup et al., 2001; Gilley et al., 2003; Nguyen et al., 2013; Trần et al., 2013; Dinh et al., 2018). To resolve this debate, it is essential to accurately determine the Moho depth where the boundary between continental blocks is usually clearly visible. The northeastern part of Vietnam, belonging to the South China terrane, is situated immediately southeast of the eastern Himalayan syntaxis. The Hoang Lien Son Mountain Range is highest in this region, with its Fansipan peak at the height of about 3,140 m above sea level. This northern part of Vietnam has a complicated tectonic setting, dominated by active faults, such as the Red River Fault (RRF), Chay River Fault (CRF), Lo River Fault (LRF) – all within the Red River Fault System (RRFS), Dien Bien Phu Fault (DBPF), Da River Fault (DRF), Ma River Fault (MRF) and Son La Fault (SLF) (Figures 6.2a and 6.2b). Most of these active faults are strike-slip faults and extends in the northwest-southeast (NW-SE) direction (Huang et al., 2009). The nature of displacements of the Da River terrane, located between the RRF and MRF, provided key constraints on the accommodation of the southward extrusion of the Indochina Peninsula. The Da River Zone represents a key area for the understanding of the geodynamic evolution of the Indochina and South China blocks during the Indonesian orogeny (Lepvrier et al., 2004). The RRFZ, located in the center of the northern part of the study region, extends 1000 km from the eastern Himalayas through southernmost China to northern Vietnam and is considered to be mechanically connected with the Indian–Eurasian collision. This fault zone is considered as a pure crustal structure (Jolivet et al., 2001; Searle, 2006). However, some authors suggested that the strike-slip RRFZ is a lithospheric structure (Gilley et al., 2003; Leloup et al., 2007). Variations in Moho and LAB depth can be used to interpret this

problem.

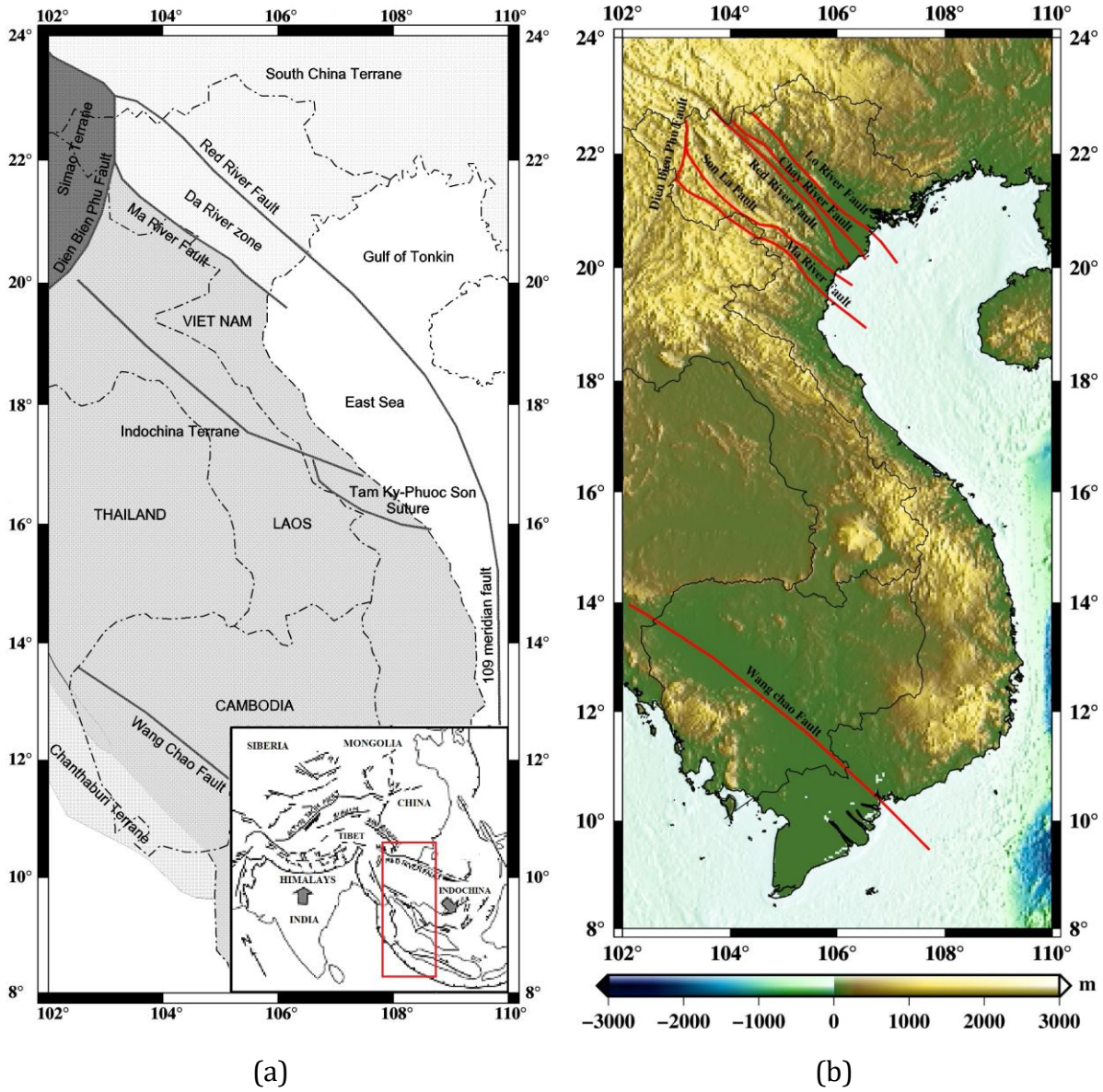

Figure 6.2. a) Tectonic situation in the study region and panel in the bottom right corner is a sketch regional tectonic map, modified from Gilley et al., (2003), and b) Topography and major active faults of the Vietnam region

According to the earthquake catalog compiled by the IGP–VAST (IGP, 2005), 90% of earthquakes in Vietnam are located in the northwest part (Huang et al., 2009); (Tran, 2012). Even if Vietnam is considered as a low-seismicity region when compared to the major tectonic activity regions in the world, it remains tectonically active, as indicated by the occurrence of moderate earthquakes (Huang et al., 2009). The earthquake catalog also indicated 30 earthquake active areas, with magnitudes of 5.5 to 6.8. Such earthquakes have caused heavy damage in the northwest as well as offshore from central Vietnam. Knowledge of the lithospheric structure is fundamental for understanding tectonic and geodynamic processes of the region and more specifically to understand the regional

consequences of collision between the Indo-Australian and Eurasian plates beneath Vietnam. For this purpose, one of the fundamental constrain to be considered is the determination of the Moho discontinuity.

6.3. Moho and LAB depth models using gravimetric geoid and DTM

In order to avoid edge effects, all computations are performed for an expanded zone 7.5^0-24.5^0N and 101.5^0-110.5^0E.

6.3.1. Geoid height and filtering

The high-accuracy GEOID_LSC gravimetric quasigeoid model was determined using the available gravity data in Vietnam. However, geoid undulations are used to determine Moho and LAB depth, so first the quasigeoid must be converted to the geoid. The grid of Bouguer gravity anomalies and the mixed SRTM model were used to compute the differences between height anomaly and geoid undulation for converting the quasigeoid to the geoid employing Eq. (2.38), called GEOID_LSC_C. This conversion procedure was not applied in recent studies using the geoid height inversion approach despite the fact that GGMs provide the height above the quasigeoid (Hofmann-Wellenhof & Moritz, 2006). The geoid is an equipotential surface of the Earth's gravity field while the quasigeoid is not. According to Hofmann-Wellenhof & Moritz, (2006), the quasigeoid-to-geoid correction can reach -0.1 m if the Bouguer gravity anomaly is -100 mGal and elevation is 1000 m. This correction varies from -0.771 to 0.020 m in the study region.

The Moho depth is often estimated by modelling gravity and/or geoid under the assumptions of local or regional isostasy. These assumptions need to be verified and this can be done using seismic data, even when sparsely distributed. First, correlation between Moho depth derived from seismic data and geoid height needs to be determined. Figure 6.3a shows correlations between Moho depth from 24 receiver functions analysis (Nguyen et al., 2013) and geoid height derived from GEOID_LSC_C and EGM2008. Thicker crusts correspond to low geoid heights. The geoid height derived from GEOID_LSC_C (R^2=0.44) agrees better than EGM2008 (R^2=0.37) with the seismic-derived Moho depths. Hence, a more accurate Moho depth beneath Vietnam is likely to be determined from GEOID_LSC_C model, even if the correlations between geoid height and Moho depth remain quite low. The explanation for such low correlation is that all masses within the Earth contribute to all wavelengths of the observed geoid. According to Bowin (1983), the degree 10 geoid i.e., wavelengths of 4000 km and longer, provides an estimation of the combined contributions from mass anomalies at the core-mantle boundary region and from the deep mantle and deeper parts, i.e., 400 km depth, of plate convergent zones. Removing the long wavelengths of the geoid height eliminates the effect of sub-lithospheric sources from geoid undulations. However, different maximum degree values have been used in past studies to filter the geoid signal for different regions. Table 6.1

shows the d/o used in several studies.

Table 6.1. Statistics of the low d/o spherical harmonics used for filtering geoid heights

N°	Model	degree/order	Country/region	Reference
1	EGM96	11	Gibraltar Arc System, Atlas Mountains	Fullea et al., (2006)
2	EGM96	11	Gibraltar Arc System, Atlas Mountains	Fullea et al., (2007)
3	EGM2008	11	Gibraltar Arc System, Atlas Mountains	Fullea et al., (2010)
4	EGM2008	11	Central Asia	Robert et al., (2012)
5	EGM2008	11	Central Eurasia	Robert et al., (2017)
6	EGM2008	8	Arabia–Eurasia collision (Iran)	Jiménez-Munt et al., (2012)
7	EGM2008	10	Southern Indian	Kumar et al., (2014)
8	EGM2008	10	Iberian Peninsula	Torne et al., (2015)
9	EGM2008	10	Africa	Globig et al., (2016)

To determine the optimum d/o for Vietnam, the removal procedure was carried out on the GEOID_LSC_C model from degree 8-11 of GOCE DIR-R5 in steps of 1 degree. The residual geoid undulations were then compared to Moho depth derived from 24 receiver functions analysis in Vietnam (Figure 6.3b). The correlation increases significantly after removing the effect of sub-lithospheric sources from long wavelengths of geoid undulations, and Figure 6.3b indicates that the optimum degree for removing the low wavelengths is 9 (R^2=0.64). After this removal, higher geoid heights correspond to thicker crust.

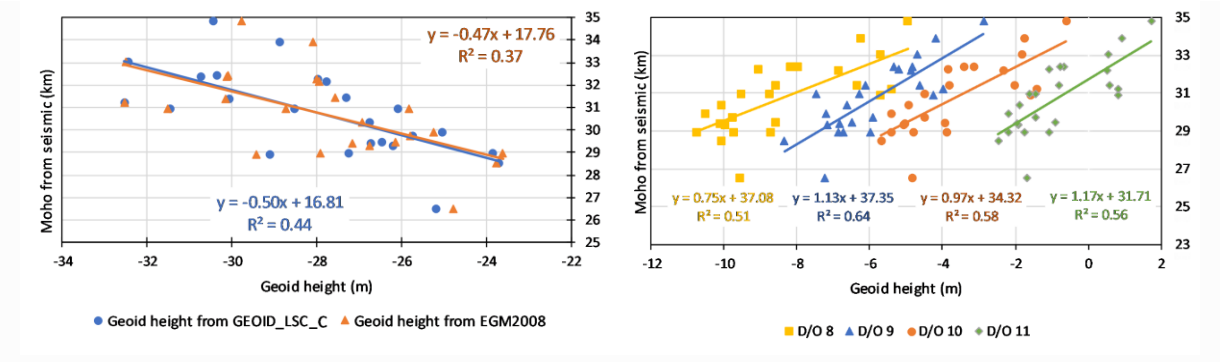

(a) (b)

Figure 6.3. Relation between Moho depths beneath seismic stations and corresponding geoid undulation retrieved from a) GEOID_LSC_C and EGM2008 and b) GEOID_LSC_C after removing low degrees

The correlation between the Bouguer gravity disturbance and Moho depth (R=-0.54) was

given by Sjöberg & Bagherbandi (2017) for South America to verify that the Bouguer gravity can be used to estimate the Moho depth. Here, the high correlation (R=0.80) between the geoid undulation and Moho depth suggests that the Moho geometry can also be estimated with geoid undulations.

Traditionally, the long wavelength components can be removed by subtracting the geoid undulations calculated from low d/o spherical harmonics corresponding to the selected long wavelength. However, according to Sandwell & Renkin (1988) a too large amplitude of residual geoid undulation between northeast and southeast Hawaii was caused by the sharp cutoff of the spherical harmonic coefficients at d/o 10. This rigorous elimination leads to side lobes in the spatial structures of the truncated fields. To minimize this effect, high-pass filtering with a 1D-Gaussian function, or a gentler cutoff was used. In the latter case, coefficients are rolled off smoothly. According to 1D-Gaussian truncation, prior to summing the series, coefficients of degree n were multiplied by:

$$w_n = exp\left[\frac{-(n-2)^2}{2(\sigma_n - 2)^2}\right] \tag{6.10}$$

when n reaches σ_n the coefficients are reduced by 0.6. In practice, σ_n was set to 9 and the coefficients for degrees range from 2-25 have been multiplied by w_n calculated using Eq. (6.10).

In gentle truncation coefficients of degree n were multiplied by:

$$w_n = \left(\frac{n - n_{min}}{n_{max} - n_{min}}\right)^4 - 2\left(\frac{n - n_{min}}{n_{max} - n_{min}}\right)^2 + 1 \tag{6.11}$$

and the rigorous truncation of coefficients at n=9 is replaced by gently cutting the spherical harmonic series from n_{min}=2 to n_{max}=16 (i.e., the coefficients for degrees range from 2-16 have been multiplied by the function w_n, Eq. (6.11)).

The resulting geoid heights from the GEOID_LSC_C model and their residuals are shown in Figure 6.4. The geoid height varies from -35.3 to 16.7 m. The low harmonic coefficients (d/o=9) from the GOCE DIR-R5 were used to remove the long-wavelengths of GEOID_LSC_C. The residuals vary from -11.9 to 0.3 m, from -7.9 to 1.5 m and from -8.8 to 1.0 m when using rigorous truncation, 1D-Gaussian function and gentle truncation, respectively. The amplitude (maximum minus minimum) after rigorous truncation (12.2 m) is much larger than after Gaussian (9.4 m) and gentle (9.8 m) truncations. The amplitudes of 1D-Gaussian and gentle truncation are at the same level with slightly better results with the Gaussian function, which is selected for computing Moho and LAB depth.

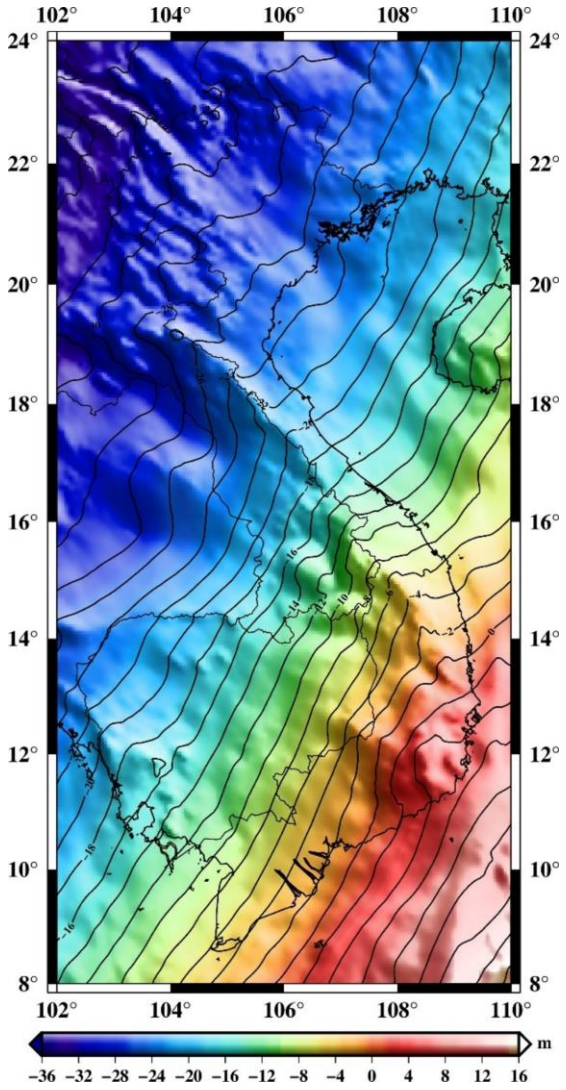
102° 104° 106° 108° 110°
24° 22° 20° 18° 16° 14° 12° 10° 8°
m
−36 −32 −28 −24 −20 −16 −12 −8 −4 0 4 8 12 16

(a)

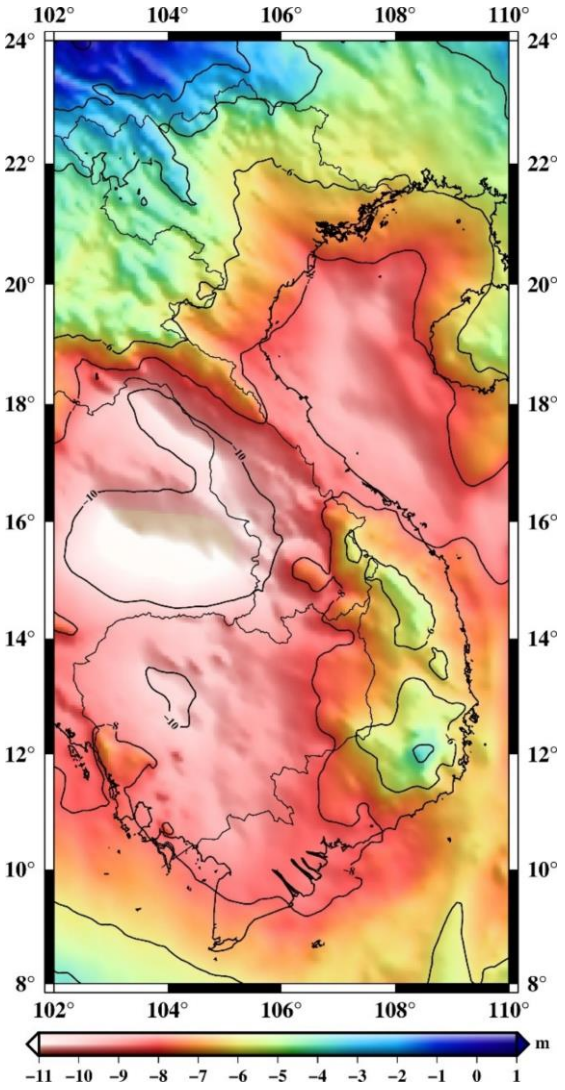
102° 104° 106° 108° 110°
24° 22° 20° 18° 16° 14° 12° 10° 8°
m
−11 −10 −9 −8 −7 −6 −5 −4 −3 −2 −1 0 1

(b)

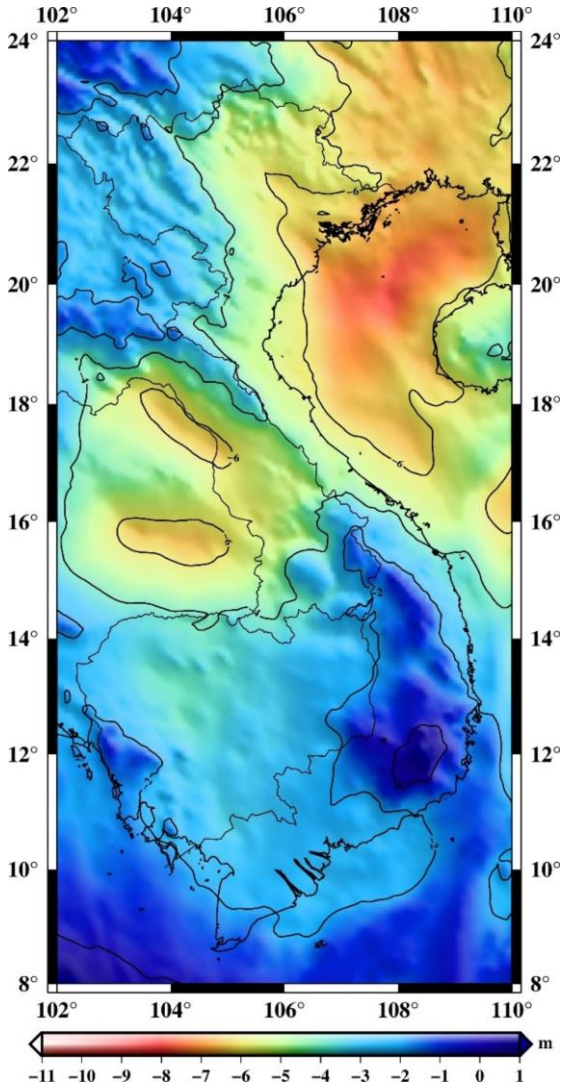

(c)

Figure 6.4. a) Geoid undulations by adding transformation from gravimetric quasigeoid to geoid, b) Residual geoid undulation by simple subtraction of low d/o from 2-9 and c) Residual geoid undulation by removing low d/o from 2-9 with a 1D-Gaussian function

6.3.2. Topography and sedimentary effect

The advantage of the isostatic hypothesis is that it removes a significant part of the influence of deep density heterogeneity to obtain a much more balanced anomaly (Kaban et al., 2016). The reality is not so simple because the isostatic anomalies may contain significant contributions due to other effects, e.g. the effect of sedimentary layers as indicated by Evans & Crompton, (1946). Therefore, sedimentary corrections should be considered before hypotheses of isostatic equilibrium. Presently, models of sedimentary basins are sufficiently reliable to calculate their effects, e.g. CRUST1.0 (Laske et al., 2012). The approach has been developed to refine the isostatic anomalies. In Bouguer gravity anomalies, the sedimentary basins, as lying on the upper part of the crust, are well-known to produce a significant gravity signal at all wavelengths. Such effect must be removed

before the gravity inversion process to estimate Moho depth (Wienecke, 2006). Sediment corrections were thus applied in many studies (Kaban et al., (2004), Braitenberg & Ebbing, (2009) Tenzer & Hamayun, (2010), Tenzer et al., (2012), Kaban et al., (2016)). Similarly, the effect of sedimentary basins in the elevation data should be also removed before applying the local isostatic assumption in combination with the geoid height to visualize the lithosphere structure. Sandwell & Renkin (1988) used the method presented by Crough (1983) to calculate the sediment correction for bathymetry. This study indicated the importance of the sediment correction on bathymetry in improving its relationship with geoid height. Despite the importance of eliminating the sedimentary effect, it was not considered in the method proposed by Fullea et al., (2007). In Globig et al., (2016), the sedimentary thickness was used to account for lateral changes in the crustal density and then the method of Fullea et al., (2007) was used to determine the lithospheric structure. However, no improvement in the accuracy of the Moho depth was obtained when compared with seismic data. In this study, the topography-corrected sedimentary basins is proposed to refine the model presented by Fullea et al., (2007) in the determination of the lithospheric structure. To compute the sedimentary effect on topography, a density-depth relationship that incorporates a sediment compaction model (Ebbing et al., 2007) is used. The function defining the density of the sedimentary basin (ρ_s) according to the depth (d) was given as follows:

$$\rho_s = \Phi_0 e^{-b_1 d}\rho_f + (1 - \Phi_0 e^{-b_2 d})\rho_g \tag{6.12}$$

where Φ_0 is the effect of porosity, ρ_f is the fluid density, ρ_g is the grain density and b_1, b_2 are the depth-decay parameters.

According to Kaban et al., (2016), the sedimentary effect was corrected on the elevation (E) as follows:

$$E^c = E - d\frac{\rho_s - \rho_{topo}}{\rho_{topo}} \tag{6.13}$$

where E^c is the elevation-corrected sedimentary layer, ρ_{topo} is the density of topography. $\rho_{topo} = 2670\ kg/m^3$ is used for the topography above the sea level, for the sea areas the density is replaced by $\rho_{topo} = 2670 - 1030 = 1640\ kg/m^3$.

The sedimentary effect is evaluated using the global sediment thickness CRUST1.0 model, which is shown in Figure 6.5a. The thickness of the sediment layer ranges from 0 to 8 km for this region. The parameters used to determine the effect of sediment on topography are listed in Table 6.2.

Table 6.2. Parameters used in the computation of the sediment effect on elevation

Parameter	Symbol	Value
Effect of porosity	Φ	0.8
Fluid density	ρ_f	1030 kg/m^3
Grain density	ρ_g	2500 kg/m^3
Depth-decay parameter	b_1	-0.9
Depth-decay parameter	b_2	-0.9

According to Fullea et al., (2006); Fullea et al., (2007) and Globig et al., (2016), the high-frequency components (wavelength of 100 km and shorter) need to be removed from the elevation data set to avoid mapping of unrealistic signals, which are related to flexural support of topographic loads, into the modeled crustal and lithospheric topography. To that end, a low-pass filter is applied to eliminate these short wavelengths from the elevation data. A simple filter was tested by averaging values of all grids being within a cutoff wavelength of the filtered grid (100 km). The disadvantage of this simple approach is that all grid nodes contribute equally. It is more realistic to use a weighting system where grid nodes close to the filtered grid node contribute more than distant nodes. Applying such a 2D-Gaussian low-pass filter instead of simple filter will lead to a smoother grid. The contribution of each grid node is weighted by a 2D-Gaussian curve as follows:

$$w(x,y) = \frac{1}{2\pi\sigma^2} exp\left[\frac{-(x^2+y^2)}{2\sigma^2}\right] \tag{6.14}$$

where σ is the standard deviation of the distribution.

The mixed SRTM model is used to derived the elevation data in the determination of the lithospheric structure. The procedure for correcting the influence of the sedimentary layer and filtering of elevation data is as follows:

- ¶ First, the 1×1^0 sediment thickness derived from CRUST1.0 model was re-gridded to 1' to compute sediment corrections for the topography using Eq (6.13). The 3 arc-second mixed SRTM model (Figure 6.5b) was also re-sampled to 1' and added the sediment corrections, called the mixed SRTM-corrected sediment, for determining the Moho depth model;
- ¶ Then, using simple or 2D-Gaussian low-pass filtering, the short-wavelengths (i.e., <100km) were removed from the mixed SRTM-corrected sediment grid, shown in Figures 6.5c and 6.5d, respectively.

The 2D-Gaussian low-pass filtered elevation data are much smoother, especially in mountainous regions with rapid elevation changes.

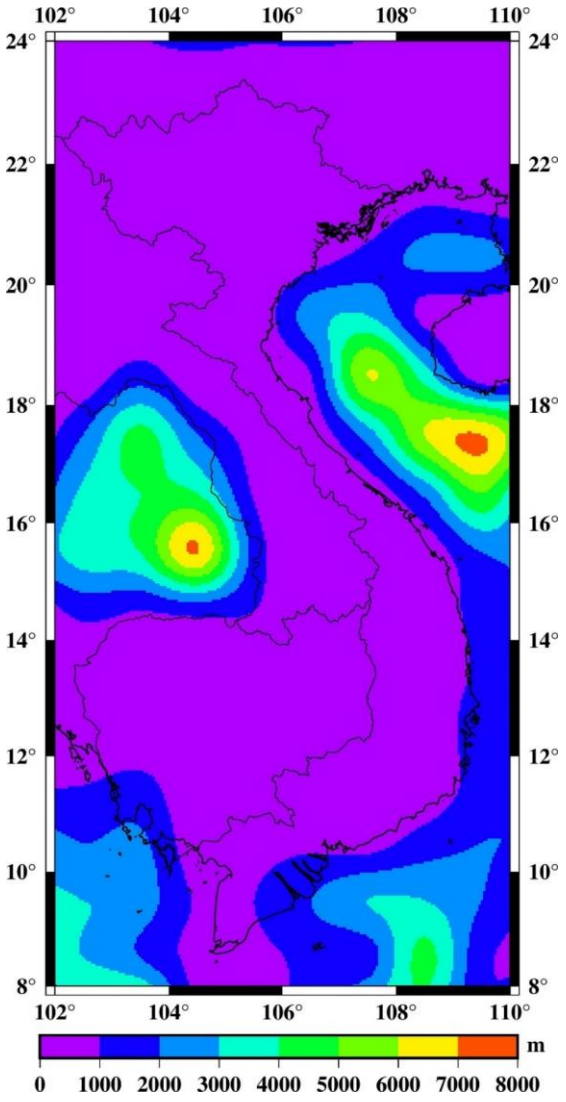
102° 104° 106° 108° 110°
24° 22° 20° 18° 16° 14° 12° 10° 8°
m
0 1000 2000 3000 4000 5000 6000 7000 8000

(a)

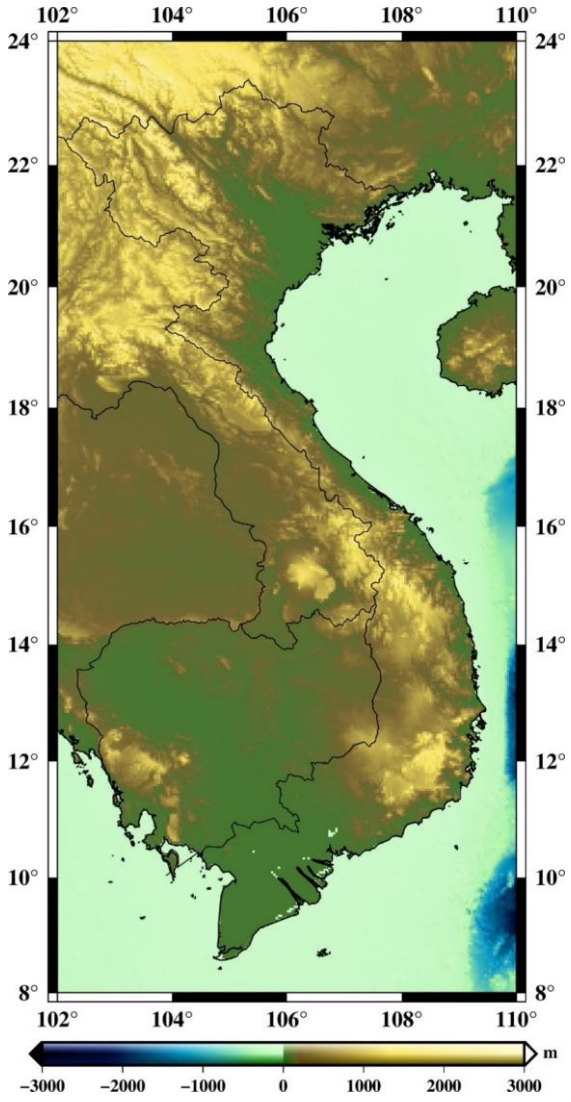
102° 104° 106° 108° 110°
24° 22° 20° 18° 16° 14° 12° 10° 8°
m
−3000 −2000 −1000 0 1000 2000 3000

(b)

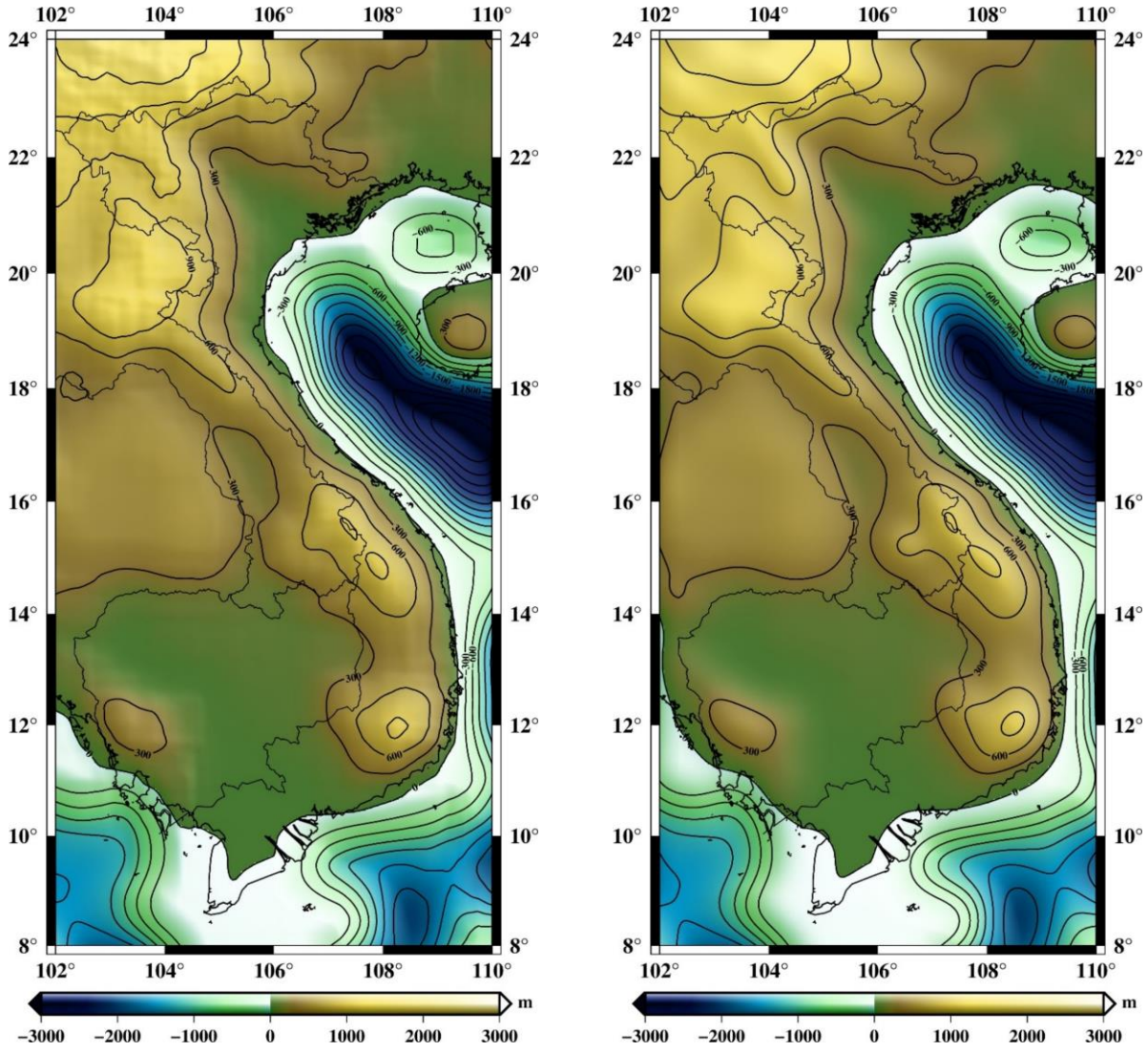

(c) (d)

Figure 6.5. a) Sediment thickness derived from the CRUST1.0 model, b) Elevation data from the mixed SRTM model, c) and d) Topography-corrected sediments after removing short-wavelengths using simple and 2D-Gaussian filter, respectively

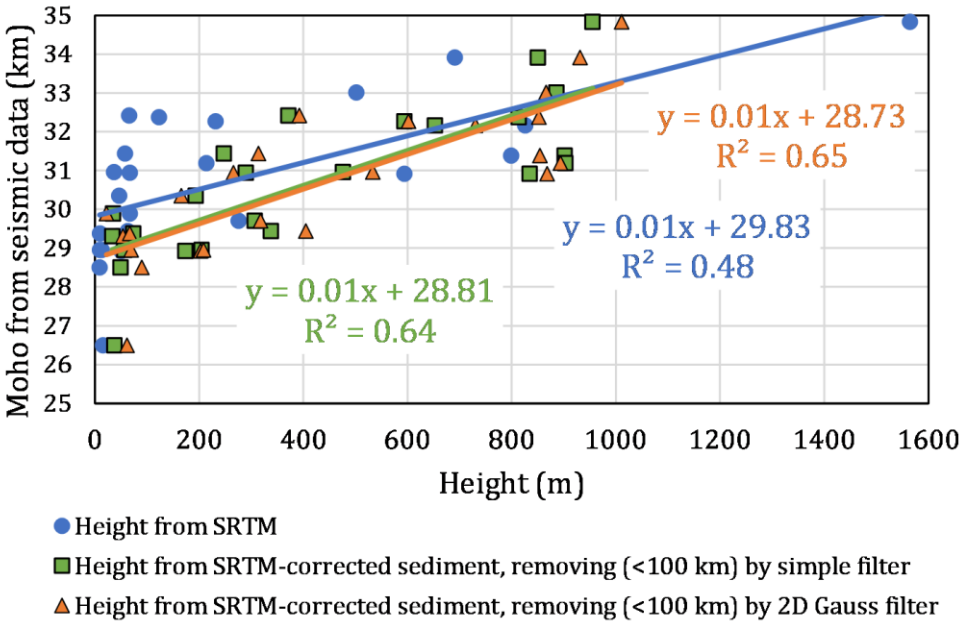

Figure 6.6. Relation between Moho depths beneath seismic stations and corresponding elevation data

The correlations between Moho depth derived from seismic data with elevation, elevation-corrected sediment removing short-wavelengths with a 2D-Gaussian or simple filter are displayed in Figure 6.6. A high correlation with elevation data after removing short-wavelength signals (R=0.81 with 2D-Gaussian filter and R=0.80 with simple filter), identical to between Moho depth with geoid height after removing long-wavelengths, can be seen. The two filtering methods give nearly identical results in terms of correlation, but the 2D-Gaussian low-pass filtered elevation data are much smoother and will be used to compute Moho and LAB depth.

Then, the geoid height, removing long-wavelengths with a 1D-Gaussian high-pass filter for low spherical harmonic coefficients (d/o 9), and elevation-corrected sediment layer data, removing short-wavelength components using a 2D-Gaussian low-pass filter (i.e., 100 km), will be used in the following section to determine Moho and LAB depth. However, in this study region, no seismic data is available on the sedimentary basins, e.g., Khorat Plateau or Gulf of Tonkin, to validate the proposed method. Therefore, a calculation is firstly performed on a test area where reliable seismic data allow to assess the efficiency of applying the sedimentary correction to topography in computation of the Moho depth. Consequently, the Moho and LAB depth will be determined for Vietnam using the proposed method.

6.3.3. Moho depth estimation in the test area

The selected test area is located in Central Eurasia where a Moho depth model was determined by Robert et al., (2017) using geoid height and elevation data derived from

EGM2008 and ETOPO1. In this area, bounded by 35-50°N and 70-100°E, lies the Tarim basin, one of the largest basins in the world. A set of relatively complete seismic data was collected to validate the model proposed by Robert et al., 2017. From these seismic data, 30 stations located on the sedimentary basins are selected to validate the proposed approach (Figure 6.7a). Similar to Robert et al., (2017), the geoid height derived from EGM2008 after removing signals to d/o 11 and elevation data from ETOPO1 after filtering wavelength shorter than 100 km are used to calculate the Moho depth. The sedimentary thickness derived from the CRUST1.0 model is used to calculate the effect on the topography. The procedure described in Section 6.3.2 is used to correct for the effect of sedimentary layer and the filtering of elevation data, and the parameters listed in Table 6.2.

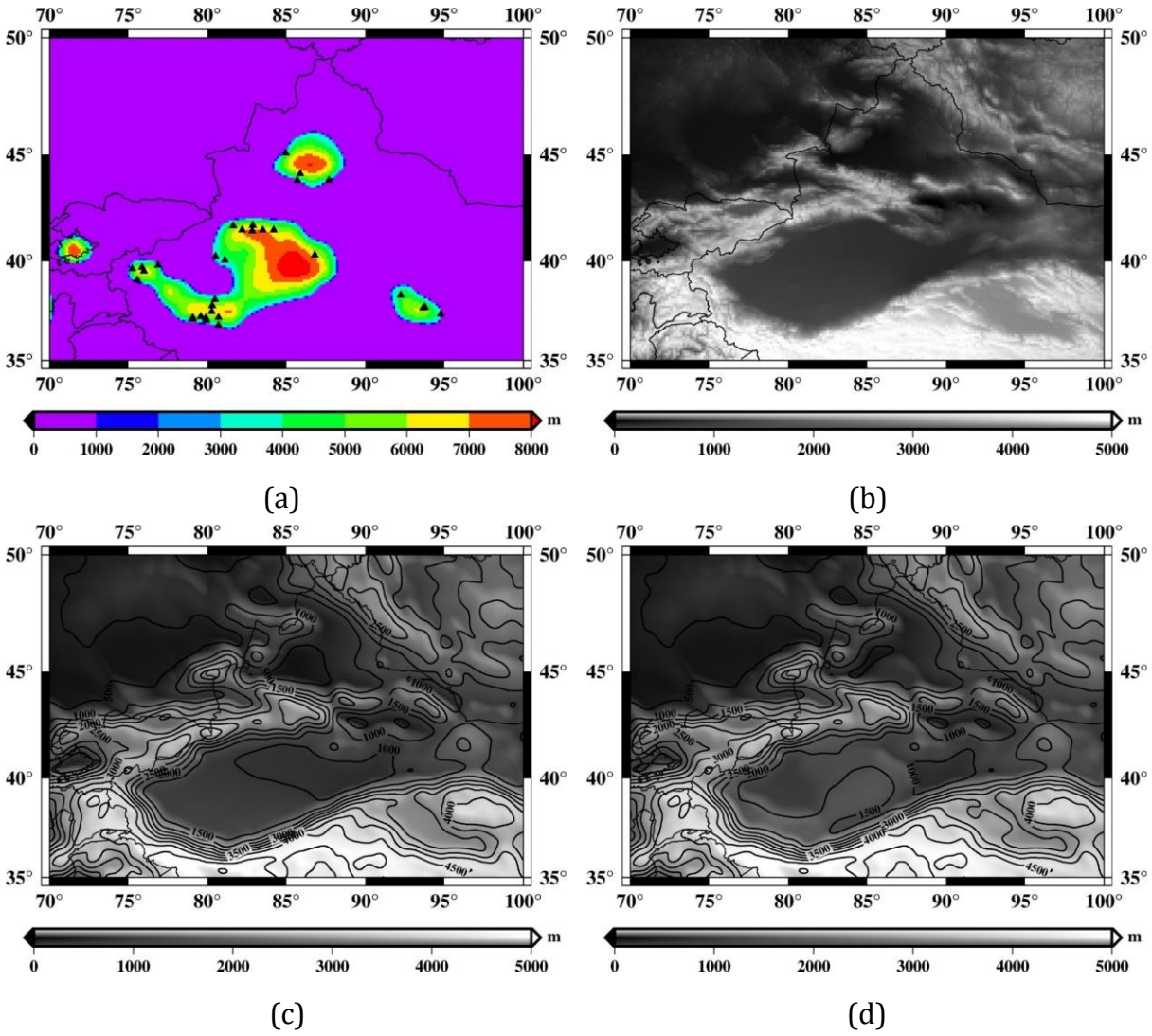

Figure 6.7. a) Thickness of sediment layer from CRUST 1.0, black triangles are seismic stations, b) topography from ETOPO1, c) topography after short-wavelengths (100 km) filtering and d) topography-corrected sedimentary effect after short-wavelengths (100 km) filtering

The thickness of sediment layer, topography, topography after short-wavelength filtering and topography-corrected sedimentary effect after short-wavelength filtering are shown in Figures 6.7a, 6.7b, 6.7c and 6.7d, respectively. The 2D-Gaussian filter is used to remove short-wavelengths.

The correlations between Moho depth and elevation after removing short-wavelengths, and elevation-corrected sediment after removing short-wavelengths were computed and are displayed in Figure 6.8. A higher correlation coefficient is obtained when the sediment effects are taken into account (R=0.64 versus R=0.59).

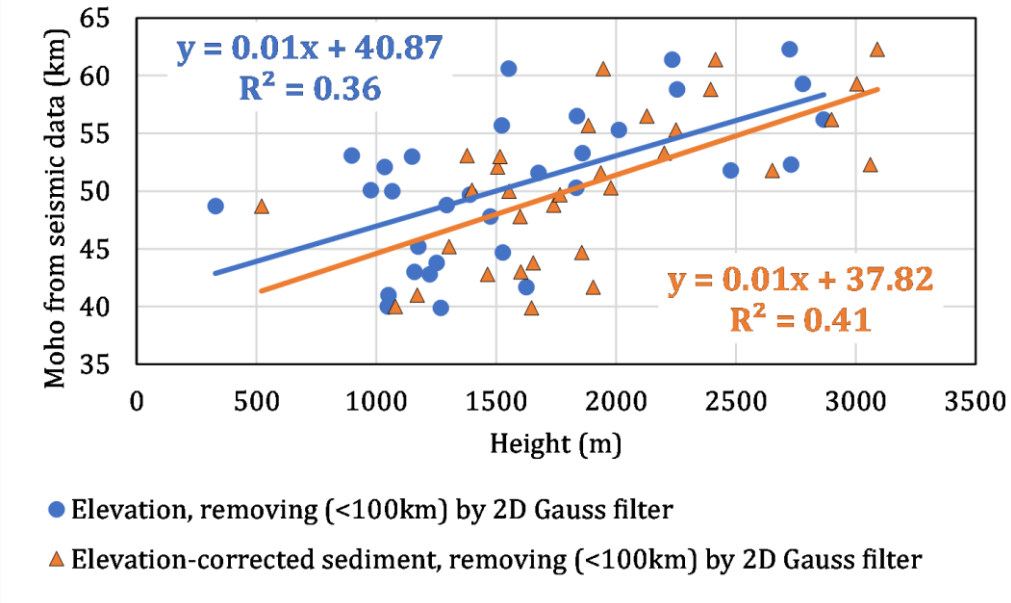

Figure 6.8. Relation between Moho depth beneath seismic stations and corresponding elevation data

The Matlab program was used to determine the Moho depth for the test region. Table 6.3 summarizes the parameters used in the calculation of the Moho depth for the test region. The absolute discrepancies beneath seismic stations, between the different estimations of Moho depth (using elevation-corrected sediment after removing short-wavelengths and elevation after removing short-wavelengths only), as well as those obtained from Robert et al., (2017) are shown in Figure 6.9. The average discrepancies are 4.2, 5.0 and 6.3 km, respectively. The comparison indicates that there is significant improvement in the accuracy of the Moho depth when the elevation correction for the sedimentary effect is used, and it will be applied in the determination of the lithospheric structure for Vietnam in the next section.

Table 6.3. Parameters used in the computation of lithospheric structure

Parameter	Symbol	Value
Upper crustal density	ρ_c^T	2700 kg/m^3
Lower crustal density	ρ_c^B	2900 kg/m^3

Seawater density	ρ_W	1030 kg/m^3
Asthenosphere density	ρ_a	3200 kg/m^3
Compensation level depth	z_{max}	300 km
Moho depth of the reference column	z_{cREF}	28.5 km
LAB depth of the reference column	z_{LREF}	129 km
Crustal surface heat production	H_s	$2.5\ 10^{-6}\ exp(-(z+E)/15000)\ W/m^3$
Linear coefficient of thermal expansion	α	3.5 10^{-5} K^{-1}
Crustal thermal conductivity	k_c	2.5 W m^{-1} K^{-1}
Mantle thermal conductivity	k_m	3.2 W m^{-1} K^{-1}
Surface temperature	T_s	15 ^{0}C
Temperature at the LAB	T_a	1350 ^{0}C

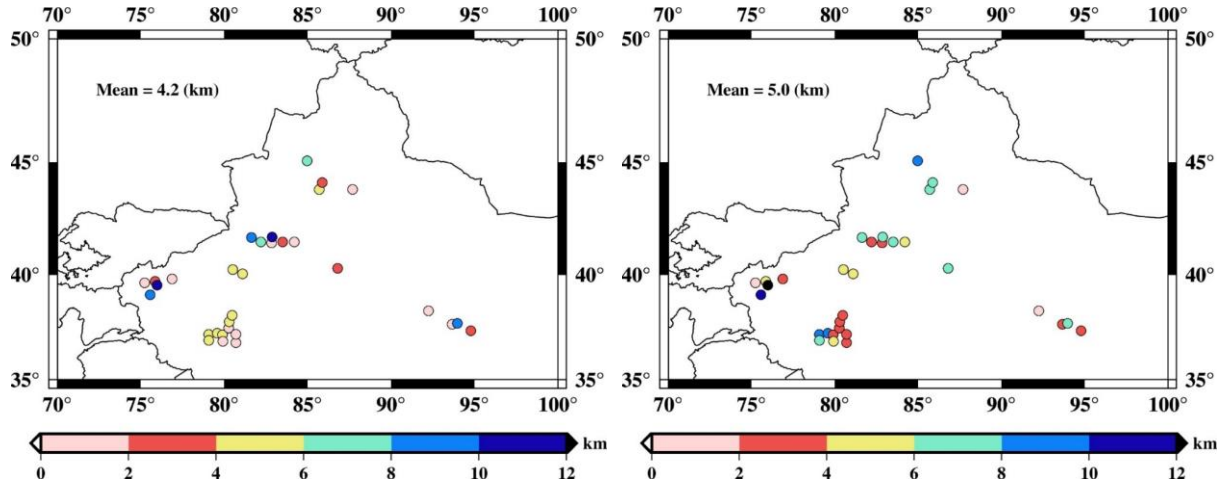

(a) (b)

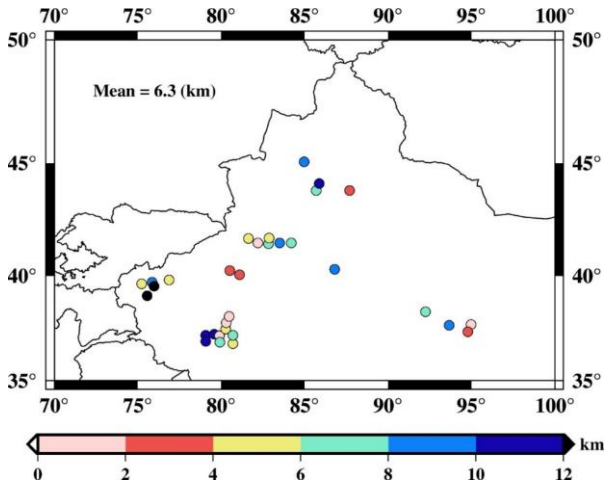

(c)

Figure 6.9. Absolute differences of Moho depth beneath seismic stations and those from the new estimations: a) Using elevation-corrected sediment after removing short-wavelengths (100 km), b) Using elevation after removing short-wavelengths (100 km) and c) Moho depth from Robert et al., (2017)

6.3.4. Moho and LAB depth estimation for Vietnam

The densities of the crust (ρ_c) and lithospheric mantle (ρ_m), and reference Moho depth (z_{cREF}) play an important role in the computation model of Moho and LAB depth using the geoid height and elevation data. The crustal density is determined by assuming a linear increase with depth between constant values at the upper ($\rho_c^T = 2670$) and lower ($\rho_c^B = 2820$) crust, corresponding to an average crustal density of 2745 kg/m^3. The lithospheric mantle density is considered to vary with temperature. To calculate the lithospheric mantle density, the temperatures at the surface and at the base of the lithosphere are fixed. For the reference Moho depth value, an average depth of 30.6 km was estimated using the 50 seismic receiver functions in the study region. One has to take into account that these stations are mainly in the north of Vietnam. There are no stations in the Mekong Delta where the depth is expected to be much thinner than in the north. The Moho depth was computed with z_{cREF} ranging from 28-31 km in steps of 0.5 km. The Moho depths were then compared to those derived from receiver functions analysis. Finally, the best Moho depth model was obtained for z_{cREF} = 28.5 km. The remaining parameters are used as listed in Table 6.3. After filtering of geoid height and elevation data, the models of Moho and LAB depth, called Moho_GEOID and LAB_GEOID, respectively, were obtained. The results are shown in Figure 6.10 and listed in Table 6.4.

The Moho depths vary from 15.3 to 37.8 km with mean and STD of 28.0 and 4.0 km, respectively. The lithospheric depths vary from 82.3 to 144.7 km with mean and STD of 123.1 and 12.3 km, respectively. Small Moho depths are generally seen over sea ranging from 15 to 25 km, increasing with topographic elevation in mainland areas with maxima in the northwest mountainous region, ranging from 32 to 35 km (up to 37 km in the south of China). The geological and geodynamic settings of the area are fairly complex there. On the mainland, local minima are observed of about 27 km in the Mekong Delta (southern Vietnam). Similar to Moho depth, LAB depth also tends to be small over sea and larger in the north of Vietnam.

Table 6.4. Statistics of Moho and LAB depth. [Unit: km]

	Min	**Max**	**Mean**	**STD**
Moho_GEOID (1 minute)	15.3	37.8	28.0	4.0
LAB_GEOID (1 minute)	82.3	144.7	123.1	12.3
Moho_GRAVITY (1 minute)	12.2	38.5	28.5	4.3
Moho_GRAVITY-Moho_GEOID	-4.3	7.5	0.5	1.3

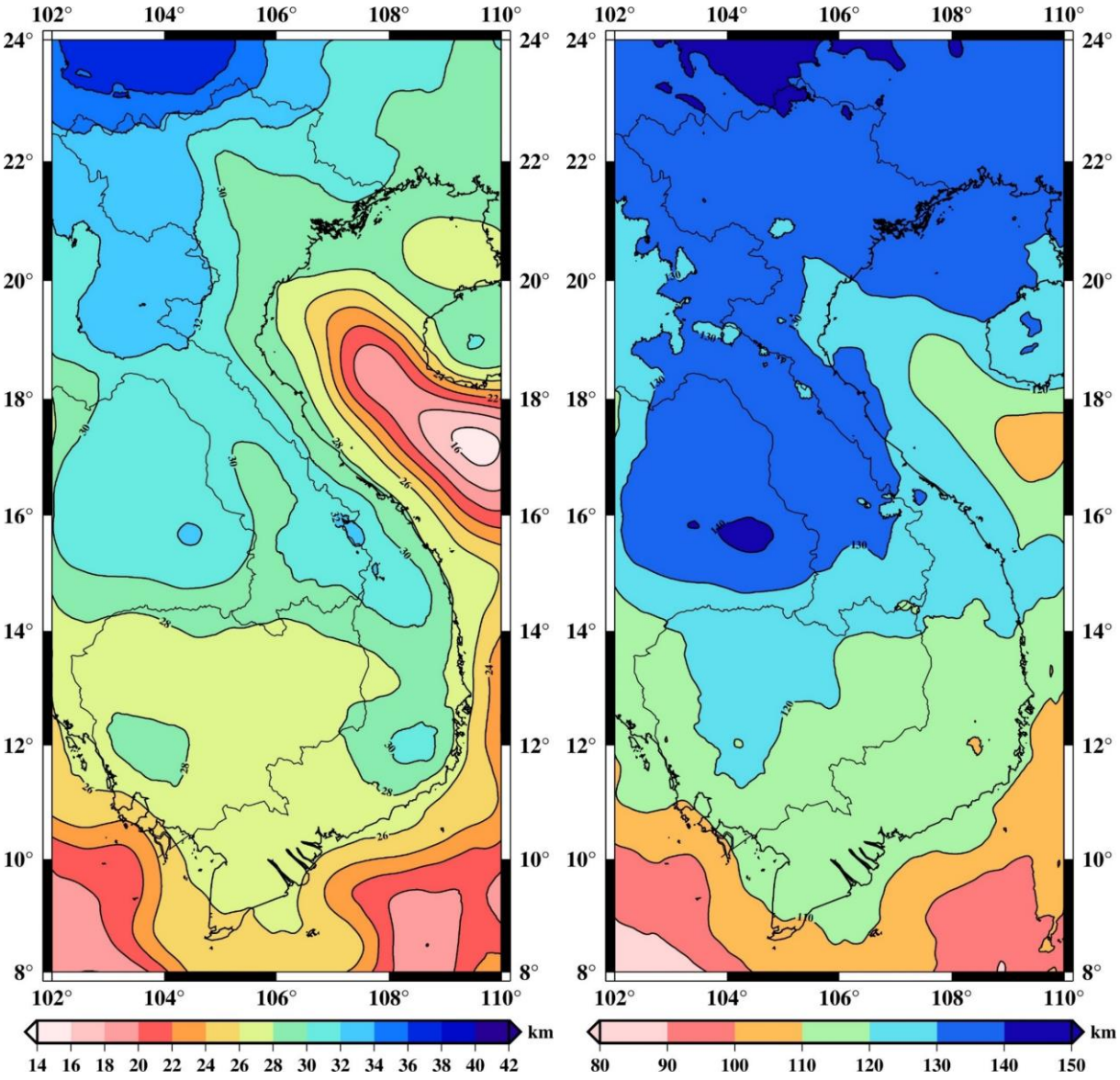

Figure 6.10. Lithospheric structure derived from elevation and geoid height data. a) Depth of the Moho (Moho_GEOID), b) Depth of the lithosphere (LAB_GEOID)

In general, most of the spatial features in the Bouguer gravity anomalies (as seen in Figure 3.7c) largely reflect the Moho depth variations. Positive anomalies over sea usually are considered to be due to thin crust, whereas negative ones are indicative of a thick crust. Lowest Bouguer gravity anomalies (-150 to -200 mGal) in the northwest region of Vietnam correspond to the thickest crust there (up to 35-37 km). The anomalies around 0 in the Mekong Delta correspond to a Moho depth of about 27 km. Similar to the Bouguer gravity anomalies, the topography-corrected sediment layer after removing short-wavelength components (<100 km) is also in good agreement with the trend in Moho depth model (Figure 6.5d). High elevations (up to 3100 m) in the northwest region are linked to a thick crust corresponding to the high loading there.

The vertically average value of the lithospheric mantle density can be also determined by using Eq. (6.4). The results are shown in Figure 6.11. This value varies from 3247 to 3263 kg/m^3. A mean value of 3252 kg/m^3 for the study region was determined from the vertically averaged density. With a mean value of the crustal density of 2745 kg/m^3, a density contrast of 507 kg/m^3 will be used to calculate the Moho depth model based on the gravity inversion method.

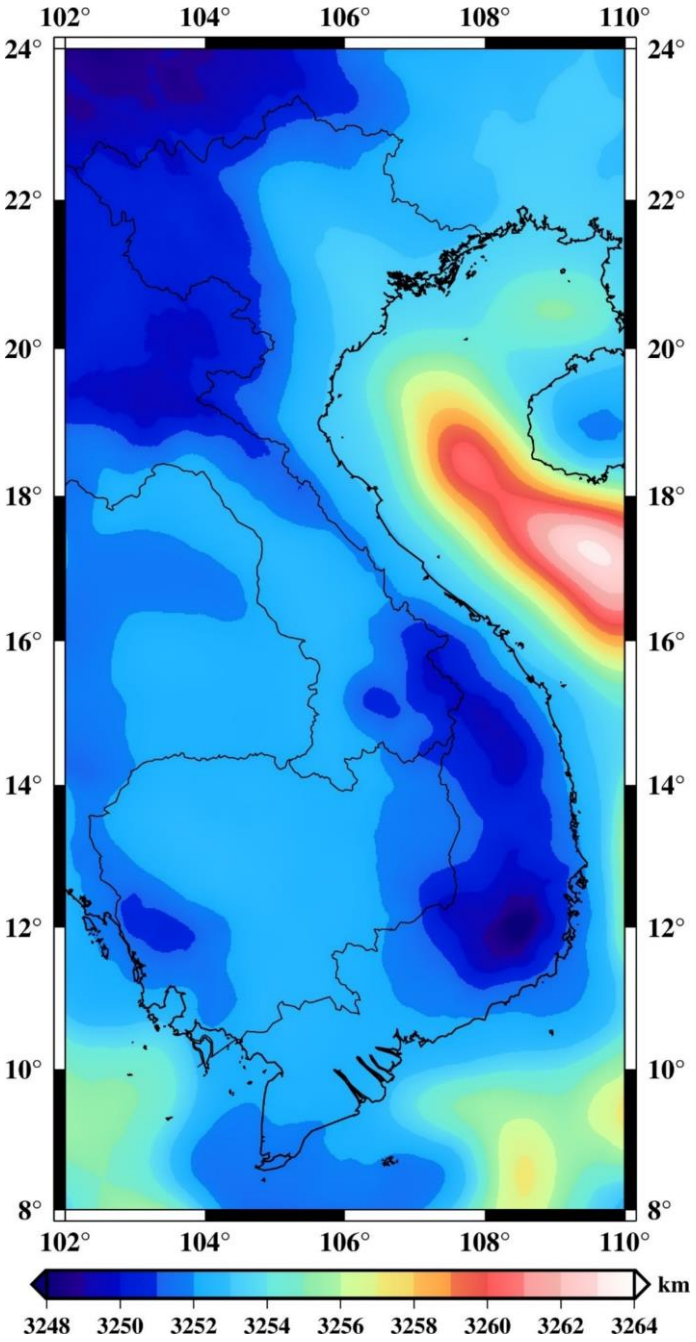

Figure 6.11. Average value of the lithospheric mantle density

6.4. Gravity data inversion for Moho depth

The new grid of Bouguer gravity anomalies is used to estimate the Moho depth model based on the inversion method. To verify that the Bouguer gravity can be used to estimate

the Moho depth, the correlations between Moho depth beneath seismic stations and corresponding Bouguer gravity anomaly interpolated from the new grid were also computed. Figure 6.12 shows correlations between Moho depth from 24 receiver functions analysis and Bouguer gravity anomalies derived from the new grid and WGM2012. Thicker crusts correspond to low Bouguer gravity anomalies. It is evident that the Bouguer gravity anomalies derived from the new grid (R^2=0.66) agree better than WGM2012 (R^2=0.51) with the seismic-derived Moho depths. As geoid height and elevation data, the high correlation (R=0.81) between the Bouguer gravity anomaly and Moho depth suggests that the Bouguer gravity anomaly is a helpful tool for estimating the Moho geometry.

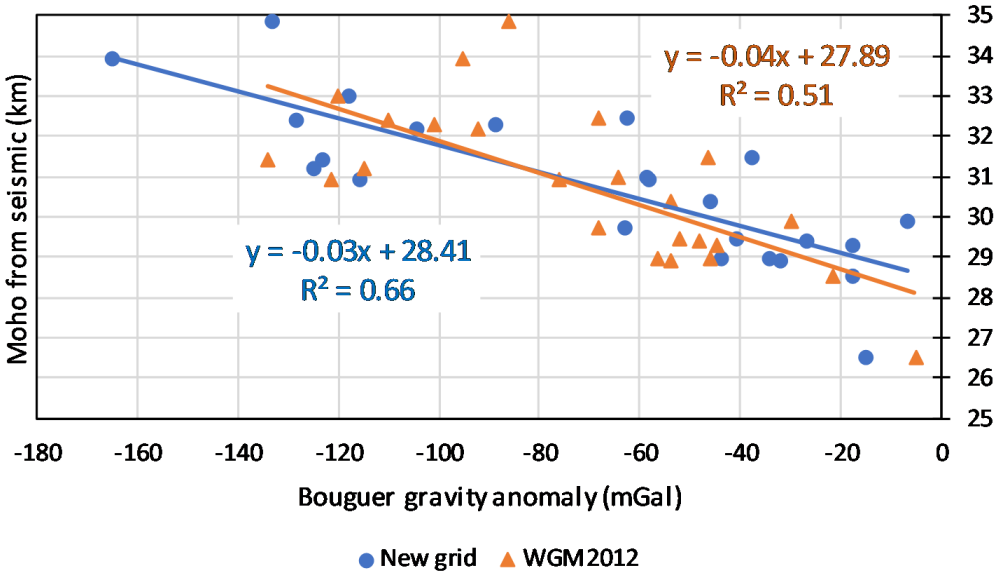

Figure 6.12. Relation between Moho depths beneath seismic stations and corresponding Bouguer gravity anomaly data

The undulating boundary corresponding to the Moho can be calculated from gravity data based on the inversion method. For this Moho depth estimation, the Bouguer anomaly is more commonly used over land, whereas Free-air anomalies are usually preferred over sea (Stephen et al., 2003; Pérez-Gussinyé et al., 2004). However, using marine Bouguer anomalies may be valuable to avoid effects of bathymetric irregularities and to visualize sub-sea floor density effects. In this study, only Bouguer anomalies were used for the whole of study region.

Similar to geoid undulation, the Bouguer gravity anomalies also need to be removed the long-wavelength components because the filter defined for the Parker-Oldenburg iterative process may be not enough to remove very long wave length effects or at least to reduce the number of iterations in the Parker-Oldenburg process. The long-wavelengths corresponding to d/o 18 were removed in Prasanna et al., (2013) for estimating Moho

depth in Sri Lanka. The long-wavelengths to d/o 18 derived from GOCE DIR-R5 were used to remove the long wavelengths in the Bouguer gravity anomalies grid.

Residual information of the gravity field mainly corresponds to the crust/mantle density contrast, but as mentioned above, sedimentary basins can also produce a long wavelength signal thus influencing the crust/mantle interface estimation by gravity inversion process (Wienecke, 2006). The gravity effect of sediments was calculated and removed using the global sediment thickness model of CRUST1.0 (Figure 6.5a) before performing the inversion procedure. Similar to calculate the sediment corrections on the topography, the sediment corrections were evaluated using the sedimentary density depends on the depth calculating by Eq. (6.12). These corrections were applied to Bouguer gravity anomalies. The Bouguer-corrected sediment anomalies after removing long-wavelengths are shown in Figure 6.13a. The 3DINVER.M (Gómez-Ortiz & Agarwal, 2005) program-based on Parker-Oldenburg's (1974) method is used to invert the Bouguer anomalies. In the 3DINVER.M program, the choice of constant density contrast and average Moho depth plays an important role in the quality of the estimated model. To be consistent with the results of Moho depth using geoid height and elevation data, the mean densities of crust and mantle are considered like in Section 6.3, i.e., a constant density contrast between crust and mantle of 507 kg/m^3. The density contrast is generally higher in mainland than in marine areas, and the constant density assumption may cause a bias. This is a common problem of Moho estimation from gravimetric methods with constant crust–mantle density contrast. But lack of seismic data over sea of the study area to validate the estimated Moho depth does not allow testing different density contrasts for mainland and marine areas. An average Moho depth of 28.5 km was also used to estimate Moho depth based on the gravity inversion method.

The new Moho depth, called Moho_GRAVITY, varies from 12.2 to 38.5 km with mean and STD of 28.5 and 4.3 km, respectively. The results are listed in Table 6.4 and shown in Figure 6.13b. The comparison between Moho_GRAVITY and Moho_GEOID was done, and the statistics are provided in Table 6.3, while Figure 6.13c illustrates the differences between the two estimated Moho depths. As seen from this comparison, the results are very close in most areas (differences are mostly within ±1 km). The differences range from −4.3 to 7.5 km with mean and STD value of 0.5 and 1.3 km, respectively. The largest differences occur in the northern and southern edges of the study region. This is due to edge effects in the calculation, but the objective is a model for Vietnam, which is not affected. It is reassuring that there are two very close Moho depth models for the study area. Both models will be validated in the next section using Moho depths derived from global and regional models as well as seismic receiver functions.

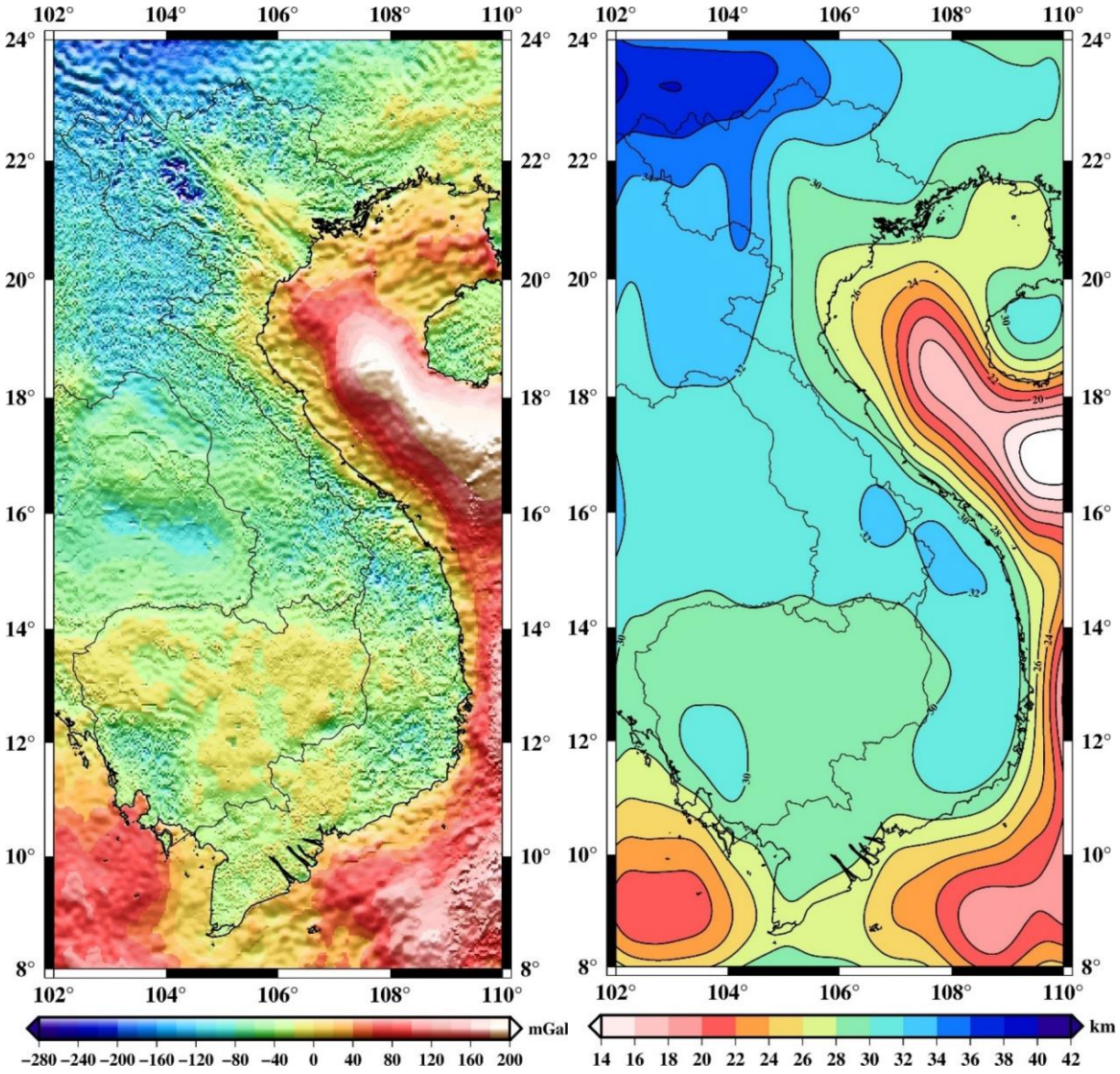
102°
104°
106°
108°
110°
24°
22°
20°
18°
16°
14°
12°
10°
8°
mGal
−280 −240 −200 −160 −120 −80 −40 0 40 80 120 160 200
km
14 16 18 20 22 24 26 28 30 32 34 36 38 40 42

(a) (b)

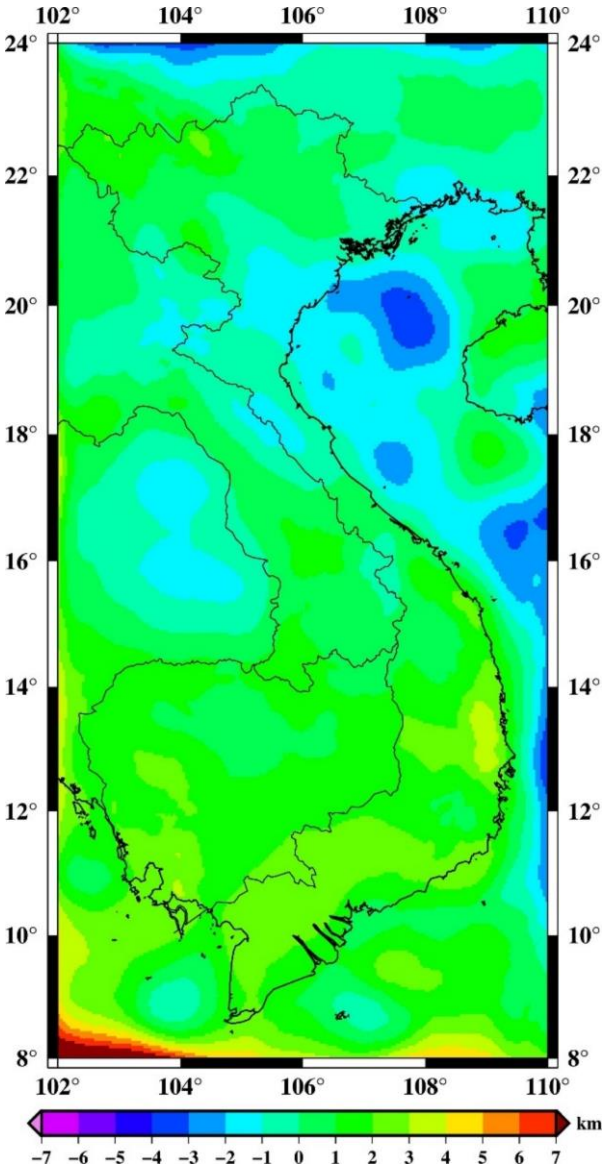

(c)

Figure 6.13. a) Bouguer-corrected sediment anomalies after removing long-wavelengths, b) Moho depth from gravity inversion (Moho_GRAVITY) and c) differences between Moho_GRAVITY and Moho_GEOID

The results obtained from the present study can be also highlighted in the context of the geodynamic evolution of the region. The lithospheric structure of the study area is not only linked to the collision between the Indochina and South China blocks but also to the extrusion process caused by the collision between the Indian Plate and Eurasian Plate, which began at about 50 Ma (Huchon et al., 1994). The rapid increase of the Moho depth in the northwest region is considered due to the southeastern extension of the eastern Tibetan plateau along the eastern Himalayan syntaxis (Dinh et al., 2018). The thinner crust in the Hanoi plain and its eastern coastal plain region is suggestive of a recent rifting process of the opening of the East Sea (Dinh, 2010). This is called the Red River rift, and it is located between the LRF and RRF (Mazur et al., 2012). Hence, an uplifted structure

characterizes the Moho surface in this section where the Moho depth is about 28 km. The obvious differences in the trends of structures in the northeast and southwest sides of RRFZ are signatures of crustal scale deformation along this fault system in northern Vietnam. These differences in Moho depth also confirm that the RRFZ may be considered to be the boundary between two continental blocks: South China and Indochina blocks. The NW-SE trend in the northern part corresponds to the extension direction of major active fault systems shown in Figure 6.2b. The Moho depth models agree that the RRFS extended southward in the sea of Vietnam and joined the 109° meridian fault zone. The 109° meridian fault, originating in the south Hainan island area, is the major fault line trends south, passing through the whole of the East Vietnam continental shelf, then the west coast of Kalimantan island until it reaches the Sunda bay of Indonesia (Figure 1a). This confirms the important role this fault plays in the tectonic movement across the sea as well as the southeastern continental shelf of Vietnam (Nguyen et al., 2012). Another hypothesis by Tapponnier et al. (1986) suggested that it is affected by the southeastward extrusion and large counter-clockwise motions of the Indochina block along the RRF and Wang Chao fault which in turn were reactivated by the collision of the Indian subcontinent with Eurasia. Obviously, deeper geological and geophysical investigations would be required to refine the complex geodynamic evolution of this region.

6.5. Validation of the Moho and LAB depth

The assessment of the Moho and LAB depth models is carried out here in two steps: first, from a comparison with available global or regional models (statistics summarized in Table 6.5) and then from a confrontation with the results derived from seismic data.

The CRUST1.0 (Laske et al., 2013) global model, based on seismic data, has a resolution of 1 arc-degree. The model includes various types of information for the Earth's crust, e.g., density, sedimentary thickness, as well as Moho depth values. Figure 6.14a shows the Moho depth of CRUST1.0 for the study region, which varies from 20.0 to 40.9 km. The comparison was made between two new models and CRUST1.0. The statistics of the differences between the Moho_GEOID and Moho_GRAVITY models with CRUST1.0 are listed in Table 6.5, and Figures 6.14b and 6.14c illustrate them. Generally, two new models present a large difference with the Moho depth in CRUST1.0 model. A southeast–northwest trend can be seen in Figures 6.10a, 6.13b and 6.14a with small Moho depths are over sea, increasing in mainland areas with maxima in the northwest. As seen from this comparison, differences are mainly within ±4 km, especially on land. These differences range from -14.4 to 6.1 km with mean bias and STD of -4.6 and 3.1 km, respectively, for Moho_GEOID model. With Moho_GRAVITY, the differences range from -15.4 to 6.7 km with mean bias and STD of -4.0 and 3.4 km, respectively. The large biases (4.6 and 4.0 km) is probably due to inaccuracies of the CRUST1.0 model for this area, as

seismic data are very sparse. Moreover, it should be stressed that two estimated models and CRUST1.0 have different resolutions (1' and 1° for the estimated models and CRUST1.0, respectively). This leads the large bias in this comparison. A comparison with the seismic data collected from recent studies will verify for this argue.

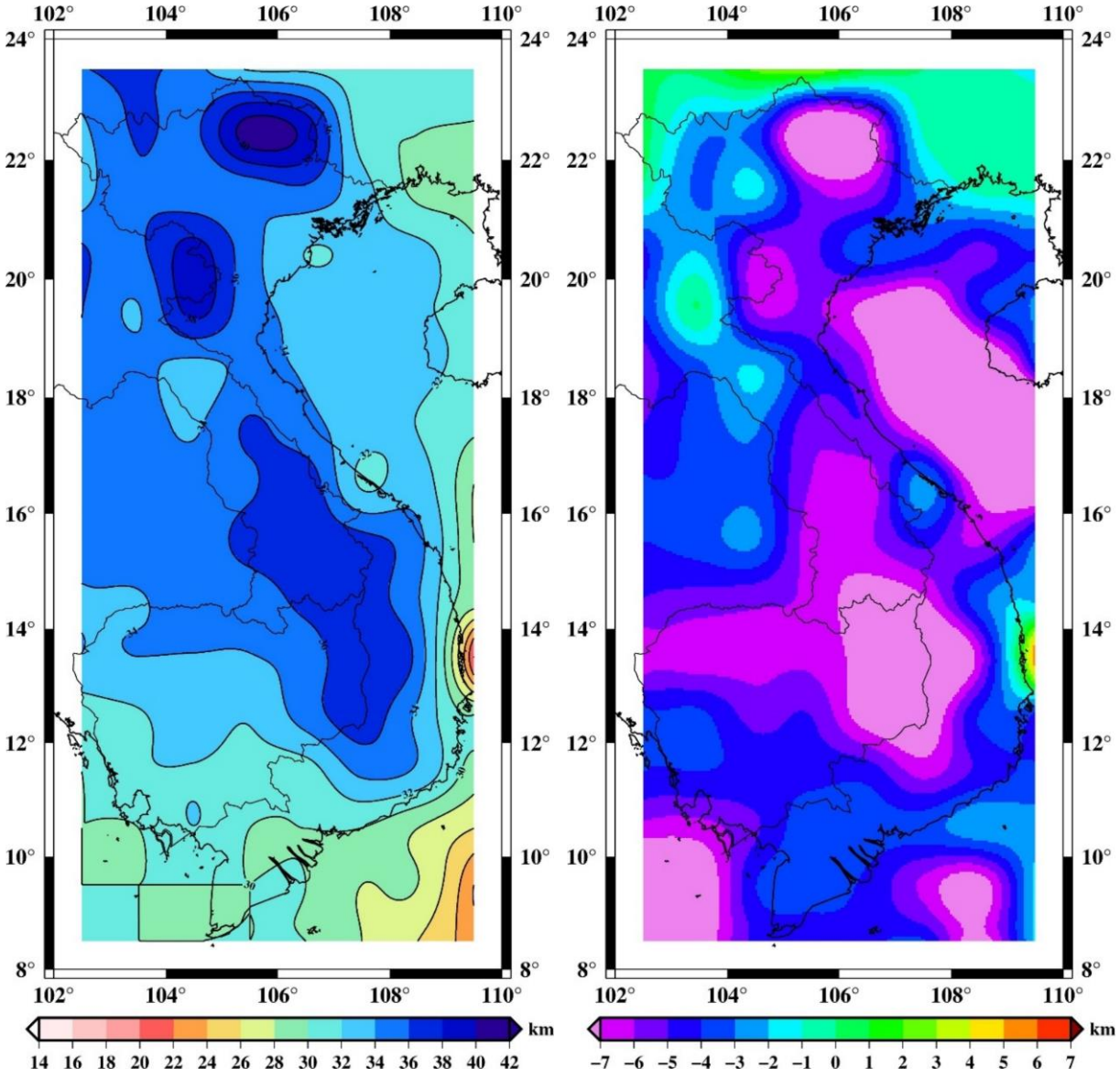

(a) (b)

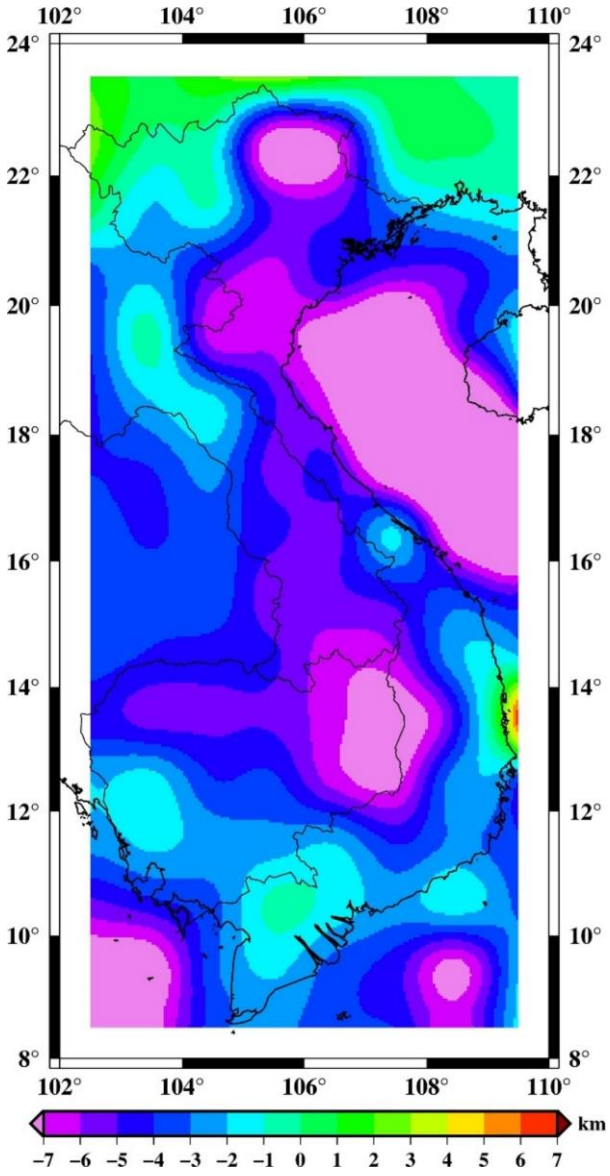

(c)

Figure 6.14. a) Moho depth derived from CRUST1.0 model, b) Differences between Moho_GEOID with CRUST1.0 and c) Differences between Moho_GRAVITY with CRUST1.0

Table 6.5. Statistics of differences of Moho depth. [Unit: km]

Model	Min	Max	Mean	STD
CRUST1.0 (1 degree)	20.0	40.9	32.7	3.3
GEMMA (0.5 degree)	17.6	54.4	33.9	6.3
Moho_GEOID-CRUST1.0	-14.4	6.1	-4.6	3.1
Moho_GEOID-GEMMA	-17.3	3.8	-5.8	4.1
Moho_GEOID- Nguyen et al 2018	-9.4	3.3	-1.2	1.8
Moho_GRAVITY-CRUST1.0	-15.4	6.7	-4.0	3.4
Moho_GRAVITY-GEMMA	-17.6	3.9	-5.2	3.7
Moho_GRAVITY-Nguyen et al 2018	-8.2	4.5	-1.1	2.0

The global gravity Moho model (GEMMA; Reguzzoni & Sampietro, 2014) was computed by inverting the global grid of second radial derivatives of the gravitational potential observed by the ESA mission GOCE and by considering the density of the crust of the CRUST2.0 model. GEMMA is available with a resolution of 0.5^0. Figure 6.15a shows the Moho depth derived from GEMMA for the study region. The statistics in Table 6.5 indicate that the Moho depths derived from GEMMA vary from 17.6 to 54.4 km. The Figures 6.10a, 6.13b and 6.15a show that variable trends of Moho_GEOID, Moho_GRAVITY and GEMMA model are close. This is reasonable because these models are based on the isostatic gravity hypothesis.

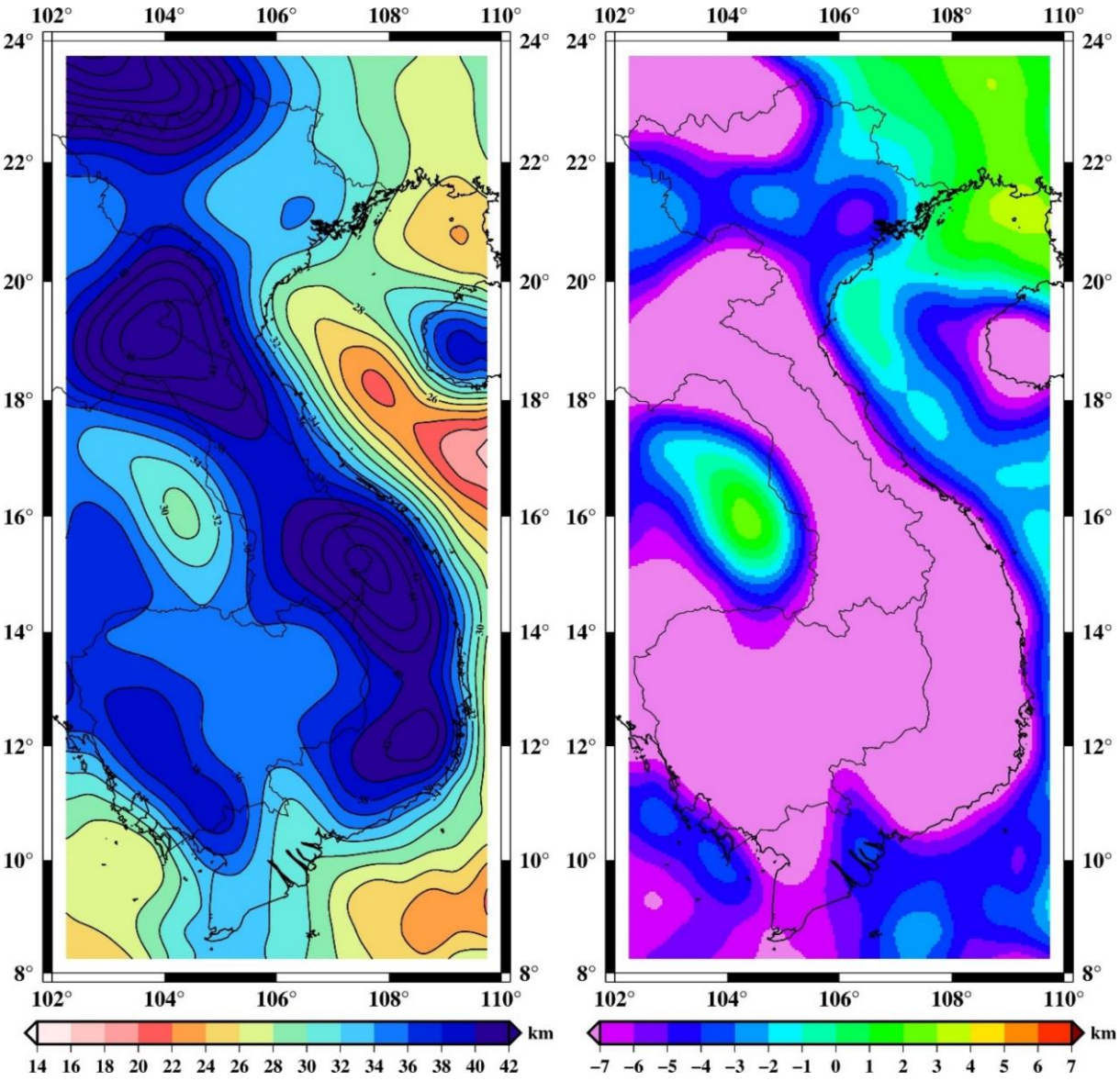

(a) (b)

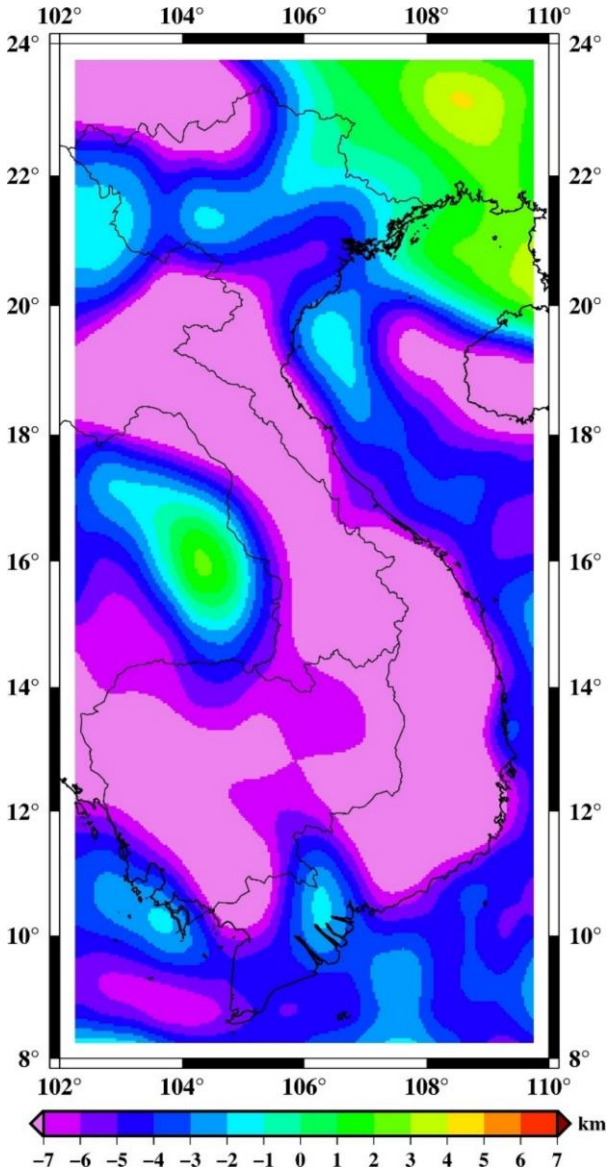

(c)

Figure 6.15. a) Moho depth derived from GEMMA model, b) Differences between Moho_GEOID and GEMMA and c) Differences between Moho_GRAVITY with GEMMA

The comparison was also made between the Moho_GEOID and Moho_GRAVITY with GEMMA. The statistics of these differences are listed too in Table 6.5, and they are displayed in Figures 6.15b and 6.15c. The differences range from -17.3 to 3.8 km with mean bias and STD of -5.8 and 4.1 km, respectively, for Moho_GEOID. With Moho_GRAVITY, the differences range from -17.6 to 3.9 km with mean bias and STD of -5.2 and 3.7 km, respectively. A possible reason for these biases is that the average density contrast of the Moho interface used in GEMMA is significantly different from the one adopted in this study. Generally, small discrepancies over sea and flat areas with differences less than 5 km can be seen, and the largest discrepancies are over rugged areas. This might be due to the resolution of GOCE of about 100 km allowing to resolve long wavelengths of Moho undulations only.

A Moho depth model was previously calculated for north Vietnam (above 16^0N), by Nguyen et al., (2018) using Bouguer gravity anomalies derived from a map at 1:500,000 in 2011 for the onshore part and satellite altimetry inferred gravity (UCSD V23.1; (Sandwell et al., 2014)) model for the offshore part.

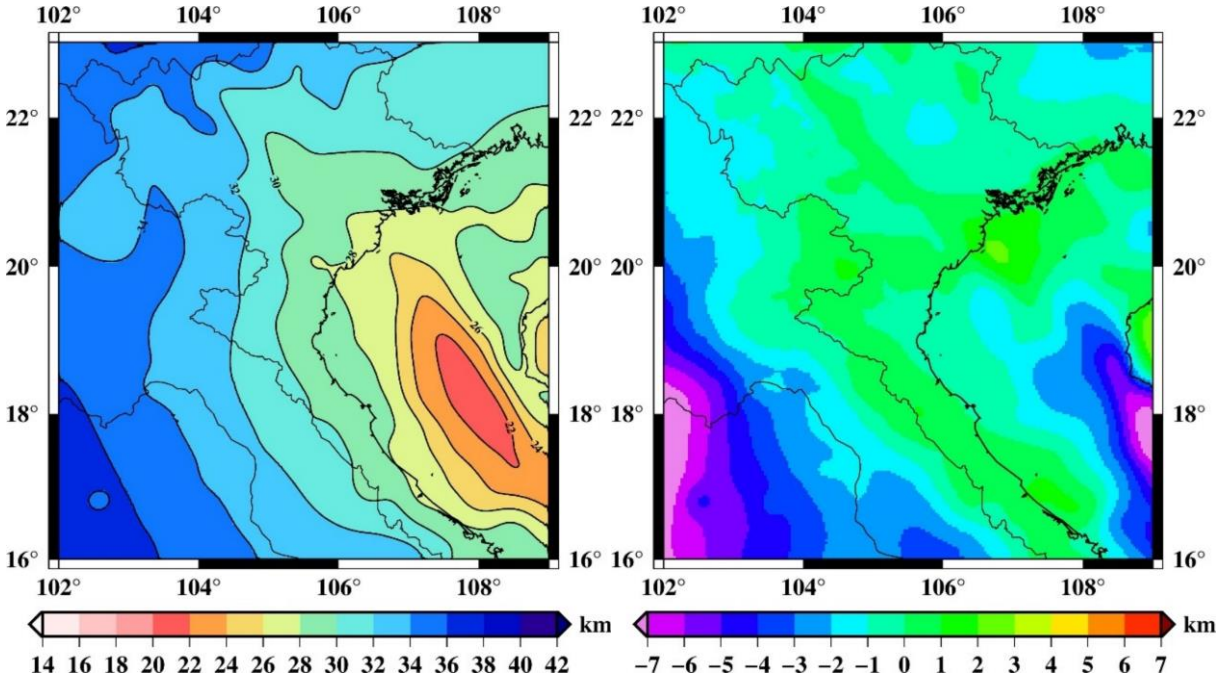

(a) (b)

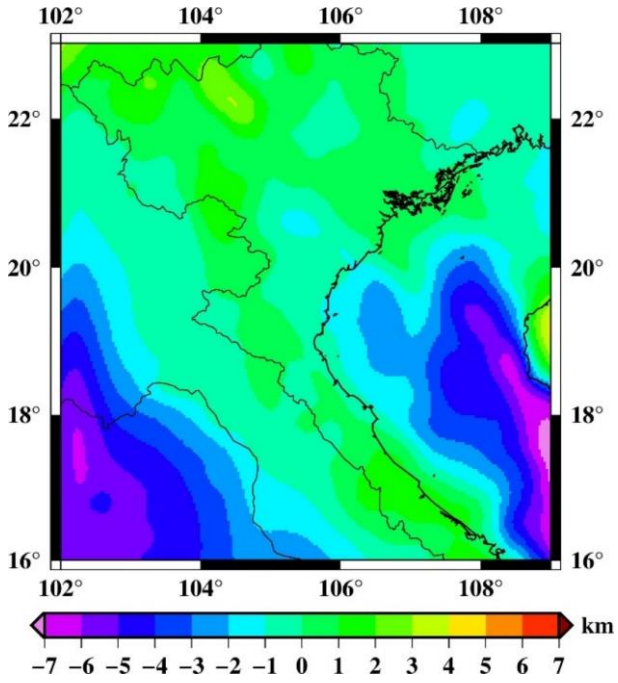

(c)

Figure 6.16. a) Moho depth from Nguyen et al., (2018), b) differences between Moho_GEOID with Nguyen et al., (2018) and c) Moho_GRAVITY with Nguyen et al., (2018)

The comparison of Moho depths in North Vietnam derived from this study and from Nguyen et al., (2018) is done. The differences are listed in Table 6.5 and they are mainly within ±1 km shown in Figures 6.16b and 6.16c. The differences range from -9.4 to 3.3 km with mean bias and STD of -1.2 and 1.8 km, respectively, for Moho_GEOID. With Moho_GRAVITY, the differences range from -8.2 to 4.5 km with mean bias and STD of -1.1 and 2.0 km, respectively. The larger differences are over sea and surrounding areas. This might be attributed to different sediment corrections and gravity data used in the calculations. Note also that the source of the gravity data used for the surrounding areas is not disclosed in Nguyen et al., (2018).

Tele-seismic results obtained from a total of 50 seismic stations were also compiled to validate the estimated Moho depth models. They include 24 stations from Nguyen et al., (2013), 2 stations from Li et al., (2008), 1 station from Noisagool et al., (2014), 13 stations from Yu et al., (2017) and 10 stations of MRF, Vietnam from Su et al., (2018). Four of the stations are in Thailand, 2 stations in southern China and 1 station on Hainan Island, China. To evaluate the possible improvement of the models developed in this study, these seismic data were also used to compare with existing Moho depth models in the study region. Moho depths derived from the receiver function are calculated beneath the topographic elevation, instead of referenced to sea level, so the elevation of seismic stations had to be subtracted before comparing the results. Statistics of these comparisons are listed in Table 6.6 and shown in Figure 6.17. Generally, the two new models reveal a significant improvement in terms of mean and STD when compared with CRUST1.0 and GEMMA. There is almost no bias between Moho depths derived from both models and all 50 tele-seismic stations, and STD is only 2.2 and 2.1 km for Moho_GEOID and Moho_GRAVITY, respectively; with CRUST1.0, mean bias and STD are -3.9 and 3.2 km, respectively, and with GEMMA -5.9 and 3.3 km, respectively. From Figures 6.17a, 6.17b and 6.17f, a significant improvement can be seen in the northern part, especially in the mountainous northwest region. This is thanks to the land gravity data included in the new estimations, whereas GEMMA was constructed with lower resolution GOCE data only, making it less accurate in mountainous areas. Figure 6.17f shows that the GEMMA model has good quality in plain areas (northeastern Vietnam), it is even better than CRUST1.0 there. Also, thanks to the ground gravity data, the models have higher accuracy in Vietnam than for surrounding regions, where fill-in data were used. This is likely to be demonstrated in Figures 6.17a and 6.17b, which show that the 3 seismic stations on the Khorat Plateau in Thailand have larger differences than those in Vietnam. The elevation of this Plateau is just 100–250 m corresponding to Bouguer gravity anomalies about -60 mGal (Figure 3.7c). The Moho depth, derived from seismic data, is up to 40 km, even if it lies in the same Indochina terrane as the northwest of Vietnam. The Bouguer anomalies in the Khorat are not sufficiently negative to explain the thick crust. According to

Noisagool et al., (2014), a simple possible explanation for the difference in Moho depth within the same terrane is the fact that the Khorat Plateau is a forefront for many past collision activities. One more reason to explain the large differences between the new models and results from seismic data is that the thickness of the sedimentary layer is up to 8 km for the Khorat Plateau. Another sedimentary density may be needed in calculating corrections for topography as well as Bouguer gravity anomalies. However, there is not enough seismic data on this plateau to determine an optimal density. This is another reason for the large difference between the new models and results from seismic data there.

The improvement with respect to CRUST1.0 in the northeast plain region (Red River Delta) is clearly seen in Figures 6.17a, 6.17b and 6.17e. This may be due to seismic data of this area not being assimilated in CRUST1.0. In contrast, in the northwestern part and central regions of Vietnam, the CRUST1.0 model has good quality and differences are only a few km. For the purpose of evaluating the accuracy of two new models in Vietnam, a set of 43 stations were selected to validate the Moho_GEOID and Moho_GRAVITY models. The results are listed in Table 6.6. A STD of 1.5 and 1.4 km for Moho_GEOID and Moho_GRAVITY, respectively, is found for the territory of Vietnam only. A set of 40 seismic stations in northern part (>16^0 in latitude) was also used to compare the new models with Nguyen et al., (2018). The results are listed in Table 6.6. The comparison indicates that the new estimation models and Nguyen et al., (2018) are consistent in terms of mean value and STD in the northern part of the study region with slight improvement of new models: STD of 1.2 and 1.2 km for the Moho_GEOID and Moho_GRAVITY, respectively, and 1.4 km for Nguyen et al., (2018).

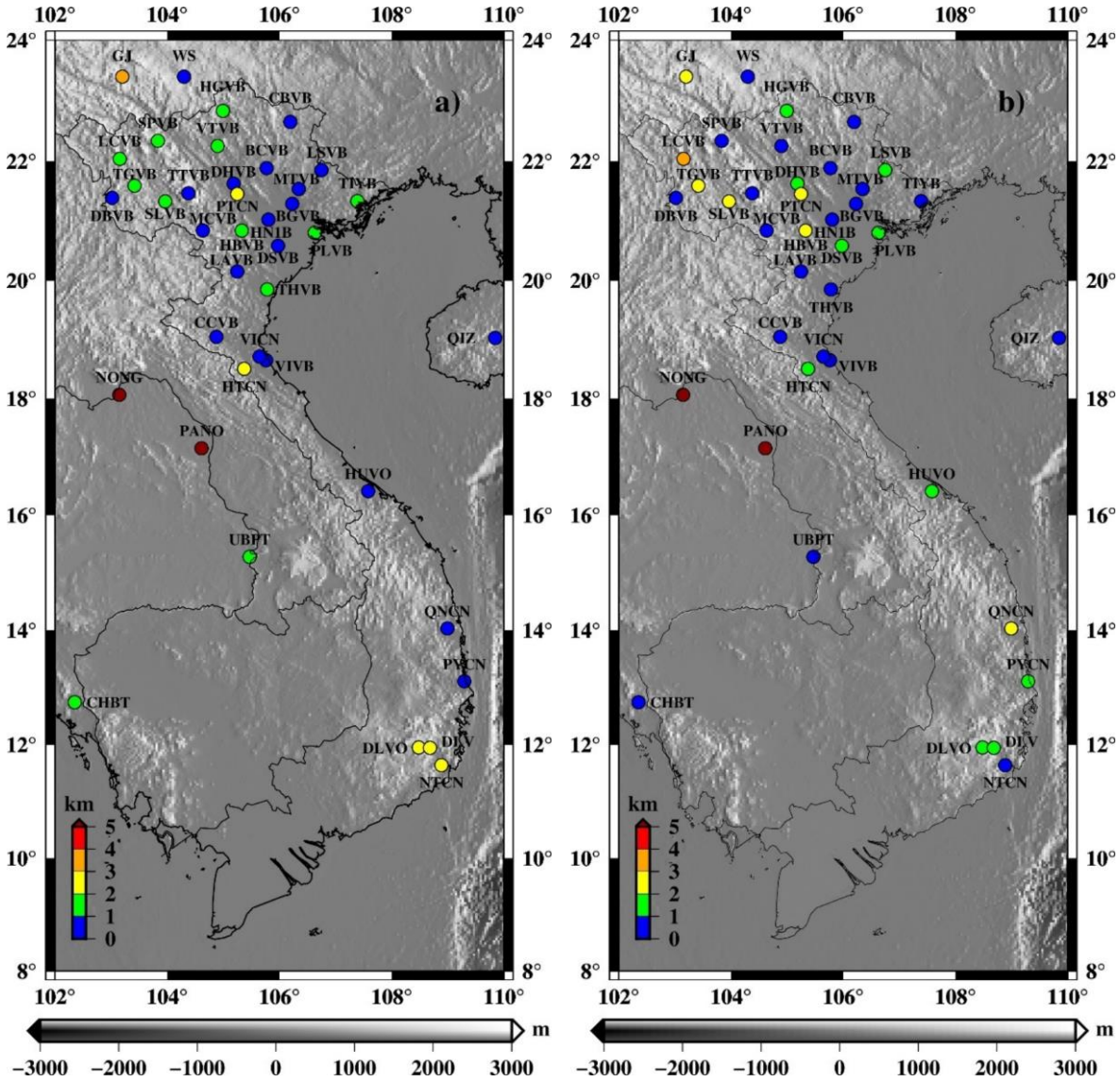
a)
b)
GJ
WS
HGVB
CBVB
SPVB
VTVB
LCVB
BCVB
LSVB
TGVB
TTVB
DHVB
MTVB
TIVB
DBVB
SLVB
PTCN
MCVB
BGVB
HNIB
HBVB
LAVB
DSVB
PLVB
THVB
CCVB
VICN
QIZ
VIVB
NONG
HTCN
PANO
HUVO
UBPT
QNCN
PVCN
CHBT
DLVO
DLV
NTCN
km
5
4
3
2
1
0
102°
104°
106°
108°
110°
24°
22°
20°
18°
16°
14°
12°
10°
8°
m
−3000
−2000
−1000
0
1000
2000
3000

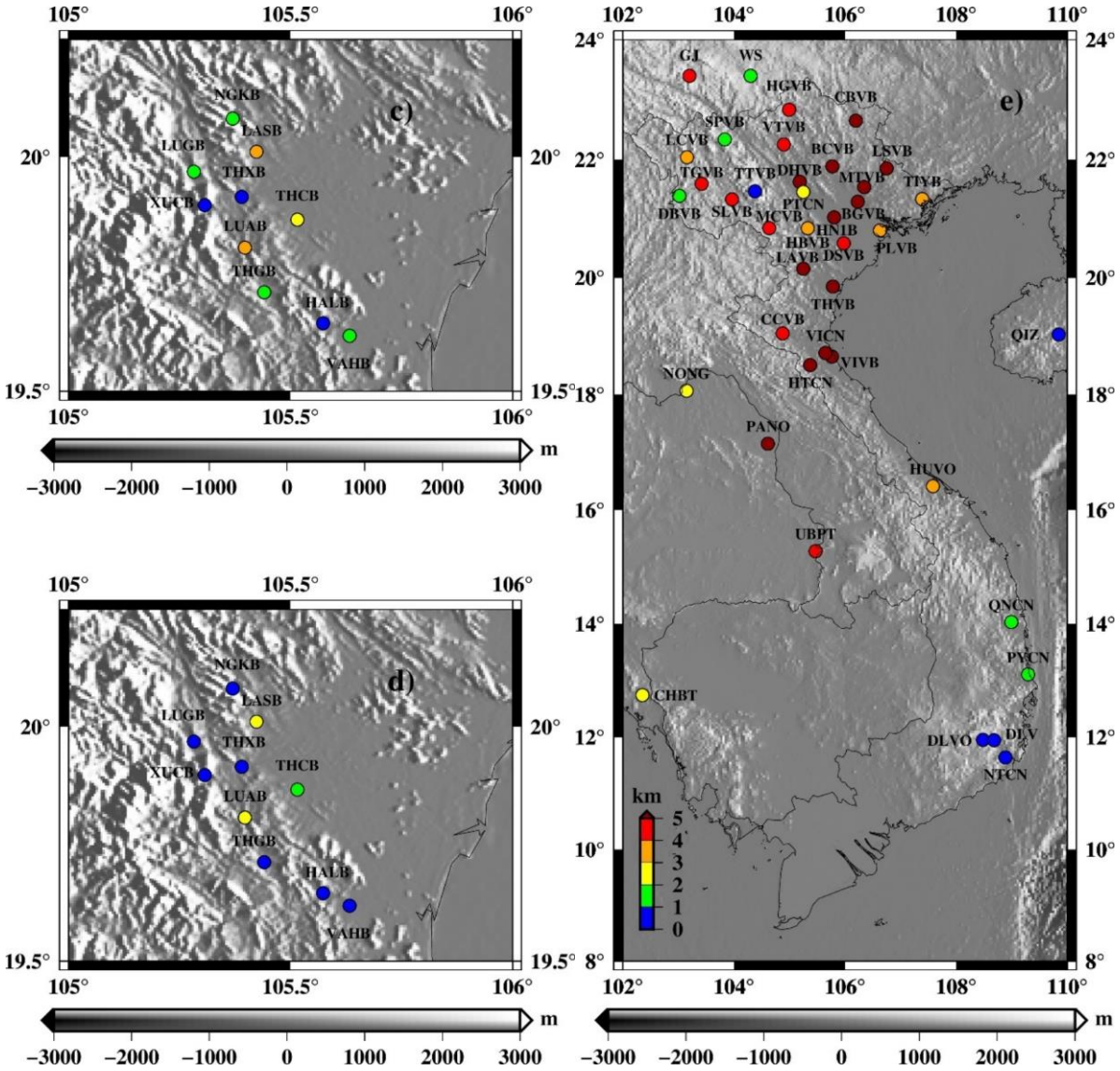
c)
d)
e)
NGKB
LASB
LUGB
THXB
XUCB
THCB
LUAB
THGB
HALB
VAHB
GI
WS
HGVB
CBVB
SPVB
VTVB
LCVB
BCVB
LSVB
TGVB
TTVB
DHVB
MTVB
TIVB
DBVB
SLVB
PTCN
MCVB
BGVB
HNIB
HBVB
PLVB
LAVB
DSVB
THVB
CCVB
VICN
VIVB
HTCN
NONG
QIZ
PANO
HUVO
UBPT
QNCN
PYCN
CHBT
DLVO
DLV
NTCN
km
5
4
3
2
1
0
105°
105.5°
106°
19.5°
20°
102°
104°
106°
108°
110°
8°
10°
12°
14°
16°
18°
22°
24°
m
−3000
−2000
−1000
0
1000
2000
3000

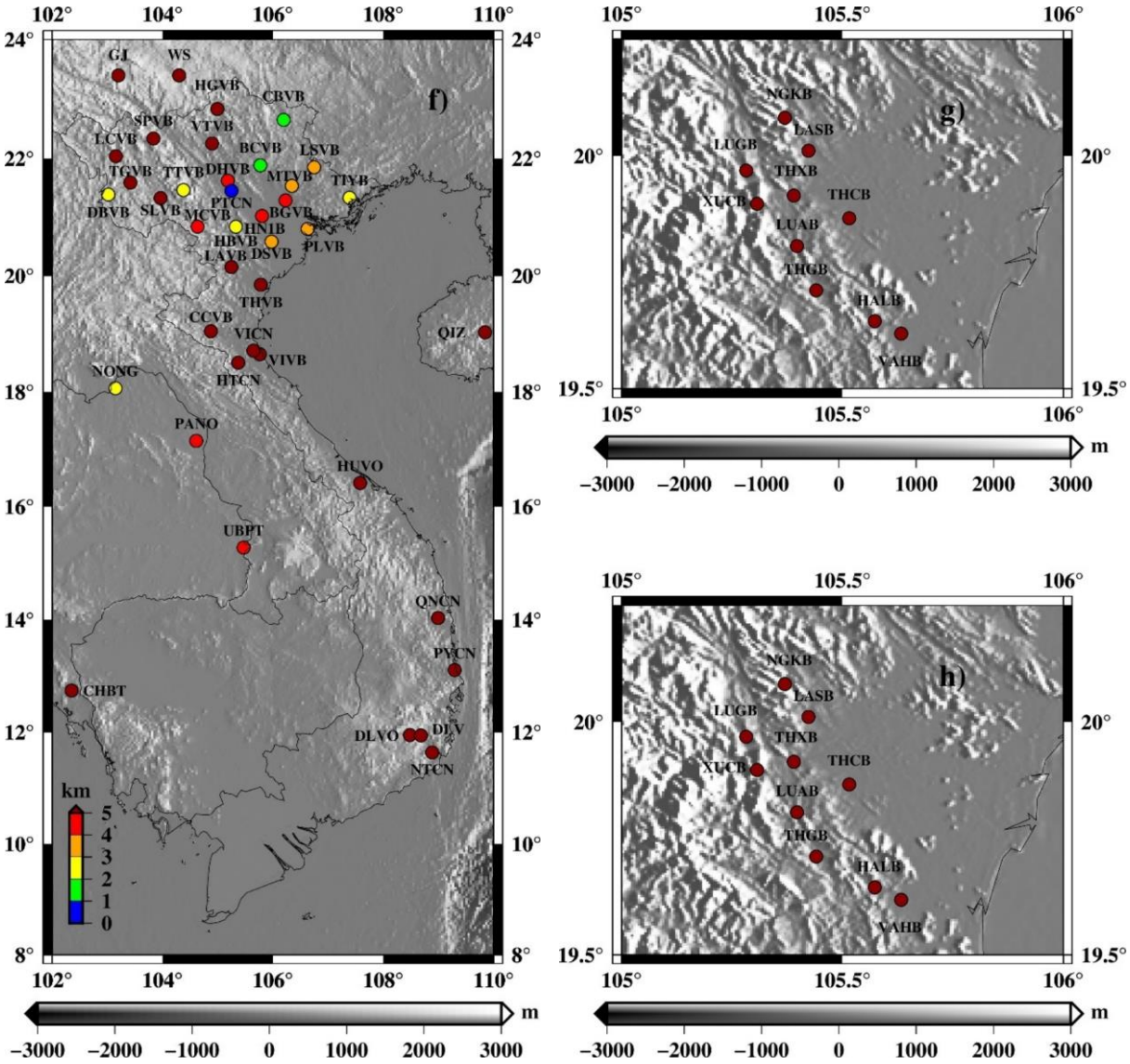

Figure 6.17. Absolute differences between Moho depths from the Moho_GEOID, Moho_GRAVITY, CRUST1.0 and GEMMA with those of 50 tele-seismic stations: a) Moho_GEOID with 40 stations, b) Moho_GRAVITY with 40 stations, c) Moho_GEOID with 10 stations of Ma River Fault, d) Moho_GRAVITY with 10 station of Ma River Fault e) CRUST1.0 with 40 stations, f) GEMMA with 40 stations, g) CRUST1.0 with 10 stations of Ma River Fault and h) GEMMA with 10 station of Ma River Fault

Table 6.6. Statistics of differences between Moho depths from the Moho_GEOID, Moho_GRAVITY, Nguyen et al., (2018), CRUST1.0 and GEMMA global model with those of 50 seismic stations. (Unit: km)

	Min	Max	Mean	STD
Moho_GEOID- seismic (all 50 points)	-3.4	9.3	0.2	2.2
Moho_GRAVITY- seismic (all 50 points)	-3.8	9.2	-0.1	2.1
CRUST1.0- seismic (all 50 points)	-9.1	6.1	-3.9	3.2
GEMMA- seismic (all 50 points)	-12.9	4.7	-5.9	3.3

Moho_GEOID- seismic (43 points in Vietnam)	-3.4	2.6	-0.1	1.5
Moho_GRAVITY- seismic (43 points in Vietnam)	-3.8	2.3	-0.5	1.4
Moho_GEOID- seismic (40 points in north)	-3.4	2.6	-0.4	1.2
Moho_GRAVITY- seismic (40 points in north)	-3.8	2.3	-0.5	1.2
Nguyen et al., (2018)- seismic (40 points in north)	-3.5	2.7	-0.5	1.4

For the assessment of the LAB depth model, the recent global tomography model SL2013sv at 0.5° resolution (Schaeffer & Lebedev, 2013) is used. S-velocity derived from this model corresponding to lithospheric depth is shown in Figure 6.18.

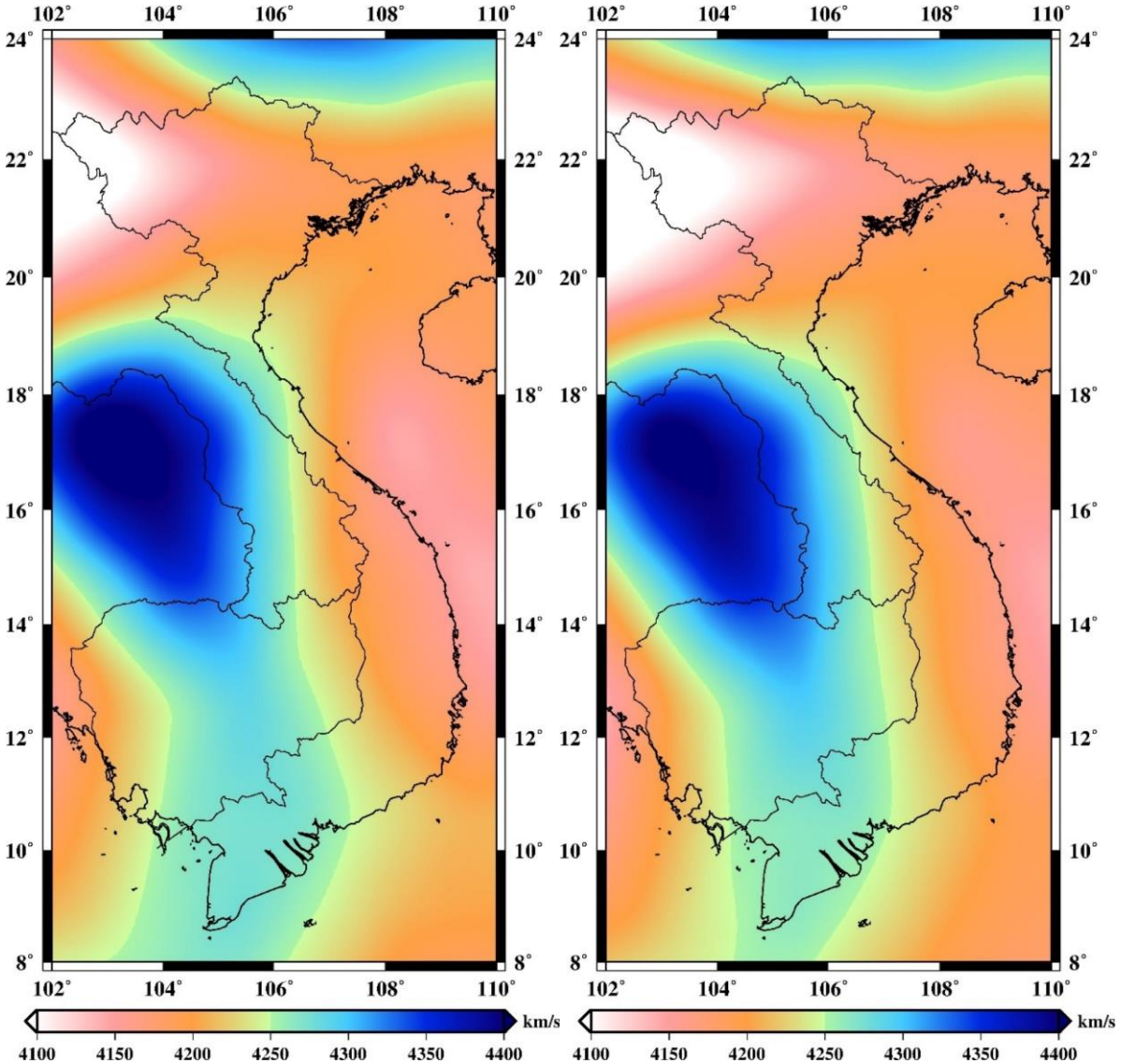

(a) (b)

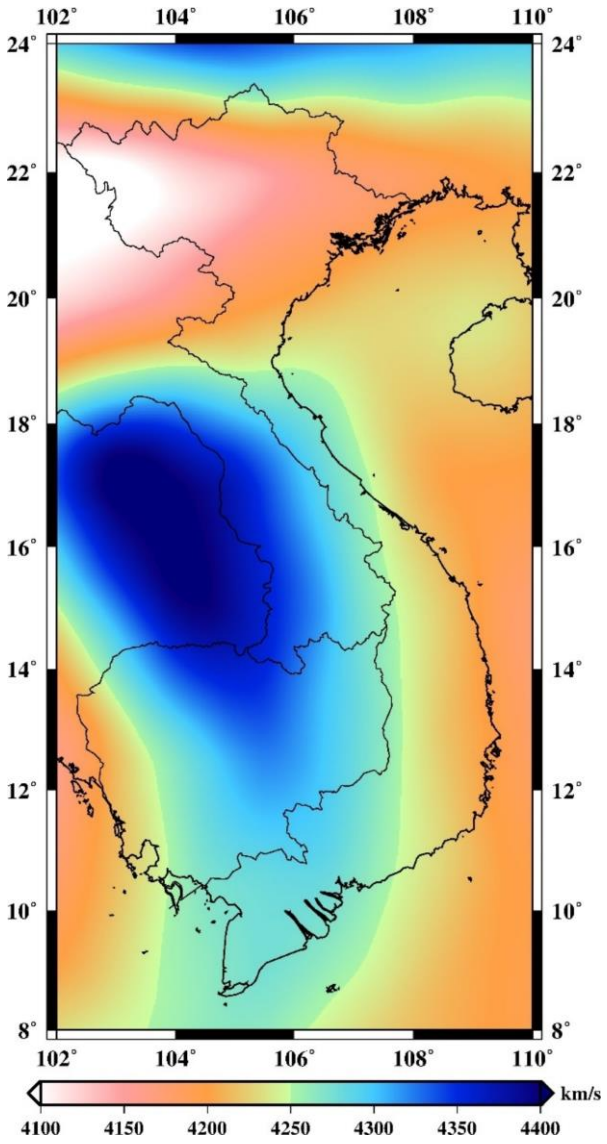

(c)

Figure 6.18. Absolute S-wave velocity (V_s) derived from SL2013sv model at a) 80 km, b) 100 km and c) 125 km

Generally, high S-velocity is located in south China and the Khorat plateau corresponding to thick lithosphere. Major differences between the new estimation and S-wave velocity derived model are observed in northern Vietnam where geological setting is fairly complicated. Moreover, the different approaches used for the lithospheric modeling can also lead to this difference.

In this chapter, the Moho and LAB depth models were determined for the study region. First, the Moho and LAB depth models were determined using the geoid height, elevation data and thermal analysis based on the local isostatic hypothesis. The elevation-corrected sedimentary thickness was proposed to improve accuracy of the estimated models. For purpose of validation of the proposed method, a calculation on the Tarim basin was tested. The results indicated that the accuracy significantly improved when compared to the

seismic data. Therefore, the proposed method was applied to determine the Moho and LAB depth for the study region. Then, the Moho depth was also determined using the Bouguer gravity anomaly data based on the inversion method. All new models are at 1' resolution. Two models are very close in most areas (differences are mostly within ±1 km). The Moho depth models were validated using the global and regional Moho models as well as seismic data. A set of 50 seismic stations distributed over Vietnam was used to validate locally the proposed models of Moho depth. This comparison indicates an agreement within 1.5 km in STD for the entire country. These new Moho depth models thus represents a significant improvement over the global models CRUST1.0 and GEMMA, which have STDs of 3.2 and 3.3 km, respectively, when compared to the same seismic data. Unlike the Moho depth, the validation of the LAB depth model cannot be more investigated due to the poor knowledge of the LAB depth in the region. This is also a more general problem of uncertainties in determining LAB depth in other regions the world. The global lithospheric model is still poorly constrained, as stated by Artemieva, (2011): "none of the geophysical or petrologic techniques can resolve the base of the lithosphere (regardless of its definition) with a resolution better than ~50 km". The high resolution of the new Moho and LAB depth models contribute to better constrain the lithospheric structure as well as tectonic and geodynamic processes of this region.

Chapter 7: CONCLUSION AND PERSPECTIVES

7.1. Conclusion in English

A set of complete gravity anomaly grids and maps i.e., Free-air, Bouguer and Isostatic, was determined for Vietnam at 1' resolution from the combination of heterogeneous data including 29,121 cleaned-up terrestrial gravity points, global gravity models, and high-resolution topographic and bathymetric data. These maps were validated by comparing with those derived from the global WGM2012 map. The results indicated that the new maps significantly improved the accuracy and resolution in the study region thanks to using the new gravity data and the fill-in data derived from the GOCE-derived gravity anomalies (GOCE DIR-R5) plus the RTM effects (using the mixed SRTM at resolution 3"). This set of grids and maps is the basic data for geodetic, geophysical and geological researches and applications in this region.

A new quasigeoid model has been generated for Vietnam and its surrounding areas from available gravity data. Two gravimetric quasigeoid solutions, called GEOID_FFT and GEOID_LSC, were computed with the Stokes' integral using the 1D-FFT approach and deterministic kernel modification as proposed by Wong–Gore, and the LSC method, respectively. These quasigeoid models were validated through a comparison with the GNSS/levelling points. The results show that both models lead to very similar results reaching a STD at the 9.7 cm level with a mean bias of 50 cm. The results of the comparison indicated the large improvement of these models over the commonly used EGM2008 and EIGEN-6C4 for Vietnam in all areas, covered or not by land gravity measurements. A significant improvement for areas with poor data coverage proves that the recent GOCE/GRACE GGM in combination with EGM2008 and RTM effects may be used to improve quasigeoid determination in the areas where gravity data are not available or insufficient, especially in mountainous regions and coastal zones. The best agreement in Vietnam was obtained with GOCE DIR-R5 used up to d/o 260, EGM2008 used up from d/o 270 to 2159 and RTM effects used equivalent to d/o 216000. The high-resolution gravimetric quasigeoid model presents various applications for Vietnam.

To apply the estimated quasigeoid model in GNSS levelling, a vertical offset model has been generated for Vietnam using the gravimetric-only quasigeoid model (GEOID_LSC) and 779 cleaned GNSS/levelling points. The annual subsidence rate grid estimated from ALOS-1 observations was used to correct and improve the accuracy for 47 GNSS/levelling points in the Mekong Delta, thereby making the average bias of this region comparable with the rest of the country. Thanks to this correction, the accuracy of the offset model is significantly improved. The cross-validation technique was used to validate the offset model, and a STD of 5.9 cm was obtained. Using the GEOID_LSC model and adding the offset model allows GNSS levelling to comply with fourth-order levelling specifications for

Vietnam and third-order levelling specifications for most of the country, excepting some mountainous areas where the quality and distribution of gravity data are not good. Especially in the area surrounding Hanoi and Ho Chi Minh City, these models allow GNSS levelling to comply with third-order levelling specifications. The vertical offset model can be applied in modernizing the height reference system in Vietnam by adding this offset model to available levelling data.

To unify the height system towards the IHRF, the zero-height geopotential value for the VLVD (W_0^{LVD}) was determined based on two approaches. First, the differences between height anomalies from high-quality GNSS/levelling data, tilt effects removed and corrected for land subsidence, and those derived from the GEOID_LSC gravimetric-only quasigeoid model were used to compute the zero-height geopotential value for the existing LVD in Vietnam. The zero-height gravity potential of the VLVD was estimated equal to W_0^{LVD} = 62,636,846.81 ± 0.70 m^2/s^2 with the global equipotential surface realized by the conventional value W_0 = 62,636,853.4 m^2/s^2. With this gravity potential value, the height system of Vietnam can presently be connected with that of the neighboring countries.

To avoid the effect of inconsistency between GNSS, levelling and gravimetric quasigeoid model for deriving height anomalies, the zero-height gravity potential of the VLVD was then directly estimated based on the GBVP approach using the GOCE global gravity field model enhanced with terrestrial gravity data. The effects of the GGM omission error, the indirect bias term and the systematic levelling error, on the estimation of the gravity potential were investigated. The results indicated that the indirect bias term is less than 0.1 m^2/s^2 (equivalent to 1 cm) if the degree of truncation is higher than 60. The objective of this work is to determine the height reference system with cm level accuracy, and so the indirect bias term can be safely neglected when using GOCE DIR-R5 up to d/o 260 in combination with the smoothing WG modification, which fully removed low harmonics up to degree N_1=220, then linearly tapered to degree N_2=230. The effect of the GOCE DIR-R5 (at d/o 260) omission error on the offset value, based on the GNSS/levelling data, was estimated by extending with EGM2008 from d/o 261-2190. It is at 0.5 m^2/s^2 (equivalent to 5 cm). This proves that the GOCE omission errors should be taken into account in the determination of the geopotential value for this region. The remaining quasigeoid signal of the mixed DIR/EGM above d/o 2190 was also estimated with the GEOID_LSC model. This signal is still significant (0.4 m^2/s^2), especially in the mountainous areas. After removing the trends in levelling data due to the systematic cumulative errors, the zero-height gravity potential of the VLVD was estimated equal to W_0^{LVD} = 62,636,846.69 m^2/s^2 with STD of 0.70 m^2/s^2 based on the GBVP approach. This value is very similar to the result calculated using GNSS/levelling-corrected data and gravimetric quasigeoid (GEOID_LSC), and the difference of 0.12 m^2/s^2 (equivalent to 1 cm) is within the limits of the study

objective.

The GBVP approach was used for direct determination of the geopotential on the surface of three GNSS-CORS stations in Vietnam. Based on time series of the vertical component derived from the GNSS observations as well as InSAR data, time variations in the geopotential were also estimated on these permanent GNSS stations. The purpose is to monitor deformation of the vertical datum. The geopotentials on the surface as well as the velocities of the three GNSS-CORS stations were estimated at epoch 2018.0 equal to W^{PHUT} = 62,636,717.46 + 0.02 m^2/s^2, W^{QNRS} = 62,636,758.62 + 0.04 m^2/s^2 and W^{BACL} = 62,636,645.40 + 0.28 m^2/s^2. The cumulative change is estimated to reach 2 m^2/s^2 within 8 years at the BACL station at the current rate. Sánchez et al., (2016) recommended an update of W_0 if the cumulative change reaches this threshold value. This study confirmed again that the geopotential values need to be monitored and determined with the time-dependent component on the permanent GNSS stations in order to plan updates. These stations may thus contribute to increase the density of reference points in the IHRF for this region.

An application of geoid/quasigeoid in geophysics is to determine the lithospheric structure. The quasigeoid was converted to the geoid to estimate Moho and LAB depth, called GEOID_LSC_C. New models of Moho and LAB depth for Vietnam and its surrounding areas were determined at 1' resolution based on very high-accuracy and -resolution GEOID_LSC_C and mixed SRTM models. Sedimentary thickness data derived from CRUST1.0 model was used to correct the elevation data. The topography-corrected sedimentary basins model is employed to refine the inverse model presented by Fullea et al. (2007). The results obtained for a test area demonstrated that a better consistency with seismic data is reached when elevation corrected for the sedimentary effect is used. The average discrepancies between the Moho depth derived from seismic data with those inferred from this study using elevation corrected for sediment and elevation data only are 4.2, 5.0 km, respectively. This elevation-corrected model was used to provide new insights in the lithospheric structure beneath Vietnam. It was determined using a linear density increase with depth in the crust and a thermal analysis for the lithospheric mantle density under the assumption of local isostasy. High-pass filtering with a 1D-Gaussian function was used to remove the long-wavelengths in the geoid height using GOCE DIR-R5 up to d/o = 9. 2D-Gaussian low-pass filtering was used to remove the short-wavelengths (i.e., <100km) from the mixed SRTM-corrected sedimentary thickness. These filtered data were used to determine the Moho and LAB depth models, called hereafter Moho_GEOID and LAB_GEOID. Moreover, the Moho depth was also determined using the Bouguer gravity anomaly data, called Moho_GRAVITY.

The Moho depths derived from Moho_GEOID vary across the study region from 15.3 to 37.8 km with mean and STD of 28.0 and 4.0 km, respectively while with Moho_GRAVITY

the Moho depths vary from 12.2 to 38.5 km with mean and STD of 28.5 and 4.3 km, respectively. As expected, the two Moho depth models are very close in most areas (differences are mostly within ±1 km). The LAB depths derived from LAB_GEOID vary from 82.3 to 144.7 km with mean and STD of 123.1 and 12.3 km, respectively. These results were compared to the seismic data as well as the global and local models of the study region. A set of 50 seismic stations was used to validate locally the models of Moho depth. This comparison indicates an agreement within 1.5 km in STD for the entire country. These new Moho depth models thus represent a significant improvement over the global models CRUST1.0 and GEMMA, which have STDs of 3.2 and 3.3 km, respectively, when compared to the same seismic data. Regarding the geoid-derived lithospheric depth model derived in this study, it is consistent with a recent global model of the S-wave velocity of this region. However, the current uncertainties in the structure of the lithosphere beneath Vietnam and its surrounding areas do not allow a more thorough evaluation. The differences in Moho depth visible in the northeast and southwest sides of RRFZ confirmed that the RRFZ may be considered the boundary between the South China and Indochina blocks.

7.2. Suggestions for future work

In the present dissertation, efforts were made in order to determine the size, physical shape and internal structure of the Earth in Vietnam using in particular the available gravity data. The results represent a big step towards applications of local geoid/quasigeoid in GNSS levelling, in height system unification and in the determination of the lithospheric structure through high-resolution gravity field modeling. However, research about this topic does not stop here. Further research can be done to improve the accuracy and resolution.

Land gravity data are not available for large parts of the mountainous region, and consequently, the knowledge of the gravity field is significantly poorer there. Improvement of the existing gravity database will require increased and homogeneous data coverage over land and sea in Vietnam and its vicinity, preferentially with airborne data and shipborne data. An airborne gravity project will be deployed in Vietnam in the near future, which should enable the gravimetric quasigeoid to be significantly improved in accuracy and resolution. Moreover, new gravity field models such as EGM2020 and UCSD V29 are also expected to improve the quasigeoid. The new DBM GEBCO_2020 at 15” resolution should be also tested to determine its impact on the quasigeoid accuracy.

On the GNSS-CORS stations, the zero-height geopotential value should also be known besides the geopotential on the Earth’s surface. Therefore, the levelling height on these stations needs to be determined to estimate the reference of a LVD from the gravity potential on the surface according to the requests of the IAG resolutions for the realization

of the IHRS.

For grids and maps of gravity anomalies, the spherical approach should be used instead of the planar approach to improve the computation of the topographic reductions. The sediment corrections are also applied in the calculation of the Isostatic gravity anomalies.

The quasigeoid-to-geoid corrections vary from -0.771 to 0.020 m in the study region. With large difference between height anomaly and geoid height, its effects on the determination of the lithospheric structure need also be estimated.

In an attempt to improve understanding of the lithospheric structure, a regional isostatic hypothesis can be used instead of local one. A thermal analysis with the variable temperature at the LAB based on the global model should be also used instead of a fixed one. This may significantly improve the accuracy of the Moho and LAB depth. Moreover, a surface crustal density model should be developed and used instead of a constant parameter to improve the accuracy of topographic effects in determining the quasigeoid as well as the grid of Bouguer gravity anomalies.

The Bouguer gravity anomalies obtained after various corrections to the observed field represent the combined responses of various masses lying at depths below the ground surface. To better discriminate the sources responsible of gravity anomalies and gain knowledge in the shallow and deep structure of the Earth, regional and residual gravity anomalies might be also determined. Based on the lithospheric structure model derived from geoid and DTM, regional gravity anomalies can be calculated. This alternative method will determine the regional/residual gravity component by assuming that the topographic relief is isostatically compensated. Therefore, the resulting regional/residual gravity field is independent on the gravity measurement, which is used in the traditional method to separate the Bouguer gravity anomalies based on a low-degree polynomial surface or a low-pass filter. This alternative method is expected to bring new insight on the regional/residual Bouguer anomaly separation.

7.3. Conclusion en français

Un ensemble de grilles et de cartes d'anomalies gravimétriques, c'est-à-dire en Air-libre, Bouguer et Isostatique, a été déterminé pour le Vietnam à la résolution 1' à partir de la combinaison de données hétérogènes comprenant 29,121 points de gravité terrestres validés, des modèles gloabaux du champ de gravité et des données topographiques et bathymétriques à haute résolution. Ces cartes ont été comparées à celles dérivées du modèle global WGM2012, incluant ces mêmes quantités (également corrigées de la topographie). Les résultats ont indiqué que les nouvelles cartes amélioraient considérablement la précision et la résolution grâce à l'utilisation des nouvelles données de gravité et des données de remplissage dérivées des anomalies de gravité dérivées de

GOCE (GOCE DIR-R5) plus les effets RTM (en utilisant le SRTM mixte à la résolution de 3"). Cet ensemble de grilles et de cartes constitue les données de base pour les recherches et applications géodésiques, géophysiques et géologiques dans cette région.

Un nouveau modèle quasigeoïde a été généré pour le Vietnam et ses régions environnantes à partir des données gravimétriques disponibles. Deux solutions quasigeoïdes gravimétriques, appelées GEOID_FFT et GEOID_LSC, ont été calculées avec l'intégrale de Stokes en utilisant l'approche 1D-FFT et la modification déterministe du noyau comme proposé par Wong–Gore et la méthode collocation par moindres carrés, respectivement. Ces modèles quasigeoïdes ont été validés par une comparaison avec les points GNSS/nivellement. Les résultats montrent que les deux modèles conduisent à des résultats très similaires atteignant un écart type de l'ordre de 9.7 cm avec un biais moyen de 50 cm. Les résultats de la comparaison ont indiqué une amélioration significative de ces modèles par rapport aux modèles globaux EGM2008 et EIGEN-6C4 couramment utilisés pour le Vietnam dans toutes les zones, couvertes ou non par des mesures de gravité terrestre. Une amélioration significative pour les zones avec une faible couverture de données prouve que le récent modèle de champ de gravité globale GOCE/GRACE en combinaison avec EGM2008 et les effets RTM peut être utilisé pour améliorer la détermination des quasigéoïdes dans les zones où les données de gravité ne sont pas disponibles ou insuffisantes, en particulier dans les régions montagneuses et les zones côtières. Le meilleur accord au Vietnam est obtenu avec le modèle GOCE DIR-R5 utilisé jusqu'à d/o 260, EGM2008 utilisé de d/o 270 à 2159 et des effets RTM utilisés équivalents à d/o 216000. Le modèle quasigeoïde gravimétrique à haute résolution présente diverses applications pour le Vietnam.

Pour appliquer le modèle quasigeoïde estimé au nivellement GNSS, un modèle de décalage vertical a été généré pour le Vietnam en utilisant le modèle quasigeoïde gravimétrique (GEOID_LSC) et 779 points GNSS/nivellement nettoyés. La grille annuelle des vitesses de subsidence estimée à partir des observations ALOS-1 a été utilisée pour corriger et améliorer la précision de 47 points GNSS/nivellement dans le Delta du Mékong, rendant ainsi le biais moyen de cette région du même ordre avec la partie restante du pays. Par conséquent, la précision du modèle de décalage est considérablement améliorée. La technique de validation croisée a été utilisée pour valider le modèle de décalage vertical, et un écart type de 5.9 cm a été obtenu. L'utilisation du modèle GEOID_LSC en combinaison avec modèle de décalage permettent au nivellement par GNSS de se conformer aux spécifications de nivellement du quatrième ordre pour le Vietnam et aux spécifications de nivellement du troisième ordre pour la majeure partie du pays, à l'exception de certaines zones montagneuses où la qualité et la distribution des données de gravité ne sont pas bonnes. Surtout dans les environs de Hanoi et Ho Chi Minh-Ville, ces modèles permettent au nivellement GNSS de se conformer aux spécifications de nivellement du troisième

ordre. Le modèle de décalage vertical peut donc être appliqué dans la modernisation du système de référence de hauteur au Vietnam en ajoutant ce modèle de décalage aux données de nivellement disponibles.

Pour unifier le système de hauteur vers l'IHRF, la valeur géopotentielle à zéro-hauteur pour le système de référence vertical local du Vietnam (W_0^{LVD}) a été déterminée en fonction de deux approches. Premièrement, les différences entre les données GNSS/nivellement à haute qualité et le modèle quasigeoïde gravimétrique GEOID_LSC ont été utilisées pour calculer la valeur géopotentielle à zéro-hauteur de la référence verticale locale au Vietnam. Le potentiel de gravité à zéro-hauteur de la référence verticale locale au Vietnam est estimé égal à W_0^{LVD} = 62,636,846.81 ± 0.70 m^2/s^2 avec la surface équipotentielle globale réalisée par la valeur conventionnelle W_0 = 62,636,853.4 m^2/s^2. Avec cette valeur potentielle de gravité, le système de hauteur du Vietnam peut actuellement être connecté à celui des pays voisins.

Pour éviter l'effet d'incohérence entre le GNSS, le nivellement et le modèle quasigéoïde gravimétrique pour dériver les anomalies de hauteur, le potentiel de gravité à zéro-hauteur de la référence verticale locale au Vietnam a ensuite été directement estimé sur la base de l'approche du problème de la valeur des limites géodésiques en utilisant le modèle de champ de gravité global GOCE amélioré avec des données de gravité terrestre. Les effets de l'erreur d'omission des modèles de champ de gravité globale, du terme de biais indirect et de l'erreur de nivellement systématique sur l'estimation du potentiel de gravité ont été étudiés. Les résultats indiquent que le terme de biais indirect est inférieur à 0.1 m^2/s^2 (équivalent à 1 cm) si le degré de troncature est supérieur à 60. L'objectif de ce travail est de déterminer le système de référence de hauteur avec une précision de niveau en cm, et donc le terme de biais indirect peut être négligé en toute sécurité lors de l'utilisation de GOCE DIR-R5 jusqu'à d/o 260 en combinaison avec la modification de Wong-Gore, qui a complètement éliminé les harmoniques basses jusqu'au degré N_1 = 220, puis a été linéairement effilée au degré N_2 = 230. L'effet de l'erreur d'omission GOCE DIR-R5 (à d/o 260) sur la valeur de décalage, sur la base des données GNSS/nivellement, a été estimé en étendant avec EGM2008 à partir de d/o 261-2190. Il est à 0.5 m^2/s^2 (équivalent à 5 cm). Cela prouve que les erreurs d'omission du modèle GOCE doivent être prises en compte dans la détermination de la valeur géopotentielle pour cette région. Le signal quasigeoïde restant du modèle DIR/EGM mixte au-dessus de d/o 2190 a également été estimé par le modèle GEOID_LSC. Ce signal est toujours significatif (0.4 m^2/s^2), en particulier dans les zones montagneuses. Après avoir supprimé les tendances des données de nivellement en raison d'erreurs cumulatives systématiques, le potentiel de gravité à zéro-hauteur de la référence verticale locale au Vietnam a été estimé égal à W_0^{LVD} = 62,636,846.69 m^2/s^2 avec un écart type de 0.70 m^2/s^2 basé sur l'approche du problème de la valeur des limites géodésiques. Cette valeur est très similaire au résultat calculé

utilisant des données GNSS/nivellement corrigées et quasigeoïde gravimétrique (GEOID_LSC), et la différence de 0.12 m^2/s^2 (équivalent à 1 cm) est dans les limites de l'objectif de l'étude.

L'approche du problème de la valeur des limites géodésiques a été utilisée pour la détermination directe du géopotentiel à la surface de trois stations GNSS-CORS au Vietnam. Sur la base de séries temporelles de la composante verticale dérivée des observations GNSS ainsi que de données InSAR, les variations temporelles du géopotentiel ont également été estimées sur ces stations GNSS permanentes. Le but est de pouvoir suivre dans le temps des variations de la référence verticale. Les géopotentiels en surface ainsi que les vitesses des trois stations GNSS-CORS ont été estimés à l'époque 2018.0 égaux à W^{PHUT} = 62,636,717.46 + 0.02 m^2/s^2, W^{QNRS} = 62,636,758.62 + 0.04 m^2/s^2 et W^{BACL} = 62,636,645.40 + 0.28 m^2/s^2. A la vitesse actuelle, la variation cumulée est estimée susceptible d'atteindre 2 m^2/s^2 d'ici 8 ans à la station BACL. Sánchez et al., (2016) ont recommandé une mise à jour de W_0 si le changement cumulatif atteint cette valeur seuil. Cette étude confirme à nouveau que les valeurs géopotentielles doivent être surveillées et déterminées avec la composante dépendant du temps sur les stations GNSS permanentes afin de planifier des mises à jour. Ces stations peuvent ainsi contribuer à augmenter la densité des points de référence dans l'IHRF pour cette région.

Une application du géoïde/quasigéoïde en géophysique consiste à déterminer la structure lithosphérique. Le quasigeoïde a été converti en géoïde, appelé GEOID_LSC_C, pour estimer la profondeur du Moho et de la limite entre Lithosphère-Asthénosphère,. De nouveaux modèles de profondeur du Moho et de la limite entre Lithosphère-Asthénosphère pour le Vietnam et ses environs ont ainsi été déterminés à une résolution de 1' sur la base des modèles de GEOID_LSC_C et de SRTM mixte à très haute précision et résolution (3" et 5' pour SRTM et GEOID_LSC_C modèles, respectivement). Les données d'épaisseur sédimentaire dérivées du modèle CRUST1.0 ont été utilisées pour corriger les données de hauteur. Le modèle de topographie corrigée des bassins sédimentaires est proposé pour améliorer le modèle inverse présenté par Fullea et al. (2007). Les résultats obtenus pour une zone d'essai ont démontré qu'une meilleure cohérence avec les données sismiques est atteinte lorsque l'élévation corrigée de l'effet sédimentaire est utilisée. Les écarts moyens entre la profondeur du Moho dérivée des données sismiques et ceux déduits de cette étude en utilisant l'élévation corrigée des données de sédiments et d'élévation seulement sont de 4.2 et 5.0 km, respectivement. Cette méthode a été utilisée pour fournir de nouvelles informations sur la structure lithosphérique sous le Vietnam. Cette dernière a été déterminée en prenant en compte une augmentation de densité linéaire avec la profondeur au Moho et une approche thermique de la densité du manteau lithosphérique sous l'hypothèse d'une isostasie locale. Un filtrage passe-haut avec une fonction 1D-Gaussian a été utilisé pour supprimer les longues longueurs d'onde dans la

hauteur du géoïde en utilisant GOCE DIR-R5 jusqu'à d/o=9. Un filtrage passe-bas 2D-Gaussian a été utilisé pour supprimer les courtes longueurs d'onde (<100 km) du SRTM mixte corrigé de l'effet sédimentaire. Ces données filtrées ont été utilisées pour déterminer les modèles de profondeur du Moho et de la limite entre Lithosphère-Asthénosphère, appelés Moho_GEOID et LAB_GEOID. A titre comparatif, la profondeur du Moho a également été déterminée en utilisant des données d'anomalie gravimétrique de Bouguer, appelée Moho_GRAVITY.

Les profondeurs du Moho dérivées du modèle Moho_GEOID varient de 15.3 à 37.8 km avec une moyenne et un écart type de 28.0 et 4.0 km, respectivement, tandis qu'avec Moho_GRAVITY, les profondeurs de Moho varient de 12.2 à 38.5 km avec une moyenne et un écart type de 28.5 et 4.3 km, respectivement. Etant basés sur les mêmes observations gravimétriques, les deux modèles de profondeur du Moho sont logiquement très proches dans la plupart des zones (les différences se situent principalement à ±1 km). Les profondeurs de la limite entre Lithosphère-Asthénosphère dérivées de LAB_GEOID varient de 82.3 à 144.7 km avec une moyenne et un écart type de 123.1 et 12.3 km, respectivement. Ces résultats ont été comparés aux données sismiques ainsi qu'aux modèles globaux et locaux de la région d'étude. Un ensemble de 50 stations sismiques a été utilisé pour valider localement les modèles proposés de profondeur du Moho. Cette comparaison indique un accord à moins de 1.5 km en écart type pour l'ensemble du pays. Ces nouveaux modèles de profondeur du Moho représentent donc une amélioration significative par rapport aux modèles globaux CRUST1.0 et GEMMA, qui ont des écarts types de 3.2 et 3.3 km, respectivement, par rapport aux mêmes données sismiques sur la région. En ce qui concerne le modèle de profondeur lithosphérique dérivé du géoïde également déduit de cette étude, il est cohérent avec un modèle global récent de la vitesse de S-wave de cette région. Cependant, les incertitudes actuelles sur la structure de la lithosphère sous le Vietnam et ses environs ne permettent pas une évaluation plus approfondie. Les différences de profondeur du Moho visibles sur les côtés nord-est et sud-ouest de la zone de faille de la Rivière Rouge semblent confirmer que cette zone de faille peut être considérée comme la frontière entre deux blocs continentaux: les blocs de Chine sud et d'Indochine. Cependant, aucune différence remarquable dans la profondeur de la limite entre Lithosphère-Asthénosphère n'a été révélée, ce qui suggère que la zone de faille de la Rivière Rouge s'est développée dans la croûte et est restée une faille crustale.

7.4. Suggestions de travaux futurs

Dans la présente thèse, des efforts ont été faits afin de déterminer la taille, la forme physique et la structure interne de la Terre au Vietnam en utilisant notamment les données gravimétriques disponibles. Les résultats représentent un grand pas vers les applications du géoïde/quasigéoïde local dans le nivellement GNSS, dans l'unification du

système de hauteur et dans la détermination de la structure lithosphérique par modélisation de champ de gravité à haute résolution. Cependant, la recherche sur ce sujet ne s'arrête pas là. Des recherches complémentaires pourront permettre d'améliorer la précision et la résolution.

Les données de gravité terrestre ne sont pas disponibles pour de grandes parties de la région montagneuse et, par conséquent, la connaissance des champs gravimétriques est très faible sur ces régions. L'amélioration des données gravimétriques nécessitera une meilleure couverture des données sur terre et en mer au Vietnam et dans ses environs. Ces régions doivent être couvertes de préférence par des données aéroportées et des données embarquées. Un projet de gravité aéroportée sera déployé prochainement au Vietnam, ce qui devrait permettre d'améliorer considérablement la précision et la résolution du quasigeoïde gravimétrique. De plus, de nouveaux modèles de champ de gravité tels que EGM2020 et UCSD V29 devraient également améliorer le quasigeoïde. Le nouveau modèle de bathymétrie numérique GEBCO_2020 à une résolution de 15" devrait également être testé pour déterminer son impact sur la précision quasigéoïde.

Sur les stations GNSS-CORS, la valeur géopotentielle à zéro-hauteur devrait également être connue en plus du géopotentiel à la surface de la Terre. Par conséquent, la hauteur de nivellement sur ces stations doit être déterminée pour estimer le géopotentiel à zéro-hauteur de la référence verticale locale à partir du potentiel de gravité à la surface en fonction des demandes des résolutions de l'IAG pour la réalisation de l'IHRS.

Pour les grilles et les cartes d'anomalies gravimétriques, l'approche sphérique devrait être utilisée à la place de l'approche planaire pour améliorer le calcul des réductions topographiques. Les corrections sédimentaires sont également appliquées dans le calcul des anomalies gravimétriques isostatiques.

Les corrections quasigeoïde-à-géoïde varient de -0.771 à 0.020 m dans la région d'étude. Avec une grande différence entre l'anomalie de hauteur et la hauteur du géoïde, ses effets sur la détermination de la structure lithosphérique doivent également être estimés.

Pour tenter d'améliorer la compréhension de la structure lithosphérique, une hypothèse isostatique régionale peut être utilisée au lieu d'une hypothèse locale abordée dans cette étude. Une analyse thermique avec la température variable à la limite entre Lithosphère-Asthénosphère basée sur le modèle global devrait également être utilisée au lieu d'une température fixe. Cela peut améliorer considérablement la précision de la profondeur du Moho et de la limite entre Lithosphère-Asthénosphère. De plus, un modèle de densité crustale de surface devrait être développé et utilisé à la place d'un paramètre constant pour améliorer la précision des effets topographiques à la détermination du quasigeoïde ainsi que de la grille des anomalies gravimétriques de Bouguer.

Les anomalies gravimétriques de Bouguer obtenues après diverses corrections au champ

observé représentent les réponses combinées de diverses masses situées à des profondeurs sous la surface du sol. Pour mieux discriminer les sources d'anomalies et ainsi acquérir des connaissances sur la structure peu profonde et profonde sous la région d'étude, des anomalies gravimétriques régionales et résiduelles doivent également être déterminées. Sur la base du modèle de structure lithosphérique dérivé du géoïde et du modèle numérique de terrain, les anomalies gravimétriques régionales peuvent être calculées. Cette méthode alternative permet de définir la composante gravimétrique régionale/résiduelle en supposant que le relief topographique est isostatiquement compensé. Par conséquent, le champ de gravité régional/résiduel est indépendant de la mesure de gravité, qui est utilisée dans la méthode traditionnelle pour séparer les anomalies de gravité de Bouguer sur la base d'une surface polynomiale de bas degré ou d'un filtre passe-bas. Cette méthode alternative est susceptible d'apporter de nouvelles perspectives sur la séparation des anomalies de Bouguer régionales/résiduelles.

References

Alber, C., Ware, R., Rocken, C., & Solheim, F. (1997). GPS surveying with 1 mm precision using corrections for atmospheric slant path delay. *Geophysical Research Letters*, *24*(15), 1859–1862. https://doi.org/10.1029/97GL01877

Altamimi, Z., & Collilieux, X. (2009). IGS contribution to the ITRF. *Journal of Geodesy*, *83*(3), 375–383. https://doi.org/10.1007/s00190-008-0294-x

Altamimi, Zuheir, Boucher, C., & Sillard, P. (2002). New trends for the realization of the international terrestrial reference system. *Advances in Space Research*, *30*(2), 175–184. https://doi.org/10.1016/S0273-1177(02)00282-X

Amante, C., & Eakins, B. W. (2009). ETOPO1 1 Arc-Minute Global Relief Model: Procedures, Data Sources and Analysis. *NOAA Technical Memorandum NESDIS NGDC-24. National Geophysical Data Center, NOAA.* doi:10.7289/V5C8276M

Amjadiparvar, B., Rangelova, E., & Sideris, M. G. (2016). The GBVP approach for vertical datum unification: Recent results in North America. *Journal of Geodesy*, *90*(1), 45–63. https://doi.org/10.1007/s00190-015-0855-8

Amjadiparvar, Babak, Rangelova, E. V., Sideris, M. G., & Véronneau, M. (2013). North American height datums and their offsets: The effect of GOCE omission errors and systematic levelling effects. *Journal of Applied Geodesy*, *7*(1), 39–50. https://doi.org/10.1515/jag-2012-0034

Amos, M. (2010). New Zealand vertical datum 2009. *New Zealand Surveyor*, *300*, 5–16.

Amos, M. J., & Featherstone, W. E. (2009). Unification of New Zealand's local vertical datums: Iterative gravimetric quasigeoid computations. *Journal of Geodesy*, *83*(1), 57–68. https://doi.org/10.1007/s00190-008-0232-y

Andersen, O. B., & Knudsen, P. (2016). *Deriving the DTU15 Global high resolution marine gravity field from satellite altimetry*. ESA Living Planet Symposium 2016. https://orbit.dtu.dk/en/publications/deriving-the-dtu15-global-high-resolution-marine-gravity-field-fr

Ardalan, A., Grafarend, E., & Kakkuri, J. (2002). National height datum, the Gauss–Listing geoid level value w0 and its time variation 0 (Baltic Sea Level Project: Epochs 1990.8, 1993.8, 1997.4). *Journal of Geodesy*, *76*(1), 1–28. https://doi.org/10.1007/s001900100211

Artemieva, I. (2011). Lithosphere. *Cambridge University Press*. https://www.academia.edu/25723063/The_Lithosphere_An_interdisciplinary_approach

Bai, L., Tian, X., & Ritsema, J. (2010). Crustal structure beneath the Indochina peninsula from teleseismic receiver functions. *Geophysical Research Letters*, *37*(24). https://doi.org/10.1029/2010GL044874

Balmino, G., Vales, N., Bonvalot, S., & Briais, A. (2012). Spherical harmonic modelling to ultra-high degree of Bouguer and isostatic anomalies. *Journal of Geodesy*, *86*(7), 499–520. https://doi.org/10.1007/s00190-011-0533-4

Balmino, G., Lambeck, K., & Kaula, W. M. (1973). A spherical harmonic analysis of the Earth's topography. *Journal of Geophysical Research*, *78*(2), 478–481. https://doi.org/10.1029/JB078i002p00478

Barzaghi, R. (2016). The Remove-Restore Method. In E. Grafarend (Ed.), *Encyclopedia of Geodesy* (pp. 1–4). Springer International Publishing. https://doi.org/10.1007/978-3-319-02370-0_19-1

Becker, J. J., Sandwell, D. T., Smith, W. H. F., Braud, J., Binder, B., Depner, J., Fabre, D., Factor, J., Ingalls, S., Kim, S.-H., Ladner, R., Marks, K., Nelson, S., Pharaoh, A., Trimmer, R., Rosenberg, J. V., Wallace, G., & Weatherall, P. (2009). Global Bathymetry and Elevation Data at 30 Arc Seconds Resolution: SRTM30_PLUS. *Marine Geodesy*, *32*(4), 355–371. https://doi.org/10.1080/01490410903297766

Block, A. E., Bell, R. E., & Studinger, M. (2009). Antarctic crustal thickness from satellite gravity: Implications for the Transantarctic and Gamburtsev Subglacial Mountains. *Earth and Planetary Science Letters*, *288*(1), 194–203. https://doi.org/10.1016/j.epsl.2009.09.022

Bonvalot, S. (2016). BGI - The International Gravimetric Bureau. In "The Geodesist's Handbook 2016." *Journal of Geodesy*, *90*(10), 907–1205. https://doi.org/10.1007/s00190-016-0948-z

Bonvalot, S. (2020). The International Gravimetric Bureau. In: Poutanen, M., Rózsa, S. The Geodesist's Handbook 2020. *Journal of Geodesy*, *94*(11), 109. https://doi.org/10.1007/s00190-020-01434-z

Bonvalot, S., Balmino, G., Briais, A., Kuhn, M., Peyrefitte, A., Vales, N., Biancale, R., Gabalda, G., Reinquin, F., & Sarrailh, M. (2012). *World Gravity Map*. Commission for the Geological Map of the World. Eds. BGI-CGMW-CNES-IRD, Paris.

Bowin, C. (1983). Depth of principal mass anomalies contributing to the earth's geoidal undulations and gravity anomalies. *Marine Geodesy*, *7*(1–4), 61–100. https://doi.org/10.1080/15210608309379476

Braitenberg, C., & Ebbing, J. (2009). *The GRACE-satellite gravity and geoid fields in analysing large-scale, cratonic or intracratonic basins*.

https://doi.org/10.1111/J.1365-2478.2009.00793.X

Braitenberg, C., Wienecke, S., & Wang, Y. (2006). Basement structures from satellite-derived gravity field: South China Sea ridge. *Journal of Geophysical Research: Solid Earth*, *111*(B5). https://doi.org/10.1029/2005JB003938

Brockmann, J. M., Zehentner, N., Höck, E., Pail, R., Loth, I., Mayer-Gürr, T., & Schuh, W.-D. (2014). EGM_TIM_RL05: An independent geoid with centimeter accuracy purely based on the GOCE mission. *Geophysical Research Letters*, *41*(22), 8089–8099. https://doi.org/10.1002/2014GL061904

Brown, N. J., McCubbine, J. C., Featherstone, W. E., Gowans, N., Woods, A., & Baran, I. (2018). AUSGeoid2020 combined gravimetric–geometric model: Location-specific uncertainties and baseline-length-dependent error decorrelation. *Journal of Geodesy*, *92*(12), 1457–1465. https://doi.org/10.1007/s00190-018-1202-7

Bruinsma, S. L., Förste, C., Abrikosov, O., Lemoine, J.-M., Marty, J.-C., Mulet, S., Rio, M.-H., & Bonvalot, S. (2014). ESA's satellite-only gravity field model via the direct approach based on all GOCE data. *Geophysical Research Letters*, *41*(21), 7508–7514. https://doi.org/10.1002/2014GL062045

Bui, C. Q. (1983). About the new results of the deep structural study of territory of Vietnam. *Journal of Earth Sciences*, *T5 (1), 27-40*. https://scholar.google.com/scholar_lookup?title=About%20the%20new%20results%20of%20the%20deep%20structural%20study%20of%20territory%20of%20Vietnam&author=C.Q.%20Bui&publication_year=1983&pages=27-40

Bullard, E. C. (1936). Gravity measurements in East Africa. *Philosophical Transactions of the Royal Society of London. Series A, Mathematical and Physical Sciences*, *235*(757), 445–531. https://doi.org/10.1098/rsta.1936.0008

Burša, M., Kenyon, S., Kouba, J., Šíma, Z., Vatrt, V., Vítek, V., & Vojtíšková, M. (2007). The geopotential value W 0 for specifying the relativistic atomic time scale and a global vertical reference system. *Journal of Geodesy*, *81*(2), 103–110. https://doi.org/10.1007/s00190-006-0091-3

Burša, M., Raděj, K., Šima, Z., True, S. A., & Vatrt, V. (1997). Determination of the Geopotential Scale Factor from TOPEX/POSEIDON Satellite Altimetry. *Studia Geophysica et Geodaetica*, *41*(3), 203–216. https://doi.org/10.1023/A:1023313614618

Carbonell, R., Levander, A., & Kind, R. (2013). The Mohorovičić discontinuity beneath the continental crust: An overview of seismic constraints. *Tectonophysics*, *609*, 353–376. https://doi.org/10.1016/j.tecto.2013.08.037

Chen, Y.-Q., & Luo, Z. (2004). A hybrid method to determine a local geoid model—Case study. *Earth, Planets and Space*, *56*(4), 419–427. https://doi.org/10.1186/BF03352495

COPERNICUS EMERGENCY MANAGEMENT SERVICE. (2019). Copernicus EMS - Mapping. Retrieved November 19, 2019, from https://emergency.copernicus.eu/mapping/list-of-components/EMSN057

COPERNICUS EMERGENCY MANAGEMENT SERVICE. (2019). Copernicus EMS - Mapping. https://emergency.copernicus.eu/mapping/list-of-components/EMSN062

Crough, S. T. (1983). The correction for sediment loading on the seafloor. *Journal of Geophysical Research: Solid Earth*, *88*(B8), 6449–6454. https://doi.org/10.1029/JB088iB08p06449

Dang, T. H. (2003). *Study on some characteristics of deep crustal structure and seismotectonic zonation in northern Vietnam* [Institute of Geophysics, VAST]. https://scholar.google.com/scholar_lookup?title=Study%20on%20some%20characteristics%20of%20deep%20crustal%20structure%20and%20seismotectonic%20zonation%20in%20northern%20Vietnam&author=T.H.%20Dang&publication_year=2003

Dayoub, N., Edwards, S. J., & Moore, P. (2012). The Gauss–Listing geopotential value W 0 and its rate from altimetric mean sea level and GRACE. *Journal of Geodesy*, *86*(9), 681–694. https://doi.org/10.1007/s00190-012-0547-6

Denker, H. (2005). Evaluation of SRTM3 and GTOPO30 Terrain Data in Germany. In C. Jekeli, L. Bastos, & J. Fernandes (Eds.), *Gravity, Geoid and Space Missions* (pp. 218–223). Springer Berlin Heidelberg.

Dinh, V. T. (2010). *Study of the earth crustal structures of Northern Vietnam by using the deep seismic, magnetotelluric investigations and gravity data (* (Vietnam National Science Project: KC.08.06/06/10).

Dinh, V. T., Harder, S., Huang, B.-S., Trinh, V.-B., Doan, V.-T., Lai, H.-P., Tran, A.-V., Nguyen, H. Q.-T., & Nguyen, V.-D. (2018). An overview of northern Vietnam deep crustal structures from integrated geophysical observations. *Terr. Atmos. Ocean. Sci*. DOI: 10.3319/TAO.2018.01.02.01

Dorman, L., & Lewis, B. (1970). Experimental Isostasy 1. Theory of the Determination of the Earth's Isostatic Response to a Concentrated Load. *Journal of Geophysical Research*, *75*, 3357–3365. https://doi.org/10.1029/JB075i017p03357

Drewes, H., Kuglitsch, F., Adám, J., & Rózsa, S. (2016). The Geodesist's Handbook 2016. *Journal of Geodesy*, *90*(10), 907–1205. https://doi.org/10.1007/s00190-016-

0948-z

Drinkwater, M. R., Floberghagen, R., Haagmans, R., Muzi, D., & Popescu, A. (2003). GOCE: ESA's First Earth Explorer Core Mission. In G. Beutler, M. R. Drinkwater, R. Rummel, & R. Von Steiger (Eds.), *Earth Gravity Field from Space—From Sensors to Earth Sciences: Proceedings of an ISSI Workshop 11–15 March 2002, Bern, Switzerland* (pp. 419–432). Springer Netherlands. https://doi.org/10.1007/978-94-017-1333-7_36

Dumrongchai, P., Wichienchareon, C., & Promtong, C. (2012). Local geoid modeling for Thailand. *International Journal of Geoinformatics*.

Eaton, D. W., Darbyshire, F., Evans, R. L., Grütter, H., Jones, A. G., & Yuan, X. (2009). The elusive lithosphere–asthenosphere boundary (LAB) beneath cratons. *Lithos*, *109*(1), 1–22. https://doi.org/10.1016/j.lithos.2008.05.009

Ebbing, J., Braitenberg, C., & Wienecke, S. (2007). Insights into the lithospheric structure and tectonic setting of the Barents Sea region from isostatic considerations. *Geophysical Journal International*, *171*(3), 1390–1403. https://doi.org/10.1111/j.1365-246X.2007.03602.x

Ekman, M. (1989). Impacts of geodynamic phenomena on systems for height and gravity. *Bulletin Géodésique*, *63*(3), 281–296. https://doi.org/10.1007/BF02520477

Entin, I. I. (1959). Main systematic errors in precise levelling. *Bulletin Géodésique (1946-1975)*, *52*(1), 37–45. https://doi.org/10.1007/BF02526861

Erban, L. E., Gorelick, S. M., & Zebker, H. A. (2014). Groundwater extraction, land subsidence, and sea-level rise in the Mekong Delta, Vietnam. *Environmental Research Letters*, *9*(8), 084010. https://doi.org/10.1088/1748-9326/9/8/084010

Evans, P., & Crompton, W. (1946). Geological factors in gravity interpretation illustrated by evidence from India and Burma. *Quarterly Journal of the Geological Society*, *102*(1–4), 211–249. https://doi.org/10.1144/GSL.JGS.1946.102.01-04.13

Farr, T. G., Rosen, P. A., Caro, E., Crippen, R., Duren, R., Hensley, S., Kobrick, M., Paller, M., Rodriguez, E., Roth, L., Seal, D., Shaffer, S., Shimada, J., Umland, J., Werner, M., Oskin, M., Burbank, D., & Alsdorf, D. (2007). The Shuttle Radar Topography Mission. *Reviews of Geophysics*, *45*(2). https://doi.org/10.1029/2005RG000183

Faure, M., Lepvrier, C., Nguyen, V. V., Vu, T. V., Lin, W., & Chen, Z. (2014). The South China block-Indochina collision: Where, when, and how? *Journal of Asian Earth Sciences*, *79*, 260–274. https://doi.org/10.1016/j.jseaes.2013.09.022

Featherstone, W., Dentith, M., & Kirby, J. (1998). Strategies for the accurate determination of orthometric heights from GPS. *Survey Review*, *34*(267), 278–296.

Featherstone, W. E. (2010). Satellite and airborne gravimetry: Their role in geoid determination and some suggestions. *In Ed. R. Lane, Airborne Gravity 2010, Geoscience Australia: Canberra*. https://www.researchgate.net/publication/268184465_Satellite_and_airborne_gravimetry_their_role_in_geoid_determination_and_some_suggestions

Featherstone, W. E., & Claessens, S. J. (2008). Closed-form transformation between geodetic and ellipsoidal coordinates. *Studia Geophysica et Geodaetica*, *52*(1), 1. https://doi.org/10.1007/s11200-008-0002-6

Featherstone, W. E., Evans, J. D., & Olliver, J. G. (1998). A Meissl-modified Vaníček and Kleusberg kernel to reduce the truncation error in gravimetric geoid computations. *Journal of Geodesy*, *72*(3), 154–160. https://doi.org/10.1007/s001900050157

Featherstone, W. E., & Filmer, M. S. (2008). A New GPS-based evaluation of distortions in the Australian Height Datum in Western Australia. *Journal of the Royal Society of Western Australia*. https://www.researchgate.net/publication/44390367_A_New_GPS-based_evaluation_of_distortions_in_the_Australian_Height_Datum_in_Western_Australia

Featherstone, W. E., & Kirby, J. F. (2000). The reduction of aliasing in gravity anomalies and geoid heights using digital terrain data. *Geophysical Journal International*, *141*(1), 204–212. https://doi.org/10.1046/j.1365-246X.2000.00082.x

Featherstone, W. E., Kirby, J. F., Hirt, C., Filmer, M. S., Claessens, S. J., Brown, N. J., Hu, G., & Johnston, G. M. (2011). The AUSGeoid09 model of the Australian Height Datum. *Journal of Geodesy*, *85*(3), 133–150. https://doi.org/10.1007/s00190-010-0422-2

Featherstone, W. E., Kirby, J. F., Kearsley, A. H. W., Gilliland, J. R., Johnston, G. M., Steed, J., Forsberg, R., & Sideris, M. G. (2001). The AUSGeoid98 geoid model of Australia: Data treatment, computations and comparisons with GPS-levelling data. *Journal of Geodesy*, *75*(5), 313–330. https://doi.org/10.1007/s001900100177

Featherstone, W. E., Lyon, T. J., & McCubbine, J. C. (2019). Potentially Misleading GPS Leveling–Based Assessment of Gravimetric Geoid or Quasigeoid Models due to Vertical Land Motion and Different GPS Processing Software. *Journal of Surveying Engineering*, *145*(4), 04019015. https://doi.org/10.1061/(ASCE)SU.1943-5428.0000293

Featherstone, W. E., & Sideris, M. G. (1998). Modified Kernels in Spectral Geoid Determination: First Results from Western Australia. In Rene Forsberg, M. Feissel, & R. Dietrich (Eds.), *Geodesy on the Move* (pp. 188–193). Springer.

https://doi.org/10.1007/978-3-642-72245-5_26

Featherstone, W., & Kuhn, M. (2006). Height Systems and Vertical Datums: A Review in the Australian Context. *Journal of Spatial Science*, *51*(1), 21–41. https://doi.org/10.1080/14498596.2006.9635062

Findlay, R. H. (1997). The Song Ma Anticlinorium, northern Vietnam: The structure of an allochthonous terrane containing an early Palaeozoic island arc sequence. *Journal of Asian Earth Sciences*, *15*(6), 453–464. https://doi.org/10.1016/S0743-9547(97)00031-7

Findlay, R. H., & Trinh, P. T. (1997). The Structural Setting of the Song Ma Region, Vietnam and the Indochina-South China Plate Boundary Problem. *Gondwana Research*, *1*(1), 11–33. https://doi.org/10.1016/S1342-937X(05)70003-4

Forsberg, R., & Sideris, M. G. (1989). On topographic effects in gravity field approximation. *Meddelelse-Geodaetisk Institut*, *58*, 129–148.

Forsberg, R, & Tscherning, C. (2008). An overview manual for the GRAVSOFT geodetic gravity field modelling programs. *DTU Space*. http://cct.gfy.ku.dk/publ_cct/cct1936.pdf

Forsberg, R. (1984). *A Study of Terrain Reductions, Density Anomalies and Geophysical Inversion Methods in Gravity Field Modelling*. Ohio State University, Department of Geodetic Science and Surveying.

Forsberg, R., & Olesen, A. V. (2010). Airborne Gravity Field Determination. In G. Xu (Ed.), *Sciences of Geodesy—I: Advances and Future Directions* (pp. 83–104). Springer. https://doi.org/10.1007/978-3-642-11741-1_3

Forsberg, R., Olesen, A. V., Einarsson, I., Manandhar, N., & Shreshta, K. (2014). Geoid of Nepal from Airborne Gravity Survey. In *Earth on the Edge: Science for a Sustainable Planet* (pp. 521–527). Springer, Berlin, Heidelberg. https://doi.org/10.1007/978-3-642-37222-3_69

Forsberg, R., Olesen, A. V., Gatchalian, R., & Ortiz, C. C. C. (2014). Geoid model of the Philippines from airborne and surface gravity. *National Mapping and Resource Information Authority*.

Forsberg, R., & Tscherning, C. C. (2008). *An overview manual for the GRAVSOFT Geodetic Gravity Field Modelling Programs*.

Förste, C., Bruinsma, Sean. L., Abrikosov, O., Lemoine, J.-M., Marty, J. C., Flechtner, F., Balmino, G., Barthelmes, F., & Biancale, R. (2014). *EIGEN-6C4 The latest combined global gravity field model including GOCE data up to degree and order 2190 of GFZ Potsdam and GRGS Toulouse* (p. 55102156 Bytes, 3 Files) [Application/octet-

stream,application/octet-stream,application/zip]. GFZ Data Services. https://doi.org/10.5880/ICGEM.2015.1

Fotopoulos, G. (2003). *An analysis on the optimal combination of geoid, orthometric and ellipsoidal height data*. https://doi.org/10.5072/PRISM/10883

Fullea, J., Fernàndez, M., Afonso, J. C., Vergés, J., & Zeyen, H. (2010). The structure and evolution of the lithosphere–asthenosphere boundary beneath the Atlantic–Mediterranean Transition Region. *Lithos*, *120*(1), 74–95. https://doi.org/10.1016/j.lithos.2010.03.003

Fullea, J., Fernàndez, M., & Zeyen, H. (2008). FA2BOUG—A FORTRAN 90 code to compute Bouguer gravity anomalies from gridded free-air anomalies: Application to the Atlantic-Mediterranean transition zone. *Computers & Geosciences*, *34*(12), 1665–1681. https://doi.org/10.1016/j.cageo.2008.02.018

Fullea, J., Fernàndez, M., Zeyen, H., & Vergés, J. (2007). A rapid method to map the crustal and lithospheric thickness using elevation, geoid anomaly and thermal analysis. Application to the Gibraltar Arc System, Atlas Mountains and adjacent zones. *Tectonophysics*, *430*(1), 97–117. https://doi.org/10.1016/j.tecto.2006.11.003

Fullea U., J., Fernàndez, M., & Zeyen, H. (2006). Lithospheric structure in the Atlantic–Mediterranean transition zone (southern Spain, northern Morocco): A simple approach from regional elevation and geoid data. *Comptes Rendus Geoscience*, *338*(1), 140–151. https://doi.org/10.1016/j.crte.2005.11.004

Gatchalian, R., Forsberg, R., & Olesen, A. (2016). *PGM2016: A new Geoid Model for the Philippines*. 27.

Gatti, A., Reguzzoni, M., Migliaccio, F., & Sansò, F. (2016). *Computation and assessment of the fifth release of the GOCE-only space-wise solution*. ResearchGate. https://www.researchgate.net/publication/316042680_Computation_and_assessment_of_the_fifth_release_of_the_GOCE-only_space-wise_solution

Gauss, C. F. (1828). *Bestimmung des Breitenunterschiedes zwischen den Sternwarten von Göttingen und Altona: Durch Beobachtungen am Ramsdenschen Zenithsector*. Bei Vandenhoeck und Ruprecht.

Gerlach, C., & Rummel, R. (2013). Global height system unification with GOCE: A simulation study on the indirect bias term in the GBVP approach. *Journal of Geodesy*, *87*(1), 57–67. https://doi.org/10.1007/s00190-012-0579-y

Gilardoni, M., & al, E. (2013). *Combining EGM2008 with GOCE Gravity Models*. https://doi.org/10.4430/bgta0107

Gilley, L. D., Harrison, T. M., Leloup, P. H., Ryerson, F. J., Lovera, O. M., & Wang, J.-H. (2003).

Direct dating of left-lateral deformation along the Red River shear zone, China and Vietnam. *Journal of Geophysical Research: Solid Earth*, *108*(B2). https://doi.org/10.1029/2001JB001726

Globig, J., Fernàndez, M., Torne, M., Vergés, J., Robert, A., & Faccenna, C. (2016). New insights into the crust and lithospheric mantle structure of Africa from elevation, geoid, and thermal analysis. *Journal of Geophysical Research: Solid Earth*, *121*(7), 5389–5424. https://doi.org/10.1002/2016JB012972

Gómez-Ortiz, D., & Agarwal, B. N. P. (2005). 3DINVER.M: A MATLAB program to invert the gravity anomaly over a 3D horizontal density interface by Parker–Oldenburg's algorithm. *Computers & Geosciences*, *31*(4), 513–520. https://doi.org/10.1016/j.cageo.2004.11.004

Grigoriadis, V. N., Kotsakis, C., Tziavos, I. N., & Vergos, G. S. (2014). Estimation of the Reference Geopotential Value for the Local Vertical Datum of Continental Greece Using EGM08 and GPS/Leveling Data. In U. Marti (Ed.), *Gravity, Geoid and Height Systems* (pp. 249–255). Springer International Publishing. https://doi.org/10.1007/978-3-319-10837-7_32

HA, M. H. (2012). *Final Report: Measurement and Improvement of Vietnam National Gravity Data*. Vietnam Institute of Geodesy and Cartography.

Ha, M. H. (2017). Construction of initial national quasi-geoid model VIGAC2017, first step to national spatial reference system in Vietnam. *VIETNAM JOURNAL OF EARTH SCIENCES*, *39*(2), 155–166. https://doi.org/10.15625/0866-7187/39/2/9702

Haagmans, R., Min, E., Gelderen, M., & von Eynatten, M. (1993). *Fast evaluation of convolution integrals on the sphere using 1D FFT, and a comparison with existing methods for Stokes'*. https://www.scienceopen.com/document?vid=71fa5d92-cd72-4ae1-9d47-e0df3d9e55f0

Hackney, R. I., & Featherstone, W. E. (2003). Geodetic versus geophysical perspectives of the 'gravity anomaly.' *Geophysical Journal International*, *154*(1), 35–43. https://doi.org/10.1046/j.1365-246X.2003.01941.x

Hastings, D. A., Dunbar, P. K., & Hittelman, A. M. (2000). Assessing the global land one-km base elsevation DEM. In K.-P. Schwarz (Ed.), *Geodesy Beyond 2000* (pp. 101–106). Springer. https://doi.org/10.1007/978-3-642-59742-8_16

Hayden, T., Amjadiparvar, B., Rangelova, E., & Sideris, M. G. (2013). Estimating Canadian vertical datum offsets using GNSS/levelling benchmark information and GOCE global geopotential models. *Journal of Geodetic Science*, *2*(4), 257–269. https://doi.org/10.2478/v10156-012-0008-4

Heck, B. (1987). *Modification of Stokes formula by combining two classical approaches*. /paper/Modification-of-Stokes-formula-by-combining-two-Heck/c16d74de3493a8c6ff426576f3fd7e375b75e1f9

Heiskanen, W. A., & Moritz, H. (1967). *Physical Geodesy*. W.H. Freeman and Company, San Francisco. http://archive.org/details/HeiskanenMoritz1967PhysicalGeodesy

Helmcke, D. (1985). The Permo-Triassic »Paleotethys« in mainland Southeast-Asia and adjacent parts of China. *Geologische Rundschau*, *74*(2), 215–228. https://doi.org/10.1007/BF01824893

Hirt, C., Featherstone, W. E., & Marti, U. (2010). Combining EGM2008 and SRTM/DTM2006.0 residual terrain model data to improve quasigeoid computations in mountainous areas devoid of gravity data. *Journal of Geodesy*, *84*(9), 557–567. https://doi.org/10.1007/s00190-010-0395-1

Hirt, C. (2013). RTM Gravity Forward-Modeling Using Topography/Bathymetry Data to Improve High-Degree Global Geopotential Models in the Coastal Zone. *Marine Geodesy*, *36*(2), 183–202. https://doi.org/10.1080/01490419.2013.779334

Hirt, C., & Kuhn, M. (2012). Evaluation of high-degree series expansions of the topographic potential to higher-order powers. *Journal of Geophysical Research: Solid Earth*, *117*(B12). https://doi.org/10.1029/2012JB009492

Hofmann-Wellenhof, B., & Moritz, H. (2006). *Physical Geodesy* (2nd ed.). Springer-Verlag. //www.springer.com/la/book/9783211335444

Hong Nguyen, P., Cong Bui, Q., & Dinh Nguyen, X. (2012). Investigation of earthquake tsunami sources, capable of affecting Vietnamese coast. *Natural Hazards*, *64*(1), 311–327. https://doi.org/10.1007/s11069-012-0240-3

Huang, B.-S., Le, T. S., Liu, C.-C., Toan, D. V., Huang, W.-G., Wu, Y.-M., Chen, Y.-G., & Chang, W.-Y. (2009). Portable broadband seismic network in Vietnam for investigating tectonic deformation, the Earth's interior, and early-warning systems for earthquakes and tsunamis. *Journal of Asian Earth Sciences*, *36*(1), 110–118. https://doi.org/10.1016/j.jseaes.2009.02.012

Huchon, P., Pichon, X. L., & Rangin, C. (1994). Indochina Peninsula and the collision of India and Eurasia. *Geology*, *22*(1), 27–30. https://doi.org/10.1130/0091-7613(1994)022<0027:IPATCO>2.3.CO;2

Hutchison, C. S. (1989). The Palaeo-Tethyan Realm and Indosinian Orogenic System of Southeast Asia. In A. M. C. Şengör (Ed.), *Tectonic Evolution of the Tethyan Region* (pp. 585–643). Springer Netherlands. https://doi.org/10.1007/978-94-009-2253-2_25

Hwang, C., Wang, C.-G., & Hsiao, Y.-S. (2003). Terrain correction computation using Gaussian quadrature. *Computers & Geosciences*, *29*(10), 1259–1268. https://doi.org/10.1016/j.cageo.2003.08.003

IGP. (2005). *Research and Forecasting Earthquakes and Ground Movements in Vietnam (Researched by Vietnam Institute of Geophysics – Chairman is Prof. Nguyen Dinh Xuyen), Hanoi, Vietnam (in Vietnamese).*

Ihde, J, Adam, J., Gurtner, W., Harsson, B. G., Sacher, M., Schlüter, W., & Wöppelmann, G. (2000). *The Height Solution of the European Vertical Reference Network (EUVN)*. 17.

Ihde, Johannes, Sánchez, L., Barzaghi, R., Drewes, H., Foerste, C., Gruber, T., Liebsch, G., Marti, U., Pail, R., & Sideris, M. (2017). Definition and Proposed Realization of the International Height Reference System (IHRS). *Surveys in Geophysics*, *38*(3), 549–570. https://doi.org/10.1007/s10712-017-9409-3

Iliffe, J. C., Ziebart, M., Cross, P. A., Forsberg, R., Strykowski, G., & Tscherning, C. C. (2003). Osgm02: A New Model for Converting Gps-Derived Heights to Local Height Datums in Great Britain and Ireland. *Survey Review*, *37*(290), 276–293. https://doi.org/10.1179/sre.2003.37.290.276

Ince, E. S., Barthelmes, F., Reißland, S., Elger, K., Förste, C., Flechtner, F., & Schuh, H. (2019). ICGEM – 15 years of successful collection and distribution of global gravitational models, associated services, and future plans. *Earth System Science Data*, *11*(2), 647–674. https://doi.org/10.5194/essd-11-647-2019

IPCC. (2014). *Climate Change 2014: Synthesis Report. Contribution of Working Groups I, II and III to the Fifth Assessment Report of the Intergovernmental Panel on Climate Change [Core Writing Team, R.K. Pachauri and L.A. Meyer (eds.)]* (p. 151). IPCC, Geneva, Switzerland,.

Ismail, M. K., Din, A. H. M., Uti, M. N., & Omar, A. H. (2018, September). *ESTABLISHMENT OF NEW FITTED GEOID MODEL IN UNIVERSITI TEKNOLOGI MALAYSIA*. ResearchGate. https://www.researchgate.net/publication/328683742_ESTABLISHMENT_OF_NEW_FITTED_GEOID_MODEL_IN_UNIVERSITI_TEKNOLOGI_MALAYSIA

Jamil, H., Kadir, M., Forsberg, R., Olesen, A., Isa, M. N., Rasidi, S., Mohamed, A., Chihat, Z., Nielsen, E., Majid, F., Talib, K., & Aman, S. (2017). Airborne geoid mapping of land and sea areas of East Malaysia. *Journal of Geodetic Science*, *7*(1), 84–93. https://doi.org/10.1515/jogs-2017-0010

Jiménez-Munt, I., Fernàndez, M., Saura, E., Vergés, J., & Garcia-Castellanos, D. (2012). 3-D lithospheric structure and regional/residual Bouguer anomalies in the Arabia–Eurasia collision (Iran). *Geophysical Journal International*, *190*(3), 1311–1324.

https://doi.org/10.1111/j.1365-246X.2012.05580.x

Jolivet, L., Beyssac, O., Goffé, B., Avigad, D., Lepvrier, C., Maluski, H., & Thang, T. T. (2001). Oligo-Miocene midcrustal subhorizontal shear zone in Indochina. *Tectonics*, *20*(1), 46–57. https://doi.org/10.1029/2000TC900021

Jolivet, L., Davy, P., & Cobbold, P. (1990). Right-lateral shear along the Northwest Pacific Margin and the India-Eurasia Collision. *Tectonics*, *9*(6), 1409–1419. https://doi.org/10.1029/TC009i006p01409

Kaban, M. K., Schwintzer, P., & Reigber, Ch. (2004). A new isostatic model of the lithosphere and gravity field. *Journal of Geodesy*, *78*(6), 368–385. https://doi.org/10.1007/s00190-004-0401-6

Kaban, M. K., El Khrepy, S., & Al-Arifi, N. (2016). Isostatic Model and Isostatic Gravity Anomalies of the Arabian Plate and Surroundings. *Pure and Applied Geophysics*, *173*(4), 1211–1221. https://doi.org/10.1007/s00024-015-1164-0

Kasenda, A., & Kearsley, A. H. W. (2002). Towards the Establishment of an Indonesian Unified Vertical Datum. In H. Drewes, A. H. Dodson, L. P. S. Fortes, L. Sánchez, & P. Sandoval (Eds.), *Vertical Reference Systems* (Vol. 124, pp. 334–338). Springer Berlin Heidelberg. https://doi.org/10.1007/978-3-662-04683-8_62

King, R., & Bock, Y. (2009). Documentation for the GAMIT GPS analysis software, release 10.2. In *Mass. Inst. Of Tech., Scripps Inst. Oceanogr*.

Kotsakis, C., Katsambalos, K., & Ampatzidis, D. (2012). Estimation of the zero-height geopotential level W o LVD in a local vertical datum from inversion of co-located GPS, leveling and geoid heights: A case study in the Hellenic islands. *Journal of Geodesy*, *86*(6), 423–439. https://doi.org/10.1007/s00190-011-0530-7

Kuhn, M., Featherstone, W. E., & Kirby, J. F. (2009). Complete spherical Bouguer gravity anomalies over Australia. *Australian Journal of Earth Sciences*, *56*(2), 213–223. https://doi.org/10.1080/08120090802547041

Kumar, N., Zeyen, H., & Singh, A. P. (2014). 3D Lithosphere density structure of southern Indian shield from joint inversion of gravity, geoid and topography data. *Journal of Asian Earth Sciences*, *89*, 98–107. https://doi.org/10.1016/j.jseaes.2014.03.028

Kuroishi, Y., Ando, H., & Fukuda, Y. (2002). A new hybrid geoid model for Japan, GSIGEO2000. *Journal of Geodesy*, *76*(8), 428–436. https://doi.org/10.1007/s00190-002-0266-5

LaFehr, T. R. (1991). An exact solution for the gravity curvature (Bullard B) correction. *GEOPHYSICS*, *56*(8), 1179–1184. https://doi.org/10.1190/1.1443138

Lai, M. G., Le, T. H., Chu, Q. K., & Kieu, H. P. (2012). The gravity anomaly maps of Vietnam

at 1:500,000 scale (mainland part), year 2011. *Journal of Geology*, 15–24.

Laske, G., Masters, G., Ma, Z., & Pasyanos, M. (2013). Update on CRUST1.0—A 1-degree global model of Earth's crust. *Abstract EGU2013-2658 Presented at 2013 Geophys. Res. Abstracts 15*, *15*, 2658.

Laske, G., Masters, G., Ma, Z., & Pasyanos, M. E. (2012). *CRUST1.0: An Updated Global Model of Earth's .14, 3743st*

Laske, G., Masters, G., & Reif, C. (2000). *CRUST 2.0: A new global crustal model at 2×2 degrees (CRUST2.0)*. http://igppweb.ucsd.edu/*gabi/rem.dir/crust/crust2.html

Lebedev, S., & Nolet, G. (2003). Upper mantle beneath Southeast Asia from S velocity tomography. *Journal of Geophysical Research: Solid Earth*, *108*(B1). https://doi.org/10.1029/2000JB000073

Lee, S. B., Auh, S. C., & Seo, D. Y. (2017). Evaluation of global and regional geoid models in South Korea by using terrestrial and GNSS data. *KSCE Journal of Civil Engineering*, *21*(5), 1905–1911. https://doi.org/10.1007/s12205-016-1096-y

Leloup, P. H., Arnaud, N., Lacassin, R., Kienast, J. R., Harrison, T. M., Trong, T. T. P., Replumaz, A., & Tapponnier, P. (2001). New constraints on the structure, thermochronology, and timing of the Ailao Shan-Red River shear zone, SE Asia. *Journal of Geophysical Research: Solid Earth*, *106*(B4), 6683–6732. https://doi.org/10.1029/2000JB900322

Leloup, P. H., Tapponnier, P., Lacassin, R., & Searle, M. P. (2007). Discussion on the role of the Red River shear zone, Yunnan and Vietnam, in the continental extrusion of SE Asia Journal, Vol. 163, 2006, 1025–1036. *Journal of the Geological Society*, *164*(6), 1253–1260. https://doi.org/10.1144/0016-76492007-065

Leloup, Philippe Hervé, Lacassin, R., Tapponnier, P., Schärer, U., Zhong, D., Liu, X., Zhang, L., Ji, S., & Trinh, P. T. (1995). The Ailao Shan-Red River shear zone (Yunnan, China), Tertiary transform boundary of Indochina. *Tectonophysics*, *251*(1), 3–84. https://doi.org/10.1016/0040-1951(95)00070-4

Lemoine, F. G., Kenyon, S. C., Factor, J. K., Trimmer, R. G., Pavlis, N. K., Chinn, D. S., Cox, C. M., Klosko, S. M., Luthcke, S. B., Torrence, M. H., Wang, Y. M., Williamson, R. G., Pavlis, E. C., Rapp, R. H., & Olson, T. R. (1998). *The Development of the Joint NASA GSFC and the National Imagery and Mapping Agency (NIMA) Geopotential Model EGM96*. 584.

Lepvrier, C., Maluski, H., Van Tich, V., Leyreloup, A., Truong Thi, P., & Van Vuong, N. (2004). The Early Triassic Indosinian orogeny in Vietnam (Truong Son Belt and Kontum Massif); implications for the geodynamic evolution of Indochina. *Tectonophysics*,

393(1), 87–118. https://doi.org/10.1016/j.tecto.2004.07.030

Lepvrier, C., Faure, M., Van, V. N., Vu, T. V., Lin, W., Trong, T. T., & Hoa, P. T. (2011). North-directed Triassic nappes in Northeastern Vietnam (East Bac Bo). *Journal of Asian Earth Sciences*, *41*(1), 56–68. https://doi.org/10.1016/j.jseaes.2011.01.002

Lepvrier, C., Maluski, H., Van Vuong, N., Roques, D., Axente, V., & Rangin, C. (1997). Indosinian NW-trending shear zones within the Truong Son belt (Vietnam) 40Ar□39Ar Triassic ages and Cretaceous to Cenozoic overprints. *Tectonophysics*, *283*(1), 105–127. https://doi.org/10.1016/S0040-1951(97)00151-0

Li, C., & Hilst, R. D. van der. (2010). Structure of the upper mantle and transition zone beneath Southeast Asia from traveltime tomography. *Journal of Geophysical Research: Solid Earth*, *115*(B7). https://doi.org/10.1029/2009JB006882

Li, Y., Wu, Q., Zhang, R., Tian, X., & Zeng, R. (2008). The crust and upper mantle structure beneath Yunnan from joint inversion of receiver functions and Rayleigh wave dispersion data. *Physics of the Earth and Planetary Interiors*, *170*(1), 134–146. https://doi.org/10.1016/j.pepi.2008.08.006

Listing, J. B. (1873). *Über unsere jetzige Kenntnis der Gestalt und Größe der Erde*. Dietrichsche Verlagsbuchhandlung, Göttingen. https://www.libreriauniversitaria.it/uber-unsere-jetzige-kenntnis-der/book/9783836422994

Marty, J. (2009). *Documentation algorithmique du programme GINS, Version 5 juillet 2009 (in French)*. http://www.igsac-cnes.cls.fr/documents/gins/GINS_Doc_Algo.html

Mayer-Guerr, T. (2015). *The combined satellite gravity field model GOCO05s*. *17*, 12364. http://adsabs.harvard.edu/abs/2015EGUGA..1712364M

Mazur, S., Green, C., Stewart, M. G., Whittaker, J. M., Williams, S., & Bouatmani, R. (2012). Displacement along the Red River Fault constrained by extension estimates and plate reconstructions. *Tectonics*, *31*(5). https://doi.org/10.1029/2012TC003174

McCubbine, J. C., Stagpoole, V., Caratori Tontini, F., Featherstone, W. E., Garthwaite, M. C., Brown, N. J., Amos, M. J., Fukuda, Y., Kazama, T., Takiguchi, H., & Nishijima, J. (2020). Evaluating temporal stability of the New Zealand quasigeoid following the 2016 Kaikōura earthquake using satellite radar remote sensing. *Geophysical Journal International*, *220*(3), 1917–1927. https://doi.org/10.1093/gji/ggz536

Meissl, P. (1971). *Preparations for the Numerical Evaluation of Second Order Molodensky Type Formulas*. 78.

Metcalfe, I. (2013). Gondwana dispersion and Asian accretion: Tectonic and palaeogeographic evolution of eastern Tethys. *Journal of Asian Earth Sciences*, *66*,

1–33. https://doi.org/10.1016/j.jseaes.2012.12.020

Minderhoud, P. S. J., Erkens, G., Pham, V. H., Bui, V. T., Erban, L., Kooi, H., & Stouthamer, E. (2017). Impacts of 25 years of groundwater extraction on subsidence in the Mekong delta, Vietnam. *Environmental Research Letters*, *12*(6), 064006. https://doi.org/10.1088/1748-9326/aa7146

Minh, D. H. T., Van Trung, L., & Toan, T. L. (2015). Mapping Ground Subsidence Phenomena in Ho Chi Minh City through the Radar Interferometry Technique Using ALOS PALSAR Data. *Remote Sensing*, *7*(7), 8543–8562. https://doi.org/10.3390/rs70708543

Miyahara, B., Kodama, T., & Kuroishi, Y. (2014). *Development of new hybrid geoid model for Japan, "GSI10. GEO2011."*

Molnar, P., & Tapponnier, P. (1975). Cenozoic Tectonics of Asia: Effects of a Continental Collision. *Science*, *189*(4201), 419–426. JSTOR.

Molodensky, M. S., Eremeev, V. F., & Yurkina, M. I. (1962). *Methods for study of the external gravitational field and figure of the Earth. Translated from Russian by the Israel program for scientific translations* (Office of Technical Services Department of Commerce, Washington, D.C).

Mooney, W. D., Laske, G., & Masters, T. G. (1998). CRUST 5.1: A global crustal model at 5° × 5°. *Journal of Geophysical Research: Solid Earth*, *103*(B1), 727–747. https://doi.org/10.1029/97JB02122

Moritz, H. (2000). Geodetic Reference System 1980. *Journal of Geodesy*, *74*(1), 128–133. https://doi.org/10.1007/s001900050278

Moritz, H. (1980). *Advanced Physical Geodesy*. Wichmann.

Nguyen, N. T., Phan, T. H., Bui, V. N., Nguyen, T. T. H., & Tran, T. L. (2018). Moho depth of the northern Vietnam and Gulf of Tonkin from 3D inverse interpretation of gravity anomaly data. *Journal of Geophysics and Engineering*, *15*(4), 1651–1662. https://doi.org/10.1088/1742-2140/aabf48

Nguyen, N.T., & Nguyen, T. T. H. (2013). Topography of the Moho and earth crust structure beneath the East Vietnam Sea from 3D inversion of gravity field data. *Acta Geophysica*, *61*(2), 357–384. https://doi.org/10.2478/s11600-012-0078-9

Nguyen, V.-D., Huang, B.-S., Le, T.-S., Dinh, V.-T., Zhu, L., & Wen, K.-L. (2013). Constraints on the crustal structure of northern Vietnam based on analysis of teleseismic converted waves. *Tectonophysics*, *601*, 87–97. https://doi.org/10.1016/j.tecto.2013.04.031

NIMA. (2000). *Deparment of Defense World Geodectic System 1984* (p. 169).

Noisagool, S., Boonchaisuk, S., Pornsopin, P., & Siripunvaraporn, W. (2014). Thailand's crustal properties from tele-seismic receiver function studies. *Tectonophysics*, *632*, 64–75. https://doi.org/10.1016/j.tecto.2014.06.014

Oldenburg, D. W. (1974). The inversion and interpretation of gravity anomalies. *GEOPHYSICS*, *39*(4), 526–536. https://doi.org/10.1190/1.1440444

O'Reilly, S. Y., & Griffin, W. L. (2010). The continental lithosphere–asthenosphere boundary: Can we sample it? *Lithos*, *120*(1), 1–13. https://doi.org/10.1016/j.lithos.2010.03.016

Pail, R., Fecher, T., Barnes, D., Factor, J. F., Holmes, S. A., Gruber, T., & Zingerle, P. (2018). Short note: The experimental geopotential model XGM2016. *Journal of Geodesy*, *92*(4), 443–451. https://doi.org/10.1007/s00190-017-1070-6

Parker, R. L. (1973). The Rapid Calculation of Potential Anomalies. *Geophysical Journal International*, *31*(4), 447–455. https://doi.org/10.1111/j.1365-246X.1973.tb06513.x

Parsons, B., & Sclater, J. G. (1977). An analysis of the variation of ocean floor bathymetry and heat flow with age. *Journal of Geophysical Research (1896-1977)*, *82*(5), 803–827. https://doi.org/10.1029/JB082i005p00803

Pavlis, N. K., Holmes, S. A., Kenyon, S. C., & Factor, J. K. (2012). The development and evaluation of the Earth Gravitational Model 2008 (EGM2008). *Journal of Geophysical Research: Solid Earth*, *117*(B4). https://doi.org/10.1029/2011JB008916

Pérez-Gussinyé, M., Lowry, A. R., Watts, A. B., & Velicogna, I. (2004). On the recovery of effective elastic thickness using spectral methods: Examples from synthetic data and from the Fennoscandian Shield. *Journal of Geophysical Research: Solid Earth*, *109*(B10). https://doi.org/10.1029/2003JB002788

Pham, H. L. (2009). *Final Report: Research on establishing the height system unification for Vietnam on the basis without using the mean sea level (in Vietnamese)*. Vietnam Institute of Geodesy and Cartography.

Piñón, D. A., Zhang, K., Wu, S., & Cimbaro, S. R. (2018). A New Argentinean Gravimetric Geoid Model: GEOIDEAR. In J. T. Freymueller & L. Sánchez (Eds.), *International Symposium on Earth and Environmental Sciences for Future Generations* (pp. 53–62). Springer International Publishing.

Poudjom Djomani, Y. H., Diament, M., & Albouy, Y. (1992). Mechanical behaviour of the lithosphere beneath the Adamawa uplift (Cameroon, West Africa) based on gravity data. *Journal of African Earth Sciences (and the Middle East)*, *15*(1), 81–90.

https://doi.org/10.1016/0899-5362(92)90009-2

Prasanna, H. M. I., Chen, W., & İz, H. B. (2013). High resolution local Moho determination using gravity inversion: A case study in Sri Lanka. *Journal of Asian Earth Sciences*, *74*, 62–70. https://doi.org/10.1016/j.jseaes.2013.06.005

Rapp, R. H. (1989). The treatment of permanent tidal effects in the analysis of satellite altimeter data for sea surface topography. *Manuscripta Geodaetica*. https://archipel-univtoulouse.hosted.exlibrisgroup.com/primo-explore/openurl?sid=google&auinit=RH&aulast=Rapp&atitle=The%20treatment%20of%20permanent%20tidal%20effects%20in%20the%20analysis%20of%20satellite%20altimeter%20data%20for%20sea%20surface%20topography&title=Manuscripta%20geodaetica&volume=14&issue=6&date=1989&spage=368&vid=33UT3_VU1&institution=33UT3&url_ctx_val=&url_ctx_fmt=null&isSerivcesPage=true

Rapp, R. H., & Balasubramania, X. (1992). *A conceptual formulation of a world height system* (No. 421). OSU Rep.

Rapp, R.H. (1998). Past and Future Developments in Geopotential Modeling. In Rene Forsberg, M. Feissel, & R. Dietrich (Eds.), *Geodesy on the Move* (Vol. 119, pp. 58–78). Springer Berlin Heidelberg. https://doi.org/10.1007/978-3-642-72245-5_9

Reguzzoni, M., & Sampietro, D. (2014). GEMMA: An earth crustal model based on GOCE satellite data. *International Journal of Applied Earth Observation and Geoinformation*, *35*. https://doi.org/10.1016/j.jag.2014.04.002

Reigber, Ch., Kang, Z., Konig, R., & Schwintzer, P. (1996, May). CHAMP, A mini-satellite mission for geopotential and atmospheric research. *Proceedings of the Spring AGU Meeting*.

Reyes, R. B., Nagai, M., Kamiya, Y., Tipdecho, T., & Ninsawat, S. (2015). Effect of sea level rise in the validation of geopotential/geoid models in Metro Manila, Philippines. *Survey Review*, *47*(342), 211–219. https://doi.org/10.1179/1752270614Y.0000000102

Robert, A., Jiménez-Munt, I., Fernàndez, M., & Vergés, J. (2012). Crustal and lithospheric mantle structures in Central Asia derived from geoid, elevation and thermal analysis. *Journal of Nepal Geological Society*.

Robert, A., Fernàndez, M., Jiménez-Munt, I., & Vergés, J. (2017). Lithospheric structure in Central Eurasia derived from elevation, geoid anomaly and thermal analysis. *Geological Society, London, Special Publications*, *427*(1), 271–293. https://doi.org/10.1144/SP427.10

Rummel, R., Gruber, T., Ihde, J., Liebch, G., Rülke, A., Schäfer, U., Sideris, M. G., Rangelova, E., Woodworth, P., & Hughes, C. (2014). *STSE-GOCE+ Height System Unification with GOCE* (Doc. No.: GO-HSU-PL-0020).

Rummel, Reiner, & Teunissen, P. (1988). Height datum definition, height datum connection and the role of the geodetic boundary value problem. *Bulletin Géodésique*, *62*(4), 477–498. https://doi.org/10.1007/BF02520239

Rychert, C. A., & Shearer, P. M. (2009). A Global View of the Lithosphere-Asthenosphere Boundary. *Science*, *324*(5926), 495–498. https://doi.org/10.1126/science.1169754

Sadiq, M., Tscherning, C. C., & Ahmad, Z. (2009). An estimation of the height system bias parameter N0 using least squares collocation from observed gravity and GPS-levelling data. *Studia Geophysica et Geodaetica*, *53*(3), 375–388. https://doi.org/10.1007/s11200-009-0026-6

Sánchez, L. (2012). Towards a vertical datum standardisation under the umbrella of Global Geodetic Observing System. *Journal of Geodetic Science*, *2*(4), 325–342. https://doi.org/10.2478/v10156-012-0002-x

Sánchez, L., Čunderlík, R., Dayoub, N., Mikula, K., Minarechová, Z., Šíma, Z., Vatrt, V., & Vojtíšková, M. (2016). A conventional value for the geoid reference potential $$W_{0}$$W0. *Journal of Geodesy*, *90*(9), 815–835. https://doi.org/10.1007/s00190-016-0913-x

Sánchez, L. (2019). *Advances in the implementation of the International Height Reference System*. 22.

Sandwell, D. T., Müller, R. D., Smith, W. H. F., Garcia, E., & Francis, R. (2014). New global marine gravity model from CryoSat-2 and Jason-1 reveals buried tectonic structure. *Science*, *346*(6205), 65–67. https://doi.org/10.1126/science.1258213

Sandwell, D. T., & Renkin, M. L. (1988). Compensation of swells and plateaus in the north Pacific: No direct evidence for mantle convection. *Journal of Geophysical Research: Solid Earth*, *93*(B4), 2775–2783. https://doi.org/10.1029/JB093iB04p02775

Sansò, F., & Sideris, M. G. (Eds.). (2013). *Geoid Determination: Theory and Methods*. Springer-Verlag. https://doi.org/10.1007/978-3-540-74700-0

Schaeffer, A. J., & Lebedev, S. (2013). Global shear speed structure of the upper mantle and transition zone. *Geophysical Journal International*, *194*(1), 417–449. https://doi.org/10.1093/gji/ggt095

Schwarz, K. P., Sideris, M. G., & Forsberg, R. (1990). The use of FFT techniques in physical geodesy. *Geophysical Journal International*, *100*(3), 485–514.

https://doi.org/10.1111/j.1365-246X.1990.tb00701.x

Searle, M. P. (2006). Role of the Red River Shear zone, Yunnan and Vietnam, in the continental extrusion of SE Asia. *Journal of the Geological Society*, *163*(6), 1025–1036. https://doi.org/10.1144/0016-76492005-144

Shin, Y. H., Choi, K. S., & Xu, H. (2006). Three-dimensional forward and inverse models for gravity fields based on the Fast Fourier Transform. *Computers & Geosciences*, *32*(6), 727–738. https://doi.org/10.1016/j.cageo.2005.10.002

Shin, Y. H., Xu, H., Braitenberg, C., Fang, J., & Wang, Y. (2007). Moho undulations beneath Tibet from GRACE-integrated gravity data. *Geophysical Journal International*, *170*(3), 971–985. https://doi.org/10.1111/j.1365-246X.2007.03457.x

Sideris, M. G., & Forsberg, R. (1991). Review of Geoid Prediction Methods in Mountainous Regions. In Richard H. Rapp & F. Sansò (Eds.), *Determination of the Geoid* (pp. 51–62). Springer. https://doi.org/10.1007/978-1-4612-3104-2_8

Sjöberg, L.E., & Bagherbandi, M. (2017). *Gravity Inversion and Integration: Theory and Applications in Geodesy and Geophysics*. Springer International Publishing. https://doi.org/10.1007/978-3-319-50298-4

Sjöberg, L.E. (2005). A discussion on the approximations made in the practical implementation of the remove–compute–restore technique in regional geoid modelling. *Journal of Geodesy*, *78*(11), 645–653. https://doi.org/10.1007/s00190-004-0430-1

Smith, W. H. F., & Sandwell, D. T. (1994). Bathymetric prediction from dense satellite altimetry and sparse shipboard bathymetry. *Journal of Geophysical Research: Solid Earth*, *99*(B11), 21803–21824. https://doi.org/10.1029/94JB00988

Smith, W. H. F., & Sandwell, D. T. (1997). Global Sea Floor Topography from Satellite Altimetry and Ship Depth Soundings. *Science*, *277*(5334), 1956–1962. https://doi.org/10.1126/science.277.5334.1956

Stephen, J., Singh, S. B., & Yedekar, D. B. (2003). Elastic thickness and isostatic coherence anisotropy in the South Indian Peninsular Shield and its implications. *Geophysical Research Letters*, *30*(16). https://doi.org/10.1029/2003GL017686

Su, C.-M., Wen, S., Tang, C.-C., Yeh, Y.-L., & Chen, C.-H. (2018). The variation of crustal structure along the Song Ma Shear Zone, Northern Vietnam. *Tectonophysics*, *734–735*, 119–129. https://doi.org/10.1016/j.tecto.2018.04.005

Tapponnier, P., Peltzer, G., & Armijo, R. (1986). On the mechanics of the collision between India and Asia. *Geological Society, London, Special Publications*, *19*(1), 113–157. https://doi.org/10.1144/GSL.SP.1986.019.01.07

Tenzer, R., & Hamayun, K. (2010). Global map of the gravity anomaly corrected for complete effects of the topography, and of density contrasts of global ocean, ice, and sediments. *Slovak Academy of Sciences. Geophysical Institute. Contributions to Geophysics and Geodesy*, *38/4*(4), 357–370.

Tenzer, R., Novák, P., Vajda, P., Gladkikh, V., & Hamayun. (2012). Spectral harmonic analysis and synthesis of Earth's crust gravity field. *Computational Geosciences*, *16*(1), 193–207. https://doi.org/10.1007/s10596-011-9264-0

Tocho, C., & Vergos, G. S. (2016). Estimation of the Geopotential Value W0 for the Local Vertical Datum of Argentina Using EGM2008 and GPS/Levelling Data W0LVD. In C. Rizos & P. Willis (Eds.), *IAG 150 Years* (pp. 271–279). Springer International Publishing. https://doi.org/10.1007/1345_2015_32

Torge, W. (2001). *Geodesy*. Walter de Gruyter.

Torge, W., & Müller, J. (2012). Geodesy. In *Geodesy*. De Gruyter. https://www.degruyter.com/view/title/33116

Torne, M., Fernàndez, M., Vergés, J., Ayala, C., Salas, M. C., Jimenez-Munt, I., Buffett, G. G., & Díaz, J. (2015). Crust and mantle lithospheric structure of the Iberian Peninsula deduced from potential field modeling and thermal analysis. *Tectonophysics*, *663*, 419–433. https://doi.org/10.1016/j.tecto.2015.06.003

Trần, Đ. T., Nguyễn, T. Y., Dương, C. C., Vy, Q. H., Zuchiewicz, W., Nguyễn, Q. C., & Nguyễn, V. N. (2013). Recent crustal movements of northern Vietnam from GPS data. *Journal of Geodynamics*, *69*, 5–10. https://doi.org/10.1016/j.jog.2012.02.009

Tran, V. H. (2012). *Study on Earthquake Ground Motion Prediction and its Application to Structural Response of Bridge in Vietnam* [Waseda University]. https://core.ac.uk/download/pdf/144448432.pdf

Tscherning, C. C. (2015). Least-Squares Collocation. In E. Grafarend (Ed.), *Encyclopedia of Geodesy* (pp. 1–5). Springer International Publishing. https://doi.org/10.1007/978-3-319-02370-0_51-1

Tscherning, C. C., & Rapp, R. H. (1974). *Closed covariance expressions for gravity anomalies, geoid undulations, and deflections of the vertical implied by anomaly degree variance models*.

van Hees, G. S. (1991). Stokes formula using Fast Fourier Techniques. In Richard H. Rapp & F. Sansò (Eds.), *Determination of the Geoid* (pp. 405–408). Springer. https://doi.org/10.1007/978-1-4612-3104-2_47

Vanicek, P., Castle, R.O. & Balazs, E.I., 1980. Geodetic leveling and its applications, Rev. Geophys., 18(2), 505–524.

Vaníček, P., & Sjöberg, L. E. (1991). Reformulation of Stokes's theory for higher than second-degree reference field and modification of integration kernels. *Journal of Geophysical Research: Solid Earth*, *96*(B4), 6529–6539. https://doi.org/10.1029/90JB02782

Vergos, G. S., Erol, B., Natsiopoulos, D. A., Grigoriadis, V. N., Işık, M. S., & Tziavos, I. N. (2018). Preliminary results of GOCE-based height system unification between Greece and Turkey over marine and land areas. *Acta Geodaetica et Geophysica*, *53*(1), 61–79. https://doi.org/10.1007/s40328-017-0204-x

Vermeer, M. (2020). Physical geodesy. 520. ISBN: 978-952-60-8940-9. https://aaltodoc.aalto.fi/handle/123456789/43774

Vu, D. T., Bonvalot, S., Bruinsma, S., & Bui, L. K. (2021). A local lithospheric structure model for Vietnam derived from a high-resolution gravimetric geoid. *Earth, Planets and Space*, *73*(1), 92. https://doi.org/10.1186/s40623-021-01415-2

Vu, D. T., Bruinsma, S., & Bonvalot, S. (2019). A high-resolution gravimetric quasigeoid model for Vietnam. *Earth, Planets and Space*, *71*(1), 65. https://doi.org/10.1186/s40623-019-1045-3

Vu, D. T., Bruinsma, S., Bonvalot, S., Bui, L. K., & Balmino, G. (2021). Determination of the geopotential value on the permanent GNSS stations in Vietnam based on the Geodetic Boundary Value Problem approach. *Geophysical Journal International*, *226*(2), 1206–1219. https://doi.org/10.1093/gji/ggab166

Vu, D. T., Bruinsma, S., Bonvalot, S., Remy, D., & Vergos, G. S. (2020). A Quasigeoid-Derived Transformation Model Accounting for Land Subsidence in the Mekong Delta towards Height System Unification in Vietnam. *Remote Sensing*, *12*(5), 817. https://doi.org/10.3390/rs12050817

Wang, Y. M., Holmes, S., Saleh, J., Li, X. P., & Roman, D. (2010). *A Comparison of topographic effect by integral and high' degree spherical harmonic expansion – Preliminary Results*. https://slideplayer.com/slide/3277420/

Wessel, P., & Smith, W. H. F. (1998). New, improved version of generic mapping tools released. *Eos, Transactions American Geophysical Union*, *79*(47), 579–579. https://doi.org/10.1029/98EO00426

Wienecke, S. (2006). *A new analytical solution for the calculation of flexural rigidity: Significance and application*. http://dx.doi.org/10.17169/refubium-4365

Witte, L. de. (1967). Truncation Errors in the Stokes and Vening Meinesz Formulae for Different Order Spherical Harmonic Gravity Terms. *Geophysical Journal of the Royal Astronomical Society*, *12*(5), 449–464. https://doi.org/10.1111/j.1365-

246X.1967.tb03125.x

Wong, L., & Gore, R. (1969). Accuracy of Geoid Heights from Modified Stokes Kernels. *Geophysical Journal International*, *18*(1), 81–91. https://doi.org/10.1111/j.1365-246X.1969.tb00264.x

Wu, H.-H., Tsai, Y.-B., Lee, T.-Y., Lo, C.-H., Hsieh, C.-H., & Toan, D. V. (2004). 3-D Shear Wave Velocity Structure of the Crust and Upper Mantle in South China Sea and its Surrounding Regions by Surface Wave Dispersion Analysis. *Marine Geophysical Researches*, *25*(1), 5–27. https://doi.org/10.1007/s11001-005-0730-8

Yu, Y., Hung, T. D., Yang, T., Xue, M., Liu, K. H., & Gao, S. S. (2017). Lateral variations of crustal structure beneath the Indochina Peninsula. *Tectonophysics*, *712–713*, 193–199. https://doi.org/10.1016/j.tecto.2017.05.023

Yun, H.-S. (2002). Evaluation of ultra-high and high degree geopotential models for improving the KGEOID98. *Korean Journal of Gematics*, 2:7-15.

Zhongolovich, I. (1952). The external gravity field of the earth and the fundamental constants connected with it. *Academy of Sciences USSR, Moscow*.

List of Figures

List of Tables

Appendix

Appendix 1: STD of the differences between the GOCE GGMs in combination with EGM2008 and the GNSS/levelling data (unit: m)

d/o	DIR-R5 + EGM2008	GOCO-R5 + EGM2008	TIM-R5 + EGM2008	SPW-R5 + EGM2008
330				0.179
320				0.182
310				0.172
300	0.173			0.177
290	0.174			0.178
280	0.168	0.170	0.167	0.171
270	0.166	0.163	0.162	0.166
260	0.160	0.167	0.164	0.167
250	0.164	0.169	0.167	0.176
240	0.162	0.163	0.161	0.164
230	0.167	0.168	0.166	0.166
220	0.176	0.176	0.174	0.175
210	0.180	0.180	0.178	0.178
200	0.188	0.188	0.187	0.187
190	0.196	0.196	0.194	0.196
180	0.197	0.197	0.196	0.196
170	0.203	0.203	0.202	0.202
160	0.203	0.202	0.202	0.202
150	0.212	0.212	0.212	0.212
140	0.236	0.236	0.235	0.235
130	0.250	0.249	0.249	0.249
120	0.274	0.274	0.273	0.273
110	0.295	0.294	0.293	0.294
100	0.281	0.281	0.280	0.280
90	0.296	0.296	0.294	0.295
80	0.294	0.294	0.293	0.294
70	0.292	0.293	0.291	0.292
60	0.292	0.293	0.292	0.292
50	0.293	0.293	0.292	0.293
40	0.293	0.293	0.292	0.293
30	0.293	0.293	0.292	0.292
20	0.293	0.293	0.292	0.292
10	0.293	0.293	0.292	0.293

Appendix 2: Result of gravimetric quasigeoid with different modified-degree kernels using Wong-Gore (unit: m)

Truncation degree	Min	Max	Mean	STD
N_1=100; N_2=110	0.126	0.874	0.493	0.118
N_1=110; N_2=120	0.115	0.861	0.489	0.115
N_1=120; N_2=130	0.102	0.847	0.489	0.113
N_1=130; N_2=140	0.098	0.834	0.491	0.110
N_1=140; N_2=150	0.102	0.825	0.494	0.107
N_1=150; N_2=160	0.111	0.830	0.497	0.104
N_1=160; N_2=170	0.124	0.840	0.500	0.101
N_1=170; N_2=180	0.130	0.844	0.502	0.099
N_1=180; N_2=190	0.132	0.845	0.503	0.099
N_1=190; N_2=200	0.133	0.843	0.504	0.098
N_1=200; N_2=210	0.133	0.837	0.504	0.098
N_1=210; N_2=220	0.140	0.827	0.506	0.098
N_1=220; N_2=230	0.136	0.815	0.506	0.097
N_1=230; N_2=240	0.130	0.802	0.504	0.100
N_1=240; N_2=250	0.123	0.787	0.501	0.103
N_1=250; N_2=260	0.116	0.784	0.499	0.106
N_1=260; N_2=270	0.109	0.790	0.497	0.110

Appendix 3: Output result from the GRAVSOFT COVFIT program

FITTING OR TABULATION OF COVARIANCE FUNCTIONS, VERS. 15 OKT 2008.

THE KINDS AND CORRESPONDING UNITS ARE AS FOLLOWS: (E=EOTVOS):

(1) THE HEIGHT ANOMALY (METERS), (2) THE NEGATIVE RADIAL DER-

IVATIVE (THE GRAVITY DISTURBANCE), (3) THE GRAVITY

ANOMALY (MGAL), (4) THE RADIAL DERIVATIVE OF (3) (E), (5) THE

SECOND ORDER RADIAL DERIVATIVE (E), (6),(7) THE LATITUDE AND

THE LONGITUDE COMPONENTS OF THE DEFLECTIONS OF THE VERTICAL

(ARCSECONDS), (8),(9) THE DERIVATIVES OF (3) IN NORTHERN AND

EASTERN DIRECTION, RESPECTIVELY (E), (10),(11) THE DERIVATIVE

OF (2) IN THE SAME DIRECTIONS (E), (12) - (15) THE SECOND

ORDER DERIVATIVES WITH RESPECT TO LATITUDE, IN NORTHERN

AND EASTERN DIRECTION * 2, WITH RESPECT TO LONGITUDE, AND

IN EASTERN MINUS NORTHERN DIRECTIONS, RESPECTIVELY (E).

(0) OR (16) DENSITY ANOMALIES IN G/CM**3*10.

(17) COEFFICIENT OF THE F.NORM. SPHERICAL HARMONIC Y(I,J),

100 ADDED INDICATES 1 OR 2-D MEAN & NEGATIVE ROTATED.

INTERACTIVE ? (T/F) ?

INPUT MODE (1-7), TEST? (T/F), FUNCTION GIVEN AS LEGENDRE SUM?

LAST COMPUTATION ? , OUTPUT TABLE TO FILE ? (T/F)

COMPUTATION MODE= 4

INPUT TYPE OF COV. FCT. MODEL (1,2,3)

INPUT INTEGER(S) IN NUMERATOR

THE MODEL ANOMALY DEGREE-VARIANCES ARE EQUAL TO

A*(I-1)
/((I-2)*(I+ 4)).

INPUT -DEPTH TO BJ.SPH.(KM), GRAVITY VARIANCE (MGAL**2),

MAX DEGREE OF ERROR DEGREE-VARIANCES (EDGV)

EDGV ALL ZERO ? (T/F),

INPUT ERROR DEG.VAR. MODEL NO., IMIN, SCALE FACTOR AND LIST?

MODEL -1 USED FROM DEGREE 2 TO 719 WITH SCALE FACTOR= 0.270000

INPUT NAME OF FILE HOLDING DEG.VAR.

DEGREE-VARIANCES INPUT FROM FILE data/dir5_egm_260_2190_ce.edg
2 719

MULTIPLICATIVE FACTOR USED

SUM OF DEGREE-VARIANCES (MGAL) = 2.94723

RATIO R/RE = 0.999035

DEPTH TO BJERHAMMAR SPHERE (R-RE) = -6150.00 M

VARIANCE OF POINT GRAVITY ANOMALIES = 90.21 MGAL**2

THE FACTOR A, DIVIDED BY RE**2 IS = 742.90 MGAL**2

INPUT NUMBER OF ITERATIONS AND 3 APRIORI WEIGHT FACTORS

THE VALUE OF TAU(J) USED IN THE CX MATRIX: CX(J,J)=TAU(J)**2

AA: 0.50, A: 0.20, RB-RE: 0.10.

(AA IS EQUAL TO THE CONSTANT SMALL A)

INPUT NO. OF DATASETS

NUMBER OF DATA SETS: 1.

INPUT NO. OF VALUES, DATA TYPE 1, DATA TYPE 2, HEIGHT1, HEIGHT2, ERROR-MODE, WEIGHT, DATA ON FILE?(T/F) WHERE ERROR-MODE=1: DATA DISTRIBUTION DEPENDENT - - - =2: COVARIANCE-VARIANCE DEPENDENT

INPUT VAR1, VAR2, FI1,2 DFI, LON1,2, DLO

DATA SET NO. 1:

NUMBER OF VALUES: 90,

BETWEEN KIND 3 AND 3,

AT HEIGHTS: 163.0 AND 163.0.

MODE FOR ERROR: 1,

ERRORS ARE CALCULATED USING:

THE VARIANCES OF THE TWO KINDS: 100.2900 100.2900,

AND AREA SPECIFICATIONS:

FI1, FI2, AND DFI: 8.0000 24.0000 0.0550,

LA1, LA2, AND DLA: 102.0000 110.0000 0.0550.

GEOMETRIC MEAN OF VARIANCES: 100.2900.

EXPECTED NUMBER OF PRODUCTS: 42314.

VAR/SQRT(N) = 0.4875.

RELATIVE WEIGHT FACTOR: 1.000.

INPUT NAME OF FILE HOLDING TABLE

INPUT OF COVARIANCES FROM FILE: table.txt

RESULT OF ITERATION NO. 0:

	AA	A	RB-RE
NEW VALUE:	0.270000	3015400.	-6150.000
LAST ADJ.:	0.270000	3015400.	-6150.000

KP	KQ	PSI	HP	HQ	OBS	MODEL	ERR	DIF/ERR
1	3	3 0.000	163.0	163.0	90.2080	85.4004	0.0778	61.7594
2	3	3 0.050	163.0	163.0	40.6245	66.5923	0.1199********	

3	3	3	0.100	163.0	163.0	33.0814	28.7033	0.1597	27.4133
4	3	3	0.150	163.0	163.0	26.8997	-2.2877	0.2113	138.1141
5	3	3	0.200	163.0	163.0	14.9263	-17.0671	0.2388	133.9880
6	3	3	0.250	163.0	163.0	5.9304	-17.8127	0.2746	86.4589
7	3	3	0.300	163.0	163.0	2.7428	-10.5947	0.3229	41.3050
8	3	3	0.350	163.0	163.0	1.8489	-1.4075	0.3638	8.9508
9	3	3	0.400	163.0	163.0	2.7550	5.5555	0.4087	-6.8517
10	3	3	0.450	163.0	163.0	3.8216	8.3936	0.4351	-10.5089
11	3	3	0.500	163.0	163.0	4.5124	7.2368	0.4420	-6.1636
12	3	3	0.550	163.0	163.0	4.0265	3.5479	0.4648	1.0298
13	3	3	0.600	163.0	163.0	1.3219	-0.7279	0.4800	4.2708
14	3	3	0.650	163.0	163.0	-1.8914	-3.9166	0.5023	4.0322
15	3	3	0.700	163.0	163.0	-3.7482	-5.0979	0.5297	2.5483
16	3	3	0.750	163.0	163.0	-4.6337	-4.2423	0.5376	-0.7280
17	3	3	0.800	163.0	163.0	-3.3799	-2.0366	0.5523	-2.4324
18	3	3	0.850	163.0	163.0	-2.5484	0.4869	0.5536	-5.4829
19	3	3	0.900	163.0	163.0	-2.7099	2.3657	0.5523	-9.1894
20	3	3	0.950	163.0	163.0	-0.6911	3.0259	0.5585	-6.6549
21	3	3	1.000	163.0	163.0	0.7912	2.4182	0.5733	-2.8379
22	3	3	1.050	163.0	163.0	0.4492	0.9543	0.5919	-0.8533

23 3 3 1.100 163.0 163.0 1.0867 -0.7051 0.5925 3.0240

24 3 3 1.150 163.0 163.0 0.8922 -1.9178 0.6097 4.6085

25 3 3 1.200 163.0 163.0 0.4990 -2.2849 0.6319 4.4054

26 3 3 1.250 163.0 163.0 -1.0884 -1.7624 0.6639 1.0152

27 3 3 1.300 163.0 163.0 -2.3544 -0.6336 0.7011 -2.4544

28 3 3 1.350 163.0 163.0 -3.0883 0.6299 0.7105 -5.2328

29 3 3 1.400 163.0 163.0 -3.9261 1.5578 0.7366 -7.4449

30 3 3 1.450 163.0 163.0 -3.3252 1.8501 0.7632 -6.7810

31 3 3 1.500 163.0 163.0 -2.9080 1.4669 0.7833 -5.5850

32 3 3 1.550 163.0 163.0 -1.2374 0.6166 0.8095 -2.2902

33 3 3 1.600 163.0 163.0 -0.7392 -0.3436 0.8210 -0.4819

34 3 3 1.650 163.0 163.0 -1.6462 -1.0511 0.8414 -0.7072

35 3 3 1.700 163.0 163.0 -1.1435 -1.2702 0.8663 0.1462

36 3 3 1.750 163.0 163.0 -1.0410 -0.9658 0.8664 -0.0868

37 3 3 1.800 163.0 163.0 0.7438 -0.2991 0.8763 1.1902

38 3 3 1.850 163.0 163.0 0.9661 0.4480 0.8745 0.5924

39 3 3 1.900 163.0 163.0 1.1194 0.9864 0.8717 0.1526

40 3 3 1.950 163.0 163.0 0.8481 1.1256 0.9027 -0.3075

41 3 3 2.000 163.0 163.0 0.0059 0.8370 0.9176 -0.9058

42	3	3	2.050	163.0	163.0	-1.6682	0.2519	0.9461	-2.0294
43	3	3	2.100	163.0	163.0	-2.4562	-0.3982	0.9600	-2.1437
44	3	3	2.150	163.0	163.0	-1.0003	-0.8731	1.0028	-0.1269
45	3	3	2.200	163.0	163.0	0.6368	-1.0130	1.0386	1.5885
46	3	3	2.250	163.0	163.0	1.4517	-0.7917	1.0708	2.0951
47	3	3	2.300	163.0	163.0	0.8771	-0.3171	1.1104	1.0754
48	3	3	2.350	163.0	163.0	-0.1020	0.2176	1.1172	-0.2860
49	3	3	2.400	163.0	163.0	0.1174	0.6101	1.1483	-0.4291
50	3	3	2.450	163.0	163.0	-0.4067	0.7249	1.1839	-0.9559
51	3	3	2.500	163.0	163.0	-0.1344	0.5386	1.1970	-0.5622
52	3	3	2.550	163.0	163.0	-1.7989	0.1418	1.2355	-1.5709
53	3	3	2.600	163.0	163.0	-0.7267	-0.3011	1.2318	-0.3455
54	3	3	2.650	163.0	163.0	-0.1243	-0.6176	1.2633	0.3904
55	3	3	2.700	163.0	163.0	1.2270	-0.6915	1.2745	1.5053
56	3	3	2.750	163.0	163.0	2.2296	-0.5032	1.2862	2.1247
57	3	3	2.800	163.0	163.0	1.7539	-0.1319	1.3274	1.4206
58	3	3	2.850	163.0	163.0	1.2812	0.2790	1.3462	0.7444
59	3	3	2.900	163.0	163.0	1.5348	0.5782	1.3862	0.6901
60	3	3	2.950	163.0	163.0	0.7315	0.6630	1.4110	0.0485
61	3	3	3.000	163.0	163.0	0.7638	0.5148	1.4318	0.1739

62 3 3 3.050 163.0 163.0 1.5092 0.2021 1.4695 0.8895

63 3 3 3.100 163.0 163.0 0.8748 -0.1498 1.4614 0.7011

64 3 3 3.150 163.0 163.0 0.2032 -0.4079 1.4842 0.4117

65 3 3 3.200 163.0 163.0 -1.0313 -0.4816 1.5146 -0.3629

66 3 3 3.250 163.0 163.0 0.0271 -0.3539 1.5231 0.2502

67 3 3 3.300 163.0 163.0 0.9094 -0.0848 1.5660 0.6349

68 3 3 3.350 163.0 163.0 0.3672 0.2151 1.5736 0.0966

69 3 3 3.400 163.0 163.0 0.1932 0.4284 1.6240 -0.1448

70 3 3 3.450 163.0 163.0 1.6377 0.4747 1.6703 0.6963

71 3 3 3.500 163.0 163.0 1.0904 0.3398 1.7127 0.4383

72 3 3 3.550 163.0 163.0 0.7436 0.0779 1.7920 0.3715

73 3 3 3.600 163.0 163.0 0.5165 -0.2111 1.8112 0.4017

74 3 3 3.650 163.0 163.0 0.4539 -0.4209 1.8449 0.4742

75 3 3 3.700 163.0 163.0 -0.1535 -0.4783 1.8839 0.1724

76 3 3 3.750 163.0 163.0 -0.2266 -0.3698 1.9185 0.0746

77 3 3 3.800 163.0 163.0 0.1744 -0.1434 1.9752 0.1609

78 3 3 3.850 163.0 163.0 0.0102 0.1112 1.9781 -0.0511

79 3 3 3.900 163.0 163.0 -0.5323 0.2981 2.0397 -0.4071

80 3 3 3.950 163.0 163.0 -0.6343 0.3510 2.0859 -0.4724

81 3 3 4.000 163.0 163.0 -0.8285 0.2572 2.1135 -0.5137

82 3 3 4.050 163.0 163.0 -1.0580 0.0600 2.1839 -0.5119

83 3 3 4.100 163.0 163.0 -0.5735 -0.1599 2.1965 -0.1883

84 3 3 4.150 163.0 163.0 0.0092 -0.3158 2.2588 0.1439

85 3 3 4.200 163.0 163.0 0.1536 -0.3480 2.3080 0.2173

86 3 3 4.250 163.0 163.0 0.0690 -0.2456 2.3367 0.1346

87 3 3 4.300 163.0 163.0 0.6777 -0.0486 2.4225 0.2998

88 3 3 4.350 163.0 163.0 1.2020 0.1682 2.4395 0.4237

89 3 3 4.400 163.0 163.0 1.9050 0.3250 2.5079 0.6300

90 3 3 4.450 163.0 163.0 1.5651 0.3665 2.5624 0.4677

RMS VALUE OF DIFFERENCES/ERRORS: 33.076342

(RELATIVE CHANGE: 1.000000).

.
.
.

RESULT OF ITERATION NO.***:

AA A RB-RE

NEW VALUE: 3.186457 86768. -28.238

LAST ADJ.: 0.000015 -2. 0.013

KP	KQ	PSI	HP	HQ	OBS	MODEL	ERR	DIF/ERR
1	3	3	0.000	163.0	163.0	90.2080	89.7269	0.0778	6.1808
2	3	3	0.050	163.0	163.0	40.6245	45.2544	0.1199	-38.6268
3	3	3	0.100	163.0	163.0	33.0814	29.7414	0.1597	20.9136
4	3	3	0.150	163.0	163.0	26.8997	19.3477	0.2113	35.7360
5	3	3	0.200	163.0	163.0	14.9263	11.3405	0.2388	15.0175
6	3	3	0.250	163.0	163.0	5.9304	5.1955	0.2746	2.6760
7	3	3	0.300	163.0	163.0	2.7428	0.8418	0.3229	5.8873
8	3	3	0.350	163.0	163.0	1.8489	-1.7943	0.3638	10.0138
9	3	3	0.400	163.0	163.0	2.7550	-2.9402	0.4087	13.9333
10	3	3	0.450	163.0	163.0	3.8216	-2.9889	0.4351	15.6538
11	3	3	0.500	163.0	163.0	4.5124	-2.4292	0.4420	15.7042
12	3	3	0.550	163.0	163.0	4.0265	-1.7391	0.4648	12.4050
13	3	3	0.600	163.0	163.0	1.3219	-1.2827	0.4800	5.4268
14	3	3	0.650	163.0	163.0	-1.8914	-1.2431	0.5023	-1.2907
15	3	3	0.700	163.0	163.0	-3.7482	-1.6083	0.5297	-4.0401
16	3	3	0.750	163.0	163.0	-4.6337	-2.2123	0.5376	-4.5040
17	3	3	0.800	163.0	163.0	-3.3799	-2.8121	0.5523	-1.0282

18	3	3	0.850	163.0	163.0	-2.5484	-3.1775	0.5536	1.1364
19	3	3	0.900	163.0	163.0	-2.7099	-3.1643	0.5523	0.8226
20	3	3	0.950	163.0	163.0	-0.6911	-2.7509	0.5585	3.6877
21	3	3	1.000	163.0	163.0	0.7912	-2.0333	0.5733	4.9266
22	3	3	1.050	163.0	163.0	0.4492	-1.1825	0.5919	2.7569
23	3	3	1.100	163.0	163.0	1.0867	-0.3835	0.5925	2.4813
24	3	3	1.150	163.0	163.0	0.8922	0.2229	0.6097	1.0978
25	3	3	1.200	163.0	163.0	0.4990	0.5774	0.6319	-0.1240
26	3	3	1.250	163.0	163.0	-1.0884	0.7083	0.6639	-2.7063
27	3	3	1.300	163.0	163.0	-2.3544	0.7084	0.7011	-4.3683
28	3	3	1.350	163.0	163.0	-3.0883	0.6922	0.7105	-5.3205
29	3	3	1.400	163.0	163.0	-3.9261	0.7520	0.7366	-6.3510
30	3	3	1.450	163.0	163.0	-3.3252	0.9257	0.7632	-5.5699
31	3	3	1.500	163.0	163.0	-2.9080	1.1878	0.7833	-5.2287
32	3	3	1.550	163.0	163.0	-1.2374	1.4634	0.8095	-3.3362
33	3	3	1.600	163.0	163.0	-0.7392	1.6596	0.8210	-2.9219
34	3	3	1.650	163.0	163.0	-1.6462	1.7005	0.8414	-3.9773
35	3	3	1.700	163.0	163.0	-1.1435	1.5539	0.8663	-3.1138
36	3	3	1.750	163.0	163.0	-1.0410	1.2414	0.8664	-2.6344
37	3	3	1.800	163.0	163.0	0.7438	0.8289	0.8763	-0.0971

38 3 3 1.850 163.0 163.0 0.9661 0.4024 0.8745 0.6446

39 3 3 1.900 163.0 163.0 1.1194 0.0389 0.8717 1.2396

40 3 3 1.950 163.0 163.0 0.8481 -0.2167 0.9027 1.1796

41 3 3 2.000 163.0 163.0 0.0059 -0.3619 0.9176 0.4008

42 3 3 2.050 163.0 163.0 -1.6682 -0.4312 0.9461 -1.3075

43 3 3 2.100 163.0 163.0 -2.4562 -0.4776 0.9600 -2.0609

44 3 3 2.150 163.0 163.0 -1.0003 -0.5497 1.0028 -0.4494

45 3 3 2.200 163.0 163.0 0.6368 -0.6717 1.0386 1.2598

46 3 3 2.250 163.0 163.0 1.4517 -0.8348 1.0708 2.1353

47 3 3 2.300 163.0 163.0 0.8771 -1.0014 1.1104 1.6916

48 3 3 2.350 163.0 163.0 -0.1020 -1.1201 1.1172 0.9114

49 3 3 2.400 163.0 163.0 0.1174 -1.1454 1.1483 1.0997

50 3 3 2.450 163.0 163.0 -0.4067 -1.0547 1.1839 0.5474

51 3 3 2.500 163.0 163.0 -0.1344 -0.8568 1.1970 0.6035

52 3 3 2.550 163.0 163.0 -1.7989 -0.5881 1.2355 -0.9801

53 3 3 2.600 163.0 163.0 -0.7267 -0.3004 1.2318 -0.3460

54 3 3 2.650 163.0 163.0 -0.1243 -0.0435 1.2633 -0.0640

55 3 3 2.700 163.0 163.0 1.2270 0.1505 1.2745 0.8446

56 3 3 2.750 163.0 163.0 2.2296 0.2750 1.2862 1.5197

57	3	3	2.800	163.0	163.0	1.7539	0.3472	1.3274	1.0597
58	3	3	2.850	163.0	163.0	1.2812	0.3982	1.3462	0.6559
59	3	3	2.900	163.0	163.0	1.5348	0.4582	1.3862	0.7766
60	3	3	2.950	163.0	163.0	0.7315	0.5440	1.4110	0.1329
61	3	3	3.000	163.0	163.0	0.7638	0.6514	1.4318	0.0785
62	3	3	3.050	163.0	163.0	1.5092	0.7574	1.4695	0.5116
63	3	3	3.100	163.0	163.0	0.8748	0.8290	1.4614	0.0314
64	3	3	3.150	163.0	163.0	0.2032	0.8357	1.4842	-0.4262
65	3	3	3.200	163.0	163.0	-1.0313	0.7617	1.5146	-1.1838
66	3	3	3.250	163.0	163.0	0.0271	0.6119	1.5231	-0.3839
67	3	3	3.300	163.0	163.0	0.9094	0.4107	1.5660	0.3184
68	3	3	3.350	163.0	163.0	0.3672	0.1938	1.5736	0.1102
69	3	3	3.400	163.0	163.0	0.1932	-0.0031	1.6240	0.1209
70	3	3	3.450	163.0	163.0	1.6377	-0.1559	1.6703	1.0739
71	3	3	3.500	163.0	163.0	1.0904	-0.2579	1.7127	0.7872
72	3	3	3.550	163.0	163.0	0.7436	-0.3192	1.7920	0.5931
73	3	3	3.600	163.0	163.0	0.5165	-0.3606	1.8112	0.4843
74	3	3	3.650	163.0	163.0	0.4539	-0.4036	1.8449	0.4648
75	3	3	3.700	163.0	163.0	-0.1535	-0.4605	1.8839	0.1630
76	3	3	3.750	163.0	163.0	-0.2266	-0.5296	1.9185	0.1580

77 3 3 3.800 163.0 163.0 0.1744 -0.5953 1.9752 0.3897

78 3 3 3.850 163.0 163.0 0.0102 -0.6346 1.9781 0.3260

79 3 3 3.900 163.0 163.0 -0.5323 -0.6259 2.0397 0.0459

80 3 3 3.950 163.0 163.0 -0.6343 -0.5578 2.0859 -0.0367

81 3 3 4.000 163.0 163.0 -0.8285 -0.4337 2.1135 -0.1868

82 3 3 4.050 163.0 163.0 -1.0580 -0.2718 2.1839 -0.3600

83 3 3 4.100 163.0 163.0 -0.5735 -0.0988 2.1965 -0.2161

84 3 3 4.150 163.0 163.0 0.0092 0.0582 2.2588 -0.0217

85 3 3 4.200 163.0 163.0 0.1536 0.1801 2.3080 -0.0115

86 3 3 4.250 163.0 163.0 0.0690 0.2610 2.3367 -0.0822

87 3 3 4.300 163.0 163.0 0.6777 0.3078 2.4225 0.1527

88 3 3 4.350 163.0 163.0 1.2020 0.3358 2.4395 0.3551

89 3 3 4.400 163.0 163.0 1.9050 0.3613 2.5079 0.6155

90 3 3 4.450 163.0 163.0 1.5651 0.3945 2.5624 0.4568

RMS VALUE OF DIFFERENCES/ERRORS: 7.314181

(RELATIVE CHANGE: 0.000020).

TAU(J) USED IN THE CX MATRIX 0.31E-01 0.13E-01 0.16E-02

RESULTS IN VARIANCE OF GRAVITY ANOMALIES:

1'TH ROW OF INVERSE MATRIX 0.1238E-04 -0.1302E-04 -0.9699E-04

2'TH ROW OF INVERSE MATRIX -0.1302E-04 0.3674E-04 0.5136E-03

3'TH ROW OF INVERSE MATRIX -0.9699E-04 0.5136E-03 0.8775E-02

STD.DEV. 0.112132E-01 0.525927E+03 0.255144E+01

STD.DEV.*RMS 0.820155E-01 0.384673E+04 0.186617E+02

RESULTS IN VARIANCE OF GRAVITY ANOMALIES: 131.06 MGAL**2.

N	RATIO	AA	A	RE-RB	VARG	IT
719	0.7314D+01	3.1865	0.8677D+05	-28.24	131.06	2000

Appendix 4: Time series of heights plots of permanent GNSS stations in Vietnam

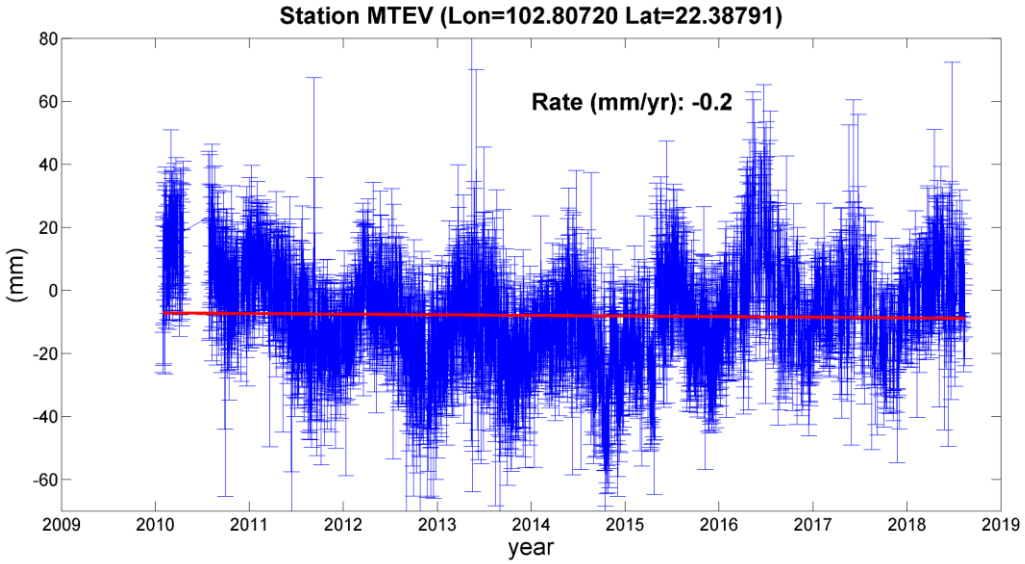

(a)

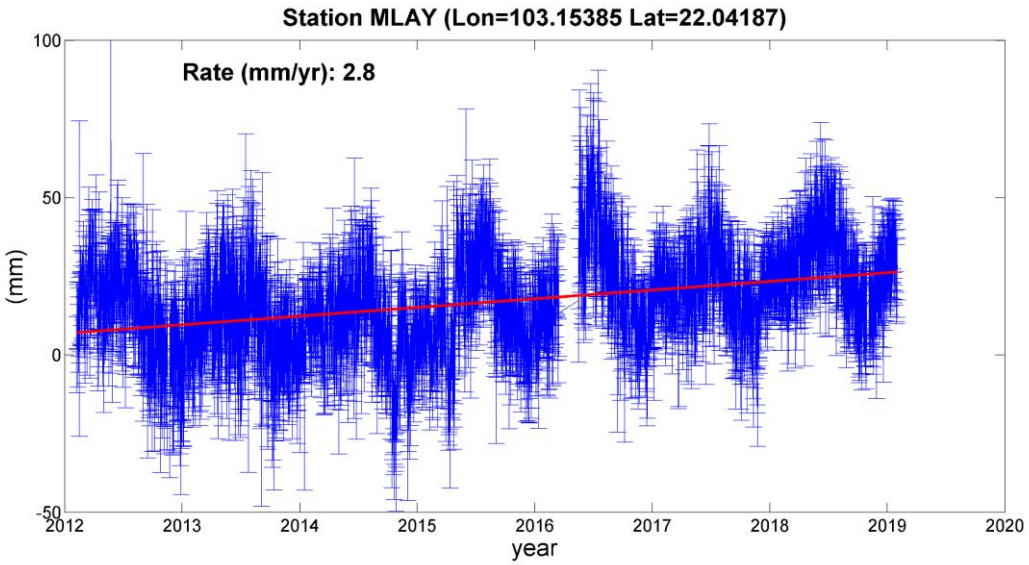

(b)

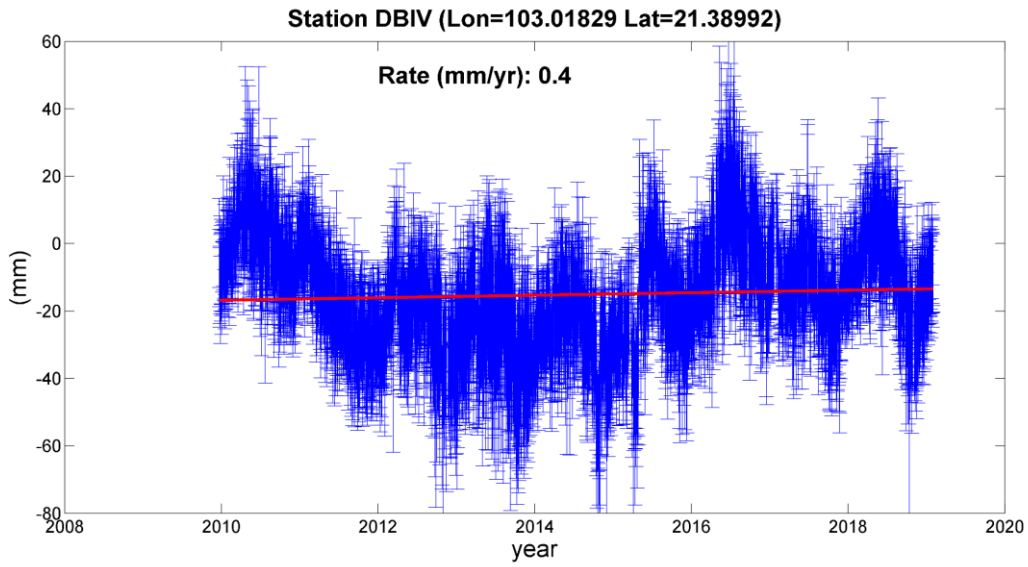
Station DBIV (Lon=103.01829 Lat=21.38992)
Rate (mm/yr): 0.4
(mm)
year

(c)

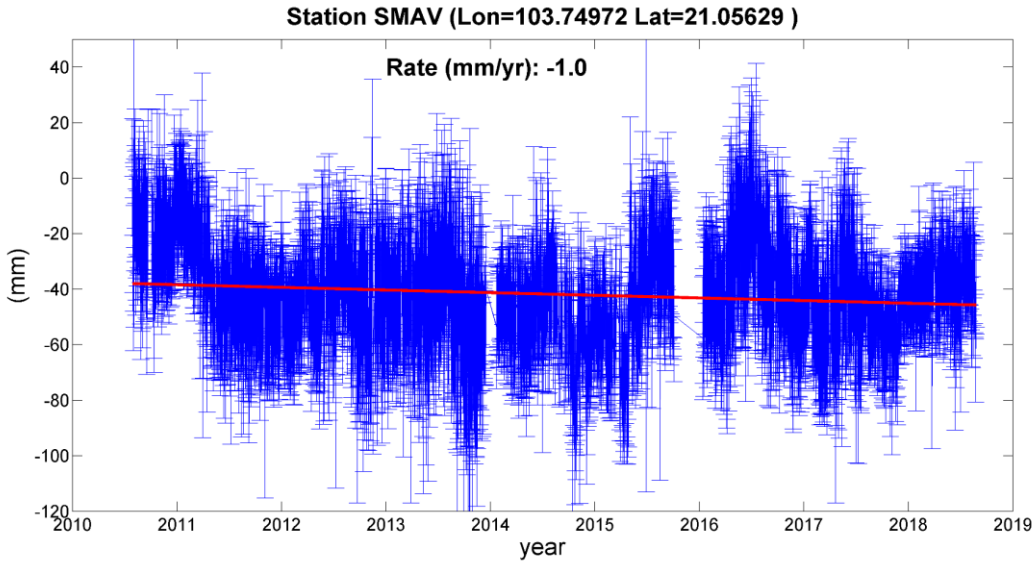
Station SMAV (Lon=103.74972 Lat=21.05629)
Rate (mm/yr): -1.0
(mm)
year

(d)

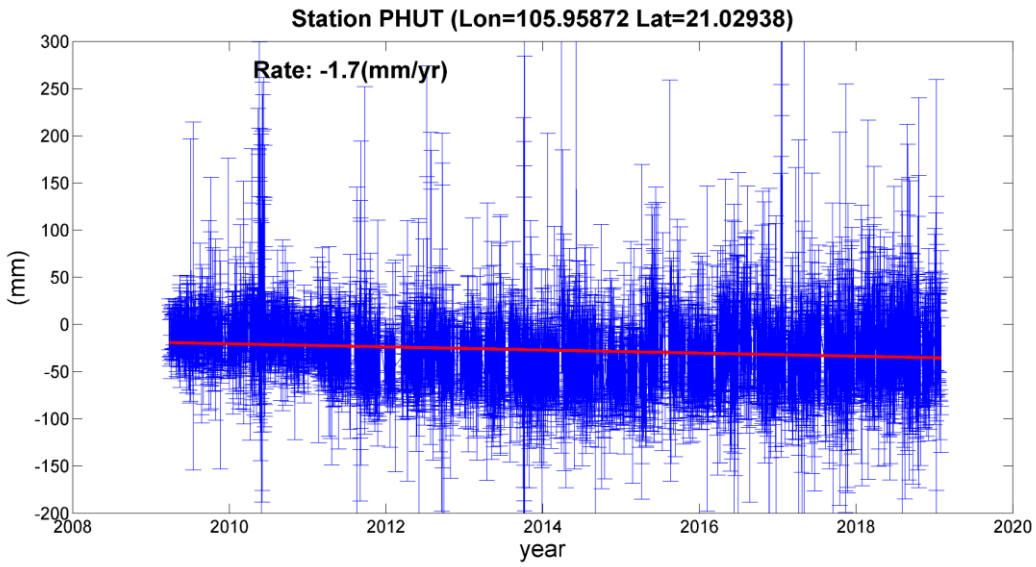
Station PHUT (Lon=105.95872 Lat=21.02938)
Rate: -1.7(mm/yr)
(mm)
year

(e)

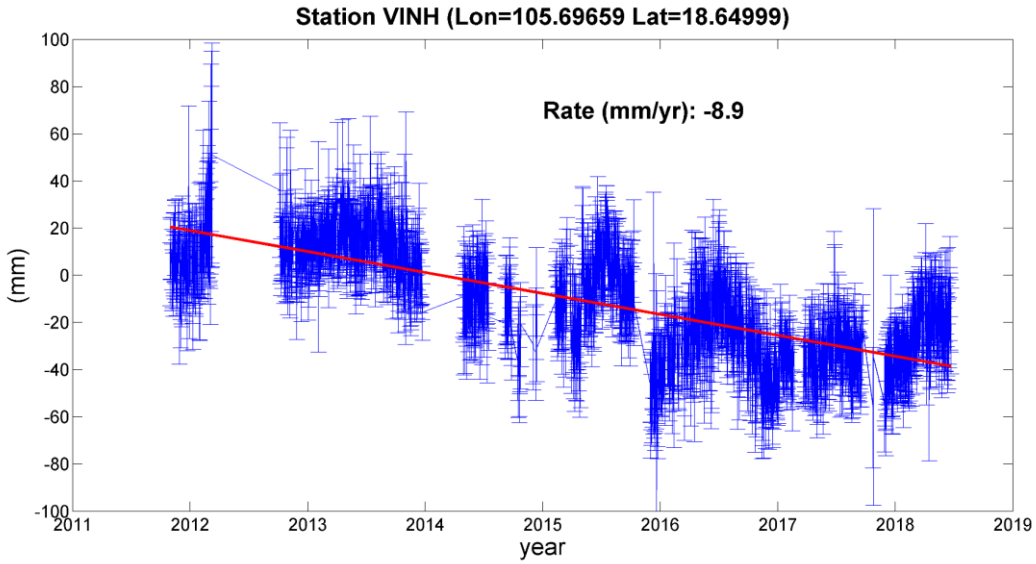
Station VINH (Lon=105.69659 Lat=18.64999)
Rate (mm/yr): -8.9
(mm)
year

(f)

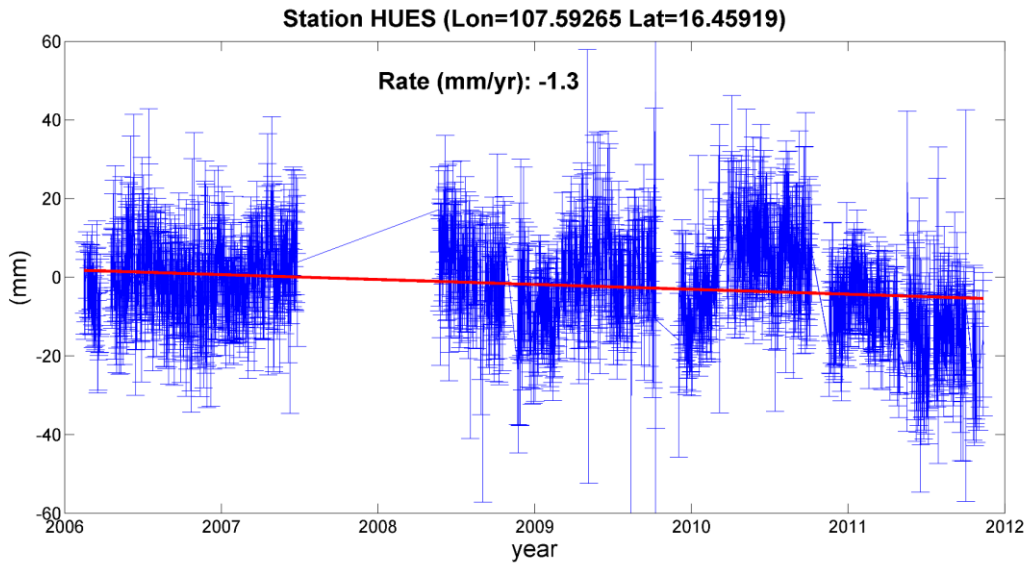

(g)

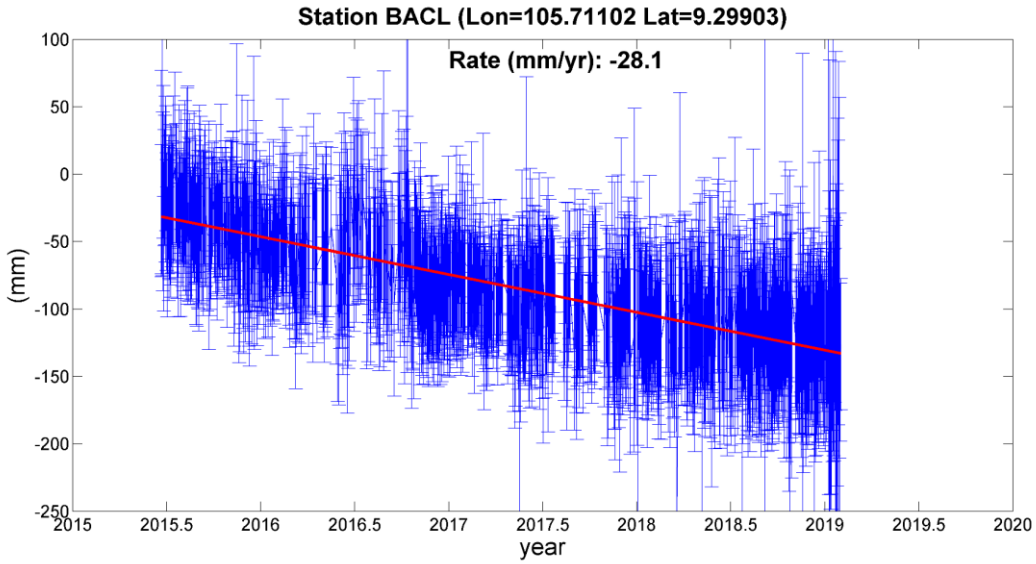

(h)

Figure A5.1. Time-series of heights plots of 8 stations provided by the Institute of Geophysics (IGP) – Vietnam Academy of Science and Technology (VAST) (a) MTEV station; (b) MLAY station; (c) DBIV station; (d) SMAV station; (e) PHUT station; (f) VINH station; (g) HUES station and (h) BACL station

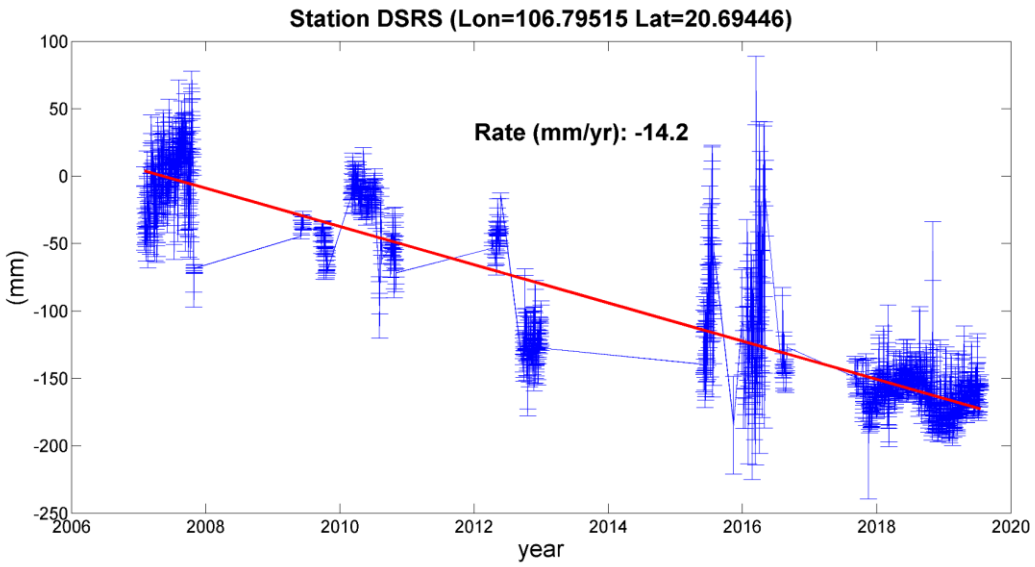
Station DSRS (Lon=106.79515 Lat=20.69446)
Rate (mm/yr): -14.2
(mm)
year
100
50
0
-50
-100
-150
-200
-250
2006
2008
2010
2012
2014
2016
2018
2020

(a)

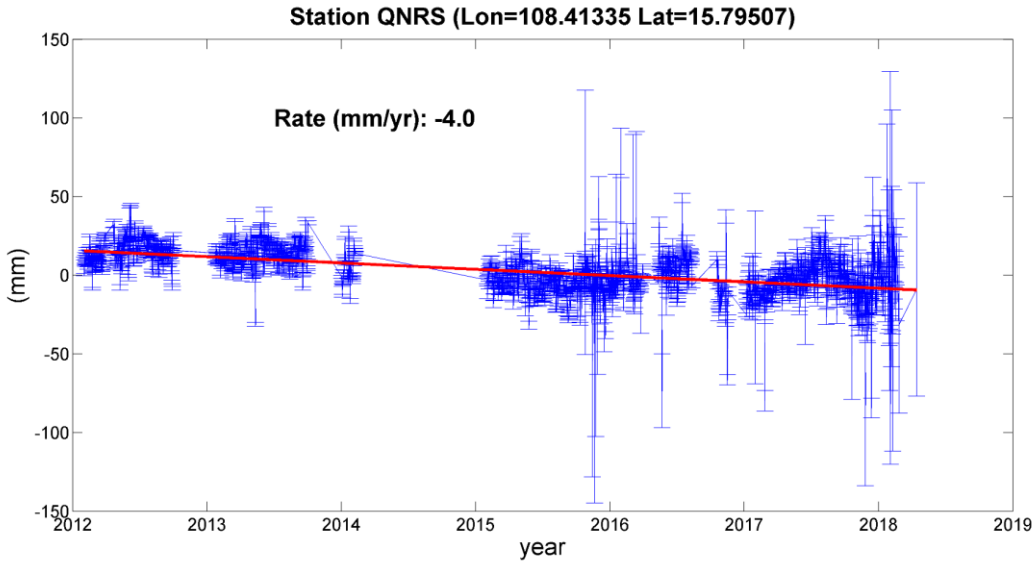
Station QNRS (Lon=108.41335 Lat=15.79507)
Rate (mm/yr): -4.0
(mm)
year
150
100
50
0
-50
-100
-150
2012
2013
2014
2015
2016
2017
2018
2019

(b)

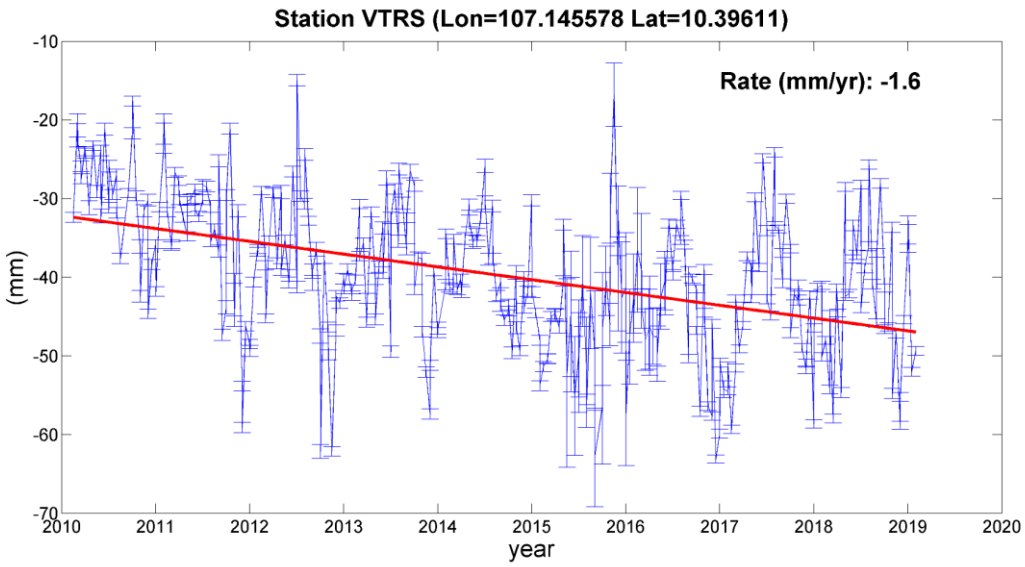

(c)

Figure A5.2. Time-series of heights plots of 3 stations provided by the Vietnam Department of Surveying and Mapping (VDSM) (a) DSRS station; (b) QNRS station and (c) VTRS station

Appendix 5: Results of time series of heights from permanent GNSS stations in Vietnam (unit: km)

	Moho depth of the reference column	Min	Max	Mean	STD
1	z_{cREF} = 28	-3.6	9.3	-0.1	2.3
2	z_{cREF} = 28.5	-3.4	9.3	0.2	2.2
3	z_{cREF} = 29	-3.3	9.5	0.5	2.3
4	z_{cREF} = 29.5	-3.1	9.6	0.6	2.3
5	z_{cREF} = 30	-3.0	9.8	0.8	2.3
6	z_{cREF} = 30.5	-2.8	10.0	1.0	2.4
7	z_{cREF} = 31	-2.6	10.1	1.2	2.4